ALLOMETRY OF THE THORACOLUMBAR REGION IN

RUNNING MAMMALS

By
Katrina Elizabeth Jones

A dissertation submitted to Johns Hopkins University in conformity with the requirements for the degree of Doctor of Philosophy.

Baltimore, Maryland
October, 2014

Abstract

  Mammals use flexion and extension of the back to increase their stride length and assist with breathing during running. The degree to which vertebral column bending increases stride length varies between dorsomobile (e.g., cheetah) and dorsostable (e.g., horse) taxa. It has been suggested that stability of the thoracolumbar region may correlate with body size because dorsomobile gaits are energetically expensive at large size. This dissertation investigates allometry of the thoracolumbar region and asks: How is vertebral structure influenced by increasing body size, and does this vary among families with different running styles? It presents new data on the influence of size and locomotion on the axial skeleton, an understudied anatomical region.

  To address these questions, three families of running mammals with a large size range were sampled: Felidae (cats, dorsomobile), Bovidae and Equidae (bovids and horses, dorsostable). Vertebral material was examined from 57 species (n=216) of felids and bovids, and five extant species and eight fossil genera (n=77) of equids. Vertebral data (linear measures, 2D and 3D landmarks) were compared to body size estimated from limb dimensions.

  Scaling of the ventral column (centra and discs) is consistent with its perceived role in body support as a dorsal compressive element, becoming craniocaudally shorter and dorsoventrally deeper with increasing body size. Morphological features of the lumbar region associated with stability are also correlated with size, but size explains a greater proportion of shape variation in bovids than felids. This suggests passive

stabilization of the lumbar region in dorsostable groups may be a size-dependent response to cursoriality.

Preliminary data suggest that the shape of the intervertebral joint complex reflects its range of motion, highlighting the utility of joint shape for understanding axial function. Specifically, craniocaudal patterns of lumbar morphology reflect differences in craniocaudal mobility between dorsomobile and dorsostable runners, which isolate mobility to the lumbosacral joint. Based on joint shape, small-bodied fossil equids (e.g., *Hyracotherium*) likely had more flexibility of the anterior lumbar region than modern horses, and therefore may have used more diverse gaits. However, specialization of the lumbosacral joint evolved early in equids, predating unguligrady and extreme digit loss.

Dissertation advisor:

Kenneth D. Rose, Johns Hopkins University

Dissertation readers:

Valerie B. DeLeon, Johns Hopkins University

John Hutchinson, Royal Veterinary College

Liza Shapiro, University of Texas

Acknowledgments

I would like to take this opportunity to thank many people who have helped me in the completion of this work, and who have made my graduate school experience so enjoyable. First and foremost, I owe a debt of gratitude to my advisor Ken Rose. He has taught me the importance of careful work, generosity, honesty and (of course) grammar! Secondly, I am extremely grateful to my dissertation readers. Dr. Valerie De Leon's patience with my never-ending questions, and her willingness to talk through statistics problems with me, bordered on the saintly. John Hutchinson and Liza Shapiro kindly stepped in to provide me with feedback on drafts of this dissertation, for which I am very grateful.

Big thanks also go out to everyone at the Center for Functional Anatomy and Evolution. My lab mates Francois Gould and Heather Ahrens have shared their good humor and scientific advice with me in equal measure, making the Rose lab a wonderful place to be! Jonathan Perry, Dave Weishampel and Chris Ruff have been excellent mentors and collaborators. Finally, I am grateful to the other grad students and post-docs who were always there to lend a helping hand: my awesome cohort Ali, Megan, Loring, Nicky, Heather K, Rachel F, Kirty, Evan, Maddy, Ryan, Janine and Rachel D.

I have also been lucky enough to have several mentors outside of the department to offer me advice and support. Special thanks go to my Master's thesis advisor Anjali Goswami, who first introduced me to mammal morphology and inspired me to pursue it. I would also like to thank Rebecca German, a friend and collaborator who has always challenged me to think about the bigger picture, and Emily Buchholtz, who first piqued my interest in the vertebral column.

Table of Contents

List of Tables

List of Figures

CHAPTER 1: INTRODUCTION

The vertebral column is a critical component of the mammalian locomotor apparatus (Howell, 1944; Slijper, 1946; Schilling, 2011). Sagittal flexion and extension of the lumbar spine are particularly important during the fastest mammalian gaits (Schilling and Hackert, 2006). These motions increase stride length, regulate positioning of the center of mass and assist with respiration (Bramble and Carrier, 1983; Alexander et al., 1985; Bertram and Gutmann, 2009; Schilling and Carrier, 2010). The magnitude of sagittal motions varies among different cursorial taxa. Some species, such as the cheetah, are dorsomobile runners and emphasize sagittal flexion; others, such as the horse, have a relatively rigid thoracolumbar region and are known as dorsostable runners (Hildebrand, 1959; Bertram and Gutmann, 2009). Factors influencing vertebral function and evolution in quadrupedal runners are poorly understood.

Sagittal bending of the trunk during running occurs at the last seven presacral joints, which mostly lie within the ribless lumbar region (Schilling and Hackert, 2006). Zygapophyses (facet joints or articular processes) in this region are sagittally-oriented to permit bending, and movement is controlled by paraxial muscles (Schilling, 2011). In addition to providing movement during locomotion, the thoracolumbar spine must also provide static support for the trunk. The center of mass for quadrupeds is between the two sets of limbs, causing a sagittal sagging moment at the mid-trunk, which is resisted in part by the vertebral column (Smit, 2002). As size increases, loading on the vertebral column also increases. Employing gaits with large sagittal vertebral flexions becomes increasingly expensive as animals become larger (Smeathers, 1981).

Therefore passive support mechanisms that stabilize the lumbar region are advantageous at large size. This leads to the prediction that there should be osteological allometry of the thoracolumbar region.

This dissertation investigates factors influencing the evolution of the vertebral column by examining thoracolumbar skeletal allometry. I used empirical data on morphological variation to address the questions: **How is the bony structure of the thoracolumbar region influenced by increasing body size in running mammals? Do dorsomobile and dorsostable runners scale differently with body size?** Three cursorial mammal groups were used to explore these questions, two extant and one including fossils. In particular, Felidae and Bovidae were included to represent extant mammals that are traditionally classified as dorsomobile and dorsostable runners, respectively. Horses are also dorsostable but small members of Equidae are extinct. Thus both fossil and extant horses were included to capture the full size-range of this family. Specifically, this dissertation uses felids, bovids and equids to:

1. Relate axial morphology to range of motion in dorsostable and dorsomobile families.

2. Investigate how thoracolumbar morphology varies with increasing size in running mammals.

3. Compare scaling in dorsostable and dorsomobile families.

Thoracolumbar movements are important in the fastest mammalian gaits. Improved knowledge of factors influencing vertebral morphology is critical to understanding the evolution of cursoriality and reconstructing locomotor capabilities in extinct taxa.

1.1 BACKGROUND

1.1.1 VERTEBRAL ANATOMY

Regions of the vertebral column

The mammalian vertebral column is made up of serially homologous units, the vertebrae, which may be divided into five regions: cervical, thoracic, lumbar, sacral and caudal (Flower, 1885). The cervical region connects the head to the trunk. In mammals the number of cervical vertebrae remains consistent across taxa at seven, with a few exceptions (Galis, 1999; Buchholtz and Stepien, 2009; Buchholtz, 2014). The thoracic vertebrae articulate with the ribs to form a rigid thoracic cage. Each vertebra articulates with one or two ribs, which articulate directly or indirectly with the sternum. The body of the vertebra articulates with the head of the rib, whereas the transverse process articulates with the tubercle (Rawls and Fisher, 2010). The head of the rib is often situated between two adjacent vertebrae, articulating onto two complementary demi-facets (Flower, 1885). The lumbar region connects the thorax to the sacrum, providing support for the abdominal region. There are no ribs, but the vertebrae have longer and more robust transverse processes. The ancestral thoracolumbar count for mammals is likely 19 vertebrae, however it is as high as 30 in some afrotheres (Narita and Kuratani, 2005). Variation of thoracic and lumbar number within this region is common, and is often inversely related (Buchholtz, 2007). Thoracics usually vary from 12 to 15 vertebrae, whereas there are between 3 and 7 lumbars (Narita and Kuratani, 2005). Total presacral count (cervical, thoracic and lumbar combined) has been proposed to be more conserved in fast running mammals due to pleiotropic effects on the lumbosacral transition (Galis et al., 2014). Sacral vertebrae are fused together to form a sacral mass, which articulates with the ilium at the sacroiliac joint. Sacral count usually varies

between 2 and 6 vertebrae, though can reach up to 9 in armadillos (Narita and Kuratani, 2005). The tail is formed from the caudal vertebrae, and their size, number and morphology are highly variable.

The boundaries of the vertebral regions are defined as follows:

Cervical-thoracic boundary - The first thoracic is the most cranial vertebra with a facet for rib articulation (Flower, 1885). There is often a change in zygapophyseal morphology across this transition too, from cervical-type widely-spaced joints to thoracic-type narrow, horizontal joints. The position of this change may vary with respect to the first rib.

Thoracolumbar boundary - The boundary between the thoracic and lumbar regions can be defined many ways (Buchholtz et al., 2011; Buchholtz, 2014). The traditional definition is the transition from ribbed to ribless vertebrae (Flower, 1885), which can be identified by the presence of a rib facet. However, another common definition is the transition from thoracic-type horizontal zygapophyses to lumbar-type sagittal zygapophyses, known as **pre-diaphragmatic** and **post-diaphragmatic,** respectively (Filler, 2007). The **diaphragmatic vertebra** has pre-diaphragmatic cranial zygapophyses and post-diaphragmatic caudal zygapophyses. Here I used rib morphology to define thoracic versus lumbar regions, but will also refer to pre- and post-diaphragmatic regions. Post-diaphragmatic thoracic vertebrae, which are common in many mammal species, will be referred to as **transitional vertebrae**. It is important to consider these two definitions separately because they seem to vary relatively independently (Williams, 2012a). The other common thoracolumbar transition marker

is the change in orientation of the neural spine from caudally inclined to cranially inclined, separated by a vertebra with a short vertical spine, known as the **anticlinal vertebra** (Slijper, 1946). This transition usually very closely approximates the diaphragmatic vertebra and is not present in all mammal taxa (Filler, 2007).

Lumbosacral boundary - The first sacral is defined as the first vertebra which is fused into the sacral mass, with auricular facets for the articulation of the pelvis (Flower, 1885).

Sacrocaudal boundary – The caudal region begins with unfused vertebrae which are usually quite robust, and quite similar in form to the lumbars with small transverse processes. Toward the tip of the tail the vertebrae tend to become more elongate and may consist only of a centrum.

Development of these vertebral regions is controlled by the interaction of two distinct mechanisms (Buchholtz, 2007). First, the number of vertebrae is determined early in development by the rate of segmentation of presomitic mesoderm into somites using an oscillating clock mechanism (Wellik, 2007; Rawls and Fisher, 2010). In contrast, the identity of vertebrae is controlled by the expression of global patterning genes, such as those from the *Hox* cluster. *Hox* genes are colinear, meaning that their position on the genome reflects their craniocaudal expression location in the embryo, and are represented in paralogs (A to D) (Wellik, 2007). For example, in *Mus*, ribs develop on lumbar vertebrae in mice that are homozygous recessive for all paralogs of *Hox10.* These results were interpreted to suggest that when active, *Hox10* can repress rib formation. The expression of *Hox10* was subsequently extended from the lumbar

region to the entire column, generating a rib-less mouse (Kessel and Gruss, 1991; Wellik and Capecchi, 2003; Vinagre et al., 2010). Variations in vertebral morphology may be classed as meristic, homeotic or morphogenetic (Polly et al., 2001; Buchholtz, 2007). **Meristic** changes are variations in vertebral count. They may result from changes in the rate of the molecular oscillators which produce segmentation. **Homeotic** changes involve shifts in the boundaries of vertebral regions without changes in total vertebral count. One example may be loss of a lumbar vertebra and its replacement by an additional thoracic, or vice versa. These changes usually relate to shifts in the expression of regionalizing genes, such as *Hox*, which determine the vertebral identity. Interestingly, some authors have suggested that all changes in presacral count are always homeotic and never meristic, because the formation of somites occurs in a anterior-to-posterior sequence (Broek et al., 2012; Galis et al., 2014). Finally, **morphogenetic** changes are variation in the morphology associated with a particular vertebral identity, and they usually occur later in development.

Parts of a vertebra

The **body** or **centrum** of the vertebra has epiphyses at each end which are known as the **endplates (**Figure 1.1.1**)**. The centra articulate with fibrocartilaginous intervertebral discs which together form the major weight-bearing portion of the axial skeleton, referred to herein as the **ventral column** (Rawls and Fisher, 2010). Dorsally, the vertebra consists of the arch and muscular processes. The arch covers and protects the spinal cord, whilst articulating with adjacent vertebrae via paired, synovial **zygapophyseal joints**. Muscles which attach to the arch may insert onto small processes, known as **anapophyses** (posterior, accessory processes) or **metapophyses**

(anterior, mammillary processes). Muscular processes provide enhanced leverage for muscles and ligaments that attach to the vertebra (Slijper, 1946). The **neural spine** protrudes dorsally to provide attachment for nuchal, supraspinous and interspinous ligaments as well as epaxial muscles (Bogduk, 1980). The **transverse processes** extend laterally, and may house the vertebral artery (in the cervical series), provide articulation for ribs (in the thoracic series) or provide attachment for intertransverse ligaments and epaxial muscles (in the lumbar series) (Flower, 1885). The size, orientation and shape of these muscular processes are highly variable and are thought to reflect *in vivo* function of the attached muscles (Slijper, 1946; Argot, 2003).
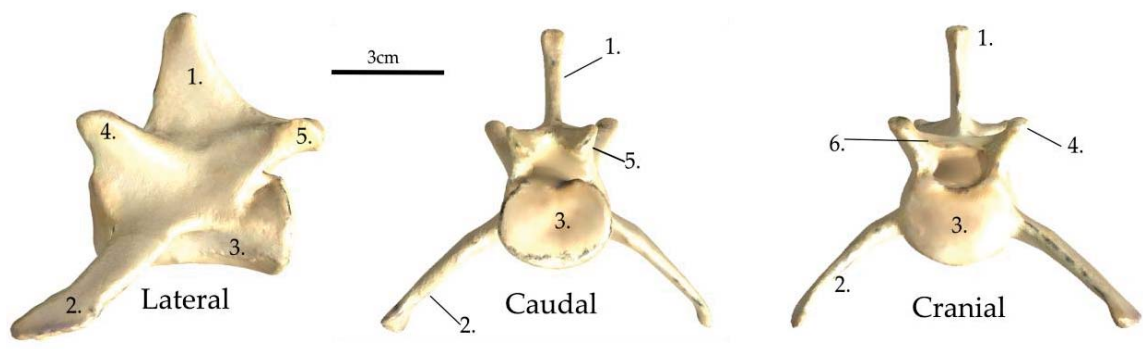
Figure 1.1.1 Anatomy of a lumbar vertebra of the cheetah, **Acinonyx jubatus**
in lateral, caudal and cranial views. 1. Neural spine, 2. Transverse process, 3. Centrum, 4. Mammillary process or metapophysis, 5. Postzygapophysis. 6. Prezygapophysis.

Intervertebral joints

Each vertebra articulates with its neighbor via an intervertebral joint, and these three structures together form a single motion segment (Denoix, 1999). The intervertebral joint consists of a single fibrocartilagenous disc connecting adjacent centra, together with paired synovial zygapophyses, connecting the arches via articular processes. The disc consists of concentric annulus fibrosus and a central nucleus pulposus. Although this joint is usually flat in mammals, in some ungulates it is slightly

convex cranially, a condition known as **opisthocoely**. These three joint features together - the disc and paired zygapophyses - will be referred to as the **intervertebral joint complex**. Four main types of motion are possible at intervertebral joints: dorsiflexion (extension), ventroflexion (flexion), lateroflexion (lateral bending) and torsion (axial rotation).

Variation in the morphology of the zygapophyseal joints is illustrated in Figure 1.1.2. The zygapophyseal joints are **horizontal** in the pre-diaphragmatic region. However, in the post-diaphragmatic region, they vary greatly in morphology and function (Townsend and Leach, 1984; Filler, 1986; Schendel et al., 1993; Pal and Routal, 1999; Boszczyk et al., 2001; Russo, 2010). There is little consensus in the literature about the proper nomenclature for these different joints, so I have defined some of the types encountered in this dissertation. In carnivores the post-diaphragmatic zygapophyses are quite **flat**. The post-zygapophyseal facet faces lateroventrally and is usually slightly convex. In contrast, artiodactyls have highly curved post-diaphragmatic zygapophyses. These **revolute** zygapophyses have a post-zygapophyseal facet with continuous dorsal-, lateral- and ventral-facing surfaces, which together form a curved c-shape (Osborn, 1900; Zhou et al., 1992; Bebej et al., 2012). These have variously been referred to as embracing, encompassing, enveloping, cylinder-interlocking and interlocking hemi-cylindrical (Slijper, 1946; Filler, 1986; Hildebrand, 1995; Boszczyk et al., 2001; Wood et al., 2011). In some cases these processes may be further expanded with an additional dorsal curvature, forming an s-shaped post-zygapophysis. Both these morphologies have been referred to as revolute, but here I differentiate the more complex s-shaped morphology using the new term: **sigmoid-revolute.** In contrast,

perissodactyls have interlocking post-diaphragmatic zygapophyses of a different nature. In this case there may be two articular facets on the post-zygapophysis. One facet faces lateroventrally (similar to the flat joint), but another is developed which faces medioventrally, forming a j-shape in transverse section. Further, the medioventral surface is pitched, such that in lateral view its long axis is inclined slightly dorsally. This produces an opposing planar surface which prevents dorsiflexion (Filler, 1986). This morphology will be referred to as **pitched interlocking** zygapophyses. In addition to the zygapophyses, perissodactyls have additional synovial joints between adjacent sets of transverse processes. These **lateral joints** form on the last two or three presacral joints and are frequently fused in *Equus caballus* (Townsend and Leach, 1984).

	Schematic	**Caudal**	**Cranial**

a. Horizontal

Equus caballus

b. Flat

Panthera leo

c. Revolute

Gazella spekei

d. Sigmoid-revolute

Bison bison

e. Pitched-interlocking

Equus caballus
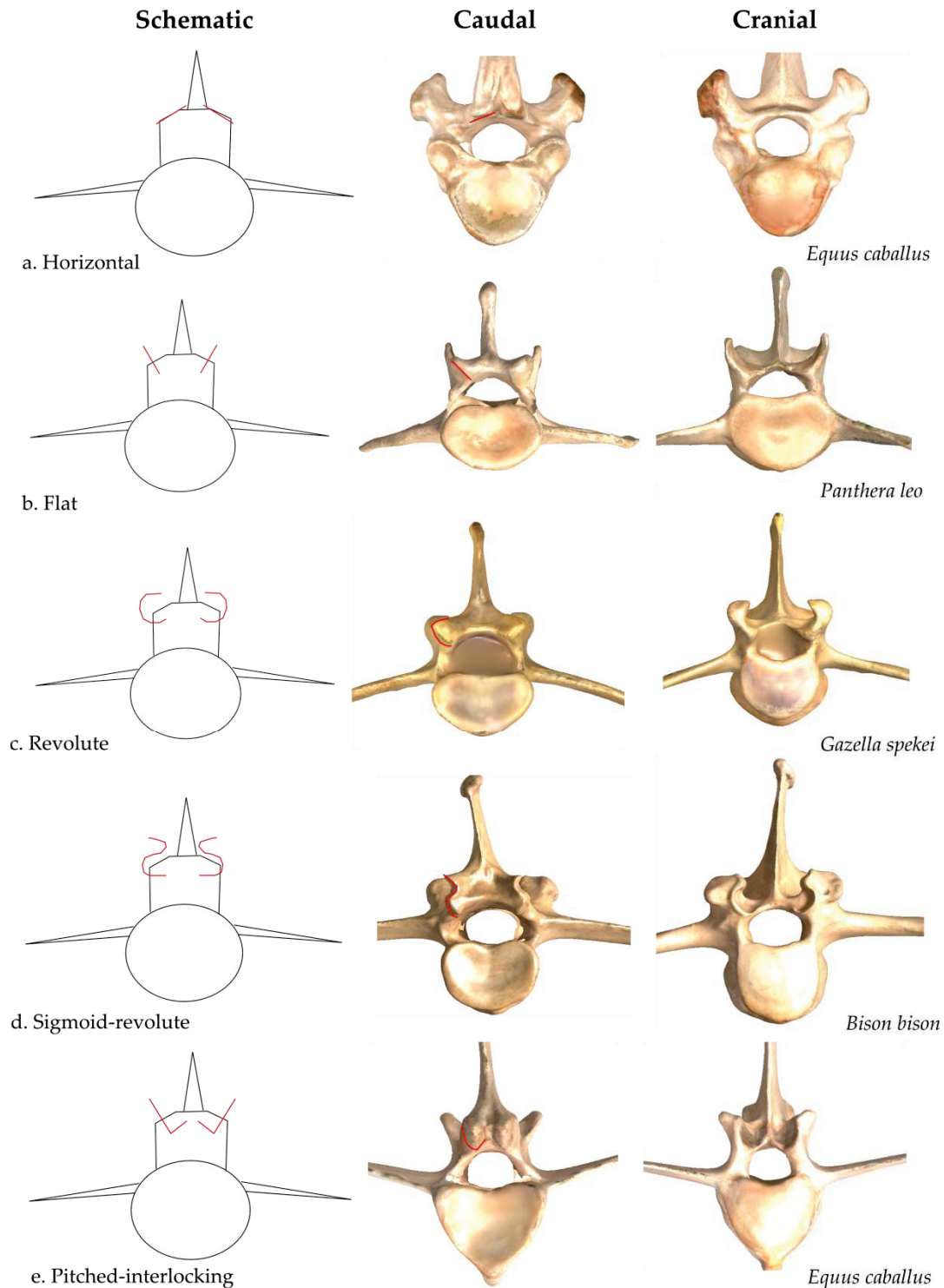
Figure 1.1.2 Variation in zygapophyseal morphology.

Schematics on the left show outline of postzygapophyses from caudal view in red.
Example taxa are shown in cranial and caudal view. Horizontal zygapophyses (a) are
typical in the pre-diaphragmatic region, whereas the other classifications are variants of
post-diaphragmatic zygapophyseal morphology.

Soft-tissues

In the thoracolumbar region, muscles play an important role in both stabilizing and mobilizing the column (Heylings, 1980; Gál, 1993; Macpherson and Fung, 1998; Schilling, 2011). The dorsal **epaxial muscles** form a long column running between sacrum and cervical region, dorsal and lateral to the arch (Figure 1.1.3). The major extensors are mm. longissimus dorsi and iliocostalis thoracis et lumborum, which originate on the sacrum. They insert segmentally along the thoracolumbar column into the neural spines, laminae or anapophyses (longissimus), and transverse processes and ribs (iliocostalis), as well as into the lumbodorsal fascia and lumbar intermuscular septum (Bogduk, 1980). Deeper transversospinalis muscles, such as multifidus, play an important role in stabilization of the vertebral column. They span one to four motion segments (Schilling, 2009) (Figure 1.3C). The **hypaxial** muscles (mm. quadratus lumborum, psoas major and psoas minor), which are located ventral to the vertebrae, and abdominal muscles are the primary flexors of the vertebral column. Unilateral contraction of the paraxials (muscles surrounding the vertebral column) or appendicular movements cause lateral flexion (Slijper, 1946; English, 1980; Schilling and Carrier, 2010) (Figure 1.1.3).

Fibroelastic ligaments play a vital role in stabilizing the thoracolumbar column (Alexander et al., 1985; Gál, 1993; Hukins and Meakin, 2000) (Figure 1.1.4). Ventrally, the ventral longitudinal ligament which runs from centrum to centrum resists extension. Dorsally, the supraspinous and interspinous ligaments, articular ligaments, ligamenta flava and dorsal longitudinal ligaments all resist excessive flexion (Denoix, 1999; Rawls and Fisher, 2010). Lateral flexion is resisted by intertransverse ligaments.

A. Paraxial muscles

Epaxials

Gluteals

Hypaxials

Abdominals

B. Erector spinae

Ilium

Longissimus lumborum et thoracis

Spinalis

T1

T14

Iliocostalis

Lumbar intermuscular septum

C. Transversospinalis

Interspinales

Multifidus

Intertransversarii medialis

Quadratus lumborum

Psoas major
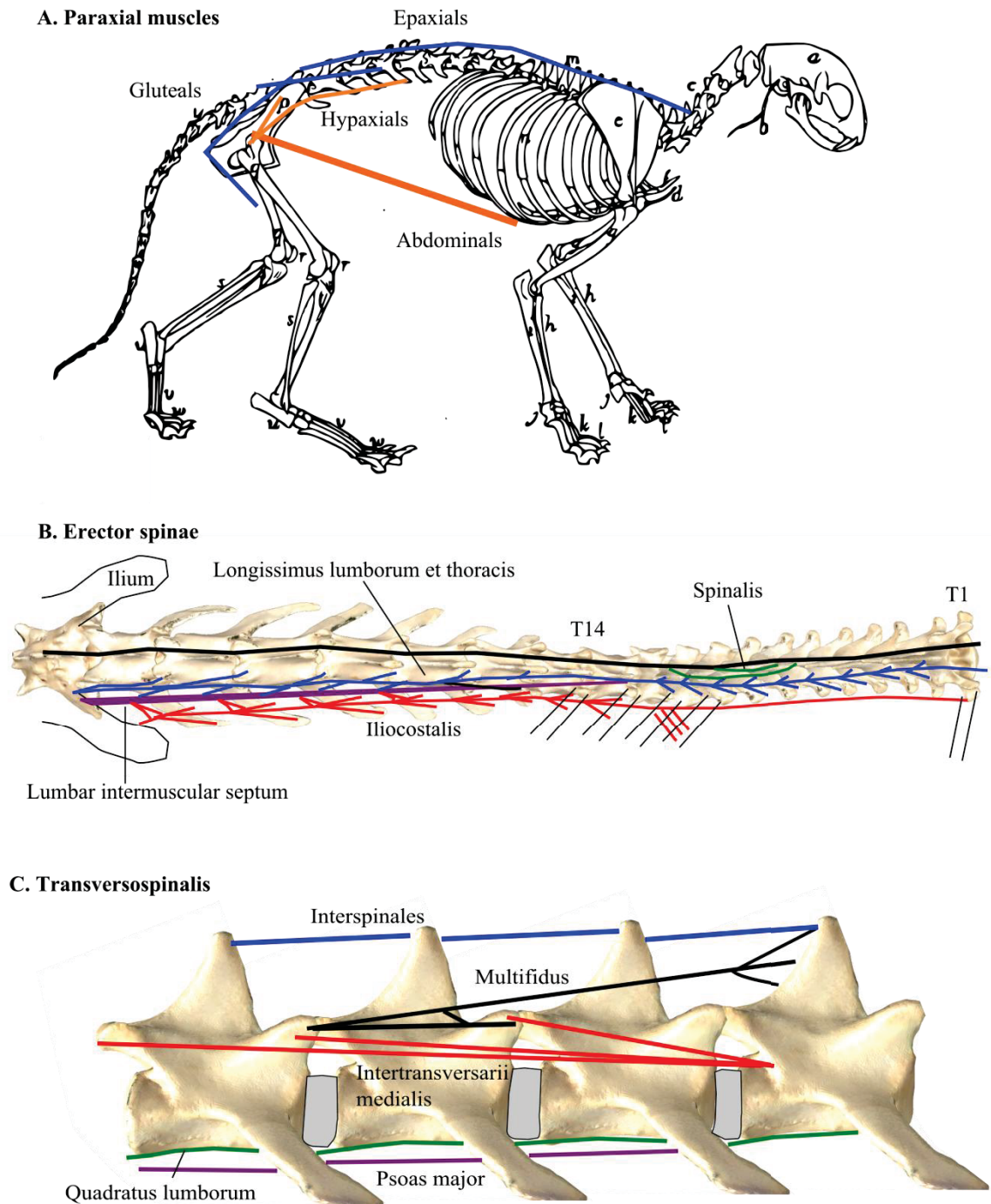
Figure 1.1.3 Muscles of the axial skeleton.
Nomenclature following Boduk (1980). A. Cat skeleton traced from Reighard and Jennings (1901), showing major muscle groupings. B. thoracolumbar column of Felis catus *with muscles represented on right side. C. Transversospinalis sketched onto lumbar vertebrae of* Acinonyx jubatus.
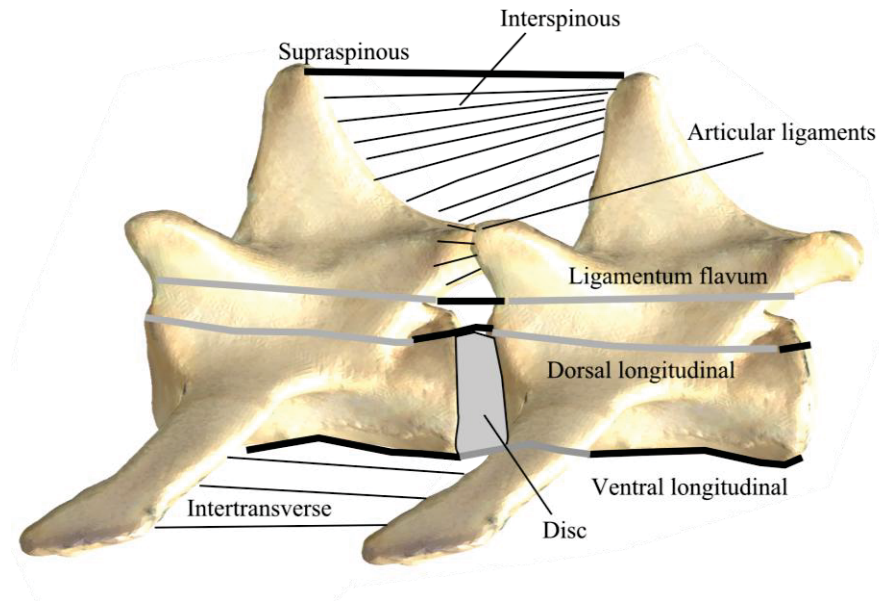
Figure 1.1.4 Intervertebral ligaments.
Demonstrated on lumbar vertebra of Acinonyx jubatus*, based on Miller's Anatomy of the Dog (Evans, 1993).*

Anatomical planes

In a quadrupedal mammal, anatomical planes of the vertebral column are defined as shown in Figure 1.1.5. The **sagittal plane** runs vertically and craniocaudally, passing through the plane of symmetry of the vertebra at the midline. The neural spine is positioned in the sagittal plane. The **transverse plane** runs mediolaterally, perpendicular to the long axis of the vertebral column. The **dorsal plane,** also known as the frontal plane, runs craniocaudally but at 90º to the sagittal plane, such that it separates dorsal from ventral (Sisson, 1975c; Evans, 1993). The transverse processes may be positioned in, or close to, the dorsal plane. When discussing features of the vertebral column, **length** refers to the craniocaudal dimension (long versus short), **width** to the mediolateral dimension (wide versus narrow) and **height** to the dorsoventral dimension (tall versus compressed). The terms cranial and anterior, and

caudal and posterior, will be used interchangeably, so that confusion with the caudal

vertebrae can be avoided.
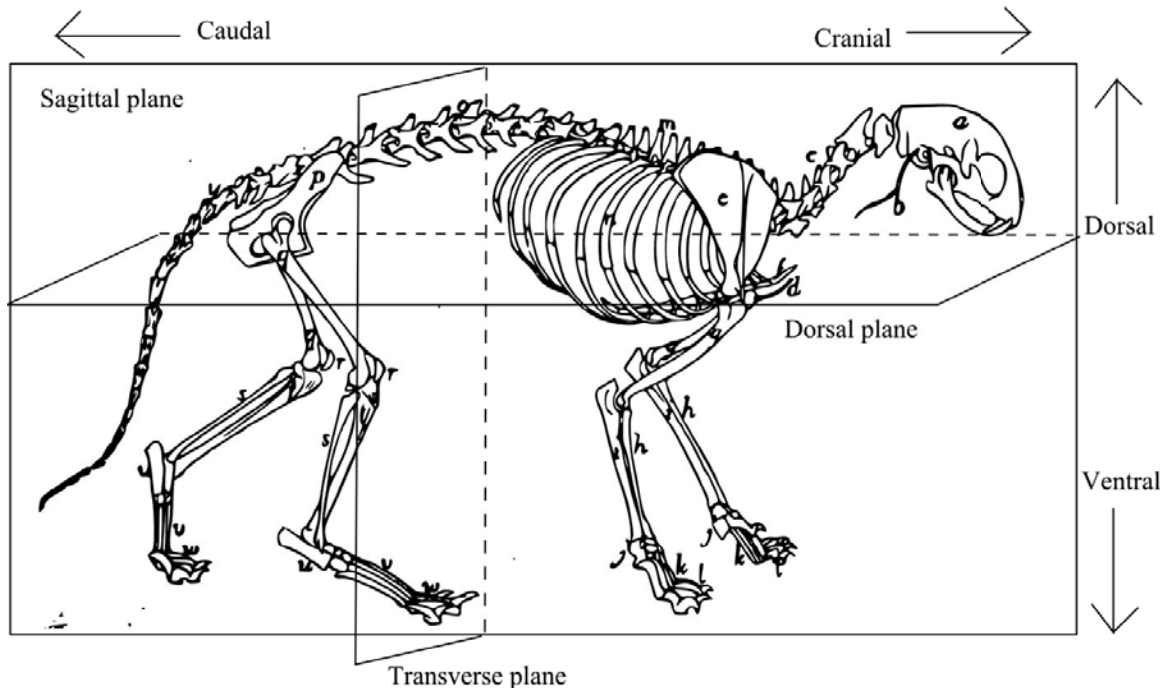
Figure 1.1.5 The anatomical planes.
Following Miller's Anatomy of the Dog, using cat skeleton traced from Reighard and Jennings (1901) (Evans, 1993).

1.1.2 MAMMALIAN GAITS

During quadrupedal locomotion, gait is defined by the sequence and timing of

the movement of the limbs. A single step of a limb consists of four parts (Gambaryan,

1974). **Touch down** occurs when the limb first makes contact with the ground. **Stance**

phase is when the limb is in contact with the ground and the body swings over the

planted limb with an inverse pendulum action. **Lift off** is the end of the stance phase

and **swing phase** is when the limb is lifted so that it may be placed in a more forward

position ready for the next step.

Symmetric gaits

During a **symmetric gait** the left and right limb pairs are evenly spaced in time, such that their footfalls are mirror images of one another (Gambaryan, 1974; Hildebrand, 1995). Examples of symmetric gaits are the **walk** and the **trot**, and may employ either lateral (same side) or diagonal footfall sequences. These slower gaits primarily use lateral bending of the vertebral column, with little vertical oscillation in the center of mass. As an animal's speed increases, the **duty factor**, or the percentage time of the gait cycle each limb spends on the ground, is reduced.

Asymmetric gaits

To reach the highest speeds, quadrupedal mammals usually switch from symmetric to asymmetric gaits. During **asymmetric gaits** the footfalls of left and right sides are unevenly spaced in time (Gambaryan, 1974; Hildebrand, 1995). The **trailing limb** is the first of the right-left pair to touch the ground, whereas the other is the **leading limb**. Duty factors are further reduced at high speed by introduction of a **flight (aerial) phase,** in which none of the limbs is in contact with the ground. An **extended flight** phase arises between hind limb lift off and forelimb touch-down, when both limbs are outstretched. A **gathered flight** phase occurs between fore limb lift off and hind limb touch-down when the limbs are gathered beneath the body. During a **gallop**, left and right sides are offset in the cycle. Different types of gallop are illustrated in Figure 1.1.6. If the leading limb is on the same side for both fore and hind limbs, it is a **transverse gallop**. In contrast, if the leading limb is different it is a **rotary gallop**. These gaits can also be distinguished based on which limb pair (fore or hind) is responsible for transitioning movement of the center of mass from a downward to an

upward direction (Bertram and Gutmann, 2009); (Figure 1.1.6). A **hind limb-initiated**

transition, usually associated with gathered flight, is common to the transverse gallop.

In contrast, a **forelimb-initiated transition** is often, but not always, associated with the

rotary gallop. In this gait the extended flight phase is usually longer, but both may be

present. Some taxa only use a hind limb-initiated (e.g., horses) or a forelimb-initiated

(e.g., cats) transition. In contrast, others (e.g., dogs) shift from hind limb- to forelimb-

initiated transitions at greater speed (Hildebrand, 1959; Bertram and Gutmann, 2009).

During the **bound** or **half-bound,** left and right sides of one or both sets of limbs move

in unison (Figure 1.1.7). Sagittal movements of the spine are conspicuous during

asymmetric gaits. Figure 1.1.7 shows radiographs of a pika half-bounding and

illustrates the importance of sagittal spinal movements to some asymmetric gaits

(Schilling and Hackert, 2006). As the pika launches with its hind limbs the vertebral

column extends, increasing its stride length considerably. When the forefeet land the

vertebral column flexes, allowing the hind feet to plant at a more advanced position

ready for the next gait cycle.

A. Horse
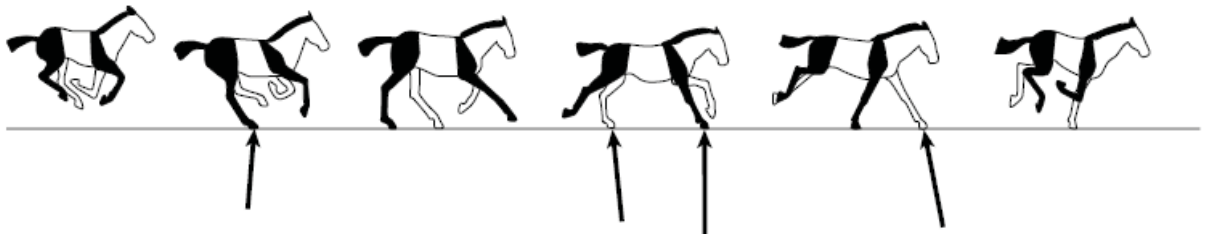
B. Cheetah
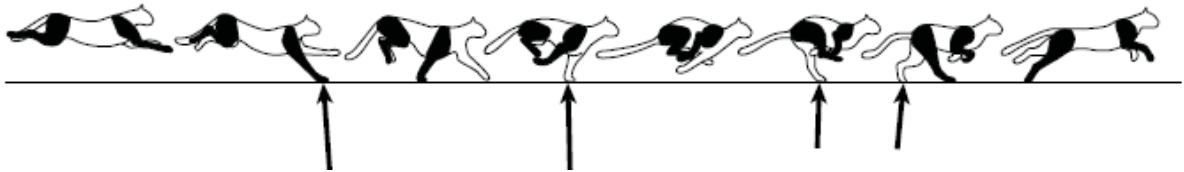
C. Dog
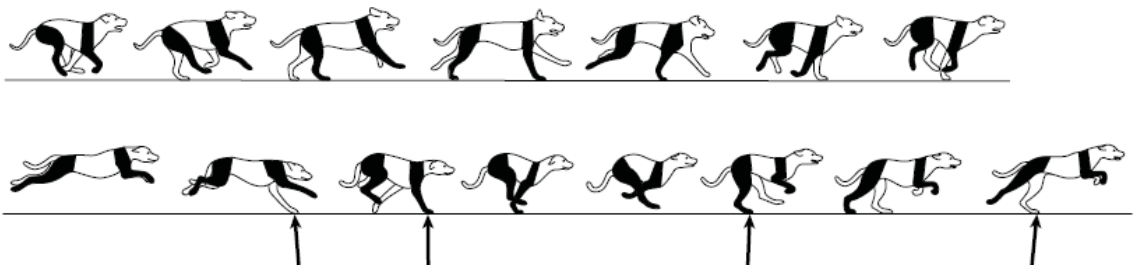
D. Rabbit
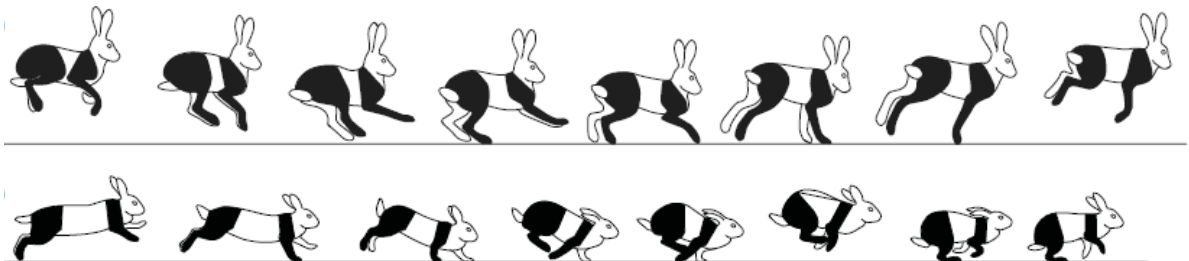
Figure 1.1.6 Footfall sequences and center of mass transitions in galloping gaits.
From Bertram and Guttman (2009). Dark limb: right side, white limb: left side. Arrows
indicate the net force vector applied by each limb. A. Equine transverse gallop with hind
limb-initiated transition. B. Rotary gallop in the cheetah with forelimb-initiated
transition. C. Dog using hind limb-initiated gallop (upper) and forelimb-initiate gallop
(lower), but using the rotary footfall pattern for both. D. Domestic rabbit using the hind
limb-initiated half-bound at slow speeds (upper) and forelimb-initiated half-bound at
high speeds (lower).

Touch-down ... **Lift-off**

1. 2. 3. 4.
5. 6. 7. 8.
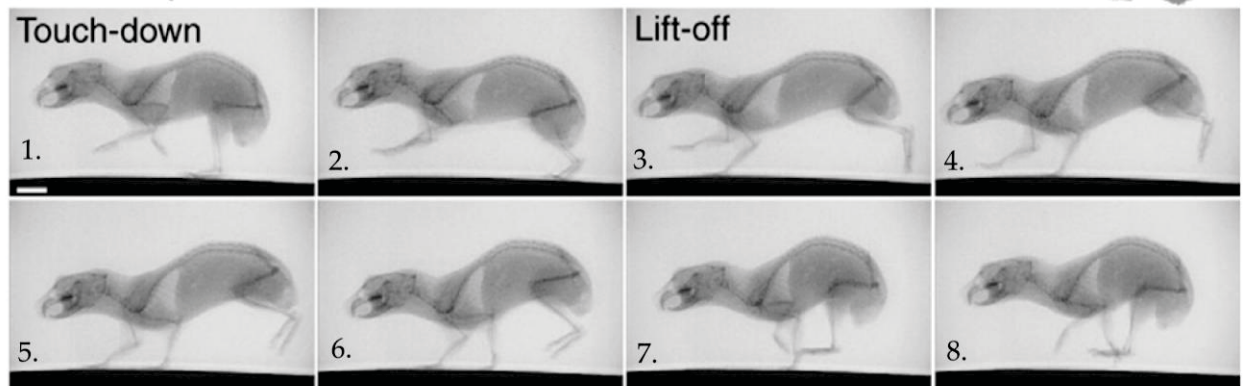
Figure 1.1.7 Spinal movements of the half-bounding pika, **Ochotona rufescens.**
From Schilling and Hackert (2005: fig. 1). Frames 1-3 depict hind limb stance phase, 4-8 depict hind limb swing phase, 3-7 depict forelimb stance phase, 8 shows gathered flight phase, between 2 and 3 is a short extended flight phase. Note the large pelvic displacements due to sagittal bending in the lumbar region.

Locomotor-respiratory coupling

The asymmetric gaits described above are unique to mammals, with the exception of crocodiles (Molnar et al., 2014). In contrast, almost all non-mammalian tetrapods use primarily symmetric gaits. The lateral trunk undulations of symmetric gaits in non-mammalian tetrapods impose a restriction on breathing, known as Carrier's constraint. During locomotion stale air is shifted from lung-to-lung by the lateral compression of each lung in turn (Figure 1.1.8); (Bramble and Carrier, 1983; Carrier, 1987; Bramble and Jenkins, 1993). This prevents running and breathing at the same time. In contrast, mammals use **locomotor-respiratory coupling** to run and breathe at the same time during asymmetric gaits. This locks lung ventilation in time with each stride. Sagittal motions of the spine assist in locomotor-respiratory coupling by changing intra-abdominal pressure, which helps ventilate the lungs via pressure on the

diaphragm (Figure 1.1.8) (Carrier, 1987; Bramble, 1989; Reilly and White, 2009). In addition, anteroposterior movements of the viscera during locomotion act like a piston, driving ventilation. Thus, by coupling asymmetric gaits with breathing, mammals achieve greater endurance for extended periods of running.
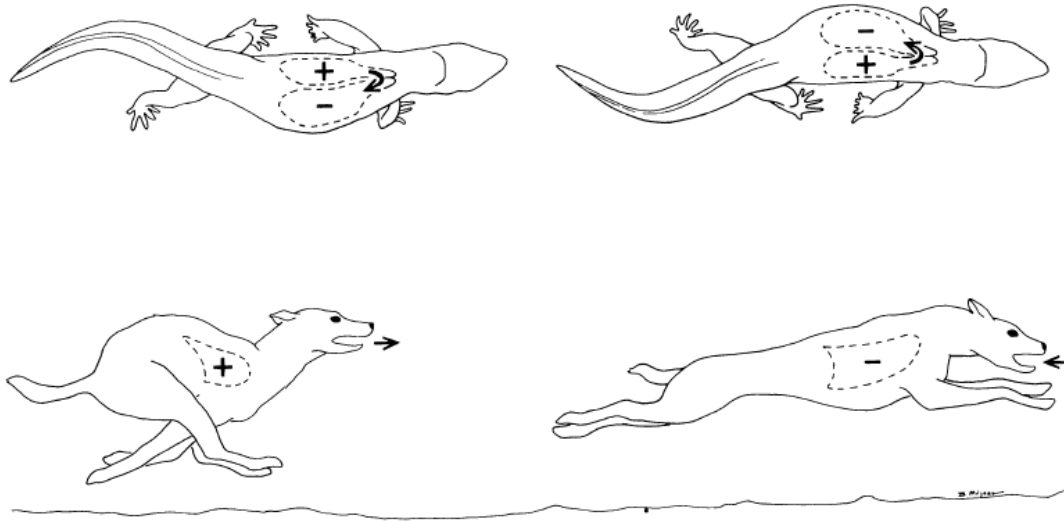
Figure 1.1.8 Reptilian versus mammalian locomotion.
From Carrier (1987: fig. 3). Lateral undulations in reptiles restrict breathing during locomotion, whereas sagittal bending of the spine during running in mammals assists with locomotor respiratory coupling. Negative pressure causes inhalation while positive pressure causes exhalation.

1.2   PREVIOUS RESEARCH

1.2.1   VERTEBRAL FUNCTION AND MORPHOLOGY

Static support in the thoracolumbar region

The thoracolumbar column plays a central role in mechanical support of the trunk. In quadrupedal mammals, body weight is supported via two sets of supporting columns, the fore- and hind limbs. The center of mass is located at a point between these two columns which depends on weight distribution between them. If one envisions the thoracolumbar region as a beam spanning the two columns, the bending moments at each point along the vertebral column may be calculated (Smit, 2002) (Figure 1.2.1). There is a ventroflexion moment around the forelimb associated with the ground reaction force and a dorsiflexion moment due to sagging at the midpoint. Various mechanical models have been proposed to explain how the vertebral column and other trunk structures, act to dissipate these loadings.
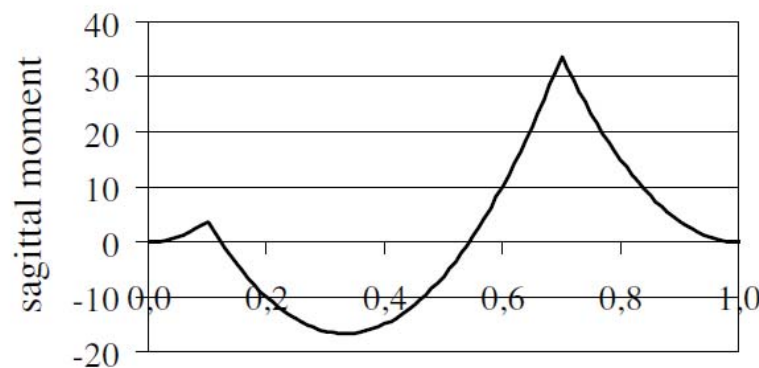
Figure 1.2.1 Bending moments on the vertebral column.
From Smit (2002), calculated based on a sheep of 750N supported by limbs 0.6m apart. X axis represents distance from tail (0m) to head (1m), limbs are at 0.1m (hind limb) and 0.7m (forelimb). Y axis is bending moment in newton meters. Note the strong dorsiflexion moment (negative scores) at the mid-trunk and the ventroflexion moment (positive scores) over the forelimb.

In 1917, D'Arcy Thompson proposed that the vertebral column was best modeled as an inverted parabolic cantilever bridge. In this model the limbs represented supporting columns, the vertebral bodies the lower pressure-element girder, the supraspinous ligament the upper tension-element girder and the neural spines as the converging diagonals, forming their characteristic anticlinal pattern (Figure 1.2.2) (Thompson, 1917). However, Slijper (1946) argued that the tail would not provide a sufficient counterweight in most mammals to support it. Instead he proposed a bow-string model. In this model the thoracolumbar column forms the bow and the abdominal muscles and sternum form the string, resulting in a primarily compressive loading on the vertebrae (Slijper, 1946) (Figure 1.2.2). Though experimental data on axial function during standing are rare, Macpherson and Ye (1998) used a combination of ground reaction forces and electromyographic data to address support of the trunk in the standing cat. They demonstrated complex vertebral curvatures in the standing cat: a strong dorsiflexed curve in the upper thoracic region and a ventroflexed curve in the lower thoracics and upper lumbars. They proposed that the dorsiflexion moment in the lumbar region is resisted by contraction of the lumbar hypaxial muscles, and not by the abdominal muscles, in contrast to the bow-string model. In the upper thoracic region, the ventroflexion moment is resisted by the scapula in the manner of a suspension bridge (Macpherson and Ye, 1998). Specifically mm. levator scapulae, serratus ventralis and the rhomboids suspend the thoracic column from the anterior pillar via the scapula. This interpretation is supported by data showing tonic activation of these muscles during quiet stance.

Fig. 5.
Inverted parabolic cantilever-bridge (Forth-bridge) which, after the opinion of THOMPSON (1917, 1942), might be compared to the vertebral column of mammals.
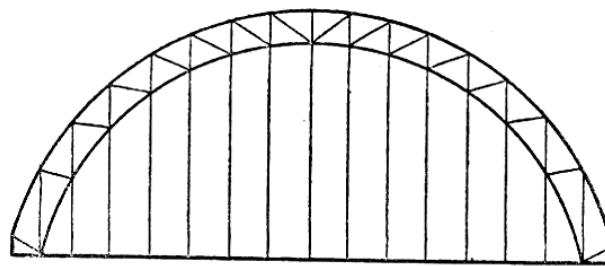
Fig. 9.
Schematic drawing of a parabolic bowstring-bridge with a bow constructed as a web (bridge at Katerveer).

Figure 1.2.2 Bridge models of the vertebral column.
From Slijper (1943: figs. 5 and 9). In his figure 5, arrows indicate the support limbs and the lower pressure element represents the ventral column, whereas the upper tension element represents the supraspinous ligament. In his figure 9, the bowstring, the upper unit represents the thoracolumbar vertebral column, whereas the lower string represents the abdominal muscles.

Kinematics of the thoracolumbar region during running

The function of the thoracolumbar column is two-fold: support and mobility. However, the kinematics of the thoracolumbar region in quadrupedal mammals are less well understood than limb kinematics, because the vertebral column is so complex in terms of its anatomy and number of moving parts (Schilling, 2011). During running, motions of the vertebral column may fulfill a range of functions. These include

22

increasing stride length, controlling vertical oscillations in center of mass, storage of

elastic energy or lung ventilation (Hildebrand, 1959; Alexander et al., 1985; Carrier,

1987; Koob and Long, 2000; Schilling and Carrier, 2010).

In vivo kinematic experiments can shed light on the movements of the vertebral

column in running mammals. Early work in this field used motion pictures to estimate

vertebral bending by observing the external anatomy. This technique was first

employed by Eadweard Muybridge (1899), who used then state-of-the-art instant

photography techniques to produce still frames of animals running. This allowed, for

the first time, detailed analysis of gait to be conducted. Interest in the specific role of

the vertebral column did not come until later. Howell (1944) pointed out that sagittal

bending of the vertebral column may increase stride length in some animals and that it

is used more in a whippet than a horse (Howell, 1944). He posited that size, relative

limb length and a heavy head were potential causative factors for lumbar stability.

Smith and Savage (1956) used Muybridge's images to investigate the contrast between

the "leaping gallop" and "horse gallop," now known as the rotary and transverse gallop

respectively (Smith and Savage, 1956). They noted that the former is characterized by

high sagittal mobility, whereas the latter is characterized by low sagittal mobility,

except at the lumbosacral joint. They also suggested that the 'horse gallop' may be

more advantageous in large animals, due to the increased costs of vertical oscillations

in center of mass associated with the "leaping gallop."

Hildebrand (1959) used slow-motion videography from Walt Disney to compare

running in the cheetah and horse. He noted that the change in angle of the pelvis

relative to the scapula during galloping was around 130º in the cheetah but only 60º in

the horse, of which 20º is due to scapular rotation in both cases (Hildebrand, 1959). The additional 70º of motion in the cheetah was achieved by sagittal bending of the vertebral column. He proposed that flexion of the spine increased both the length and the speed of the stride. English (1980) combined videography with electromyographic (EMG) data to examine the role of the lumbar spine in the stepping cat. Data suggested that the epaxial muscles serve mostly to stabilize the column during symmetric gaits, whereas they contribute to step length via flexion and extension during half-bounding and galloping (English, 1980). Bertram and Gutman (2009) suggested a modification of the definition of the transverse and rotary gallops to focus on dynamics instead of footfall patterns. They proposed the forelimb- versus hind limb-initiated transition from downward to upward trajectory of the center of mass, as a more mechanically appropriate definition of these gallop types. The authors dubbed these running modes 'flexed backed' and 'stiff backed' respectively, due to the increased role of thoracolumbar bending in the forelimb-initiated gallop (Bertram and Gutmann, 2009).

Cineradiographic studies have provided data on movements of individual bones and joints during *in vivo* locomotion. Pridmore (1992) used radiographs of *Monodelphis* to measure overall vertebral motions during walking, trotting and half-bounding. He noted lateral-bending during walks and trots but sagittal-bending during half-bounds (Pridmore, 1992). Schilling and Hackert (2006) expanded on this work by examining sagittal movements at individual intervertebral joints in five mammalian species during bounding or galloping (Schilling and Hackert, 2006). They found that across diverse mammal species the last seven (plus or minus one) presacral joints contributed to the total pelvic displacement in the sagittal plane during asymmetric

gaits, irrespective of thoracic or lumbar identity (Figure 1.1.7). Amplitudes of motion

increased caudally, and were related to caudal increases in glycolytic fiber composition

of paraxial muscles. Precise *in vivo* vertebral rotations in the horse were measured by

placing pins into the neural spines at several locations and recording their 3D

movements using cameras. Low levels of flexion and extension occurred during

walking and trotting but greater amplitudes were measured during canter (Haussler et

al., 2001), though overall amplitudes were lower than in the small-mammal study. This

finding is supported by anatomical and muscle activation data, which suggest that the

longissimus dorsi of the horse primarily acts to stiffen the back, and does not produce

sagittal bending (Ritruechai, 2009). Sagittal motions during canter were greatest at the

lumbosacral joint and were correlated with running speed (Faber et al., 2001a; Faber et

al., 2001b).

Morphological features associated with function

Various morphological features of the vertebrae have been linked to function

using comparative anatomy. Slijper (1946) implicated variations in morphology of the

epaxial musculature and processes in determining vertebral function. Specifically, he

suggested that neural spines develop perpendicular to the direction of muscle force

acting upon them by either multifidus (in carnivores and primates) or spinalis and

longissimus (monotremes, marsupials, edentates and rodents) or a combination thereof.

Thus highly inclined neural spines reflected strong action of epaxial extensors (Slijper,

1946). Boszczyk et al. (2001) examined variation in intervertebral joint morphology in

mammals and concluded that increased dimensions of the centrum reflected resistance

to flexion in that plane, whereas wide zygapophyses resisted torsion. Those workers

also proposed that horizontal zygapophyses may resist ventral shear whereas revolute zygapophyses might resist dorsal shear (Boszczyk et al., 2001). In contrast, Filler (1986) implicated sigmoid-revolute zygapophyses as a method of resisting dorsiflexion. He suggested they reflect transmission of load through the arch structures, dubbing it 'dorsal element compression'(Filler, 1986). In other species, he proposed that the transverse processes and tension in the intertransverse ligaments restricted dorsiflexion. Generally, revolute or sigmoid-revolute zygapophyses are thought to resist torsion or increase the stiffness of the lumbar region (Slijper, 1946; Gambaryan, 1974; Hildebrand, 1995), though little empirical data on their function exists.

The relationship between form and function in the vertebral column can be tested using bending experiments on *ex vivo* excised vertebral columns. Gál (1993a, b) examined sagittal motion and stiffness of lumbar joints in several mammalian species, before and after lesion of key vertebral structures. There was considerable range in the extent of sagittal mobility across mammal taxa. The lowest mobility was found in a primate (*Macaca fascicularis*) and the highest mobility was found in the semi-aquatic seal (*Phoca vitulina*). Impaction of the zygapophyses restricted dorsiflexion in all taxa, in spite of their varying morphology. In contrast, ventroflexion was restricted by both intervertebral discs and the ligamenta flava, depending on the taxon. Long et al. (1997) performed a similar study on the saddleback dolphin. They found that the interspinous ligaments contributed to the sagittal stiffness of vertebral joints (Long et al., 1997). Comparison of a rabbit and goat revealed that flexural stiffness was much greater in the sagittal plane in the goat (Smeathers, 1981). Increased flexibility in the rabbit was attributed to increased space between the muscular processes, ligaments with lower

strains, flat rather than revolute zygapophyses, pinnate arrangement of paraxial muscle fibers, inclined transverse processes, arched back and enlarged volume of paraxial muscles. In horses, range of motion in the sagittal plane varies strongly along the column. Specifically, large sagittal motions are restricted to the first thoracic and lumbosacral joints (Jeffcott and Dalin, 1980; Townsend et al., 1983; Wilke et al., 1997a; Denoix, 1999). In the thoracolumbar region of horses, dorsiflexion is limited primarily by the zygapophyses and the ventral longitudinal ligament, whereas ventroflexion is restricted by a tall, broad neural spine and strong interspinous ligaments (Townsend and Leach, 1984; Denoix, 1999). Lateroflexion and torsion are restricted by the zygapophyses, transverse processes and lateral joints. *Ex vivo* joint stiffness was correlated with centrum width and height, neural spine angle and lamina width in Nile crocodiles (Molnar et al., 2014). There was relatively high sagittal stiffness compared to the lumbar regions of mammals, despite the fact that both employ asymmetric gaits.

Examining correlations between locomotor behavior and vertebral morphology can shed light on vertebral functional morphology. There is a strong link between axial morphology and arboreal locomotion, and there are two main morpho-functional types. Arboreal taxa that emphasize leaping and running, whilst maintaining pronograde postures, have highly mobile thoracolumbar regions (Hurov, 1987; Shapiro, 1993, 1995; Johnson and Shapiro, 1998; Argot, 2003; Russo, 2010). This has been linked with longer lumbar regions, dorsoventrally compressed centra, inclination of the transverse processes and development of anapophyses. In contrast, climbing that involves bridging, suspensory movement or orthograde clinging and leaping is

associated with a more rigid lumbar region (Jenkins, 1970). These behaviors are associated with wide, straight neural spines and shorter lumbar regions (Shapiro, 1993; Shapiro and Simons, 2002; Chen et al., 2005; Shapiro et al., 2005). The evolution of bipedalism in hominoids is associated with further stiffening of the spine, with features including reduced lumbar count, caudal placement of the diaphragmatic vertebra, lumbar wedging, increasing zygapophyseal width and increased endplate area (Ward and Latimer, 1993; Sanders, 1998; Chen et al., 2005; Russo, 2010; Williams, 2012a, b). Rigidity has also been linked to digging behaviors in quadrupedal mammals, and in particular the evolution of accessory xenarthrous articulations in some species (Jenkins, 1970; Gaudin and Biewener, 1992). In contrast, subterranean locomotion in tunnels has been linked to long trunks with well developed stabilizing muscles in ferrets (Moritz et al., 2007a, b). Vertebral movements are also extremely important in aquatic locomotion, though adaptations vary depending on the relative importance of hind limb versus forelimb in producing thrust (Gingerich et al., 1994; Long et al., 1997; Buchholtz, 2001; Pierce et al., 2011; Bebej et al., 2012). The axial skeleton also forms a major propulsive organ for quadrupedal jumping (Hatt, 1932; Harty, 2010).

Gallop type has been related to morphological and ecological variables. Morphometric analysis suggests that rotary gallopers, as defined by footfall pattern, have a lower height:body length ratio and lower body masses. This suggests that slower, larger animals with relatively longer and thicker limbs tend to employ transverse gallops (Biancardi and Minetti, 2013). Further, rotary galloping is associated with more closed or variable terrains, or species that emphasize maneuverability, whereas transverse galloping is associated with open habitats. Running has also been

associated with variability in presacral vertebral count via developmental constraints (Galis et al., 2014). Specifically, presacral count changes are hypothesized to cause an increased likelihood of developmental anomalies at the lumbosacral transition, such as asymmetric fusion of lumbars. In turn, these anomalies may hinder flexion at the lumbosacral joint which is important during running. Therefore, both inter- and intra-specific variation in presacral count were hypothesized to be limited via pleiotropy with running function. Galis et al. (2014) presented increased variability of presacral count in mammals classified as slow moving in support of this idea.

Linking form and function in running mammals

Combining the above data from anatomical comparisons, bending experiments and *in vivo* kinematics produces a coherent picture of the role of the vertebral column in quadrupedal running. Sagittal flexion and extension in the lumbar region (i.e., ventroflexion and dorsiflexion) to increase stride length are motions that are particularly associated with rotary, forelimb-initiated galloping (Slijper, 1946; Hildebrand, 1959; Smeathers, 1981; Hildebrand, 1995; Schilling and Hackert, 2006). The degree of sagittal flexibility may be reflected in the morphology of the vertebral column. Based on previous studies, a joint with high mobility should have a dorsoventrally compressed centrum, vertical, flat zygapophyses, short neural spine, elastic spinous and ventral longitudinal ligaments, and strongly inclined processes (Slijper, 1946; Smeathers, 1981; Gál, 1993; Shapiro, 1993; Boszczyk et al., 2001). In contrast, stable joints should have a dorsoventrally tall centrum, with a strong keel for the ventral longitudinal ligament, tall neural spine, revolute zygapophyses, and wide, horizontal and robust transverse processes (Slijper, 1946; Smeathers, 1981; Townsend

and Leach, 1984; Filler, 1986; Gál, 1993; Shapiro, 1993; Denoix, 1999; Boszczyk et al., 2001).

1.2.2   ALLOMETRY OF THE POSTCRANIAL SKELETON

Scaling in biology

Life exists on an extraordinary array of scales and the importance of size in shaping anatomy and physiology has long been appreciated (Thompson, 1917; Huxley, 1932). Allometry is defined as the change in the characteristics of an organism that is associated with a change in its size (Brown et al., 2000). Early workers such as D'Arcy Thompson and Julian Huxley realized that certain physical and mathematical principles which govern the function of organisms change with size. Therefore, similar organisms at different scales might have inherently different functions. Consequently, some biological traits must vary with size to maintain constant function, a concept known as self-similarity (Schmidt-Nielsen, 1984). The relationship of features with size can be described using an allometric or power-law equation as shown below:

$$\text{Log } Y = b \text{ Log } M + Y_o$$

In which Y is the biological parameter, M is a size variable, usually mass, Y_o is the y-intercept and b is the scaling co-efficient. The null hypothesis of scaling is generally that of **geometric similarity** (GS, a form of isometry), which preserves constant shape with increasing size. Under this model a linear dimension will have the exponent b=0.33, whereas an area would have b=0.66, when compared to body mass (Schmidt-Nielsen, 1984; Brown et al., 2000) (Figure 1.2.3). However, in the postcranial skeleton many parameters vary significantly from this null expectation of geometric similarity, as outlined below.

Allometry of the limbs in quadrupeds

The limbs must safely support body mass and withstand stresses generated during locomotion (Gambaryan, 1974). However, as size increases limbs must adapt to the increased mechanical loading from both of these functions. In 1973, McMahon proposed a model to explain the scaling of beam-like elements in biology, including mammal limbs, which he named the **elastic similarity** (ES) model. This model states that elongate elements (in which length is at least 25 times greater than diameter) may be subject to Euler bucking forces which are proportional to their length (McMahon, 1973). Thus, to limit elastic deformations to a similar magnitude, a longer beam must have a relatively larger diameter. Specifically, he calculated that length should scale with diameter as b=2/3, and each scales with mass by b=0.25 (length) and b=0.375 (diameter) respectively (Figure 1.2.3). Early studies found support for elastic similarity in the scaling of the limb bones of bovids (McMahon, 1975a, b; Alexander, 1977). However, later work suggested that elastic similarity was likely a peculiar characteristic of bovids only, and that geometric similarity was much more typical for limb scaling (Alexander et al., 1979; Bertram and Biewener, 1990). When more limb dimensions were measured, Scott (1985) showed that although many limb lengths scaled negatively in bovids, not all matched elastic similarity (Scott, 1985). Campione et al. found elastic scaling only in humeral circumference of bovids, a pattern which was shared with a diversity of other tetrapod groups (Campione and Evans, 2012).

Cross-family analyses reveal that scaling is not linear in mammals. In particular, larger mammals tend to have stronger allometry than smaller ones (Economos, 1983; Bertram and Biewener, 1990). Biewener (1983) proposed a model to explain this

discrepancy in which smaller mammals primarily accommodate for increases in body size by straightening their limb posture, whereas larger mammals use structural allometry. A more upright posture brings the limb closer in line with its ground reaction force (Figure 1.2.4). This reduces the turning moment at the joint and the peak stress experienced by the bone (Alexander et al., 1981; Biewener, 1983, 1989). Peak stresses and safety factors (failure stress/maximum applied stress) remain constant over a range of body sizes (Biewener, 1989, 1990). Further, while limb bone dimensions of smaller mammals scale close to geometric similarity, limb angle scale with negative allometry, supporting postural versus structural allometric adaptations (Bertram and Biewener, 1990; Biewener, 2000, 2005). However, structural allometry of the limb is found in larger mammals. Ursids, proboscideans and bovids scale with elastic similarity, while ceratomorphs have even stronger negative allometry (McMahon, 1975b; Prothero and Sereno, 1982; Bertram and Biewener, 1990; Christiansen, 2007). This pattern suggests that postural changes are constrained in large mammals (those over 300 kgs). One exception to this pattern is felids, which do not seem to conform to the postural allometry model. Instead of limb postural allometry, they show allometry of structural limb parameters (Day and Jayne, 2007; Doube et al., 2009).

Limb bone scaling across mammals does not follow either the geometric or the elastic similarity models, instead intermediate exponents for most features were recovered (Christiansen, 1999a, b). This work suggests that limb allometry is controlled by multiple complex factors and thus cannot be explained by a single unifying model across all mammals. Similarly, across tetrapods (including reptiles) there was variation in scaling exponents of length of proximal limb bones. However, their circumferences

consistently scaled with negative allometry in diverse groups, suggesting this measure

is more universally related to size (Campione and Evans, 2012).
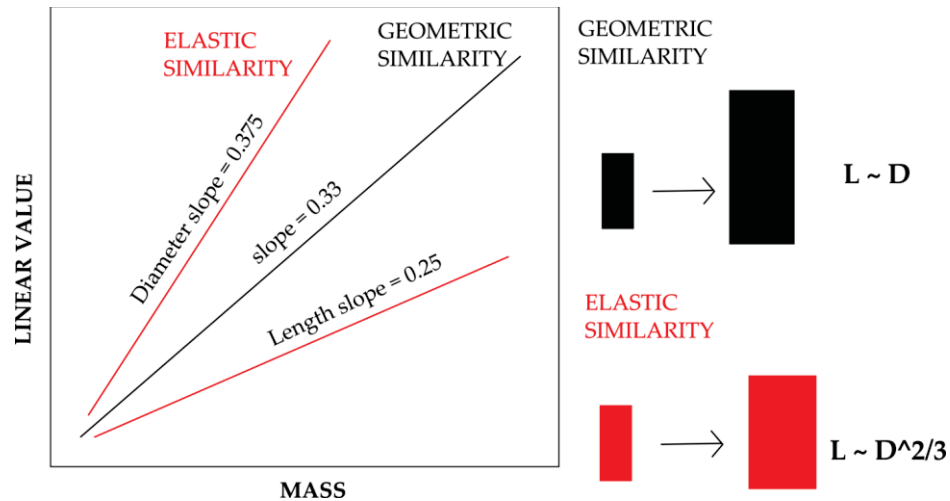
Figure 1.2.3 Elastic versus geometric scaling.

Note slope differences between lengths and diameters in the elastic similarity model (red). Shapes on right indicate geometrically similar shapes of different sizes (black), versus the change in shape associated with elastic similarity (red). L - length, D – diameter.
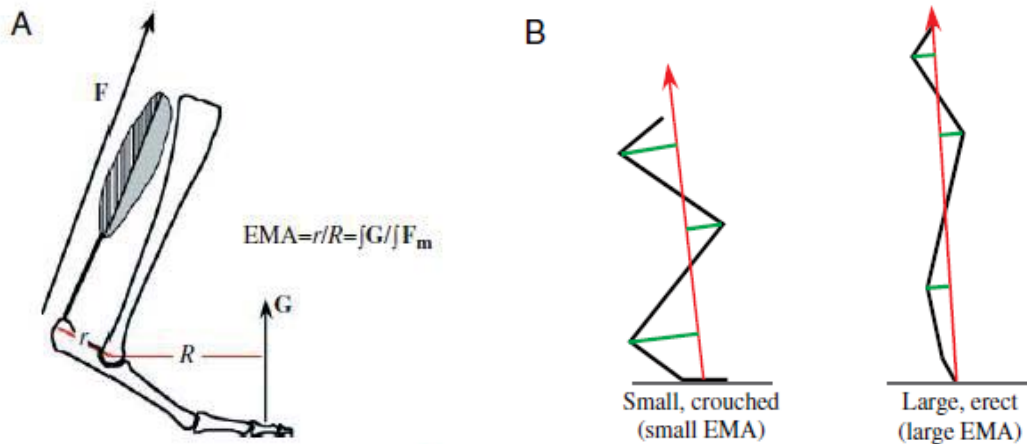
Figure 1.2.4 Postural allometry of the limbs.

From Biewener (2005:fig. 2). EMA – effective muscle advantage. A. EMA is the relationship of the moment arm (R) of the ground reaction force (G) to the muscle moment arm (r). B. In larger animals, an erect posture reduces R at each joint (green lines), therefore reducing the total moment from G.

Vertebral allometry

Relatively fewer data exist on allometry of the vertebral column than on the

limbs. Although the vertebral column does not function as a direct support column, some studies have compared it to the elastic similarity model (Halpert et al., 1987; Majoral et al., 1997). Experimental work in humans has shown that the lumbar region buckles in response to axial loading in a similar manner to that predicted from a Euler column (Crisco et al., 1992). Further, comparable loadings are found in quadrupedal and bipedal columns, suggesting application of the elastic similarity model to the quadrupedal axial skeleton is valid (Wilke et al., 1997a; Smit, 2002). In particular, the ventral column is most appropriate for analysis because it is the primary compressive element of the vertebral column, and therefore most important in resisting buckling.

Most investigations of vertebral allometry have focused on primates (Shapiro, 1993; Ward and Latimer, 1993). Total column length of a broad sampling of primates scales with both positive and negative allometry relative to geometric similarity, but the lumbar region has the most variable scaling (Majoral et al., 1997). Catarrhines have strong negative allometry in all vertebral regions, indicating that the vertebral column becomes shorter with increasing size. In contrast, platyrrhines show positive allometry in the cervical region and negative allometry more posteriorly. Finally, prosimians have strong positive allometry in the cervical and lumbar regions but negative allometry in the thoracic region. These variable exponents are attributed to variation in locomotor types within primate groups (Majoral et al., 1997). In contrast, lumbar region length was not significantly different to geometric similarity in strepsirrhines (Shapiro and Simons, 2002). Centrum cranial surface area scaling generally exceeds geometric similarity (b=0.8-0.9) relative to mass in lumbar vertebrae of cercopithecoids and platyrrhines. However, when lumbar length is taken into account groups scale similarly

(Nakatsukasa and Hirose, 2003). Further, the correlation between length and area in the two groups is stronger when the zygapophyseal rather than the rib definition of the lumbar region is used (see 'vertebral regions').

Analysis of 3D shape and density of hominoid thoracic vertebrae using CT data revealed that shape of the vertebrae and axial compressive strength scales with geometric similarity, but that bending strength has positive allometry (Hernandez et al., 2009). Trabecular thickness and number also scales with negative allometry to body mass, though measures of the distribution of trabeculae are scale independent (Cotter et al., 2009a; Cotter et al., 2009b). In strepsirrhines, both thoracic trabecular thickness and bone mass and microarchitecture of the last lumbar vertebra scale with geometric similarity, suggesting structural changes do not compensate for increasing size (Fajardo et al., 2005; Fajardo et al., 2013). However, primates may not provide a good model for understanding other quadrupeds. For example, sagittal and transverse diameters of lumbar vertebrae scale with negative allometry relative to body length in most primate groups, compared to positive allometry in non-primates (Rose, 1975).

Outside primates, data on vertebral allometry are even scarcer. Halpert et al. (1987) found elastic similarity of craniocaudal length and dorsoventral height of the lumbar centra against body mass, but geometric similarity of mediolateral width. They also showed a reduction in the angle of the transverse process and an increase in complexity of the zygapophyseal joints with increasing size using discrete measures. These data combined with kinematic data on four species of bovids were used to suggest decreasing sagittal mobility of the lumbar region with increasing size in bovids (Halpert et al., 1987). Relative epaxial muscle mass scales with negative allometry in a

small sample of bovids, further supporting a reduction in axial mobility in large bovids (Grand, 1997). However, Alvarez et al. (2013) did not find a significant correlation of penultimate lumbar shape with mass in a broad sample of medium-small mammals using 2D landmarks from the dorsal view (Alvarez et al., 2013).

Though few empirical data exist, many previous authors have proposed a link between body size and reduced sagittal mobility of the vertebral column in running mammals. In particular, transverse galloping that is associated with dorsostability may be energetically favorable to rotary galloping at large size (Smith and Savage, 1956; Hildebrand, 1959; Biancardi and Minetti, 2013). Further, the energetic cost of muscular support increases with size, as body weight scales as a cube whereas muscle force output scales with its cross-sectional area, favoring dorsostability at large sizes (Smeathers, 1981).

1.3   SYNTHESIS

Previous research has demonstrated that the thoracolumbar spine plays an important role in both static support and quadrupedal running. These competing functions--sagittal stiffness to resist sagging and sagittal flexibility to enhance stride length--must both be accommodated by vertebral morphology. A mobile column, with strong paraxial musculature and flexible joints, requires active support while providing sagittal flexibility. In contrast, a stable column sacrifices flexibility for passive support. As size increases, the trade-off between the energetic cost of sagittal mobility and the advantage of increased stride length may shift (Smeathers, 1981). Furthermore, leaping gaits which use sagittal flexion become difficult at large size due to the energetic cost of vertical motions of the center of mass. Thus several authors have proposed that dorsostable running may be directly related to size (Slijper, 1946; Smith and Savage, 1956; Hildebrand, 1959; Smeathers, 1981; Hildebrand, 1995).

Few quantitative data exist on morphological variation in the thoracolumbar region of running mammals. This dissertation helps to resolve this problem by examining the influence of size on thoracolumbar morphology. **How is the structure of the bony thoracolumbar region influenced by increasing body size in running mammals? Do dorsomobile and dorsostable runners scale differently?** The vertebral column is an important missing piece in our understanding of the locomotory system, particularly with respect to cursoriality. Collecting empirical data about the effect of size on vertebral morphology will help to tease apart some of the complex factors influencing vertebral evolution and provide improved context for interpreting fossils.

To address the questions posed above, study groups must be selected from which morphological data can be collected. Three groups were selected as case studies of size variation in running mammals: Felidae, Bovidae and Equidae. They were selected because: a) each is monophyletic, b) each group spans a large range of body sizes, and c) they frequently use asymmetric gaits. Further, groups were selected to span a range of vertebral functions, incorporating both dorsostable and dorsomobile groups.

1.4 STUDY GROUPS

1.4.1 FELIDAE

Felidae is a family of feliform Carnivora, first known from the Oligocene, which consists of 14 genera and 40 extant species (Wilson and Reeder, 2005; Vaughan et al., 2011). They range from 2 to 200 kg in mass (Van Valkenburgh, 1990; Anyonge, 1993; Rose, 2006) and are highly skilled predators. Felids catch their prey via rapid short distance chasing and pouncing, using a forelimb-initiated rotary gallop that involves extreme spinal mobility (Gambaryan, 1974; Day and Jayne, 2007; Bertram and Gutmann, 2009; Biancardi and Minetti, 2013). They also use the spine extensively for jumping (Harty, 2010) and many have good arboreal capabilities (Van Valkenburgh, 1985). The cheetah is the most cursorial felid, and indeed the fastest land mammal; and experimental data have indicated that spinal movements contribute significantly to stride length, and ultimately speed, in this species (Hildebrand, 1959; Bertram and Gutmann, 2009). Systematics of felids have been controversial and generic nomenclature has changed many times (Wilson and Reeder, 2005). Here I follow the taxonomy and phylogenetic arrangement proposed by Nyakatura and Bininda-Emonds (2012), which uses a supertree approach combining both morphological and molecular data to find species-level relationships of the Carnivora (Figure 1.4.1). The relationships of felids recovered in this study are in general agreement with those from other recent work (Johnson et al., 2006). Felids were used in this dissertation to typify dorsomobility and rotary, forelimb-initiated galloping during locomotion.
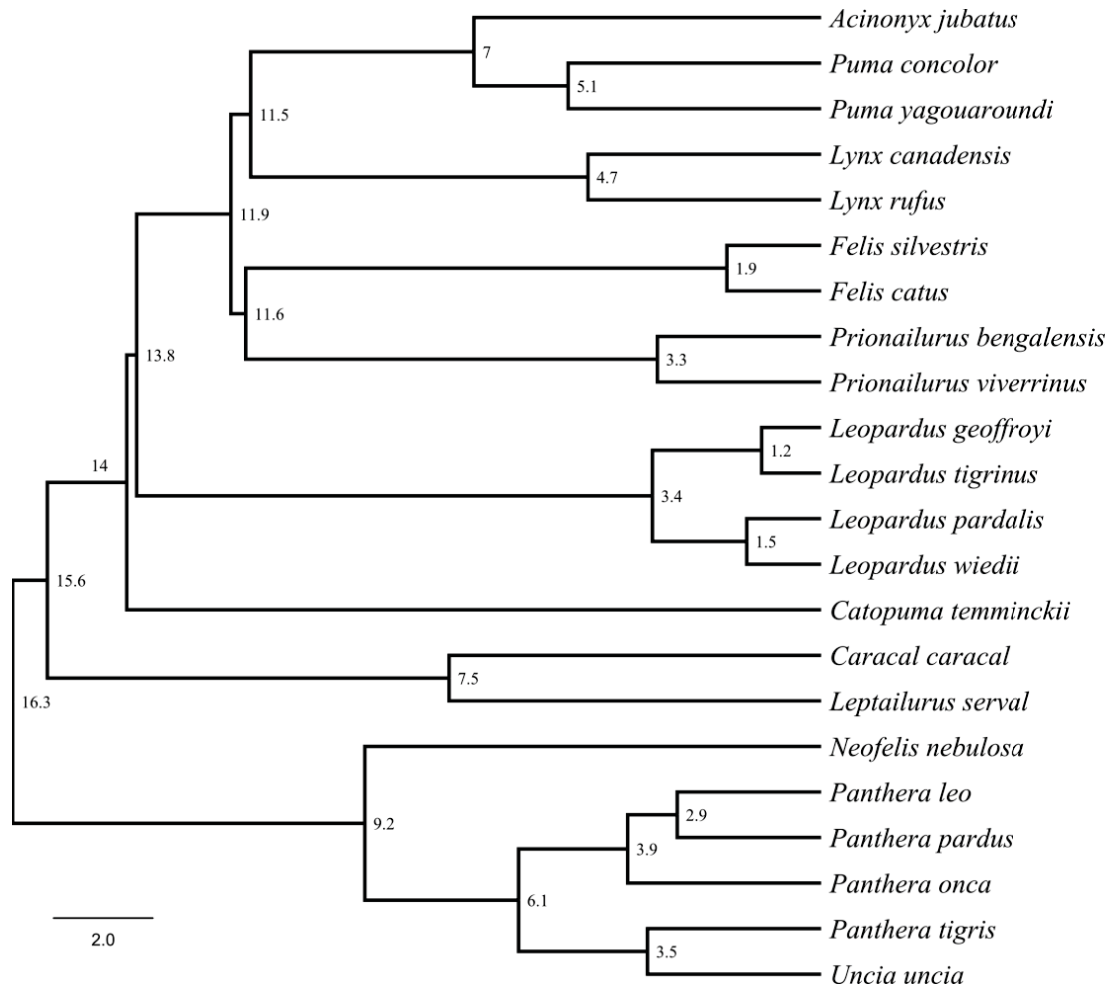
Figure 1.4.1 Felid phylogeny.
Subset from the supertree of Nyakatura and Bininda-Emonds (2012), showing only taxa included in this study. Node ages are shown in Ma and are taken from the same study.

1.4.2   BOVIDAE

Bovids are a diverse family of Artiodactyla, originating in the Miocene, which includes 50 genera and 139 extant species (Wilson and Reeder, 2005). They have been particularly popular for allometric studies because of their enormous extant size range, which spans 2.5 to 1000 kgs (Scott, 1983; Scott and Janis, 1993). The family underwent several phases of rapid radiation in the Miocene, and through both migration and speciation became especially diverse in Africa (Hassanin and Douzery, 1999). I follow

previous authors in focusing my sample on these African bovids, which span the largest

size range (Alexander, 1977; Halpert et al., 1987; Grand, 1997). Bovidae are

specialized for terrestrial running, using both the transverse and rotary gallop

(Hildebrand, 1962; Gambaryan, 1974; Biancardi and Minetti, 2013). They are strictly

terrestrial, though their habitat ranges from open grasslands, mountains, deserts,

swamps or dense forest (Vaughan et al., 2011). For phylogenetic comparative analyses

I will utilize the topology and divergence times of Bibi (Bibi, 2013). This study used

mitochondrial DNA data collected from a previous study (Hassanin et al., 2012) and 16

additional fossil calibration points to produce a more finely calibrated phylogeny.

Seven species included in my study were not present in Bibi's analysis. These species

were added in the position described by Fernandez and Vrba (2005) to form a

composite tree (Figure 1.4.2). Bovids were used in this dissertation to typify an extant

dorsostable group.
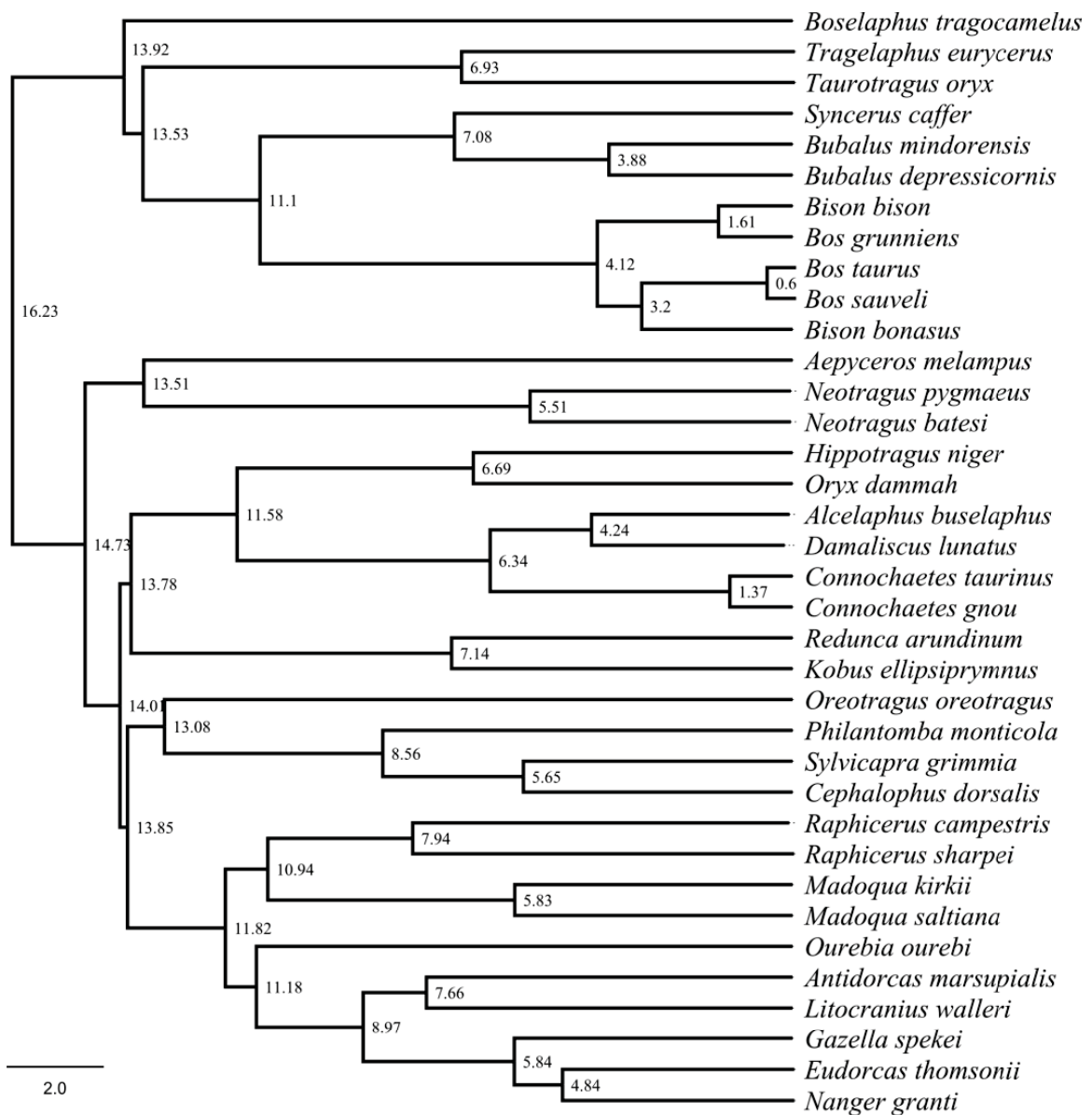
Figure 1.4.2 Composite phylogeny of bovids.
Based on Bibi (2013) and Fernandez and Vrba (2005), showing only taxa included in this study. Node ages are shown in Ma and are taken from or computed using the same studies.

1.4.3   EQUIDAE

Equidae (horses) are represented today by only one extant genus and seven

species, yet the family has a rich evolutionary history and fossil record dating back to

the Eocene (Vaughan et al., 2011). Equids range in body size from 9 to ~500 kg

(MacFadden, 1986; Wood et al., 2011). To sample the full size diversity of this family,

fossil equids were also included. The Equidae are one of the best studied fossil mammal

groups, and their sytematics, diversification, body size radiation, and adaptation to

changing environmental conditions are well understood. Here, I follow the taxonomy of

MacFadden and a composite phylogeny presented by Stromberg (2006), which is based

on MacFadden (1998) and Hulbert and MacFadden (1991) (Figure 1.4.3).

Fossil equids are subdivided into three subfamilies: Hyracotheriinae,

Anchitheriinae and Equinae. Though their evolution was once characterized as linear, it

was more likely a complex, branching pattern of interrelated clades (Simpson, 1951;

MacFadden, 1992). Since vertebral material is so rare, this dissertation focuses on a few

well-known equid genera at key stages through their evolution, as representatives of

important functional grades. The phenacodontid condylarth *Phenacodus* is used as the

phylogenetic outgroup of Perissodactyla (Radinsky, 1966). Eocene hyracotheres were

the smallest equids and are typified by the genus *Hyracotherium,* a primitive browser

with four digits on the forefoot (MacFadden, 1986). The systematics of this genus are

controversial (in particular *Hyracotherium grangeri* has been transferred to

Arenahippus; ((Froehlich, 2002); however, for simplicity I use *Hyracotherium sensu*

lato following Wood et al. (2011) and other authors (Rose, 2006; Stromberg, 2006;

Wood et al., 2011) to refer to North American early Eocene equids. Within the

anchitheres I examined *Mesohippus, Archaeohippus* and *Parahippus.* Oligocene

Mesohippus is well known from the White River Formation of Nebraska and the

Dakotas. It has a larger body mass, a tridactyl manus and subunguligrade foot posture

44

(MacFadden, 1992). The later anchitheres *Archaeohippus* and *Parahippus,* which are known from the Miocene of Florida, still had three digits, but the lateral ones are greatly reduced. Primitive members of the Equinae are grouped in *Merychippus,* though this genus is paraphyletic (Hulbert and MacFadden, 1991). These are the first horses adapted for a grazing lifestyle like modern horses; they were relatively large, had hypsodont teeth and unguligrade foot posture (MacFadden, 1986, 1992). Multiple increases in size during the Miocene are thought to be linked to shifts within the group toward a more open-plains lifestyle in response to the spread of grasslands in North America (MacFadden, 1986). Within Equinae, *Nannippus* was a hipparionine horse with secondarily reduced body size more similar to that of anchitheres, though it retained derived limb morphology. *Pliohippus,* from the late Miocene, is interpreted to have given rise to *Equus* and may or may not have achieved true monodactyly (Hulbert and MacFadden, 1991).

Modern horses are highly specialized cursors that use the transverse gallop for efficient long-distance running (Hildebrand, 1959; Pilliner et al., 2002). Cursorial features of the limbs of modern equids include reduced (monodactyl) digits with hooves, elongated limbs that are restricted to movements in the parasagittal plane, and a complex system of limb ligaments to store elastic energy during locomotion (Hussain, 1975; MacFadden, 1992). These features have been well characterized in fossil taxa and are associated with increasing size in some lineages (Hussain, 1975; Thomason, 1985; Thomason, 1986; Hermanson and MacFadden, 1996). A fully unguligrade but three-toed manus evolved in *Merychippus,* whereas *Mesohippus* was subunguligrade with a digital pad (Sondaar, 1968; Thomason, 1986). Passive stay apparatuses which

use ligaments to facilitate long periods of standing are found first in the knee in

primitive equines, then later in the shoulder in Pleistocene *Equus* (Hermanson and

MacFadden, 1992, 1996).

The lumbar region of the modern horse is highly stabilized using strong

intervertebral ligaments, interlocking zygapophyses and vertebral fusions (Jeffcott and

Dalin, 1980; Townsend and Leach, 1984; Ritruechai, 2009; Zaneb et al., 2013). In

contrast the lumbosacral joint is more sagittally mobile. Lateral joints facilitate sagittal

motions but restrict lateral bending or torsion (Townsend et al., 1983; Denoix, 1999;

Haussler et al., 2001). Equids were included in this dissertation as the best understood

dorsostable runners, with fossil equids added to sample small-bodied species.
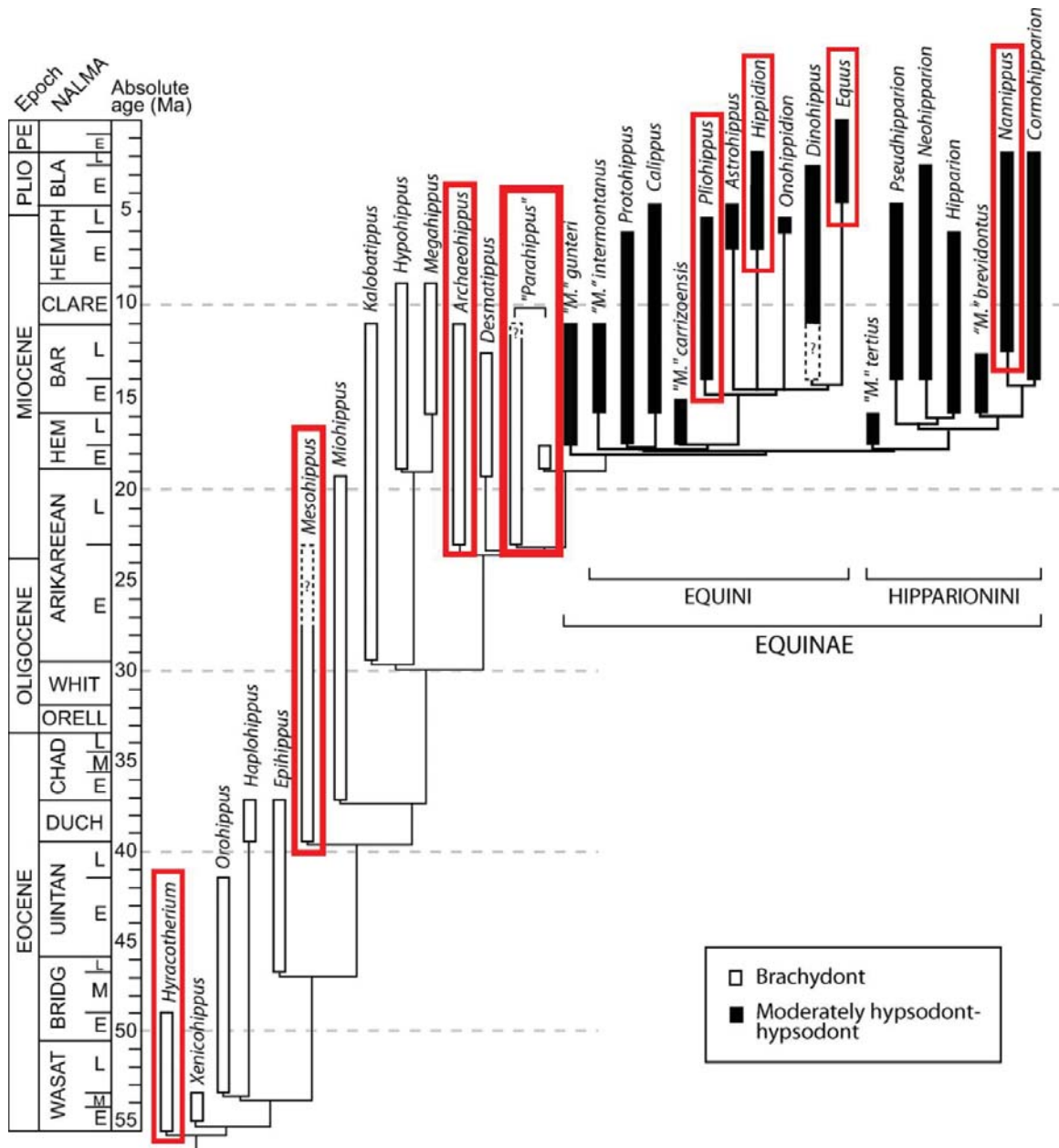
Figure 1.4.3 Equid phylogeny.
From Stromberg (2006), based on MacFadden (1998) and Hulbert and MacFadden
(1991). Taxa included in this study are outlined in red.

1.5   OBJECTIVES AND HYPOTHESES

Objective 1.   Collect preliminary data to assess the link between <u>form and function</u> in the thoracolumbar region of running mammals.

Objective 1 was addressed using one representative species from each group, whose vertebral function has been measured: cats (*Felis catus*), sheep (*Ovis*) and horses (*Equus caballus*). Range of motion data were gathered from the literature and morphological data from osteological material were collected. The relationship between range of motion and morphology was examined using correlation analysis, and digital models were used to identify interactions of bony features limiting mobility. Results of **Objective One** are presented in **Chapter Three**. Experimental range of motion and morphologic data were used to test the following hypotheses:

H1. Sagittal range of motion is correlated with morphology. Specifically, it may be restricted:

A) in dorsiflexion by impaction of the zygapophyses, tension in the ventral longitudinal ligament and compression of the dorsal portion of the disc (Gál, 1993; Denoix, 1999).

B) in ventroflexion by tension in the supraspinous ligament, ligamenta flava and dorsal longitudinal ligaments, and compression of the ventral disc (Gál, 1993; Long et al., 1997; Denoix, 1999).

Thus it is predicted that low sagittal mobility is correlated with one or more of the following features: a tall arch with dorsally-placed zygapophyses, a tall

endplate, a strong ventral keel, and a tall neural spine (Townsend and Leach, 1984; Boszczyk et al., 2001; Molnar et al., 2014).

H2. Lateroflexion is restricted by tension in the intertransverse ligaments, compression in the lateral portion of the disc and impaction of the zygapophyses (Denoix, 1999). Therefore, it is predicted that limited lateroflexion should be correlated with a wide transverse process, widely spaced zygapophyses or a wide endplate (Boszczyk et al., 2001).

H3. Torsion is restricted by impaction of the zygapophyses (Shirazi-Adl, 1994; Russo, 2010). Therefore limited torsion should be correlated with sagittally-oriented or wide zygapophyses (Boszczyk et al., 2001).

Objective 2.   Examine the role of the <u>ventral column</u> (centra and discs) in providing <u>static support</u> with increasing size.

Objective 2 was addressed by calculating the scaling exponents for felids and bovids, and comparing them to mechanical predictions. As the ventral column resists body weight, its shape is predicted to change with size in order to maintain a similar vulnerability to buckling. Scaling exponents are therefore compared to those predicted under the elastic similarity model. Results of **Objective Two** are presented in **Chapter Four**. Using osteological samples, lengths of vertebral regions and cross-sectional dimensions were compared to body mass estimated from limb dimensions. Scaling exponents were calculated and used to test the following hypotheses:

H1. Craniocaudal length of the ventral column (regions and individual centra)

scales with exponent 0.25 (elastic similarity), indicating the column becomes relatively shorter with increasing size.

H2. Dorsoventral height of the ventral column scales with exponent 0.375 (elastic similarity), indicating it becomes relatively deeper with increasing size.

H3. Mediolateral width of the ventral column scales with exponent 0.33 (geometric similarity), indicating isometry, because major weight -bearing forces are in the sagittal, not mediolateral, plane.

Objective 3.   **To characterize <u>allometry of the lumbar region</u> and look for association of <u>stabilizing features</u> with increasing size.**

Objective 3 was addressed by correlating lumbar morphology with body mass in felids and bovids. Morphology of the lumbar region was measured in two ways:

A) Three-dimensional lumbar morphology was measured at one vertebral position (penultimate lumbar), using 3D geometric morphometrics. The shape variation associated with increasing size was characterized using multivariate regression. The results of this analysis are presented in **Chapter Five**. The 3D shape most correlated with increasing size was calculated and used to test the following hypotheses:

H1. The centrum becomes craniocaudally shorter and dorsoventrally taller with increasing size.

H2. The zygapophyses become horizontal or more interlocking and metapophyses become larger with increasing size.

H3. The processes (spinous and transverse) become more robust, craniocaudally longer, dorsoventrally/mediolaterally wider and less inclined from the primary planes of the vertebra with increasing size.

B) Two-dimensional lumbar morphology was measured at three positions along the lumbar region (first, middle and last lumbar), using linear measures and 2D geometric morphometrics taken from photographs. Craniocaudal variations in lumbar allometry were tested using an analysis of covariance. The results of this part are presented in **Chapter Six**. Allometry of two-dimensional shape of vertebrae along the lumbar region was used to test the following hypotheses:

H1. There is an effect of size on lumbar shape. Specifically, increasing size is associated with a taller centrum, increased lever arm of the neural spine and arch, and decreased angle between the neural spine and transverse process.

H2. The effect of size varies among vertebral positions and families. Specifically:

A. Size and position. Allometric slopes vary along the lumbar region.

B. Size and family. Allometric slopes vary between families.

C. Family and position. Craniocaudal patterns vary between families. Specifically, there is stronger craniocaudal variation in bovids than felids because bovids enhance mobility at the lumbosacral joint relative to the rest of the lumbar region. In particular, the last lumbar may have a shorter centrum, arch or neural spine.

Objective 4.   Examine allometry in the lumbar region of the <u>Equidae</u> using both extant and <u>fossil </u>taxa (to include small-bodied species).

Objective 4 was addressed by examining vertebral material of fossil equids and modern *Equus*. Digital models were created from lumbar vertebrae from eight genera of equids encompassing the entire size range of the family. Joint complex shape was measured using 2D landmarks and compared to size. Features associated with lumbar function in *Equus* were mapped onto a phylogeny of fossil equids to reconstruct their evolution. Results of **Objective 4** are presented in **Chapter Seven**. Data on the morphology of the lumbar region in fossil equids were used to test the following hypothesis:

H1. Dorsostable running evolved in Miocene horses of the subfamily Equinae e.g., *Merychippus*, in association with increased body size. This is indicated by:

A. Lumbar joints: Dorsoventrally tall centra, with a strong ventral keel for the ventral longitudinal ligament and pitched-interlocking zygapophyses.

B. Processes: Robust, long neural spines with a strong dorsal ridge, indicating a strong supraspinous ligament, and wide transverse processes which are not ventrally or cranially inclined.

C. Lumbosacral joint: A hinge-like lumbosacral joint which is dorsoventrally compressed, but mediolaterally wide, with lateral joints to resist lateroflexion and torsion.

CHAPTER 2: MATERIALS AND METHODS

2.1 SAMPLE

2.1.1 TAXONOMIC SAMPLE

Primary dataset

Felid and bovid sample - The thoracolumbar region of 93 felid and 123 bovid specimens were examined from the osteological collections of the United States National Museum of Natural History (USNM, Washington DC), American Museum of Natural History (AMNH, New York) and Natural History Museum (NHM, London), constituting 23 felid species and 34 bovid species (Table 2.1.1 and Appendix 1). This dataset will be referred to herein as the 'felid and bovid sample.' Specimens with complete disarticulated thoracolumbar columns which were free of obvious pathology were selected. Wherever possible, wild specimens were used. Only fully-grown adult individuals were used, which was verified by fusion of the vertebral epiphyses. I aimed to examine 3-5 specimens per species, although this was not always possible (Table 2.1.1). During examination the thoracolumbar column was reassembled to ensure that the column was complete, by establishing that all vertebrae articulated tightly with the next.

Table 2.1.1 Felidae and Bovidae included in the sample.

Body masses were estimated from limb dimensions. BM, body mass; SD, standard deviation; N, sample size.

SPECIES	MEAN BM (Kg)	SD	N
Bovidae			
Neotragus pygmaeus	2.0	.	1
Neotragus batesi	2.6	0.2	5
Madoqua saltia	4.0	0.3	2
Philantomba monticola	4.7	0.4	5
Madoqua kirkii	5.8	0.7	5
Raphicerus sharpei	8.4	1.2	3
Raphicerus campestris	9.7	2.4	3
Sylvicapra grimmia	14.2	1.8	4
Oreotragus oreotragus	14.4	1.9	2
Gazella spekei	17.0	1.0	3
Ourebia ourebi	17.0	2.2	5
Cephalophus dorsalis	17.8	3.4	3
Eudorcas thomsonii	21.4	3.9	5
Antidorcas marsupialis	32.8	5.2	5
Litocranius walleri	41.3	6.2	2
Aepyceros melampus	45.1	8.5	4
Redunca arundinum	50.9	11.8	5
Nanger granti	52.5	8.8	5
Bubalus depressicornis	83.8	.	1
Oryx dammah	116.2	20.2	5
Damaliscus lutus	120.7	10.4	5
Alcelaphus buselaphus	135.3	21.4	5
Connochaetes gnou	138.2	30.3	3
Bosephalus tragocamelus	153.6	.	1
Hippotragus niger	182.2	18.5	5
Kobus ellipsiprymnus	182.4	28.5	3
Connochaetes taurinus	196.6	5.9	5
Bubalus mindorensis	200.7	.	1
Tragelaphus eurycerus	227.4	5.9	3
Bos grunniens	231.3	.	1
Bos sauveli	306.3	15.1	2
Bison bosus	483.4	.	1
Taurotragus oryx	536.0	94.6	3
Bison bison	605.2	113.1	5
Syncerus caffer	647.2	93.5	5
Bos taurus	655.5	.	1

Felidae			
Leopardus tigrinus	2.2	.	1
Prionailurus bengalensis	2.3	.	1
Felis catus	4.5	1.1	5
Leopardus wiedii	4.8	1.1	3
Felis silvestris	5.4	1.2	5
Leopardus geoffroyi	5.9	2.2	4
Puma yagouaroundi	7.9	0.0	2
Prionailurus viverrinus	11.1	2.7	3
Lynx lynx	11.2	.	1
Caracal caracal	12.7	0.6	4
Catopuma temminckii	13.5	1.8	3
Leopardus pardalis	14.0	3.7	5
Leptailurus serval	14.2	3.3	4
Lynx rufus	14.5	3.3	5
Lynx canadensis	15.0	2.0	5
Neofelis nebulosa	16.5	3.5	4
Acinonyx jubatus	40.6	10.2	5
Uncia uncia	44.9	13.5	4
Panthera pardus	52.0	7.9	5
Puma concolor	66.8	24.8	5
Panthera onca	80.7	21.0	5
Panthera tigris	151.3	49.2	8
Panthera leo	195.0	39.9	5

54

Equid sample - Thirteen extant equid specimens, constituting five species of the genus *Equus*, were measured at the USNM, using the same selection criteria described above for felids and bovids (Table 2.1.2, Appendix 2). Vertebral material of fossil equids was compiled from collections across North America. Fossilized vertebrae are rarely preserved and frequently damaged, so finding sufficient material was extremely challenging. The sampling focused on the lumbosacral region (except where complete columns were available) because the lumbosacral region is functionally important during asymmetric gaits (Townsend and Leach, 1984). Specimens were examined at USNM, AMNH, Harvard Museum of Comparative Zoology (MCZ), Yale Peabody Museum (YPM) and University of Florida Museum of Natural History (UF) (see Appendix 2). A digital copy of the vertebral column of *Hyracotherium grangeri* was also supplied by Aaron Wood, which was created by the authors using as NextEngine surface scanner (Wood et al., 2011). The fossil sample included 67 specimens from 9 genera, representing 105 lumbar vertebrae scanned (Table 2.1.2). This sample will be referred to herein as the 'equid sample.'

Table 2.1.2 Equid species included in the sample.
Specimen numbers are provided in Appendix 2.

SPECIES	GROUP	N
Hyracotherium grangeri	Hyracotheriinae	1
Hyracotherium sp.	Hyracotheriinae	5
Mesohippus sp.	Anchitheriinae	12
Mesohippus westoni	Anchitheriinae	1
Mesohippus bairdii	Anchitheriinae	4
Archaeohippus blackbergi	Anchitheriinae	4
Parahippus leonensis	Anchitheriinae	19
Merychippus republicanus	Equinae	1
Nannippus sp.	Equinae	7
Merychippus quartus	Equinae	1
Merychippus proparvulus	Equinae	1
Merychippus campestris	Equinae	1
Merychippus isoneus	Equinae	1
Pliohippus pernix	Equinae	1
Equus kiang	Equinae	1
Merychippus sp.	Equinae	1
Equus burchellii	Equinae	4
Equus zebra	Equinae	1
Equus caballus	Equinae	4
Equus grevyi	Equinae	2
Equus sp.	Equinae	5

Additional datasets

Range of motion (ROM) sample - Three species were selected from within these groups to examine the relationship between vertebral morphology and joint mobility. The cat, sheep and horse were selected as representatives of my groups of interest because of the availability of experimental range of motion data from the literature (English, 1980; Townsend et al., 1983; Townsend and Leach, 1984; Nagel et al., 1991; Wilke et al., 1997a; Wilke et al., 1997b; Macpherson and Fung, 1998; Macpherson and Ye, 1998; Denoix, 1999). Vertebral elements were assembled from five cats (*Felis catus*), five horses (*Equus caballus)* and six sheep, using both specimens from the primary dataset and additional specimens. The sheep sample consisted of a mixture of domestic and bighorn sheep (*Ovis aries* and *Ovis canadensis*) because there was insufficient material available of *O. aries* alone. Visual inspection of the material indicated that both species had very similar vertebral morphology, so the samples were pooled. This sample will be referred to herein as the 'ROM sample'.

Radiograph sample - Radiographs were also obtained for a small sample of felids and bovids to examine variation in intervertebral space length. These data were used for method validation. In particular, vertebral region lengths were calculated from centra alone, but examining the relationship between centrum length and intervertebral space length can test the effect of excluding the intervertebral spaces on the allometric analyses. Radiographs of adult animals with healthy spines in the lateral view were selected (Felidae:n=5, Bovidae:n=6). Species represented were *Felis silvestris* (n=2)*, Caracal caracal* (n=1)*, Acinonyx jubatus* (n=1)*, Puma concolor* (n=1)*, Oryx dammah* (n=3)*, Capra hircus* (n=1)*, Nanger dama* (n=1) and *Gazella spekei* (n=1)*. This sample

will be referred to herein as the "radiograph sample." Individuals with unfused epiphyses, signs of osteoarthritis or disc collapse were excluded. Bovid radiographs were obtained from the Smithsonian Veterinary Hospital courtesy of Jess Seigal-Willcott, and felid radiographs were provided courtesy of Natalia Kennedy and Blaire Van Valkenburgh.

2.1.2 VERTEBRAL SAMPLE

Vertebrae are serially homologous structures that vary on multiple levels: along the column, between individuals within a species and between species (O'Higgins and Johnson, 1993; Filler, 2007). Vertebral formula (the number of vertebrae in each particular anatomical region) may vary both within and between species. However, in order to make meaningful comparisons, vertebrae with equivalent function and morphology must be compared. In this dissertation I overcame the problem of comparison of individual vertebrae from taxa with variable vertebral counts by selecting 'homologous' vertebral positions. For this purpose six homologous positions were defined:

1. First thoracic (T1) - the most cranial vertebra with a facet for a rib

2. Mid-thoracic (MT) - the median thoracic vertebra, even numbers were rounded up

3. Diaphragmatic (D) - the vertebra with thoracic-type prezygapophyses but lumbar-type postzygapophyses

4. First lumbar (L1) - the first vertebra without a facet for a rib, usually bearing a small transverse process

5. Mid-lumbar (ML) - the median lumbar vertebra

6. Last lumbar (LL) - the caudal-most lumbar (articulates with the sacrum)

These six positions sample the full variation of thoracolumbar morphology. Sub-sampling the column in this way was also useful when combining vertebrae in a single analysis as it lessens the effect of pseudo-replication, in which a single morphology is represented multiple times in the analysis because adjacent vertebrae are highly integrated. Instead these six positions represent semi-independent morphotypes that can characterize variation in a single column, and various combinations of them will be used in the subsequent analyses. In addition, the penultimate lumbar was used to represent a typical lumbar vertebra in the 3D shape analysis. The scanning protocol for this analysis was time-consuming, so it was important to choose a vertebra which was not required for the other data collection (one of the six described here). This vertebra was suitable because it has more pronounced transverse processes than the more cranial lumbars (e.g., L2), and can be easily identified in columns with different lumbar counts.

2.2 DATA COLLECTION

2.2.1 FELID AND BOVID SAMPLE

Body mass estimation

Osteological collections of mammal postcrania in museums rarely have associated body mass data. However, comparing shape data directly to body mass is preferable in order to determine which shape variable may be driving allometric patterns (Christiansen, 1999a). Species-averaged body masses can be taken from the literature and compared to species-mean shape. However, this method introduces error because intraspecific mass variations are not taken into account. This is particularly problematic in species with marked sexual dimorphism (such as many bovids) as the sex of the specimen is not always known (Scott, 1983). There are strong relationships between the dimensions of limb bones and body mass (Ruff, 1986; Biewener, 2000) which can also be used to estimate body mass in specimens for which mass is unknown (Scott, 1983; Anyonge, 1993). Allometric relationships may vary among taxonomic groups, so it is best to use relationships calculated from a phylogenetically constrained sample when estimating body mass (Gingerich et al., 1982; Bertram and Biewener, 1990), though some measures may scale consistently across groups (e.g., Campione and Evans, 2012).

Relationships of body mass and limb dimensions from the literature were used to estimate body mass in the felid and bovid sample. I used separate regressions for felids and bovids because these family-specific relationships are likely to provide more sound estimations than broader clade or cross-mammal analyses (Scott, 1990; Anyonge, 1993). Three limb measures were selected as mass predictors for each group,

due to their low standard error of the estimate, including both forelimb and hind limb measures. For bovids, mediolateral width of the distal femur, distal humerus and distal radius were taken (Table 2.2.1). For felids, the circumference of the femur and humerus at the mid-shaft and distal femoral articular area were taken. All dimensions were measured twice using digital calipers, then the average taken. Circumferences were calculated from mediolateral and anteroposterior diameters using the following approximation (Wang et al., 2012):

$$p \approx \pi \left[3(a + b) - \sqrt{(3a + b)(a + 3b)} \right]$$

Where a is the semi-major axis and b is the semi-minor axis. Separate estimates of body mass were calculated from each of these measures then averaged to provide a best estimate of mass and a range of variation.

Table 2.2.1 Allometric equations used to estimate body mass from limb dimensions in felidae and bovidae.
Int., intercept; R, correlation coefficient; %SEE, percent standard error of the estimate.

Family	Source	Measure	Slope	Int.	R	%SEE
Felidae	Anyonge (1993)	Femur circumference	2.92	-3.46	0.96	38
	Anyonge (1993)	Femur distal condyle area	1.32	-2.16	0.98	24
	Anyonge (1993)	Humerus circumference	2.65	-3.00	0.97	30
Bovidae	Scott (1983)	Mediolateral distal femur	2.91	-0.077	0.95	31
	Scott (1983)	Mediolateral distal humerus	2.62	0.276	0.96	28
	Scott (1983)	Mediolateral distal radius	2.48	0.464	0.96	29

Error study on body mass estimation - An error study was conducted to estimate measurement error and the repeatability of estimates based on different limb

measures. A subset of specimens was selected encompassing the full size range of the groups and including ten bovid species (n=38) and seven felid species (n=29). Each limb measure was taken twice and used to estimate body mass from the allometric relationships above (three measures), resulting in a total of six estimates for each individual. Error due to measurement repeats was very small; however, there was some variation between the body mass estimates produced by the three limb measures (Figure 2.2.1). Visual inspection of the data revealed that femoral condyle area in felids gave a consistently higher estimate than the circumferential measures. This metric was also the most difficult to measure using calipers because the joint has a complex three-dimensional shape. Hence, I decided to exclude this measure *a posteriori*. This decision was confirmed by comparing the mass estimations to one specimen of *Neofelis nebulosa* which had associated mass data (actual mass = 14.2kg, condyle area mass = 25kg, other measures = 17.5kg). An ANOVA with factors species and individual (nested within species) revealed that despite variation in the mass estimates produced from different linear measures, it was still possible to distinguish among species based on mass estimates (felids $p<0.001$, bovids $p<0.001$). For bovids, it was additionally possible to distinguish individuals within a species ($p=0.007$). The average variation among measures was around 10% of specimen mass, though this also varied from species to species.
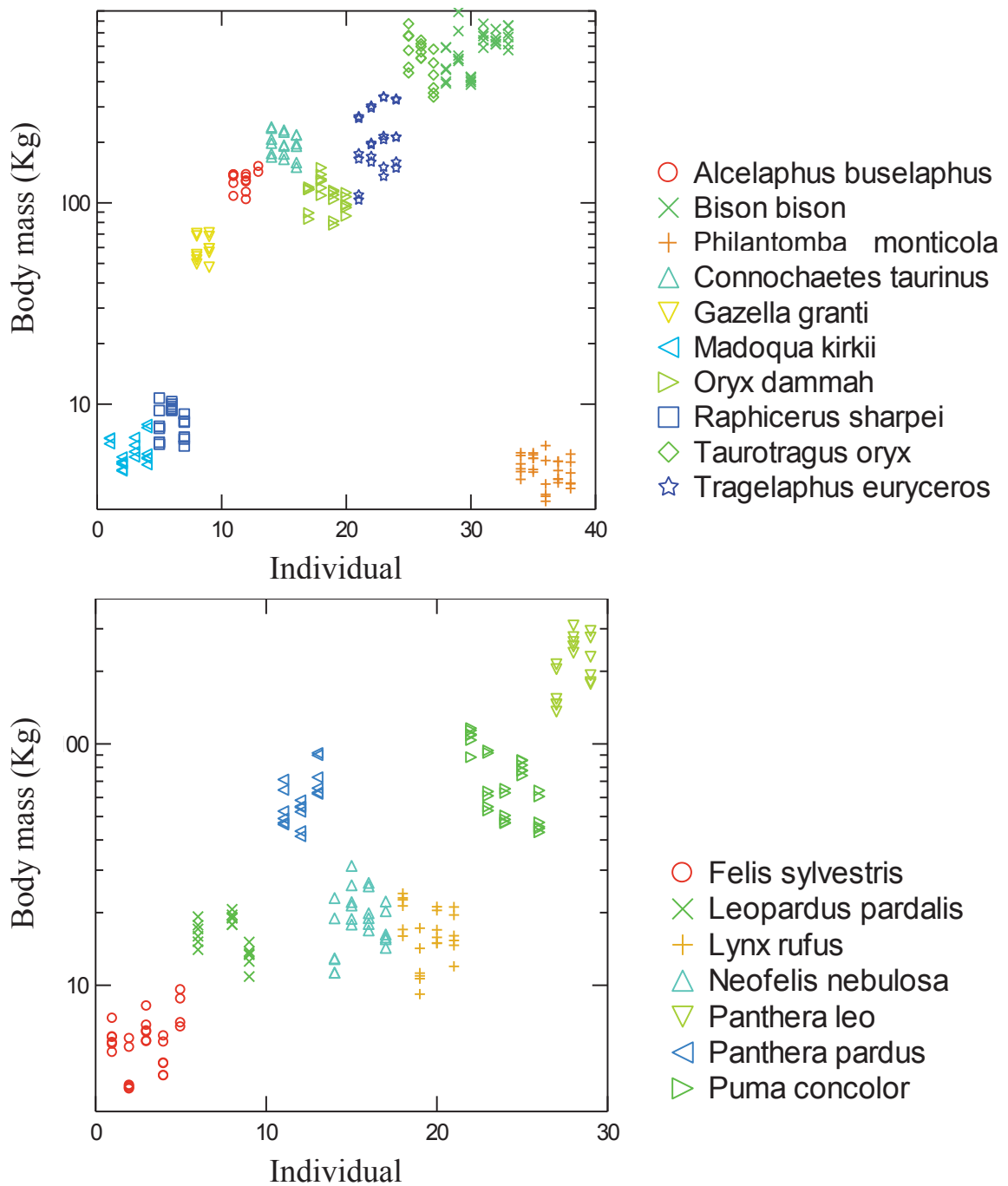
Figure 2.2.1 Variation in body mass estimates.

Each individual is represented by six data points which include two repeats of three limb measures used. Species are indicated by color and symbol. Upper: bovids, lower: felids. Though the body mass estimates for each individual do vary, the variation is relatively small compared to that among species and the size range as a whole.

Centrum dimensions

Mitutoyo digital calipers were used to measure the dimensions of the thoracolumbar centra (length, width, height) in the felid and bovid sample. All linear centrum measures were taken twice and averaged to minimize error due to measurement. Maximum craniocaudal length of each thoracolumbar centrum was measured and summed to provide an estimate of total thoracolumbar length (excluding intervertebral spaces). Length of the thoracic, lumbar, pre-diaphragmatic and post-diaphragmatic regions was also calculated. Centrum width and height at the caudal endplate were measured on the mid-thoracic, diaphragmatic and mid-lumbar vertebrae, which were selected to measure cross-sectional diameters of the ventral column in the thoracic, transitional and lumbar regions. Endplate areas were also calculated from these dimensions. This produced a total of 17 linear measures describing ventral column shape. All data were log-transformed prior to analysis. This dataset constituted between 50 and 60 measurements per specimen and around 10,800 total measurements.

Error study on centrum dimensions - Measurement error was examined in the same dataset described above in the previous section (Body mass estimation, Section 2.2.1.2). Caliper measurements from centra were used as the dependent variable instead of estimated body mass in the ANOVA. The nested ANOVA had highly significant effects of both species and individual, indicating that measurement error was very small compared to the effect of the factors ($p < 0.001$ for all effects), and that dimensions can be clearly discerned among species.

Surface scans

     A. Creating a digital model - Three-dimensional models of the penultimate lumbar vertebrae of the samples of felids and bovids were created using a NextEngine surface scanner. Each scan consisted of 16 individual scans taken about 360º using a rotating platform. The vertebra was secured with clay, with the center of rotation about its long axis (craniocaudal), and then this process was repeated with the vertebra secured about its dorsoventral axis. The surface models created were realigned and merged in Scan Studio (Scan Studio HD, 2006). Next, any extraneous material in the scans was removed and the two views (craniocaudal and dorsoventral) were merged into a single model using Geomagic (Geomagic Studio, 2010). Finally, the models were smoothed and small holes filled. The final product is an almost complete surface model. Sometimes the inside of the vertebral canal was not captured, but no landmarks were collected from this region.

     B. Collecting landmarks – Coordinates for 120 3D landmarks were collected for each specimen to capture the shape of the penultimate lumbar vertebra in felids and bovids. This consisted of 40 fixed landmarks and four curves of 20 landmarks each. Several types of landmarks exist (Adams et al., 2004; Zelditch et al., 2004). Type 1 landmarks are homologous points clearly defined by biological structures, whereas type 2 landmarks are defined by their position relative to biological structures (e.g., 50% of the height of the spine). Type 3 landmarks are constrained only by their position on a curve, along which they are allowed to slide during the semi-landmark optimization step. The penultimate lumbar is geometrically complex with few clear type 1 landmarks. Its shape can be captured using a combination of type 2 landmarks and

sliding semi-landmarks (Type 3). See Section 2.4.1, Sliding semi-landmarks, for a discussion of their implementation and appropriateness.

Forty fixed landmarks were taken in Geomagic using the point coordinate tool (Figure 2.2.2, Table 2.2.2) (Geomagic Studio, 2010). To assist with repeatable positioning of type 2 landmarks, a number of guideline curves were first defined on the vertebra in Geomagic using three principal planes of the vertebra. The sagittal plane was defined by the midline symmetry plane, the dorsal plane was defined by the dorsal surface of the centrum and the transverse plane was defined by the posterior endplate. Next, points were calculated at 50% and 10% from tip to base of both transverse and the neural processes. An additional point was defined at 50% the craniocaudal length of the centrum. Finally, guidelines were created on the surface model in the sagittal plane at the base, 50% and 10% of the transverse processes; in the dorsal plane at 50% and 10% neural spine height; and in the transverse plane midway along each postzygapophysis. The use of guidelines in defining landmarks is shown in Table 2.2.2, along with any calculations used in their placement.
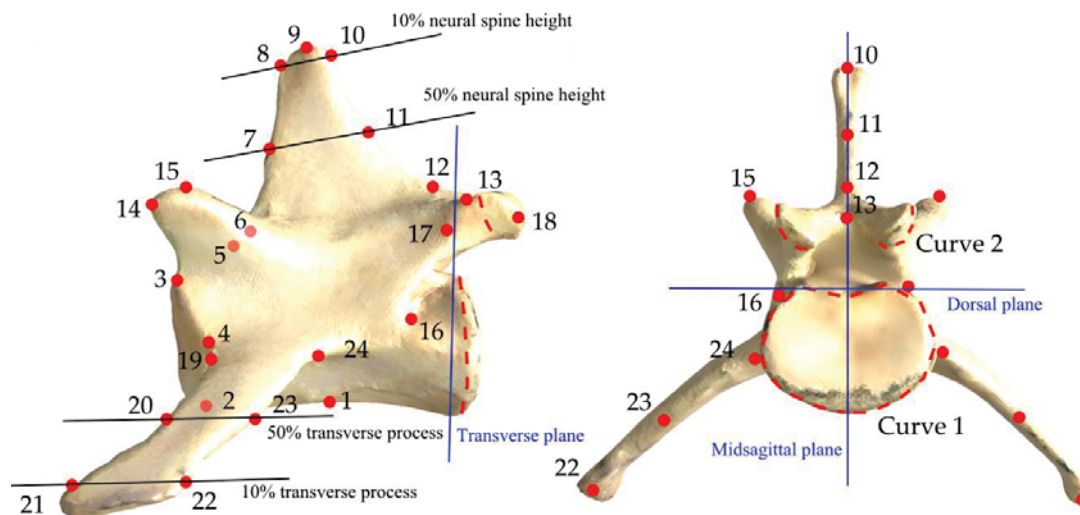
Figure 2.2.2 Three-dimensional fixed landmarks and curves.
Shown on a penultimate lumbar of Acinonyx jubatus *in lateral and caudal view. Type 2*
landmarks: Red dots; type 3 landmark curves: red dashed lines. Bilateral landmarks are
shown on the left side only. Curves, consisting of 20 sliding semi-landmarks, are
bilateral. Blue planes were used to create guidelines (black) to assist in the placement of
type 2 landmarks. Landmark descriptions can be found in Table 2.2.2.

Table 2.2.2 Landmarks taken from 3D digital models of the penultimate lumbar
Twenty-three fixed landmarks and two curves (each with 20 sliding semi-landmarks).
Guidelines and calculations used in landmark placement are indicated. Ant., anterior;
post., posterior.

No.	Name	Guideline Used?	Calculation	Midline or bilateral?	Region
1	Mid-keel	Sagittal	50% keel length at midline	midline	Body
2	Ant. endplate - ventral	Sagittal	Ventral extreme	midline	Body
3	Ant. endplate - dorsal	Sagittal	Dorsal extreme	midline	Body
4	Ant. endplate - lateral	no	Lateral extremes	bilateral	Body
5	Anterior lamina	Sagittal	At margin	midline	Arch
6	Neural spine - ant. base	Sagittal	Anterior base	midline	Processes
7	Neural spine - ant. midheight	Sagittal, dorsal	50% distance from tip to base	midline	Processes
8	Neural spine - ant. top	Sagittal, dorsal	10% distance from tip to base	midline	Processes
9	Neural spine - tip	Sagittal	Dorsal extreme	midline	Processes

10	Neural spine - post. top	Sagittal, dorsal	10% distance from tip to base	midline	Processes
11	Neural spine - post. midheight	Sagittal, dorsal	50% distance from tip to base	midline	Processes
12	Neural spine - post. base	Sagittal	Posterior base	midline	Processes
13	Posterior lamina	Sagittal	At margin	midline	Arch
14	Metapophysis - anterior	no	Anterior extreme	bilateral	Arch
15	Metapophysis - dorsal	no	Dorsal extreme	bilateral	Arch
16	Intervertebral notch	no	Anterior extreme	bilateral	Arch
17	Postzygapophysis - anterior	no	Anterior extreme	bilateral	Arch
18	Postzygapophysis - posterior	no	Posterior extreme	bilateral	Arch
19	Transverse process - ant. base	no	Anterior base	bilateral	Processes
20	Transverse process - ant. midway	Sagittal	50% distance from tip to base	bilateral	Processes
21	Transverse process - ant. end	Sagittal	10% distance from tip to base	bilateral	Processes
22	Transverse process - post. end	Sagittal	10% distance from tip to base	bilateral	Processes
23	Transverse process - post. midway	Sagittal	50% distance from tip to base	bilateral	Processes
23	Transverse process - post. base	no	Posterior base	bilateral	Processes
Curve 1	Margin of caudal endplate	no	20 landmarks	bilateral	Body
Curve 2	Postzygapophysis surface (along plane of endplate)	Transverse	20 landmarks	bilateral	Arch

Twenty curve points were taken on each of four sliding semi-landmark curves, totaling eighty landmarks. Curves were taken on both the posterior endplate and zygapophyses, to describe the shape of the posterior intervertebral joint complex. Curves were drawn bilaterally around the posterior endplate beginning and ending at the sagittal plane of symmetry. Taking landmarks bilaterally ensured that symmetry of the landmarks was preserved throughout the shape analysis. The first and last landmarks of the curve (the superior and inferior intersection with the midline) were

fixed and did not slide. Curves were also drawn on the zygapophyseal joint surface along the transverse plane, midway along the postzygapophyseal joint (Figure 2.2.2). These four curves were collected in Geomagic and exported as thousands of points in an object file. They were then re-sampled using the software 'resample' (Reddy et al., 2006) that calculated 20 evenly spaced landmarks along each curve.

C. Mirroring missing landmarks - Unilateral missing landmarks were estimated using symmetry filling. A plane of symmetry was created through the vertebra, and missing landmark positions were estimated based on their position on the opposite side. This procedure was executed using the OSymm script for R (R, 2009) written by Annat Haber, available through the Stony Brook website (http://life.bio.sunysb.edu/morph/soft-R.html). This code was looped over all the specimens in the analysis using custom code provided for me by Dr. Haber. The majority of missing data constituted broken transverse processes. Since there was large asymmetry in transverse processes, all the landmarks on the whole process were mirrored and never a subset of them.

D. Shape coordinates - Raw landmarks were converted to shape co-ordinates using a two-step procedure. First, size, orientation and position were removed using Procrustes superimposition and the semi-landmarks on the curves were allowed to slide. Next, principal components analysis was used as a data reduction tool to describe most of the variation in just a few variables. See the statistical considerations section for more details on these techniques.

Error study on 3D landmarks - To estimate the error associated with landmark data collection, an error study was conducted on a subsample of two bovid and two felid species (n=12). A large and a small species were selected from each group, represented by three specimens per species (bovids: *Eudorcas thompsonii, Taurotragus oryx*, felids: *Felis sylvestris, Panthera leo*). These 12 specimens were each landmarked three times using the method described above, producing 36 landmark configurations. Visualization of the data via PCA shows that repeats cluster much more closely in shape space than specimens of the same species or different species in both groups (Figure 2.2.3). A multivariate analysis of variance (MANOVA) on the first ten PCs (99% of shape variance) had highly significant effects of both species and specimen ($p<0.0001$). This indicates the method is precise enough to distinguish specimens successfully. Univariate ANOVAs on each Procrustes coordinate were used to identify coordinates with the highest error. Though variation due to repeats was generally small relative to between-specimen variation, there was relatively large variation in the zygapophyses, particularly of felids. Hence, greater care was taken when placing the beginning and end of the postzygapophysis curves, to minimize error.
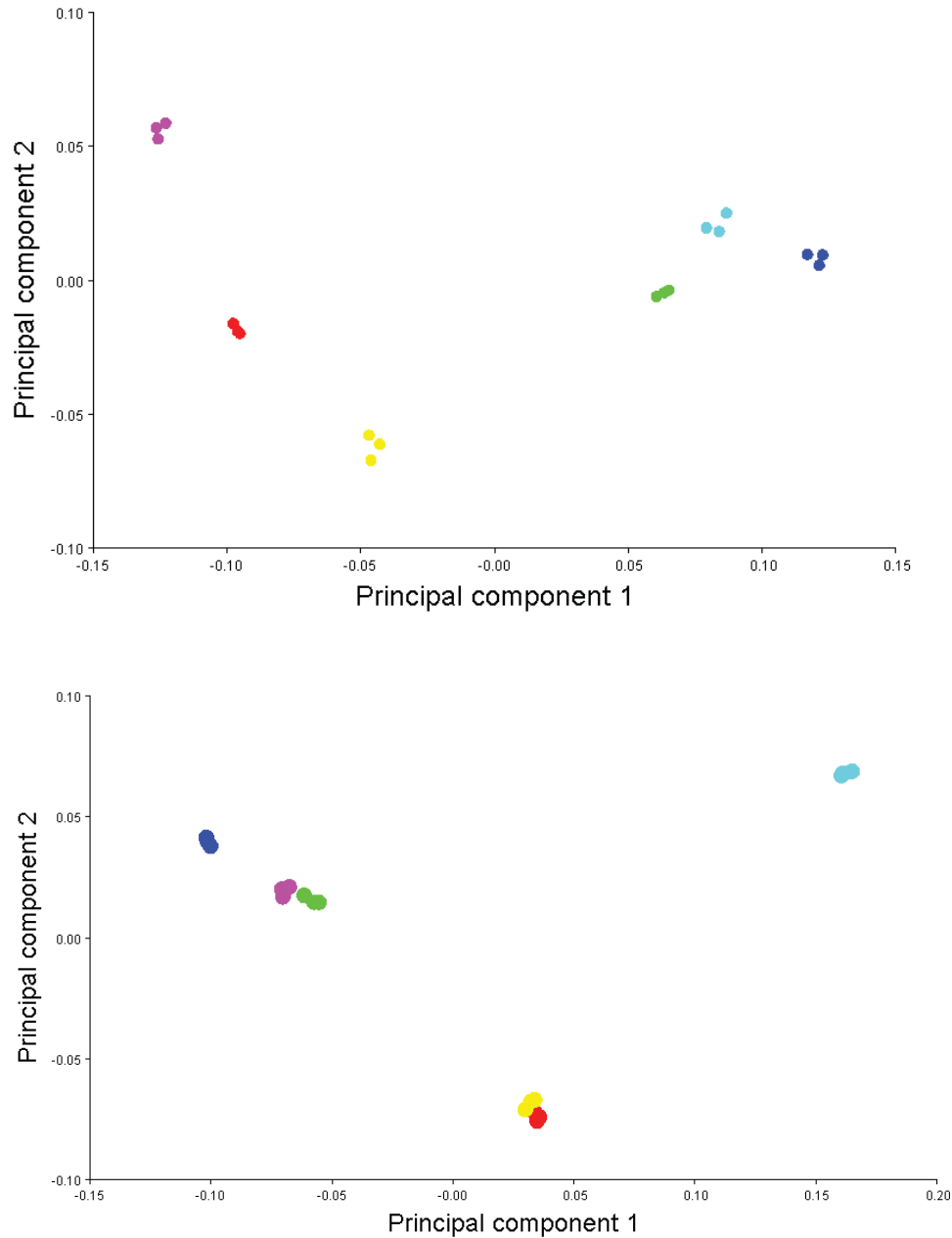
Figure 2.2.3 PC1 and PC2 of principal components analysis of error study data for felids (upper) and bovids (lower).

Each color represents an individual measured with multiple repeats. Note the close clustering of repeats relative to individuals suggesting the error due to the method is less than intraspecific variation between individuals. The variance represented is 73%/11% and 64%/23% for PC1/PC2 of felids and bovids respectively.

Photographs

      Photographs were taken of the caudal view of each vertebra at the six vertebral positions (see Vertebral sample, Section 2.1.2). The vertebra was placed with caudal endplate facing toward the camera on a photography stand. The camera was secured at least 30 cm above the specimen to limit the effects of lens aberration. A scale was placed next to the specimen at the same level as the caudal endplate, using clay where necessary. In addition, a label containing the specimen number and vertebral position was placed within the frame. Of these six photographs, the three lumbar positions—first lumbar, mid-lumbar and last lumbar—were used for data collection in the felid and bovid sample. A total of 556 images of L1, mid-lumbar and last lumbar vertebrae, including 224 felid and 332 bovid images, were examined. Linear measures and 2D landmarks were taken.

      Linear measurements - Six linear measurements and one angular measurement were taken from each photograph in TPSdig (Rohlf, 2005). First the scale bar was used to set the scale in the photograph, and then the following distances were measured: centrum height, centrum width, arch height, neural spine height, transverse process width, zygapophysis width and transverse process angle (Figure 2.2.4, Table 2.2.3). Lateral measurements were always taken on the left side, unless the feature was missing on that side. These measures were used to calculate six new variables (see Table 2.2.3). Transverse process angle was a dimensionless metric. The other parameters were scaled to remove the effect of pure size using square root of the caudal endplate area (CW multiplied by CH). A vertebra-specific size measure was selected for scaling because there were craniocaudal variations in vertebral size that may

overwhelm other types of variation if body mass was used. In particular, endplate area was selected because this has been used to reflect vertebral loading in previous studies (Christian and Preuschoft, 1996; Sanders, 1998; Pierce, 2013). If endplate area itself scales with positive allometry, this scaling measure will result in an underestimate of positive allometric slopes and an overestimate of negative allometric slopes, relative to pure body size. Square-root of endplate area scaled by cube-root of body mass was also calculated as a measure of endplate scaling and craniocaudal variations in the size of the vertebrae.
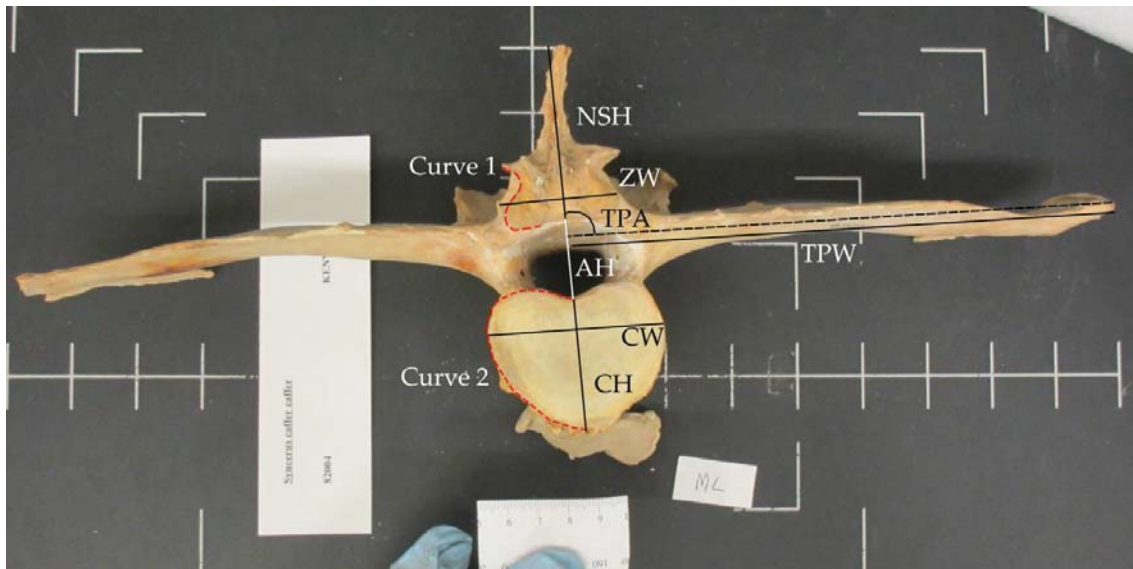
Figure 2.2.4 Photograph of a middle lumbar of* Syncerus caffer *with linear measures (black lines) and 2D curves (red dashed lines).

AH, arch height; CH, centrum height; CW, centrum width; NSH, neural spine height; TPA, transverse process angle (dashed line); TPW, transverse process width; ZW, zygapophysis width. Curves were used to calculate 20 (centrum) and 10 (zygapophyses) 2D semi-landmarks on both left and right sides. Descriptions of linear measures can be found in Table 2.2.3.

Table 2.2.3 Vertebral dimensions calculated from linear measures.
Pure size removed by scaling by square-root endplate area or cube-root body mass. AH, arch height; BM, body mass; LA, lever arm, NSH, neural spine height; TPA, transverse process angle; TPW, transverse process width; ZW, zygapophysis width. Linear measures are shown in Figure 2.2.4.

MEASURE	DESCRIPTION	SCALE
CH	Centrum height	Area
CW	Centrum width	Area
Endplate area	CH * CW	BM
Arch LA	(CH/2) + Arch height	Area
Neural Spine LA	(CH/2) + Arch height + Neural spine height	Area
Transverse process LA	TPW: Tip of transverse process to the midline	Area
Zygapophysis width	ZW: Maximum width of zygapophysis	Area
Transverse Process angle	TPA: Angle between neural spine and transverse process	No

2D Landmarks - Two bilateral curves were drawn on the image: the outline of the endplate and the outline of the zygapophyses, using TPSdig2 (Figure 2.2.4). These curves capture the shape of the intervertebral joint complex, which constitutes both the disc and paired zygapophyseal joints, and is important in determining vertebral mobility. These curves were then resampled to 20 and 10 evenly spaced landmarks, respectively. Only 10 zygapophysis landmarks were taken in this case (as opposed to 20 in the 3D analysis in Chapter Five) because the resolution of the images was relatively lower than that of the 3D scans. Size was removed from these landmark data using GPA, during which the landmarks were allowed to slide into positions which minimized the bending energy of the curve, using the software TPSrelw (Rohlf, 2010) (see statistical considerations).

Error study on linear measures and 2D landmarks - An error study was conducted to estimate the magnitude of error associated with photographing and

measuring specimens. Three small bovid specimens (two *Madoqua kirkii,* one *Redunca arundinium*) were photographed three times over the course of a day. Between each set of photographs the specimens were removed from the photo stand and then set up anew for each repeat. This resulted in three images of first lumbar, mid-lumbar and last lumbar, culminating in a total of 9 images per specimen for three specimens (n=27). Linear measures and 2D landmarks were taken from the images in TPSdig. The effect of position and specimen, relative to measurement and photography error, was tested using a MANCOVA in SYSTAT. Morphology (linear measures or PC scores) were the dependent variables, while vertebral position and species were factors. Specimen was nested as a factor within species.

Linear measures were significantly influenced by both position (p<0.001) and specimen (p=0.012), indicating that the error was sufficiently small that both craniocaudal and between-specimen variation could be detected (Figure 2.2.5). Principal components analysis of the 2D joint shape landmarks resulted in three significant components (83.7%, 10.3% and 2.1% of variation respectively). A similar MANCOVA on these PCA data also resulted in significant effects of position and specimen (p<0.001 for both). Figure 2.2.6 shows that repeated measurements of the same specimen (A, B or C) cluster more closely together in morphospace than specimens or positions (green, red or blue).
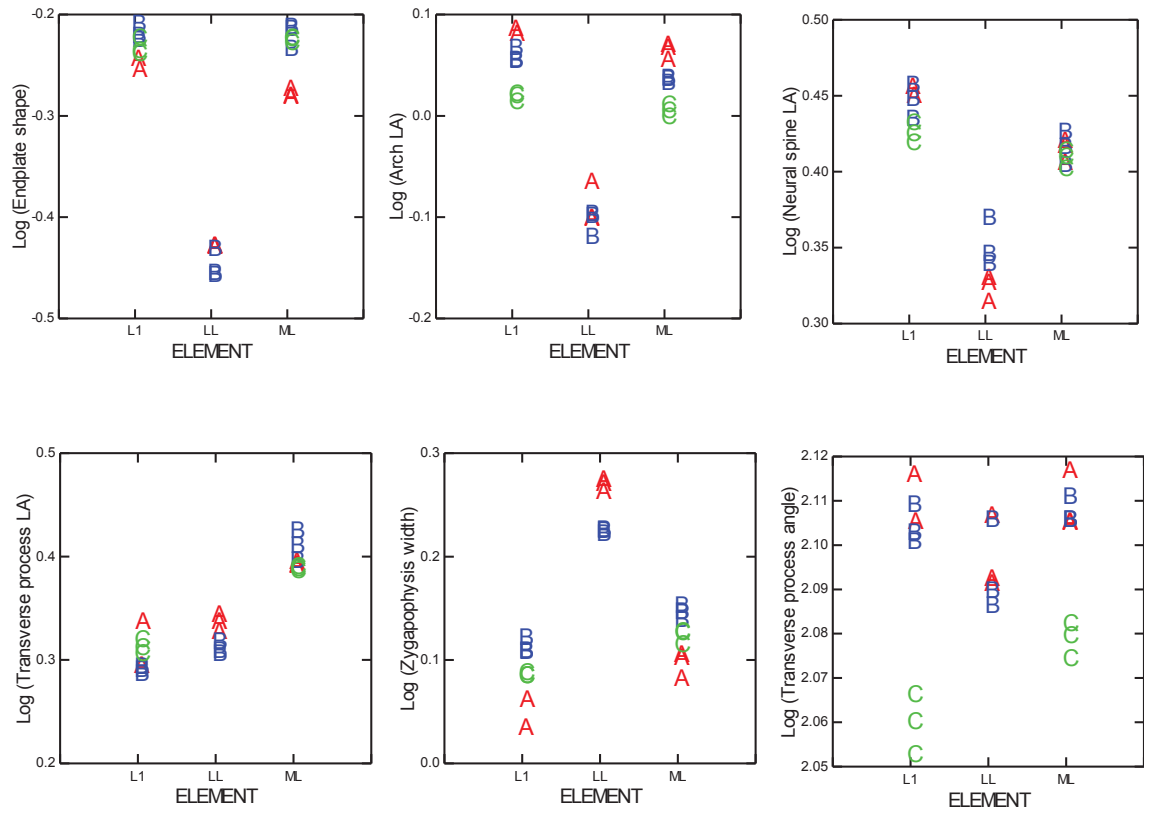
Figure 2.2.5 Error study on 2D linear measures

L1: first lumbar, ML: mid-lumbar, LL: last lumbar. Letters and colors indicate separate specimens (A, B or C). Within-specimen variation is smaller than between-specimen or between-position variation. LA, lever arm. Endplate shape is the ratio of height and width.
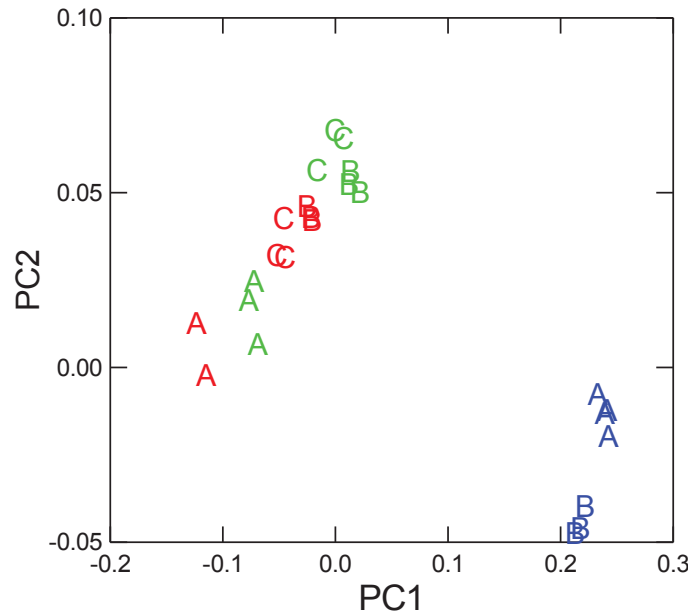
Figure 2.2.6 PC1 and PC2 of 2D landmark error study data.
Letters represent specimens, colors represent position. Red: L1, green: mid-lumbar, blue: last lumbar. Repeats cluster closely together indicating photography and measurement error is relatively small.

2.2.2   EQUID SAMPLE

Data collection for extant equids mirrored that of the felid and bovid sample.

For fossil equids, three-dimensional models were created of all vertebrae available for

study, using the scanning method described above, from which measurements could be

taken directly. Since the exact position of isolated fossil vertebrae could not be directly

assessed, vertebrae were classified as proximal, middle or distal lumbar based on their

morphology, appreciating that these assignments are not exactly equivalent to those of

the extant sample. A number of specimens had complete lumbar regions which allowed

vertebral position to be assessed directly and guided assignment in isolated specimens.

Isolated proximal lumbars were identified by their smaller size, narrow zygapophyses

and short origin for the transverse process (usually broken), whereas distal lumbars

were identified primarily by their articulations for lateral transverse joints. Specimens were frequently broken or distorted. The best preserved portion of the vertebra was the centrum and zygapophyses, whereas the processes were most poorly preserved. Hence, the analysis of fossil equids focused primarily on centrum dimensions and joint shape.

Centrum dimensions were measured directly from the 3D models of the fossil equid specimens in Geomagic (Geomagic Studio, 2010). To assess craniocaudal variation in centrum dimensions of fairly complete skeletons, centrum length, width and height were scaled and plotted against vertebral position to create a "vertebral profile." Centrum width and height were scaled by square-root of centrum area. Centrum length was scaled by the length of the mid-thoracic vertebra where the whole column was available, and L1 where only the lumbar region was available. The scaling metric chosen was arbitrary and was applied to compare the different measures on the same axis, because the purpose of these plots was to examine craniocaudal trends which were unchanged by the scaling.

Shape of the intervertebral joint complex was measured using 2D landmarks taken from curves on the centrum and zygapophyses, as described in the Photographs section (2.2.1.4). For extant equids, the protocol used was the same. However, for fossil equids the method was slightly altered. Instead of using a camera to obtain 2D images, caudal screenshots were taken of the 3D model of the vertebra using the screen capture function in Geomagic (Geomagic Studio, 2010). Each vertebra was aligned such that the caudal endplate was perpendicular to the screenshot and a scale was included. This was useful because many of the fossil specimens were damaged and therefore would have been difficult to place in a correct position on a photostand, but could be easily

manipulated as 3D models. Where one side of the specimen was damaged or missing in the image, the other side was copied, mirrored and used to replace it. Landmarks were subject to GPA and PCA prior to analysis, as described previously.

Lateral transverse joints are additional synovial joints which form between the transverse processes in the posterior lumbar region of equids. Sagittal and mediolateral dimensions of the lateral transverse joints were measured directly from the specimen in Geomagic and used to calculate joint shape, which is the ratio of the sagittal to mediolateral dimension of the lateral joint on one side (Geomagic Studio, 2010). Inclination of the neural spine and transverse processes, where present, were measured from lateral and caudal screenshots of the vertebra in ImageJ (Rasband, 2004).

2.2.3   ADDITIONAL DATASETS

Range of Motion sample
  Experimental data - Maximum intervertebral range of motion (**ROM**) data were taken from the literature for each of the three species which make up the ROM sample, as a measure of joint function (Townsend et al., 1983; Wilke et al., 1997a; Macpherson and Ye, 1998). Data on thoracolumbar function in mammals are relatively rare. These sources were selected because they provide data for the whole thoracolumbar column and use reasonable samples (> four individuals). Maximum range of motion in total sagittal bending, lateral bending and torsion was measured at each of the six positions, where motion is measured in the joint caudal to that position. Additional data were available for dorsiflexion and ventroflexion separately in the cat, and all positions except last lumbar in the sheep. However, it should be noted that the nature of the data collection technique in each study is slightly different.

MacPherson and Ye (1998) used live, sedated cat specimens which were manipulated into positions of maximum dorsiflexion, ventroflexion and lateroflexion and then radiographed to measure the angle at each vertebral joint. Angles were measured from a line directly connecting the two adjacent neural canals, which means that some joints were considered flexed even when they were maximally extended. Wilke et al. (1997) dissected out vertebral columns from sheep cadavers, and then examined bi- or tri-segmental portions, removing muscles but leaving discs and segmental ligaments intact. The range of motion was calculated using a spine tester to produce a loading curve by applying force at a constant rate. Maximum range of motion was measured from the mechanically neutral zone. The authors did not include the lumbosacral joint, which would not fit into their experimental apparatus, so data for that joint were taken from a separate study (Nagel et al., 1991). The latter study used both *in vivo* and *ex vivo* data, but only considered the last lumbar and lumbosacral joints. Similar values were obtained for the last lumbar joint in both studies, suggesting that these data are comparable. Townsend et al. (1983) also used cadaveric horse specimens, but in this case the column was left complete. Pins were placed in vertebrae and the column was photographed while being maximally loaded. Due to the contrasting data collection methods used in these studies, the data were analyzed within each species separately, but were not directly compared between the different taxa.

Morphologic data - To assess craniocaudal variation in lumbar morphology, measurements were collected from the vertebral columns of the cats, sheep and horses from the ROM sample. Linear and landmark data were taken from photographs of the caudal aspect of six vertebrae from each column, as described in the Photographs

section above (2.2.1.4). These photographs were the source of linear measures and 2D landmarks (See 2.2.1.4). Angle of the transverse process was not measured so that thoracic vertebrae could be included. Centrum width and centrum height were combined into endplate shape (height divided by width) to reduce the total number of variables because the number of cases in some of the levels was very small (see variables to cases rule, Assumptions section, 2.4.4).

Osteological range of motion (O-ROM) - The thoracolumbar region of one specimen of each species was 3D laser scanned in order to create a digital model, using the method described above. This model was used to examine osteological range of motion (O-ROM) and 3D bony interactions of the joint caudal to the six vertebral positions. A single specimen was used because scanning is very time-consuming, and intraspecific variation in joint morphology is small compared to the between-species and along-column variation.

To measure osteological range of motion and interactions at a particular joint, digital models of two adjacent vertebrae were created and imported into the same virtual space. The vertebrae were re-oriented such that the major axes of the vertebrae were aligned with the global axes of the model, so that angles of movement could be measured. A small gap was left between the vertebrae to represent the intervertebral disc, whose length was based on data from the literature (Townsend and Leach, 1984; Wilke et al., 1997b) or from direct measurement from radiographs (cat). The center of rotation for the caudal vertebra rotating about the cranial vertebra was defined. Placement of the center of rotation for joint movement can have a large effect on estimated mobility. The center of rotation for cat and sheep joints was placed within the

disc, slightly dorsal to the center of the endplate (Thompson et al., 2003). In the horse, the center of rotation has been measured experimentally and is situated caudal to the joint itself, within the centrum of the more posterior vertebra in the motion segment. However, at the lumbosacral joint it is located in the more typical position within the joint (Denoix, 1999). Though the center of rotation can move during motions at the joint, it was assumed to be stationary to simplify the model.

Maximum angular displacement was measured by rotating the caudal-most vertebra about the cranial-most vertebra until the surfaces of the model touched. This procedure was repeated in four planes: dorsiflexion, ventroflexion, lateroflexion and torsion. Combined movements in multiple planes were not considered, although they likely occur *in vivo* (Denoix, 1999). The maximum angle and vertebral joint structures which first touched were noted. The angle at which this first collision occurred represents the maximum potential range of motion because in life soft tissues may restrict the joint further.

Radiograph sample
The effect of excluding intervertebral spaces on estimating thoracolumbar length was assessed by measuring the length of centra and intervertebral spaces on radiographs using ImageJ (Rasband, 2004). The position of the intervertebral disc was identified by its relationship to related structures such as ribs and the sacrum, and the orientation of the neural spines. Maximum length of the centrum and intervertebral space were measured in lateral view, and each measurement was taken twice and the mean calculated.

2.3 DATA ANALYSIS

In this section I will summarize the data analysis methods used in each chapter to address its specific question. A summary of the analyses implemented in each chapter can be found in Table 2.3.1. Additional details of particular analytical methods are presented in the Statistical Considerations section (2.4).

2.3.1 DOES VERTEBRAL MORPHOLOGY REFLECT RANGE OF MOTION?

Chapter three examines the relationship between vertebral morphology and range of motion in the thoracolumbar region using the ROM sample. Three steps were taken to test if vertebral morphology reflects function: a) bone-bone interactions during joint movement were characterized using a digital model; b) significant differences in morphology along the column within each taxon were tested using a MANOVA; c) the correlation of morphology with range of motion was tested using a Spearman's rank correlation.

To provide insights into which structures might limit intervertebral range of motion, O-ROM was measured from the digital models and qualitatively compared to experimental ROM data. The bone-bone interactions limiting mobility were noted and recorded using screenshots in Geomagic (Geomagic Studio, 2010).

Multivariate analysis of variance (MANOVA) was used to test for significant differences in morphology between the six vertebral positions within each taxon (see statistical considerations 2.4.2.2). Prior to the MANOVA, PCA was run on Procrustes scores (landmarks) and linear measures to reduce the number of dependent variables in the analysis to just a few key axes summarizing shape variation. Principal components that represented more than 95% percent of total variation were included in the

MANOVA. All data were log transformed. Morphologic data were the dependent variables, and vertebral position was the factor (Table 2.3.1). Multivariate significance of the effect of vertebral position on morphology was tested using the Pillai's trace test statistic. Also univariate f-tests were used to examine the influence of vertebral position on individual variables. Significant results indicate that there are shifts in joint morphology along the column. Morphological variation was visualized using scatter plots of PC1 and PC2, and wireframes (landmarks) or variable loadings (linear measures).

To examine the link between form and function, Spearman's rank correlation analyses were run to test relationships of morphologic data with experimental ROM data. Correlation analysis was most appropriate because neither range of motion nor morphology of the joints were predetermined. Non-parametric Spearman's rank was used because this method makes no assumptions about the distribution of the data. This was important because the data were highly non-normal due to the unusual sampling scheme used. In particular, mean range of motion data for each position and species were taken from the literature, whereas morphologic data were collected for multiple specimens of each species, resulting in strongly non-normal distributions. Bonferroni corrections were used to adjust the significance level for the effect of multiple comparisons. This correction reduces the p-value required to reject the null hypothesis because many tests were run. For the landmark data, log-transformed PC scores were used in the correlation analysis, with log range of motion in each plane. For the linear measures, original data were used in the correlation analysis instead of PC scores because this made the results easier to interpret. A two-pronged approach was taken.

First, correlations with only the specific morphologies predicted *a priori* in the

hypotheses were tested. This resulted in relatively few comparisons, which therefore

had greater power to detect differences due to the lower Bonferroni correction-level.

Second, a "shotgun" approach was taken, in which all possible pairs were compared but

Bonferroni correction-levels were much greater.

Table 2.3.1 Summary of the analyses applied in each chapter of this dissertation.

CS, centroid size; LS, least-squares regression; PC, principal component; RMA, reduced major axis regression; ROM, range of motion.

QUESTION	SAMPLE	ANALYSIS	INDEPENDENT VARIABLE	DEPENDENT VARIABLES	HYPOTHESIS TESTED
Does vertebral morphology reflect ROM?	ROM	1.MANOVA 2.Spearman's rank correlation	1. Vertebral position	1. PC scores of landmarks and linear measures	1. shape = position 2. shape ~ experimental ROM
How do thoracolumbar centra scale?	Felid and bovid	1. LS & RMA regression 2. ANCOVA	1. Log body mass 2. Log body mass & Family	1 & 2. Log linear measures (raw and contrasts)	1. dimension=mass 2. dimension = mass + family + mass:family
How does the penultimate lumbar scale?	Felid and bovid	Multivariate regression	1 & 2. Log body mass	1. PC scores (raw and contrasts) 2. Procrustes co-ordinates	1 & 2. shape = mass
How does scaling differ along the lumbar region?	Felid and bovid	MANCOVA	1. Log body mass, position & family 2. Log body mass & position (families separate)	1 & 2. Scaled linear measures (raw and contrasts) 2. PC scores (raw and contrasts)	1. shape = mass + position + family + mass:position + mass:family + position:family 2. shape = mass + position + mass:position
How does the lumbar region scale in extant and extinct equids?	Equid	MANCOVA	1. Log centroid size, position & family 2. Log centroid size & position (equid only)	1 & 2. PC scores	1. shape = CS + position + family + CS:position + CS:family + position:family 2. shape = CS + position + CS:position

86

2.3.2 HOW DO THORACOLUMBAR CENTRA SCALE?

Chapter four compares scaling of ventral column dimensions to predictions of geometric or elastic similarity in the felid and bovid sample. Centrum dimensions were regressed on body mass (estimated from limb dimensions) to provide an estimate of the allometric slope. Slopes were calculated using RMA regression, and compared to results using least-squares and phylogenetically-corrected slopes. Length of the whole thoracolumbar region was estimated by summing centrum lengths. The radiograph sample was used to test if excluding the intervertebral spaces might influence allometry estimates based solely on the centra.

Regression slopes were calculated between ventral column dimensions and body mass in log-log space for each family separately. Species mean values were calculated for thoracolumbar length; region lengths; height, width, and area of the centrum at three vertebral positions; and body mass. Slopes and confidence intervals were then calculated using both least-squares and reduced major axis regressions (see Statistical Considerations, 2.4.2, for comparison) and statistically compared to predicted slopes for geometric and elastic models (SYSTAT 13 for Windows, 2009). Elevation differences between families were tested using an ANCOVA, with family as the factor. In addition, a phylogenetically-corrected series of analyses was run. Independent contrasts were calculated using the PDAP package of Mesquite to felid and bovid phylogenies (See 1.5 Study Groups, and 2.4.3 Correcting for Phylogeny). These data were used to estimate reduced major axis slopes in Mesquite (Maddison and Maddison, 2010). Appropriateness of the branch lengths for calculating contrasts was tested as described in the Statistical Considerations section below (2.4.3).

Intervertebral spaces – The radiograph sample was used to examine the scaling of intervertebral spaces relative to centra. The significance of region and family effects on intervertebral space length was tested using an ANCOVA. Log intervertebral space length was the dependent variable and log centrum length was the covariate, while family and region (thoracic versus lumbar) were factors. Regressions were used to test the slope of log intervertebral space length on log centrum length for each region. Felids and bovids were pooled in this analysis because of the limited sample sizes for which radiographs were available. A slope of one in this analysis would indicate the centrum and intervertebral spaces were scaling similarly. This would show that excluding the intervertebral space from length estimates (as is necessary when calculating length from osteological specimens, as above) has little effect on estimating the scaling exponent of length, and provides a validation for the use of osteological measures for this purpose.

2.3.3   HOW DOES THE PENULTIMATE LUMBAR SCALE?

Chapter five characterizes the allometry of the penultimate lumbar vertebra in three dimensions using the felid and bovid sample. Three-dimensional landmarks were used to measure the shape of the penultimate lumbar vertebra (see Data Collection, 2.2.1.3). Shape variables were regressed on log body mass, which was estimated from limb dimensions (2.2.1.1). Lumbar allometry was tested in two ways: a) Significance of the influence of size on shape was tested using a multivariate regression of principal component scores on body mass, and b) the shape most correlated with size was visualized by creating an allometric vector using multivariate regression of all Procrustes co-ordinates on body mass. To correct for phylogeny, independent contrasts of PC scores and body mass were also used. The relative influence of size on different

regions of the vertebra was assessed using separate regressions on the body, arch and processes.

Generalized Procrustes analysis (GPA) was run on landmarks for each family separately. This was because the zygapophyses were revolute to interlocking in bovids but close to flat in felids. Therefore, the curves in these two groups were not equivalent, and attempting to include them in one Procrustes fit led to bunching of the landmarks during the sliding process. Hence, the analyses were kept separate when the zygapophyseal curves were very dissimilar. Landmarks were symmetrized and species-mean shapes were calculated in MorphoJ (Klingenberg, 2011b). Principal components describing 95% of total variation were then used as dependent variables in a multivariate regression against log body mass to test the relationship of size to lumbar shape.

To correct for phylogeny, the contrasts of mass and PC scores were calculated in Mesquite (Maddison and Maddison, 2010). Next, a multivariate regression on body mass, through the origin, was conducted on the contrasts in SYSTAT (SYSTAT 13 for Windows, 2009). This tests the significance of the relationship of shape to size when the effects of phylogeny have been removed. To investigate allometry of different vertebral regions, modularity of the vertebra was tested. Autonomy of the centrum, arch and processes as modules was tested by comparing within-module co-variation to between-module co-variation (see Table 2.2.2 for landmark assignments). This value, known as the "RV coefficient," was compared to the RV coefficient calculated from 10,000 randomly generated, contiguous partitions of the landmarks in MorphoJ to test its significance (Klingenberg, 2011a). If modularity was detected, then the allometric

analysis was rerun on the landmarks from each module separately, and the percentage variance explained by size in each module calculated.

The allometric vector was calculated using a multivariate regression of all Procrustes coordinates on log body mass. This method preserves all of the shape variation in the sample because no shape is excluded (i.e., when low PCs are excluded in the PCA multivariate regression). Therefore, it allows reconstruction of the shape changes which are most correlated with body mass. Wireframes were used to visualize the allometric vector in MorphoJ (Klingenberg, 2011b).

2.3.4 How does scaling differ along the lumbar region?

Chapter six examines allometry at three vertebral positions within the lumbar region, using the felid and bovid sample. Morphology of the lumbar region was assessed using photographs from three lumbar positions, which were used to generate 2D landmarks and linear measures (see Data Collection, 2.2.1.4). The influence of family, position and body size on morphology was tested using MANCOVAs.

Species-mean values were calculated from principal component scores from 2D landmark data and scaled linear measurements. Principal components representing 95% or more of the total variation were selected for the landmark analysis of joint complex shape. Species-mean log body mass was calculated using estimates based on limb dimensions (2.2.1.1). Procrustes fits and subsequent analyses of landmarks were kept separate for felids and bovids to avoid homology problems, as described above. To test craniocaudal variation in allometry, morphological data were used as dependent variables in a MANCOVA, in which log body mass was the covariate and position and

90

family were factors. Significant effects of body mass indicated allometry, whereas significant effects of the factors indicated elevation differences between families or vertebral positions. Significant interactions between body mass and factors indicate differences in allometry between vertebral positions or families. Since there were significant slope differences between families, the linear measurements MANCOVAs were rerun on each family separately with only position as a factor (equality of slopes assumption, see Statistical Considerations section, 2.4.4).

To correct for phylogeny, independent contrasts were calculated in Mesquite. These contrasts were then used as dependent variables in a MANCOVA through the origin in SYSTAT, with a similar design to that used for the raw data (SYSTAT 13 for Windows, 2009; Maddison and Maddison, 2010). This provides an estimate of the allometric relationships when the effect of phylogeny is removed. Branch length assumptions on contrasts were tested prior to analysis (see Statistical Considerations).

2.3.5 HOW DOES THE LUMBAR REGION SCALE IN EXTANT AND FOSSIL EQUIDS?

Chapter seven investigates allometry of the equid lumbar region using the equid sample. Lumbar vertebrae were examined from eight genera of fossil horses spanning their taxonomic, temporal and size range, and their morphology was described. Images of these vertebrae were used as the source for 2D landmarks, which were compared to similar data from bovids, representing extant ungulates of a comparable size range (see Data Collection, 2.2.1.4). The influence of size, position and family on joint shape was tested using a MANCOVA, with centroid size as a size proxy. Size of the lateral transverse joints and orientation of the processes was also measured and compared among taxa.

Lumbar vertebrae were qualitatively described and compared among the eight key genera examined. Centroid size (taken from landmarks during Procrustes fit, see Statistical Considerations, 2.4.1) was used as a proxy for vertebral size, as many specimens lacked associated limb material from which to estimate body mass. The effect of size and position on equid lumbar joint shape was quantitatively tested using two MANCOVAs. First, joint landmarks for equids and bovids were combined in a single Procrustes fit and principal components analysis. Species-mean PC scores were used as dependent variables in a MANCOVA, with log centroid size as the covariate and family and position as factors. Second, this analysis was rerun on equids only, after a separate equid-only Procrustes fit. The shape of the lateral transverse joints at penultimate and last lumbar vertebrae was compared to size using an ANCOVA, to test for allometry. Angles of the transverse and spinous processes were qualitatively compared among genera due to low sampling of these features.

2.4 STATISTICAL CONSIDERATIONS

This section provides additional information on the data analysis methods used in this dissertation and their associated assumptions.

2.4.1 GEOMETRIC MORPHOMETRICS
Sliding semi-landmarks

When clear homologous landmarks are hard to define, sliding semi-landmarks can be used (Zelditch et al., 2004). These are landmarks which are placed along a curve or surface, but are allowed to "slide" until they reach a "best position" as defined by a particular optimality criterion (Adams et al., 2004). Sliding semi-landmarks were used to describe the shape of the caudal endplate and zygapophyses by placing two bilateral curves along their surfaces (four in total), which are functionally important but difficult to describe using standard type 2 landmarks. First, landmarks were placed at equal distances along the curve; then they were allowed to slide during the GPA step (see below). Minimized bending energy was used as the optimality criterion, which has a number of favorable properties (Bookstein, 1997). Once the points have been slid they may be treated in the same way as the other fixed landmarks.

The sliding semi-landmark method for capturing complex shape has been used extensively on post-crania (e.g., De Groote et al., 2010; Fabre et al., 2013; Sylvester, 2013; Gould, 2014). It is preferable to static (traditional) semi-landmarks because bending energy is a more meaningful measure of equivalency between specimens than the absolute distance from the beginning of the curve. As sliding occurs along a tangent to the curve, not on the curve itself, it is essential to take sufficient sampling of landmarks. Therefore curves were sampled densely enough to properly represent the

curvatures. This method results in a relatively greater sampling of landmarks from the joint surface than the rest of the vertebra. However, examination of the principal components of variation (from PCA) suggests that the semi-landmarks are not dominating the variation patterns, which is likely because they strongly co-vary with one-another.

Generalized Procrustes analysis (GPA)

Geometric morphometric data were collected in the form of 2D or 3D landmarks. However, in order to analyze these data they must first be converted into shape coordinates, which allows specimens collected in separate shape spaces to be directly compared. Here I used a two step protocol of Procrustes superimposition followed by principal components analysis. To calculate shape coordinates, the landmarks were first brought into the same shape space by generalized Procrustes analysis (GPA). This method minimizes the distance between the same landmarks in different specimens. Landmarks were scaled, translated and rotated in order to superimpose the specimens onto one another. Each specimen was scaled to a similar size and the scaling factor, known as the centroid size, was saved as a measure of its original size (Zelditch et al., 2004). GPA and landmark-sliding were carried out using the GPAgen command in the software geomorph for 3D landmarks (Adams and Otarola-Castillo, 2013) and in TPSrelwar for 2D landmarks (Rohlf, 2010). The new, superimposed landmarks (known as Procrustes coordinates) were imported into MorphoJ for subsequent analysis. Object symmetry was imposed on the landmarks by separating symmetric and asymmetric components of the variance (i.e., they were symmetrized; (Klingenberg, 2011a).

Principal components analysis (PCA)

Once the landmarks were converted into shape co-ordinates, or Procrustes co-ordinates, they were ready to analyze. However, when there are many landmarks, there are also many Procrustes co-ordinates. In the case of 3D landmarks, there will be three times the original number of landmarks. Therefore it is advantageous to reduce the number of variables prior to analysis using dimension reduction techniques. Here I used principal components analysis to summarize the variation in all the Procrustes coordinates using just a few variables. This technique does not alter the position of the specimens relative to one another in shape space, but instead produces new axes from combinations of the variables. These new variables, known as principal components (PCs), are independent of one another. Each PC describes relatively less variance, such that the first few PCs usually describe the majority of the variation in the dataset (Zelditch et al., 2004). How concentrated the variation is on a few axes depends upon how integrated the data are, or how much co-variation there was in the Procrustes coordinates. By analyzing just the top PC's, the majority of variation can be included in the analysis, while drastically reducing the number of variables analyzed. However, some variation is inevitably excluded by this method (<5%). PCA was performed in MorphoJ on symmetrized landmarks (Klingenberg, 2011b).

2.4.2 TESTING RELATIONSHIPS BETWEEN VARIABLES

Correlation

In order to understand the relationship of two variables to one another, such as size and shape, univariate correlation or regression may be used. Correlation does not assume that one variable is dependent upon the other, but rather measures the degree of

association between the variables. Its application is most appropriate where both variables are measured and neither has been controlled or determined *a priori.* In contrast, regression analysis describes the dependence of the Y variable on the predictor X, assuming there is a causal relationship.

A correlation analysis measures the relationship of two variables using a correlation coefficient (r), which can vary from zero (no relationship) to either minus one or plus one (perfect negative and positive relationship respectively) (Zar, 1999). Spearman's rank is a non-parametric correlation analysis which ranks the cases in both variables, then calculates their association based on the distance between their rankings. Spearman's rank does not require normality or linearity, only that variables are monotonic, i.e., as one increases so does the other (Zar, 1999). Significance of the relationship was determined using a bootstrap analysis on 1000 resamples to produce a probability that the variables are not correlated in SPSS (SPSS for Windows, 2001).

When many univariate comparisons are carried out simultaneously the chance of obtaining a p-value of 0.05 or less purely by chance increases. Therefore, a Bonferroni correction was applied to the alpha level, such that the acceptable p-value for significance was alpha of 0.05 divided by the number of comparisons. This ensures that the significance levels exceed those expected from comparisons of many unrelated variables. Correlation coefficients, p-values and Bonferroni corrected alpha levels were reported.

Regression

Regression analyses determine the dependence of Y on X by fitting a line whose

slope reflects their relationship. Two types of regression are commonly used: least-squares and reduced major axis (RMA). Least-squares regression fits the line based on summed-square errors only on the Y axis, whereas RMA takes into account error on both the X and Y axes. An RMA regression was preferable to least squares because there was likely error on both the X and Y axes in this case, due to errors in the estimation of body mass; but both were calculated for comparison and should produce similar results if the correlation is high. Standard errors and confidence intervals on the slope were calculated (Zar, 1999) and the difference of each value from its predicted slope was tested. All analyses were carried out in SYSTAT (SYSTAT 13 for Windows, 2009).

Multivariate regression - When morphology cannot be described adequately using a single variable, it is better to use a multivariate regression. This analysis determines the relationship of multiple dependent (shape) variables on a single independent variable, in this case size. Slopes and intercepts are estimated for every independent variable. Here, multivariate regression was used on both Procrustes coordinates and PC scores as dependent variables in MorphoJ in Chapter 5 (Klingenberg, 2011b). Using PC scores was more suitable for parametric testing because the number of variables was less than the number of specimens. However, the analysis with Procrustes coordinates was also useful as it allowed reconstruction of the shape associated with size, or allometric vector.

Including a factor: ANCOVA and MANCOVA - In some cases it was necessary to include one or more categorical predictor variables, known as factors, to test for differences in elevations or slopes. Analysis of covariance (ANCOVA) or

multivariate analysis of covariance (MANCOVA) tests the influence of both

continuous and categorical variables on one or more dependent variables. These

analyses can test for differences in elevation between the levels of the factors (factor

effect), significance of the slope (covariate effect) as well as differences in slopes

between the levels (interaction of covariate and factor), and differences in magnitudes

of elevations between the levels (interaction of factors). A full model tests the

significance of both the slope of the covariate, any elevation differences between the

factors and any interactions. The multivariate significance of the model was tested

using the Pillai's Trace statistic in SYSTAT (SYSTAT 13 for Windows, 2009). Where

interactions were insignificant they were removed from the model.

2.4.3   CORRECTING FOR PHYLOGENY

Statistical analyses assume that all data points included are independent of one

another. However, the hierarchical nature of evolution means that some species in a tree

have been evolving independently for a longer time period than others (Felsenstein,

1985; Grafen, 1989; Garland et al., 1993; Garland and Ives, 2000).This can result in

non-independence of the data at the tips of the tree, i.e., the species means. Moreover,

evolutionary transitions that occurred once at a phylogenetic node will be falsely

represented as multiple occurrences in each of the descendant taxa, which is known as

phylogenetic pseudo-replication. To take into account the phylogenetic non-

independence of taxa on the relationships of morphological traits with size, I used

phylogenetic independent contrasts analysis (PIC) (Felsenstein, 1985). Instead of using

values from the terminal branches or tips of the tree, PIC calculates the contrasts

between branches at each node. These new data points are truly independent of one

another and were used as the basis for a new regression analysis. PIC is equivalent to phylogenetic generalized least squares with strong phylogenetic signal, when Brownian motion is assumed.

All analyses were run in the Phenotypic Diversity Analysis Program (PDAP) module for Mesquite (Maddison and Maddison, 2010). Relationships and branch lengths of felids and bovids used in this analysis were taken from the literature, as described in the Introduction (Hassanin and Douzery, 1999; Fernandez and Vrba, 2005; Nyakatura and Bininda-Emonds, 2012; Bibi, 2013). Once generated, contrasts could be exported from Mesquite and used as data in any of the above-described analyses. However, regressions run on contrasts must always be run through the origin, so the effect of the constant was removed from the model (Garland et al., 1992).

All contrasts were standardized by the standard deviation of their branch lengths. To ensure proper standardization, the branch lengths used must meet certain criteria for each variable. The most accepted method for testing validity of branch lengths is to ascertain that there is no correlation between the absolute contrasts and the square-root of the sum of the branch lengths. If this criterion is not met, branch lengths may be transformed, either by log-transform or using a Grafen-rho transformation. To test which transformations were appropriate for my data, I calculated the correlation coefficient between absolute contrasts and square-root sum of corrected branch lengths for each variable under analysis using raw, log-transformed and Grafen rho transformed branches. Whichever had the lowest correlation coefficient was most appropriate (Christiansen, 1999b). Frequently, different variables had better fits with different branch lengths. However, for multivariate analyses all branch lengths must be the same

in order to compare variables, so a single transformation with the most low correlations was used for all variables (Garland et al., 1992).

2.4.4 ASSUMPTIONS

In order to use inferential statistics to test how well a model fits a set of data, several assumptions must be met:

Random sampling

Each measurement in the sample is a random pick from a larger population without bias toward one particular subset of the population. I minimized this problem with my experimental design by selecting species from throughout the size range of the groups of interest and sampling as broadly as was permitted by the availability of specimens.

Independence of measurements

Each measurement should represent a unique and independent draw from the population. There are two ways in which this is problematic in natural history studies. First, there is non-independence due to phylogenetic relationship. This was addressed using phylogenetic independent contrasts analysis, which uses contrasts between taxa instead of tip values and is explained above (Section 2.4.3). Second, there is non-independence due to morphological integration. Vertebrae at different positions are correlated with one another due to serial homology. The effects of pseudo-replication were limited by sub-sampling vertebrae that are spaced far enough apart to have relatively independent morphology.

Observations to variables rule

There should be more observations than variables when using parametric

statistics. The large sample sizes collected here ensured that this rule was adhered to, except in the case of Procrustes coordinates in which variables were numerous. In this case a non-parametric test of relationship was used, and the data were reanalyzed after data reduction using Principal Components Analysis.

Linearity

Where relationship of one variable to another is being tested using regression or ANCOVA designs it is very important that the relationship between the variables is linear. Non-linearity will lead to inappropriate estimations of slope and fit. Non-linear variables can often be made linear via log transformation. Linearity was tested by examining a plot of residual versus predicted regression values and looking for a 'bowed' distribution (Zar, 1999).

Normality

A normal distribution is assumed a) for the residuals about a regression and b) within the factors for both univariate and multivariate samples. Normality of the error distribution or of univariate continuous variables was tested using a Shapiro-Wilk Test, with the null hypothesis of normality. For multivariate distributions, marginal normality of individual variables was tested for each variable using Shapiro-Wilk, and the joint normality was tested using the Mardia skewness and kurtosis measures. Normality can be improved by log-transforming the data or removing outliers. However, in MANOVA departures from normality have only a slight effect on the type I error rate (Zar, 1999).

Equality of variances and co-variances

Where multiple groups or factors are being compared it is assumed that each group has similar variance, an assumption known as homoscedasticity. This can be

tested using a Levene's test, with the null hypothesis of equal variances. Variance models such as ANOVA (particularly the Pillai's Trace statistic) are fairly robust to small variations in variance.

Equality of slopes

Where a covariate is included as well as factors, it is also important that the relationship between the covariate and dependent variables is similar across the groups (similar slopes) when testing for differences between factors. Similarity of slopes was tested by first including in the model an interaction between the covariate and factors. If this interaction was large, slopes varied between the groups, and elevation differences between the groups could not be tested by the ANCOVA. However, since sample sizes here were large, there was high power to detect small significant differences in slope, even though they may be too small to affect the elevation analysis. If slope differences between levels seemed very large, the analyses were run separately for each level.

CHAPTER 3: FORM AND FUNCTION IN THE THORACOLUMBAR REGION

This chapter is a preliminary investigation of the link between form and function in the thoracolumbar region of three representative model species of my families of interest: Felidae (the cat *Felis catus)*, Bovidae (the sheep *Ovis* spp*.)* and Equidae (the horse *Equus caballus*). Experimental data on joint range of motion were taken from the literature as a measure of vertebral function in these species. Joint mobility at six positions along the thoracolumbar column was then related to bony morphology in three ways: 1. Digital models were created and used to examine bone-to-bone interactions during various movements; 2. Joint shape (measured using 2D landmarks) was correlated with mobility; and finally 3. Linear measurements thought to reflect biomechanical function of the centrum, arch and processes were correlated with mobility.

3.1   HYPOTHESES

In this chapter I explore whether **vertebral morphology reflects range of motion in these three mammal species** by addressing the following specific hypotheses:

H1. Sagittal range of motion is correlated with morphology. Specifically, it may be restricted:

A) in dorsiflexion by impaction of the zygapophyses, tension in the ventral longitudinal ligament and compression of the dorsal portion of the disc (Gál, 1993; Denoix, 1999).

B) in ventroflexion by tension in the supraspinous ligament, ligamenta flava

and dorsal longitudinal ligaments, and compression of the ventral disc (Gál, 1993; Long et al., 1997; Denoix, 1999).

Thus it is predicted that low sagittal mobility is correlated with one or more of the following features: a tall arch with dorsally-placed zygapophyses, a tall endplate, a strong ventral keel, a tall neural spine and horizontal zygapophyses (Townsend and Leach, 1984; Boszczyk et al., 2001; Molnar et al., 2014).

H2. Lateroflexion is restricted by tension in the intertransverse ligaments, compression in the lateral portion of the disc and impaction of the zygapophyses (Denoix, 1999). Therefore, it is predicted that limited lateroflexion should be correlated with a wide transverse process, widely spaced zygapophyses or a wide endplate (Boszczyk et al., 2001).

H3. Torsion is restricted by impaction of the zygapophyses (Shirazi-Adl, 1994; Russo, 2010). Therefore limited torsion should be correlated with sagittally-oriented or wide zygapophyses (Boszczyk et al., 2001).

3.2   RESULTS

3.2.1   EXPERIMENTAL DATA

Range of motion (ROM) data for cats, sheep and horses were taken from the literature. The methodologies used in collecting the experimental data for each species were compared in the methods section (2.2.3.1). Data are shown in Figure 3.2.1 and Table 3.2.1, where the joint is named according to its more cranial vertebra. Joint abbreviations are as follows: T1, first thoracic; MT, mid-thoracic; D, diaphragmatic; L1, first lumbar; ML, mid-lumbar; LL, last lumbar. Vertebral range of motion was highly variable between the species and along the column. Total sagittal range of motion for the entire thoracolumbar column for these species was 218º, 152º and 82º for the cat, sheep and horse respectively.

Joint mobility in the cat thoracolumbar region was measured in dorsiflexion, ventroflexion and lateroflexion, from a position in which adjacent centra form a straight line, in live, sedated animals (Macpherson and Ye, 1998). Maximum flexion was the position the sedated animal could reach during manipulation by the experimenter. Dorsiflexion and ventroflexion were inversely related to each other, but overall sagittal mobility was high throughout the column (Macpherson and Ye, 1998). In the anterior thoracic region, dorsiflexion was greater, with relatively limited ventroflexion and moderate lateroflexion. Though exact angles of torsion were not measured, this study reported that high levels of torsion occurred between T4 and T11, totaling 180º of total flexion. The posterior thoracic region was habitually ventroflexed such that even when maximum dorsiflexion was applied, the joint did not reach the neutral position (when adjacent centra form a straight line). High ventroflexion was possible in this region.

The lumbar region was capable of high to moderate ventroflexion and moderate to low dorsiflexion. Lateral flexion at the lumbosacral joint was too small to measure and so was recorded as 0.01° in the subsequent analysis.

Sheep vertebral joints were measured in excised cadaveric material, using a material properties tester, and maximum range of motion was determined from their load-deformation curves (Wilke et al., 1997a). Sagittal mobility of the sheep was slightly higher in the lumbar region, and significantly higher at the lumbosacral junction. Although the lumbosacral data are from a different study than the rest of the column, Nagel et al. (1991) compared the lumbosacral junction with the lumbar-lumbar joints and found very similar levels of sagittal mobility to Wilke et al. (1997a), justifying inclusion of these data here. Unlike in the cat, dorsiflexion and ventroflexion in the sheep were evenly distributed about each joint, which likely reflects the fact that the bending neutral zone was measured mechanically and not geometrically in this study. This reinforces the fact that these data are not directly comparable and should be analyzed separately. Lateral mobility is moderate throughout and slightly higher at T1. Torsion in the sheep spine was entirely restricted to the pre-diaphragmatic vertebrae.

The horse data also come from cadaveric specimens, whose maximum bending by manual manipulation was recorded using photographs (Townsend et al., 1983). Of the three species examined here, the horse had the most restricted spine in terms of sagittal mobility. In fact, sagittal mobility was almost entirely restricted to the lumbosacral joint, where levels were relatively similar to those of the sheep. Elsewhere in the thoracolumbar column, sagittal mobility was negligible, except at T1. In contrast, lateral mobility was relatively high in the horse, reaching a maximum of 10° around the

mid-column. Torsion was quite restricted and reached a maximum of 5º in the posterior thoracic region, which consists entirely of pre-diaphragmatic vertebrae in this species.

Table 3.2.1 Range of motion data from the literature.

Range of motion in degrees. DFL: Dorsiflexion, VFL: Ventroflexion, SAG; total sagittal, LAT: Lateroflexion, TOR: Torsion. For DFL and VFL in the cat, negative values indicate degrees of dorsiflexion away from the zero position, whereas positive values indicate a ventroflexed position. The zero position for the joint in this case is when the adjacent centra form a straight line, and does not necessarily correspond with the neutral position for bending. In contrast, for the sheep absolute value of dorsiflexion and ventroflexion, from a mechanically neutral position, are cited.

SPECIES	POSITION	DFL	VFL	SAG	LAT	TOR	SOURCE
CAT	First thoracic	-22	2	23			Macpherson and Ye (1998)
	Mid-thoracic	-13	3	17	3		
	Diaphragmatic	-1	6	6	3		
	First lumbar	-1	11	11	4		
	Mid-lumbar	-3	7	8	2		
	Last lumbar	-3	7	8	0.01		
HORSE	First thoracic			7	2	3	Townsend et al. (1983)
	Mid-thoracic			3	8.5	4	
	Diaphragmatic			3.5	5	1.8	
	First lumbar			2	4.5	1.8	
	Mid-lumbar			2	3	1	
	Last lumbar			23	0.5	2.5	
SHEEP	First thoracic	3.5	4.6	8.1	12.9	10	Wilke et al. (1997)
	Mid-thoracic	3.0	3.5	6.5	6.2	7.0	
	Diaphragmatic	1.9	2.6	4.5	6.2	4.3	
	First lumbar	4.0	5.7	9.7	6.2	1.3	
	Mid-lumbar	4.0	4.6	8.6	4.3	0.7	
	Last lumbar			20			Nagel et al. (1991)
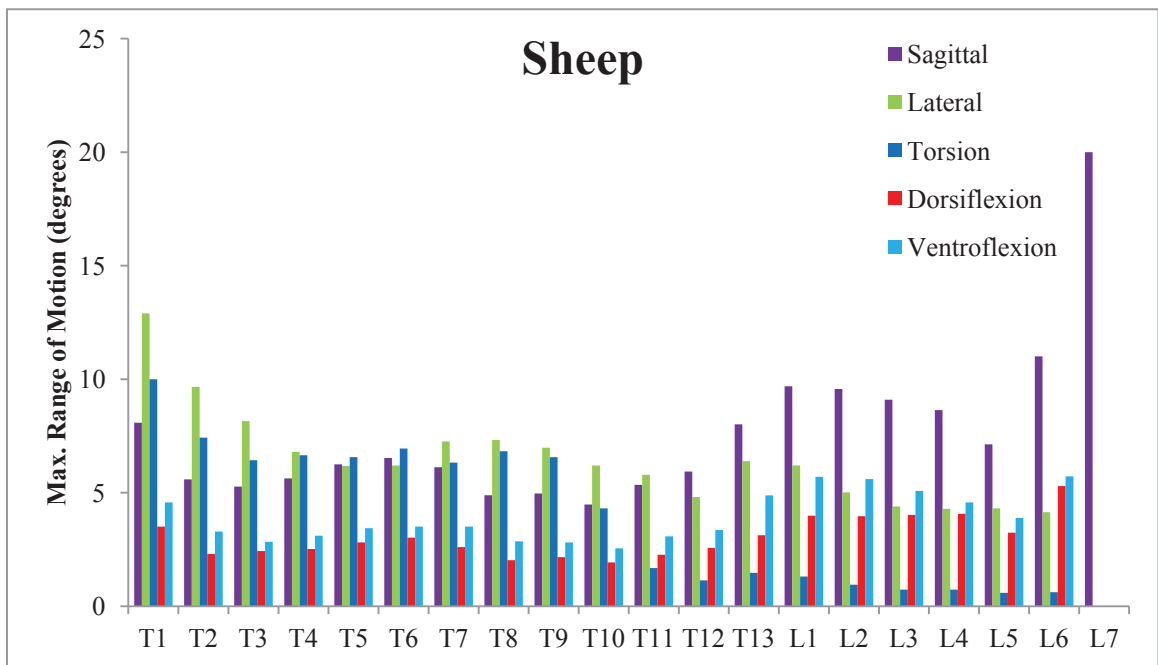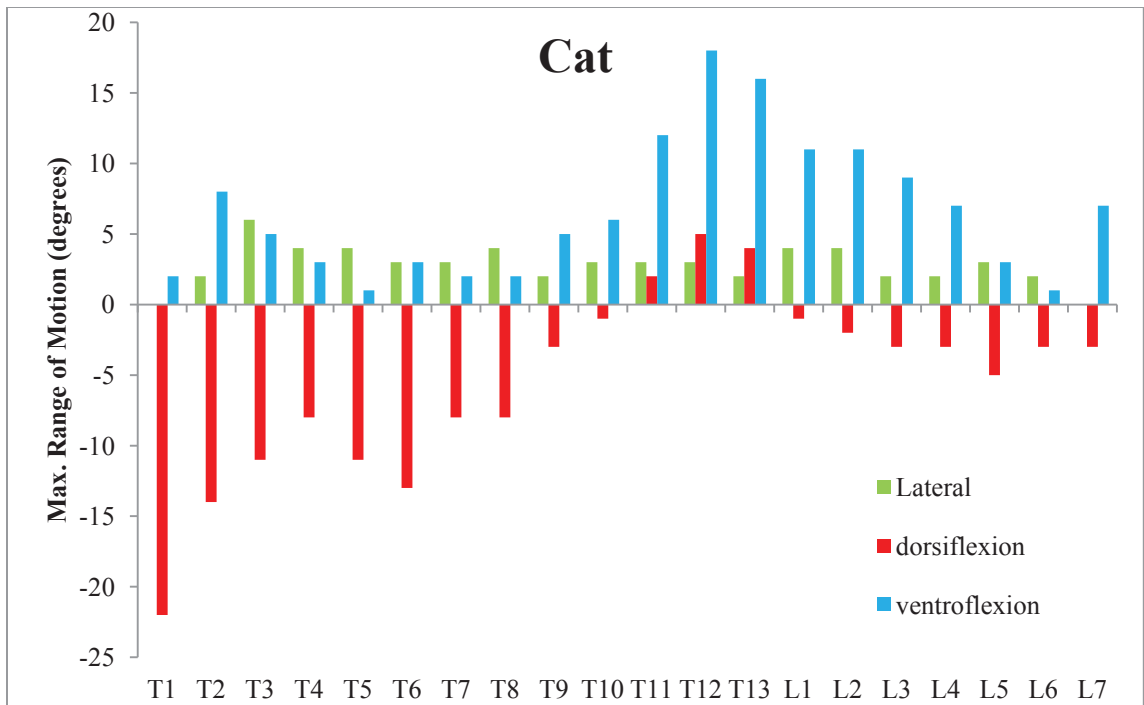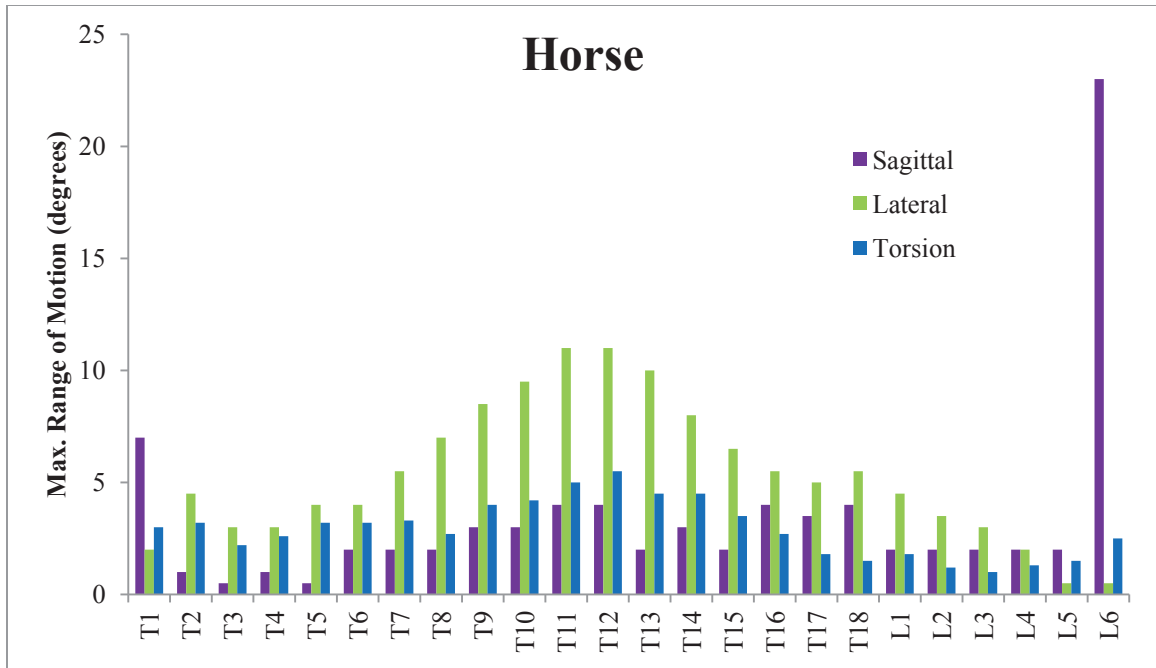
Figure 3.2.1 Range of motion in degrees.
Separate dorsiflexion and ventroflexion data were available for the whole column in the
cat and all but the last lumbar in the sheep. For the cat, negative values indicate degrees
in dorsiflexion from a position in which the centra form a straight line, while positive
values indicate ventroflexion from the same position. Note relative emphasis of sagittal
mobility on the last lumbar joint in the sheep and horse, and inverse relationship between
dorsiflexion and ventroflexion in the cat.

3.2.2   DIGITAL MODELING OF BONY JOINT INTERACTIONS

Three-dimensional models were created of the first thoracic, mid-thoracic,

diaphragmatic, first lumbar, mid-lumbar and lumbosacral joints by positioning models

of two adjacent vertebrae into articulation. Osteological range of motion (OROM) was

measured and the bony features restricting mobility were observed. Details of the

centers of rotation and intervertebral spacing used can be found in the Methods section

(2.2.3.1) and Table 3.2.2. Results are described in Table 3.2.2 and compared to the

experimental range of motion data in Figure 3.2.5, Figure 3.2.6 and Figure 3.2.7.

OROM in the cat was limited by zygapophyseal contact in dorsiflexion, lateroflexion and rotation, and by contact of the ventral body in ventroflexion (Table 3.2.2, Figure 3.2.2). When OROM data are compared to experimental ROM, it is clear that OROM drastically overestimated mobility for some measures (Figure 3.2.5). This suggests that soft tissues play an important role in limiting mobility *in vivo*. OROM dorsiflexion patterns closely reflect both experimental dorsiflexion and total sagittal mobility patterns. Similarly, high torsion in the posterior pre-diaphragmatic region (reported qualitatively in the original study) was mimicked by the model. In contrast, Lateroflexion in the digital model was a poor match for the experimental data. These patterns suggest that these zygapophyseal interactions are important for limiting torsion but not lateroflexion *in vivo*.

A similar pattern of bone-bone interactions was seen in the sheep joints. Zygapophyses limited dorsiflexion, lumbar lateroflexion and torsion, whereas the centrum limited ventroflexion and thoracic lateroflexion (Table 3.2.2, Figure 3.2.3). During dorsiflexion the inferior portion of the zygapophyses made contact, whereas during lateroflexion and torsion the superior portion of the facet also touched. OROM estimates of sagittal mobility roughly reflected experimental values, though they are an overestimate in all except dorsiflexion (Figure 3.2.6). High lateroflexion seen in thoracic region of the model did not match experimental data, suggesting that soft tissues or ribs restrict lateroflexion in the thoracic region. Interactions of the zygapophyses in resisting torsion in the digital model provided a close estimate to real mobility patterns in the sheep.

In the horse, dorsiflexion was limited by the zygapophyses, whereas

110

ventroflexion was limited, where it could be estimated, by the ventral body (Figure

3.2.4). Lateroflexion was limited by the lateral body, zygapophyses or transverse

process joints at the last lumbar position, and torsion was limited by the zygapophyses.

Morphology of the zygapophyses permitted far greater dorsiflexion at the last lumbar

joints than more cranial lumbar joints. OROM estimates of joint mobility fit

experimental data best in the horse of all the species examined (Figure 3.2.7). The

model dorsiflexion was a near perfect fit for total sagittal mobility of the column.

Experimental data were only available for total sagittal flexion in the horse

(dorsiflexion and ventroflexion combined) but the close fit of these data with

dorsiflexion in the model suggests that ventroflexion may be limited. OROM estimates

of both lateroflexion and torsion fit the experimental data well, despite overestimating

mobility at the middle thoracic position.

Table 3.2.2 Osteological range of motion (degrees) determined from manipulation of digital models of vertebrae.

Maximum angles (in degrees) in dorsiflexion, ventroflexion, lateral flexion and torsion. Intervertebral spacing in mm, IV, intervertebral. Int., Interactions between osteological components which limit motion are as follows: LB, lateral bodies; L/S, lamina with neural spine; TPJ, transverse process joints; VB, ventral bodies; Z, zygapophyses; Z/M, zygapophysis with caudal metapophysis. DFL: Dorsiflexion, VFL, Ventroflexion, SAG, total sagittal, LAT, Lateroflexion, Tor, Torsion. MT, midthoracic; D, diaphragmatic; ML, midlumbar; LL, last lumbar.

Species	Pos.	Joint	IV spacing	DFL	Int.	VFL	Int.	LFL	Int.	Tor	Int.
CAT	T1	T1-2	0.6	15	Z	16	VB	15	Z	3	Z
	MT	T7-8	0.5	2	Z	20	VB	10	Z	14	Z
	D	T11-12	0.9	3	Z	22	VB	5	Z	2	Z
	L1	L1-2	1.2	8	Z	42	VB	13	Z/M	2	Z
	ML	L3	1.5	7	Z	36	VB	15	Z/M	2	Z
	LL	L6	1.5	8	Z	44	VB	12	Z/M	1	Z
SHEEP	T1	T1-2	4.5	6	Z	35	VB	25	LB	18	Z/M
	MT	T6-7	2.6	2	Z	22	VB	25	LB	12	Z/M
	D	T11-12	3.2	13	Z	15	VB	26	LB	4	Z
	L1	L1-2	4.4	7	Z	30	VB	2	Z	1	Z
	ML	L3-4	4.2	7	Z	35	VB	5	Z	1.5	Z
	LL	L6-S	4.5	16	Z	28	VB	2	Z	0	Z
HORSE	T1	T1-T2	5.9	17	Z	N/A		10	Z	2	Z
	MT	T9-10	2.3	4	Z	11	VB	17	LB	9	Z
	D	T17-18	2.4	4	Z	24	VB	9	Z/M	3	Z
	L1	L1-2	2.5	3	L/S	31	VB	2	Z	2	Z
	ML	L3-4	2.6	6	Z	N/A		3	Z	2	Z
	LL	L6-S	3.6	22	Z	26	VB	1	TPJ	2	Z
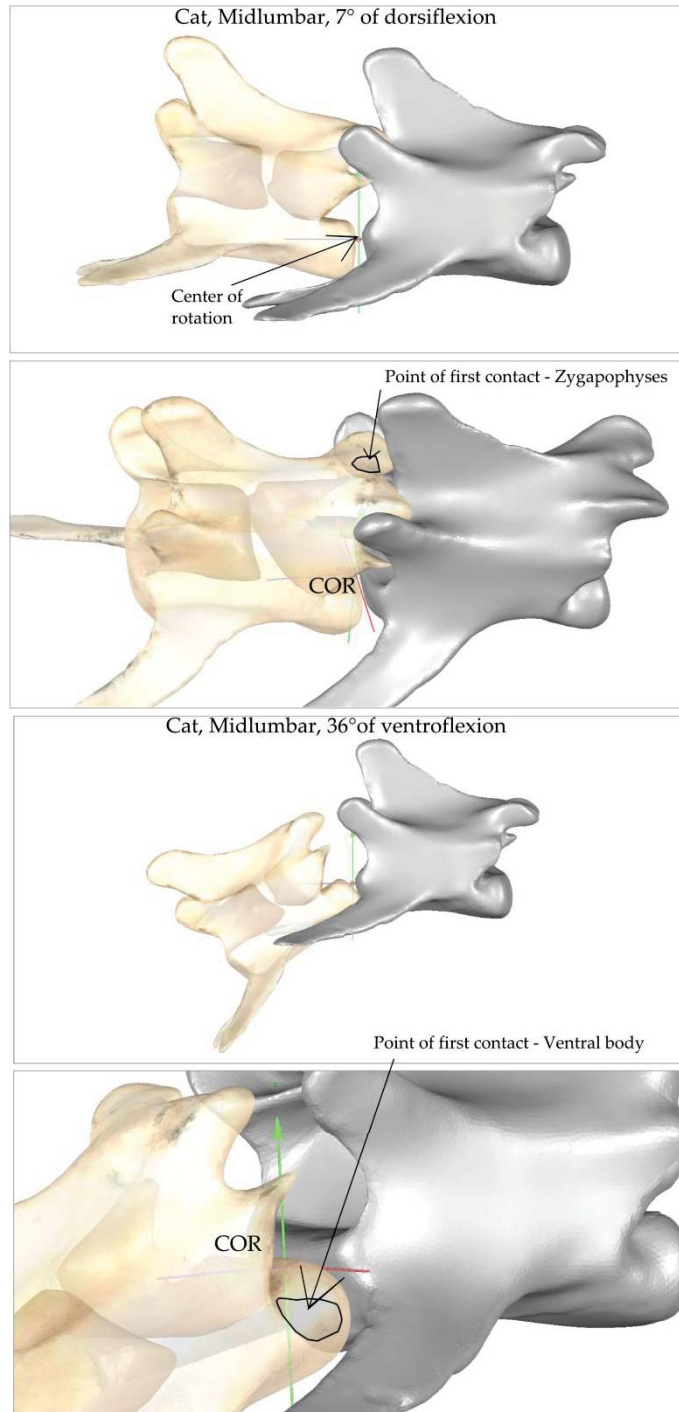
Figure 3.2.2 Bony joint interactions at the mid-lumbar joint of the cat.
COR, center of rotation. Cranial vertebra (color, ghosted) rotates relative to caudal vertebra. Arrows indicate primary (x, y, z) planes. Note there are no bony structures to inhibit ventroflexion until the vertebral bodies contact.

113

Sheep, Midlumbar, 7° of dorsiflexion

Point of first contact -
inferio-lateral zygapophyses

COR

Sheep, Midlumbar, 5° of lateroflexion

Point of first contact -
supero-lateral zygapophyses,
contralateral side

COR

Sheep, Midlumbar, 2° of torsion

Point of first contact -
superior and lateral zygapophyses,
ipsilateral side

COR
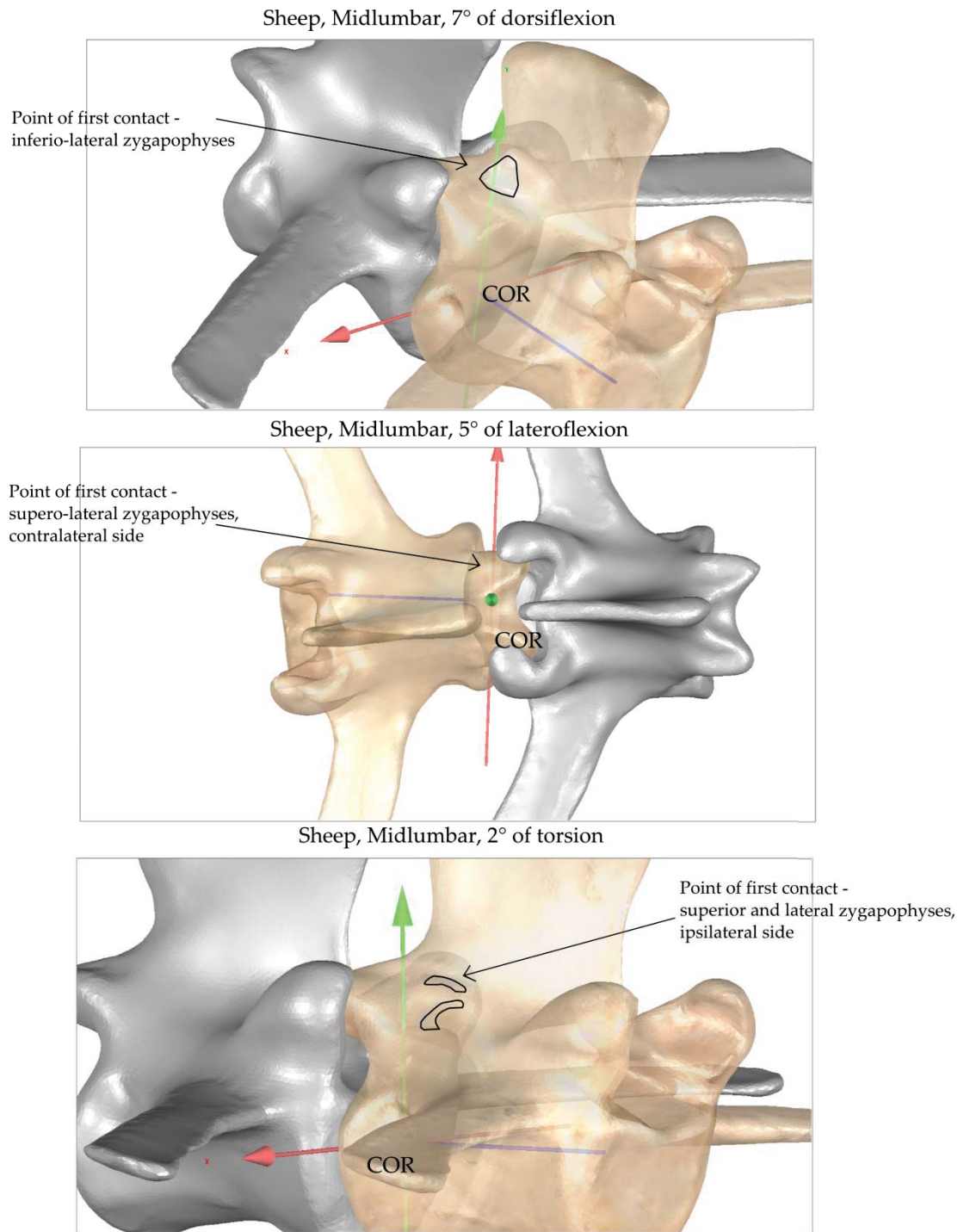
Figure 3.2.3 Bony joint interactions in the mid-lumbar joint of the sheep
in dorsiflexion, lateroflexion and torsion. Superior (dorsal) facet of revolute
zygapophysis comes into contact during torsion and lateroflexion.

Horse, Midlumbar, 5° of dorsiflexion

Point of first contact -
caudal zygapophyses

COR

Horse, Last-lumbar, 22° of dorsiflexion

Point of first contact -
inferio-caudal zygapophyses

COR

Horse, Last-lumbar, 1° of lateroflexion

Point of first contact -
Lateral transverse joint

COR
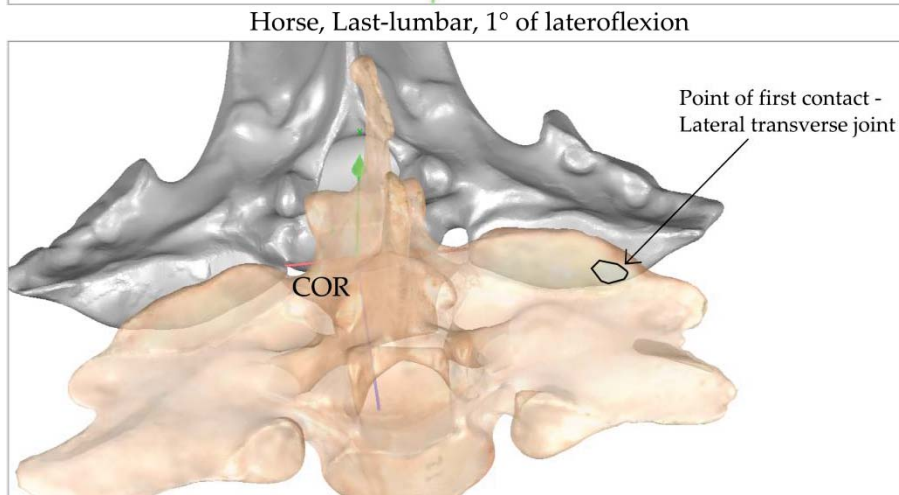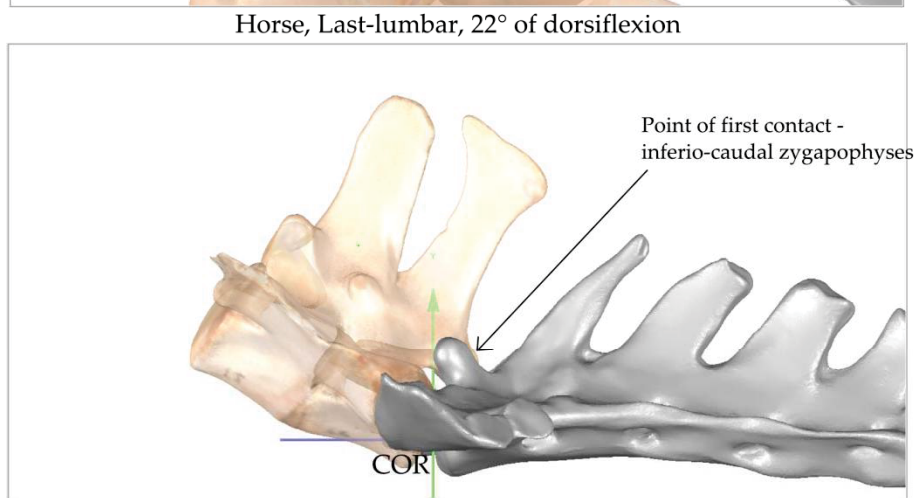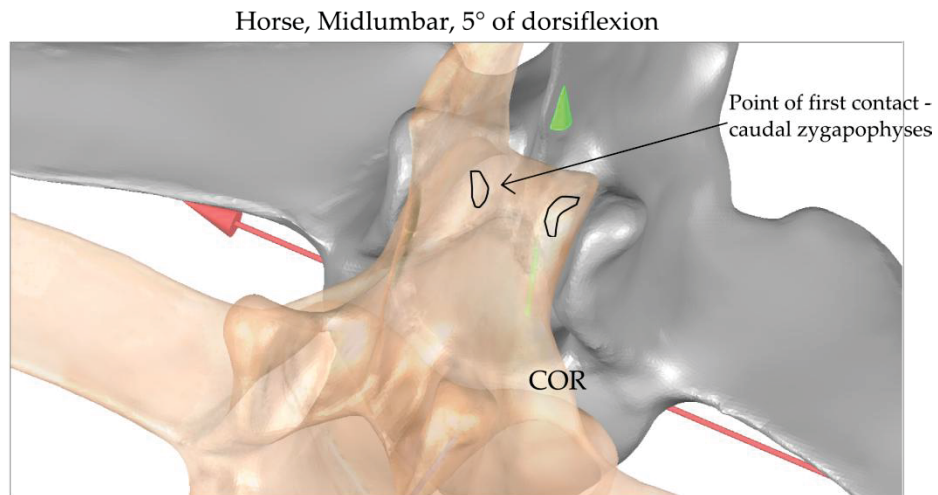
Figure 3.2.4 Bony joint interactions of the horse.
Note the increased dorsiflexion at the lumbosacral joint relative to the mid-lumbar joint.
Lateral joints come into contact during lateroflexion.
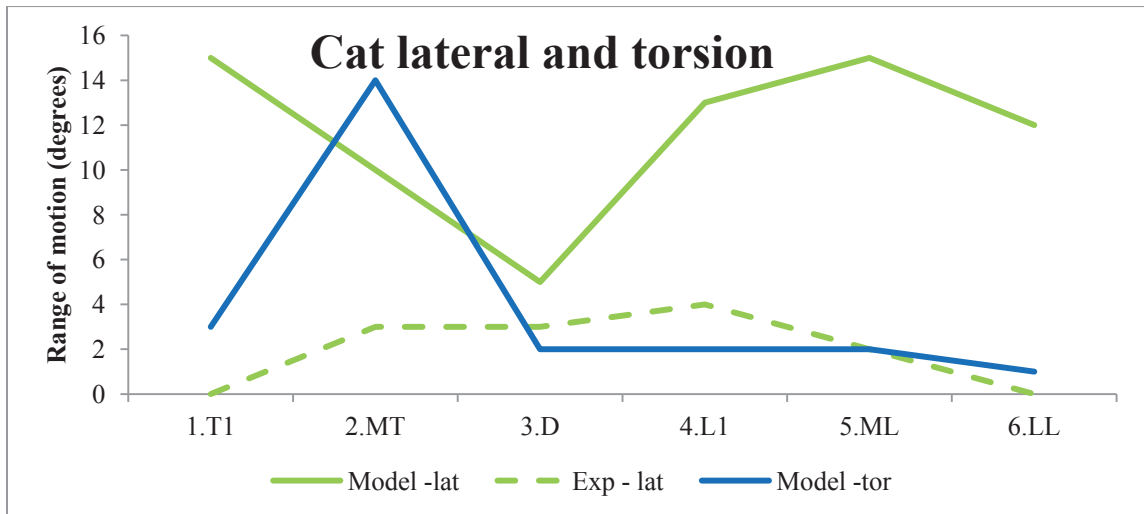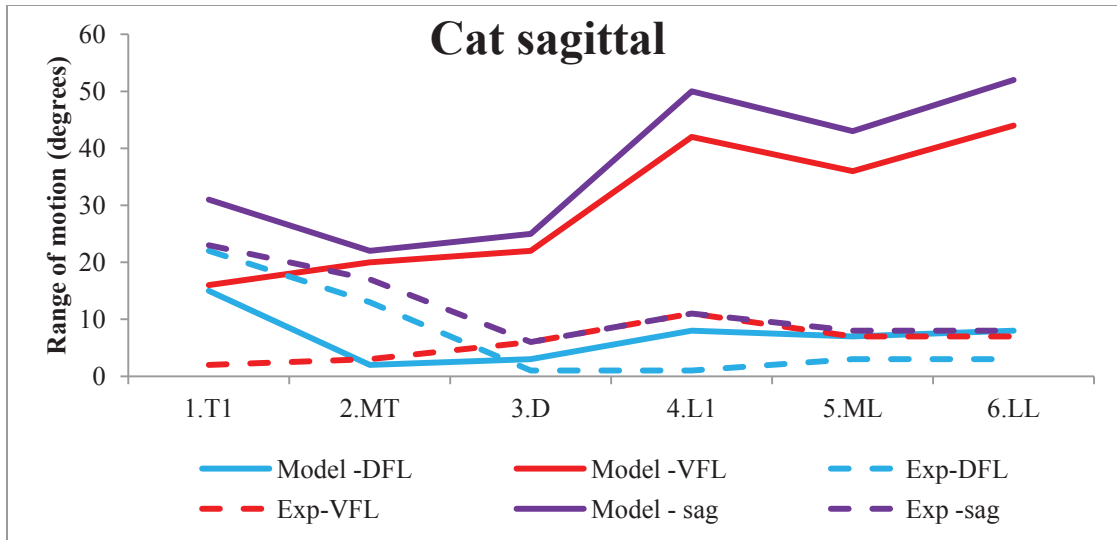
Figure 3.2.5 Comparison of experimental versus osteological range of motions for the cat.

Dashed lines indicate experimental data, solid lines indicate osteological range of motion collected from digital model. Color scheme for sagittal motion-- Pale blue: dorsiflexion, red: ventroflexion, purple: total sagittal. Color scheme of lateral and torsion motions-- green: Lateroflexion, dark blue: torsion. Osteological range of motion tends to overestimate relative to experimental data. T1, first thoracic; MT, mid-thoracic; D, diaphragmatic;L1, first lumbar; ML, mid-lumbar; LL, last lumbar. DFL, dorsiflexion; VFL, ventroflexion; Sag, sagittal; exp, experimental data.
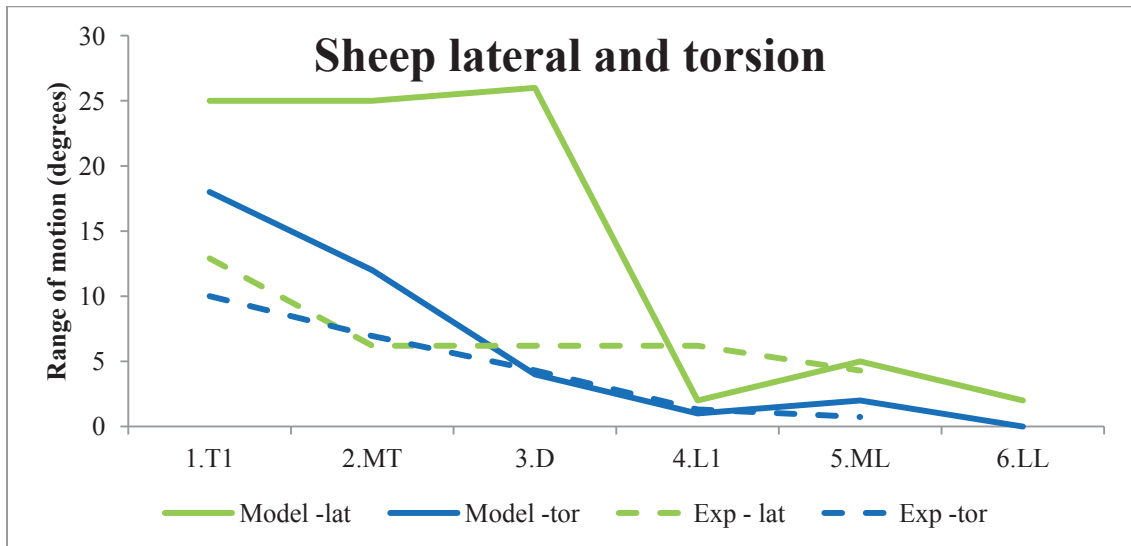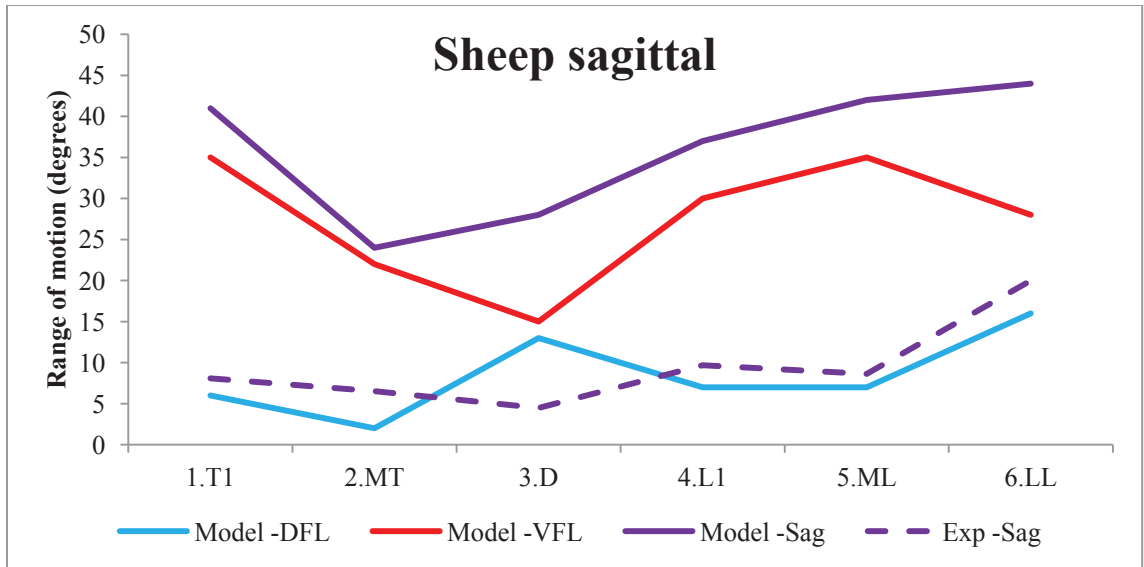
Figure 3.2.6 Comparison of experimental versus osteological range of motions for the sheep.

Dashed lines indicate experimental data, solid lines indicate osteological range of motion collected from digital model. Color scheme for sagittal motion-- Pale blue: dorsiflexion, red: ventroflexion, purple: total sagittal. Color scheme of lateral and torsion motions-- green: Lateroflexion, dark blue: torsion. MT, mid-thoracic; D, diaphragmatic; ML, mid-lumbar; LL, last lumbar. Dorsiflexion and torsion most closely match experimental values. . DFL, dorsiflexion; VFL, ventroflexion; Sag, sagittal; exp, experimental data.
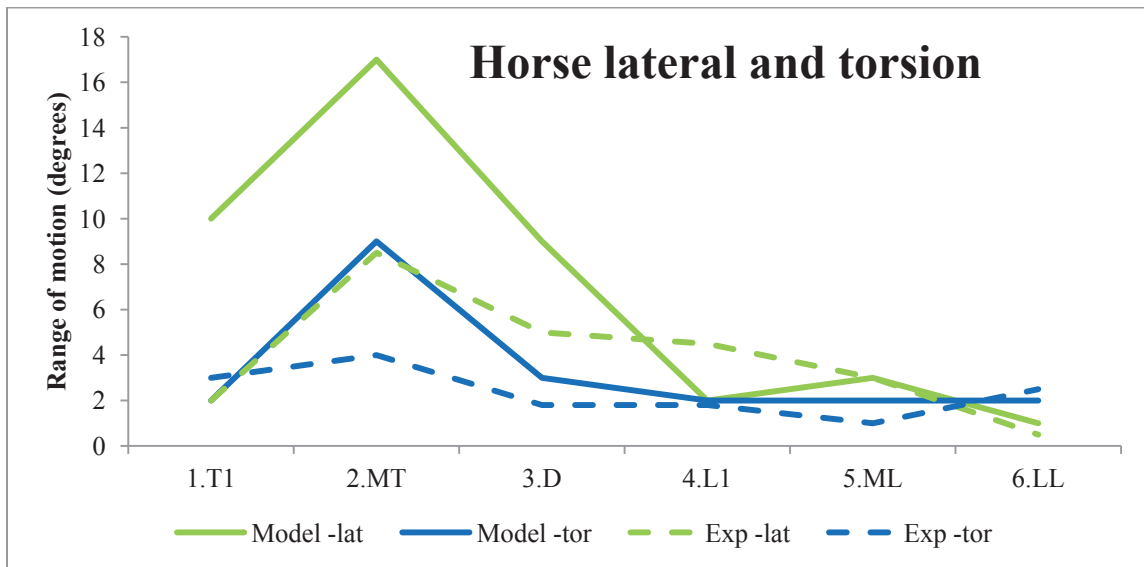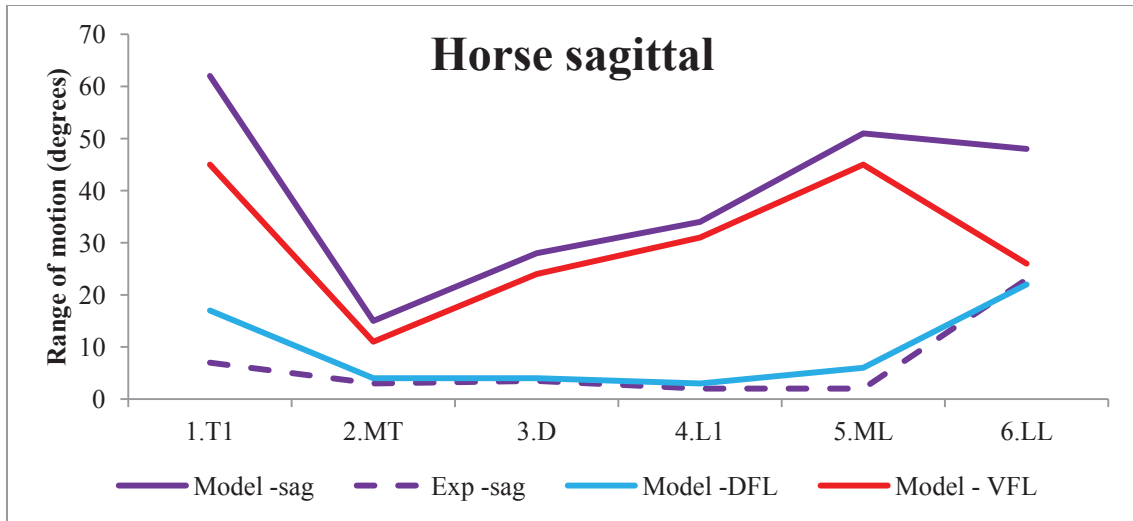
Figure 3.2.7 Comparison of experimental versus osteological range of motions for six intervertebral joints.

Dashed lines indicate experimental data, solid lines indicate osteological range of motion collected from digital model. Color scheme for sagittal motion-- Pale blue: dorsiflexion, red: ventroflexion, purple: total sagittal. Color scheme of lateral and torsion motions-- green: Lateroflexion, dark blue: torsion. MT, mid-thoracic; D, diaphragmatic; ML, mid-lumbar; LL, last lumbar. There is a good match with experimental data, except for ventroflexion. . DFL, dorsiflexion; VFL, ventroflexion; Sag, sagittal; exp, experimental data.

3.2.3 SHAPE OF INTERVERTEBRAL JOINT COMPLEX

PC1 and PC2 from a principal components analysis of landmarks from the joint complex (centrum and zygapophyses) for each species are presented in Figure 3.2.8, and the contribution of each axis to total variation can be found in Table 3.2.3. Correlations between range of motion data and shape revealed significant relationships, which are shown in Table 3.2.4.

PC1 and PC2 for the cat account for approximately 86% of the total variation. PC1 distinguishes the T1 and last lumbar (LL) vertebrae from the others due to their extremely wide zygapophyses, while PC2 distinguishes pre-diaphragmatic and post-diaphragmatic vertebrae based on zygapophyseal morphology. Multivariate analysis of variance confirmed that there was an effect of vertebral position on shape (PC1:PC3, $p<0.001$) and Tukey's HSD revealed that T1, MT and LL were significantly different from the other positions. In the cat, dorsiflexion was correlated with both negative PC1 and positive PC2 scores, representing pre-diaphragmatic joint morphology. Lateroflexion was positively correlated with PC1, which represents variation from wide to narrowly-spaced zygapophyses, suggesting wide zygapophyses might restrict lateral bending.

For the sheep, the first two PCs account for 87% of variation. Pre-diaphragmatic vertebrae were distinguished by positive scores on PC2 and negative scores on PC1, whereas LL was separated from the other post-diaphragmatic vertebrae based on its wide and dorsoventrally compressed endplate and zygapophyses. The effect of position in a MANOVA was highly significant ($p<0.001$), with differences between all the

vertebrae except T1/MT and ML/L1 revealed by a Tukey's HSD. Sagittal mobility in the sheep was positively correlated with PC1, reflecting wider and more sagittal zygapophyses and a dorsoventrally compressed centrum. Lateroflexion and torsion were related to taller endplates with horizontal zygapophyses as reflected by negative correlations on PC1, and torsion was additionally correlated with positive PC2 scores.

PC1 and PC2 contributed about 85% of variation in the horse. As in the cat, PC1 distinguishes T1 and LL from the other vertebrae based on wider zygapophyses and endplate. The mid-thoracic vertebra (MT) is separated on PC2 based on its flat zygapophyses and tall centrum. There is a significant effect of vertebral position ($p<0.001$), which reflects the clustering of positions on PC1 and PC2, and all vertebrae were different except the cluster of D/L1/ML. In the horse, sagittal mobility is positively correlated with PC1, reflecting wide zygapophyses and compressed centrum. Lateroflexion is negatively correlated with PC1 but positively correlated with PC2, reflecting a mediolaterally narrow centrum and pre-diaphragmatic-type zygapophyses. Torsion is correlated with positive PC2, indicating horizontal pre-diaphragmatic-type zygapophyseal joints.

Generally, similar craniocaudal morphology patterns are seen across the families, with vertebral positions clustering closely on the first two PCs in all analyses, suggesting that craniocaudal position is a major determinant of variation in joint shape. In particular, this analysis distinguishes pre- and post-diaphragmatic vertebrae, and the last lumbar also tends to have a distinctive morphology.
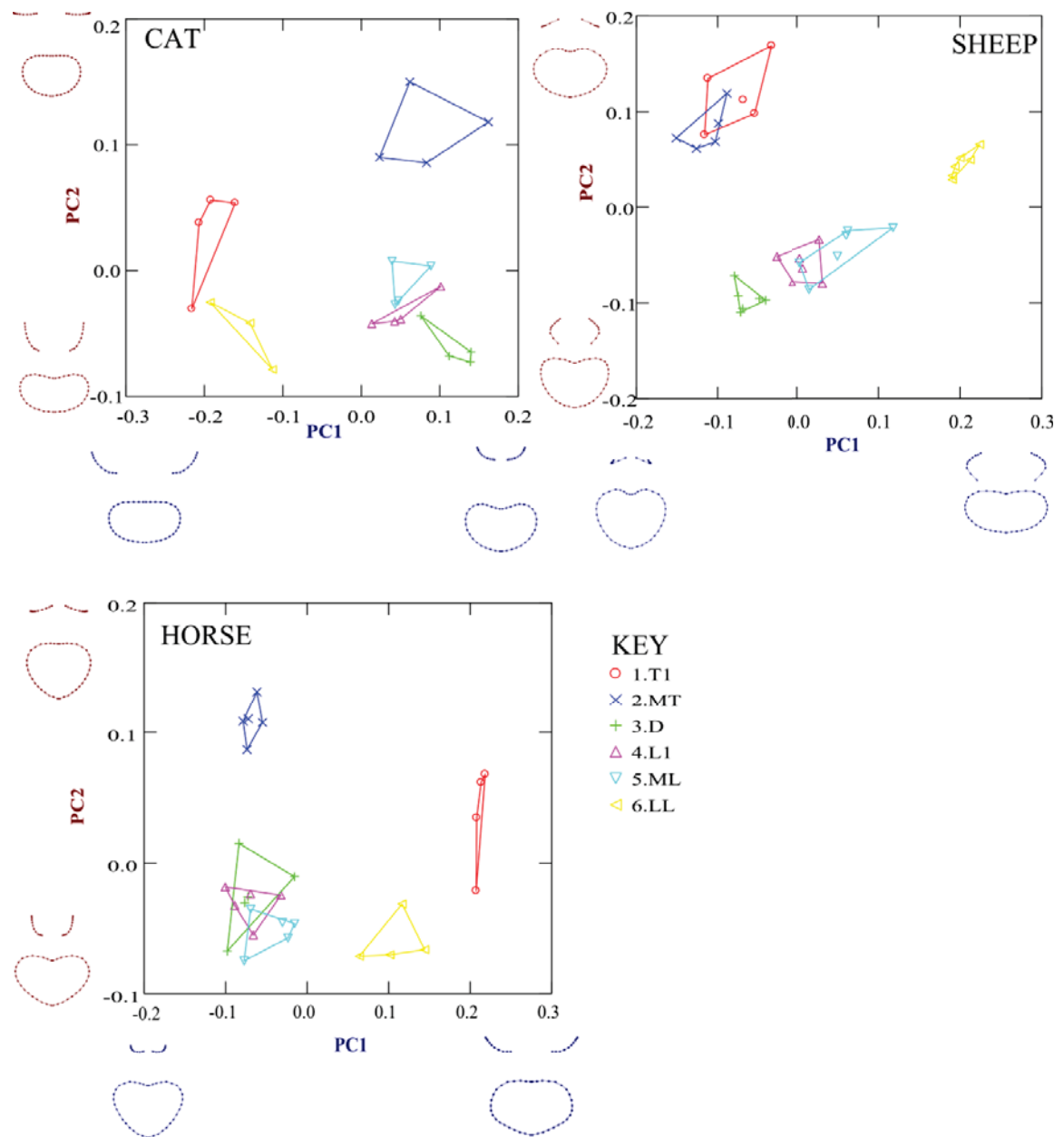
Figure 3.2.8 Shape changes associated with PC scores.

Extremal shapes shown as wireframes near the axes. T1, first thoracic; MT, mid-thoracic; D, diaphragmatic; L1, first lumbar; ML, mid-lumbar; LL, last lumbar. Vertebral positions can be clearly distinguished by their joint complex morphology.

Table 3.2.3 Eigenvalues (% variance) from joint shape PCA .

PC	CAT	SHEEP	HORSE
1	67.9	56.8	61.9
2	17.9	29.4	23.1
3	6.9	5.4	6.8
4	3.7	3.1	4.5
5	1.7	1.9	1.3

Table 3.2.4 Correlation analysis of joint shape (PC Scores) and mobility for cat, sheep and horse.

Rho, Spearman's rank correlation coefficients reflect the strength of the correlation between the variables. Bold values indicate significance at Bonferroni-corrected levels. Significant correlations indicate the types of shape variation (PCs) which may be influencing mobility in specific planes.

CAT	Sagittal		Dorsiflexion		Ventroflexion		Lateroflexion	
	rho	P	rho	P	rho	P	rho	P
PC1	-0.489	0.018	**-0.532**	**0.009**	0.188	0.391	**0.657**	**0.001**
PC2	**0.673**	**>0.001**	**0.712**	**>0.001**	-0.495	0.016	-0.118	0.592
PC3	0.289	0.181	0.144	0.513	-0.267	0.218	-0.52	0.814

Bonferroni corrected p (alpha=0.05) = 0.0042

SHEEP	Sagittal		N	Lateroflexion		Torsion		N
	rho	P	N	rho	P	rho	P	N
PC1	**0.818**	**>0.001**	34	**-0.602**	**0.001**	**-0.825**	**>0.001**	28
PC2	0.139	0.433	34	0.405	0.032	**0.533**	**0.003**	28
PC3	-0.058	0.744	34	0.326	0.091	0.227	0.245	28

Bonferroni corrected p (alpha=0.05) = 0.0056

HORSE	Sagittal		Lateroflexion		Torsion	
	rho	P	rho	P	rho	P
PC1	**0.531**	**0.004**	**-0.695**	**>0.001**	0.243	0.212
PC2	0.039	0.844	**0.557**	**0.002**	**0.68**	**>0.001**
PC3	-0.241	0.217	0.056	0.777	-0.354	0.065

Bonferroni corrected p (alpha=0.05) = 0.0056

3.2.4 **LINEAR MEASURES**

To test for craniocaudal variation in vertebral shape, principal components analysis of scaled linear measures was used to reduce the dimensionality of the dataset (from five to four variables). Results are shown in Figure 3.2.9 and show that vertebral positions can be distinguished by their shape. Loadings on the principal components, which describe the variables driving each axis, can be found in Table 3.2.5. To examine the relationship between morphology and mobility, Spearman's Rank correlation between linear measures and mobility was conducted. First only the *a priori* hypothesized relationships were tested. Evidence was found for some of the *a priori* hypotheses and is presented in Table 3.2.6. Subsequently a pairwise analysis of all data was conducted to look for alternative relationships. Pairwise correlations of all variables are presented in Table 3.2.7.

PC1 and PC2 in the cat account for 65% of the variance in the sample. There is a significant effect of vertebral position on multidimensional shape ($p<0.001$), with pairwise differences between all positions except T1 and ML. Positive PC1 scores were driven by increasing transverse process width and zygapophyseal width, whereas increasing PC2 scores were driven by taller endplates and neural spines.

The first two axes explain approximately 84% of variance in the sheep, distinguishing lumbar and thoracic vertebrae. The effect of vertebral position was significant ($p<0.001$), and there are pairwise differences between all positions except L1 and ML. Positive PC1 scores are driven by tall endplates, tall neural spines, narrow transverse processes and narrow zygapophyses. PC2 reflects a tall arch, whereas PC3 relates to wide transverse processes.

In the horse 78% of the variance is contained in the first two PCs, which reflect craniocaudal patterns and distinctive T1 shape. MANOVA revealed a significant effect of vertebral position ($p<0.001$) and significant pairwise differences for all positions except ML with L1 and LL. Positive PC1 is related to a taller endplate, taller neural spine and narrower transverse processes. Positive PC2, which is typified by T1, reflects a taller arch and wider zygapophyses. Positive scores on PC3 were driven by a taller endplate and taller but anteroposteriorly shorter arch.

Sagittal motion is significantly correlated with a dorsoventrally compressed centrum in both the horse and the sheep. Conversely, sagittal motion is correlated with a taller endplate in cats. Short neural spines are related to high sagittal mobility in the sheep, and to ventroflexion in the cat, but a tall neural spine is associated with dorsiflexion in the cat. Short transverse processes and narrow zygapophyses are correlated with lateroflexion in the cat and the horse. In addition, a relatively narrow centrum is correlated with lateroflexion in the horse. Zygapophysis width is not significantly correlated with torsion in either the sheep or the horse. A few additional, unpredicted correlations were found in addition to those described above (Table 3.2.7). In the sheep sagittal mobility was additionally correlated with long transverse processes and wide zygapophyses, lateroflexion was correlated with a tall neural spine, and torsion was correlated with a tall neural spine and short transverse processes. In the horse, torsion was also correlated with a tall neural spine and short transverse processes, likely reflecting the emphasis of torsion on the thoracic region where the withers are high.

Table 3.2.5 Loadings of each linear measurement in the PCA.

PCA used to test for craniocaudal differences in vertebral shape. Bold values indicate measurements that contributed the most to each PC. LA, lever arm.

	CAT				SHEEP				HORSE			
	PC1	PC2	PC3	PC4	PC1	PC2	PC3	PC4	PC1	PC2	PC3	PC4
% Variance	36.9	28.2	15.3	23.1	59.9	24.2	9.2	5.4	43.5	33.8	12.4	8.3
Endplate shape (H/W)	-0.241	**0.741**	0.445	0.441	**0.851**	-0.312	0.265	0.312	**0.797**	-0.378	**0.431**	0.061
Arch LA	0.49	0.529	**-0.647**	0.223	0.339	**0.899**	0.235	-0.115	0.411	**0.788**	**0.419**	0.094
Neural spine LA	0.439	**0.668**	0.2	**-0.565**	**0.817**	0.44	-0.272	0.209	**0.808**	-0.016	**-0.428**	0.402
Transverse process LA	**0.81**	-0.354	0.318	0.156	**-0.863**	0.188	**0.405**	0.201	**-0.848**	0	0.201	0.487
Zygapophysis width	**0.921**	-0.095	0.085	0.129	**-0.864**	0.274	-0.309	0.259	-0.009	**0.961**	-0.181	-0.047
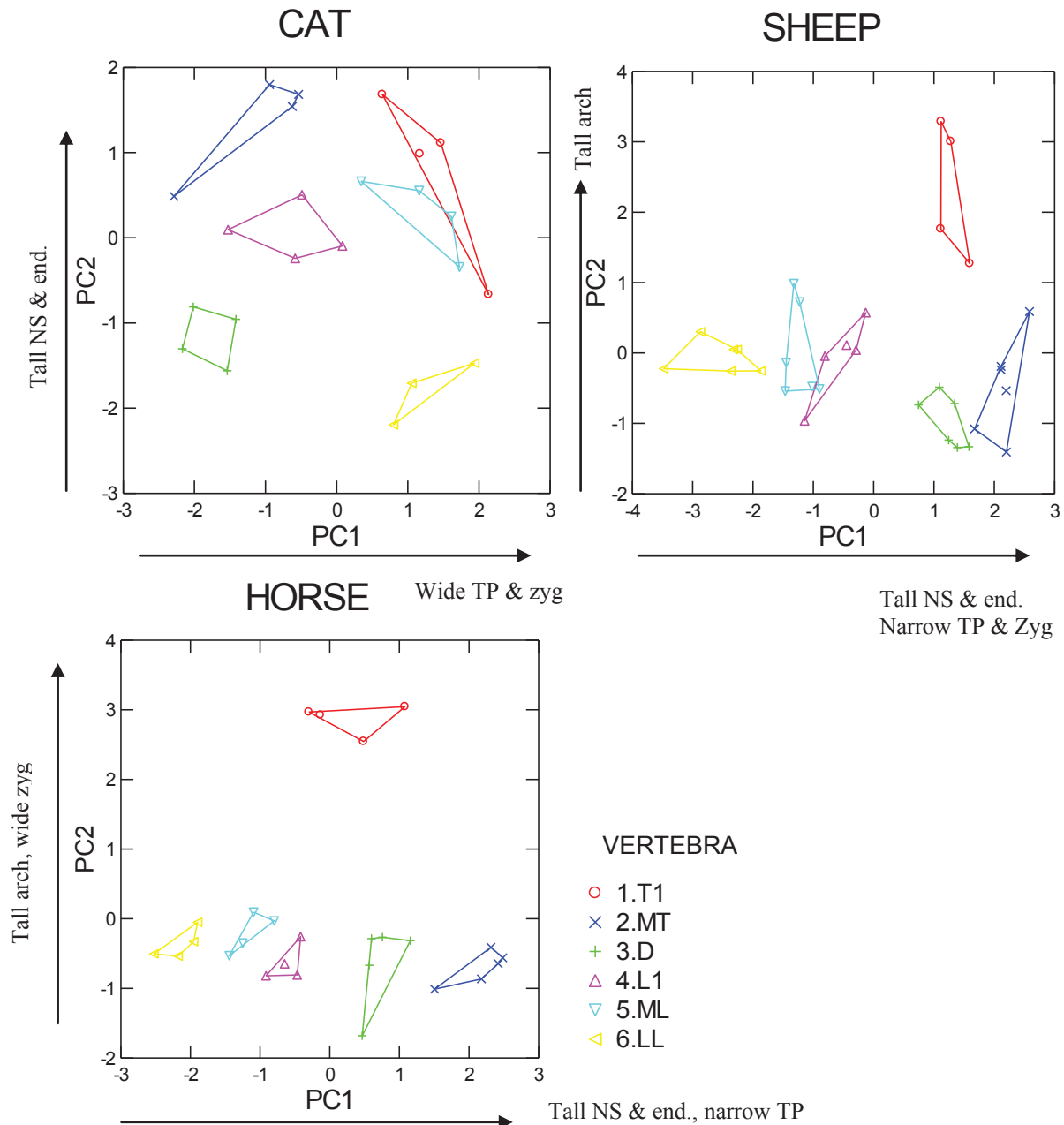
Figure 3.2.9 PCA of linear measurements from vertebrae.

T1, first thoracic; MT, mid-thoracic; D, diaphragmatic; L1, first lumbar; ML, mid-lumbar; LL, last lumbar. End, endplate; NS, neural spine; TP, transverse process; Zyg, zygapophyses. Vertebral positions can be distinguished based on linear measurements.

Table 3.2.6 Spearman's rank correlation on mobility and linear measures for a priori hypotheses.

Rho: Spearman's correlation coefficient. Bold values are significant to the Bonferroni-corrected alpha level which is shown in brackets next to p. Sagittal motion and lateroflexion meet some of the a priori hypotheses

SAGITTAL	CAT		SHEEP						HORSE		
	Sagittal		Dorsiflexion		Ventroflexion		N	Sagittal		N	Sagittal	
	rho	P(0.0056)	rho	p(0.0056)	rho	p(0.0056)	N	rho	P(0.017)	N	rho	p(0.017)	N
Endplate shape	**0.562**	**0.005**	0.409	0.053	-0.139	0.528	23	**-0.712**	**>0.001**	33	**-0.479**	**0.01**	28
Arch height	0.252	0.246	0.174	0.427	0.16	0.466	23	-0.151	0.403	33	-0.107	0.589	28
Neural spine	**0.742**	**>0.001**	**0.898**	**>0.001**	**-0.72**	**>0.001**	23	**-0.663**	**>0.001**	33	0.021	0.92	26

LATERAL	CAT			SHEEP			HORSE		
	rho	p(0.017)	N	rho	p(0.017)	N	rho	p(0.017)	N
Endplate shape	0.127	0.565	23	0.019	0.921	29	**0.939**	**>0.001**	28
Transverse process lever arm	**-0.788**	**>0.001**	23	-0.391	0.036	29	**-0.612**	**0.001**	28
Zygapophysis width	**-0.737**	**>0.001**	23	-0.224	0.242	29	**-0.612**	**0.001**	28

TORSION	SHEEP			HORSE		
	rho	P(0.025)	N	rho	p(0.025)	N
Zygapophysis width	-0.379	0.042	29	0.294	0.129	28

Table 3.2.7 Pairwise comparisons of all linear measurements with mobility.
Rho: Spearman's correlation coefficient. Bold values indicate significance at Bonferroni corrected alpha levels which are p=0.0025 for the cat and p=0.0033 for the sheep and horse. Some additional correlations beyond the a priori hypotheses are detected in the sheep and horse.

CAT	Sagittal		Dorsiflexion		Ventroflexion		Lateroflexion		
	rho	p	rho	p	rho	p	rho	p	N
Endplate shape	0.562	0.005	0.409	0.053	-0.139	0.528	0.127	0.565	23
Arch height	0.252	0.246	0.174	0.427	0.16	0.466	-0.019	0.931	23
Neural spine	**0.742**	**>0.001**	**0.898**	**>0.001**	**-0.72**	**>0.001**	-0.476	0.022	23
Transverse process	0.045	0.84	0.419	0.047	-0.011	0.96	**-0.788**	**>0.001**	23
Zygapophysis width	0.286	0.186	0.41	0.052	0.048	0.828	**-0.737**	**>0.001**	23

SHEEP	Sagittal			Lateroflexion		Torsion		
	rho	p	N	rho	p	rho	p	N
Endplate shape	**-0.712**	**>0.001**	33	0.133	0.509	0.366	0.06	27
Arch height	-0.151	0.403	33	0.417	0.03	0.309	0.117	27
Neural spine	**-0.663**	**>0.001**	33	**0.723**	**>0.001**	**0.908**	**>0.001**	27
Transverse process	**0.748**	**>0.001**	33	-0.459	0.016	**-0.652**	**>0.001**	27
Zygapophysis width	**0.861**	**>0.001**	33	-0.321	0.103	-0.479	0.012	27

HORSE	Sagittal		Lateroflexion		Torsion		
	rho	p	rho	p	rho	p	N
Endplate shape	-0.479	0.01	**0.939**	**>0.001**	0.183	0.353	28
Arch height	-0.107	0.589	0.023	0.907	0.018	0.928	28
Neural spine	0.021	0.92	0.501	0.009	**0.596**	**0.002**	26
Transverse process	-0.376	0.049	**-0.612**	**0.001**	**-0.586**	**0.001**	28
Zygapophysis width	0.473	0.011	**-0.612**	**0.001**	0.294	0.129	28

3.3 DISCUSSION

3.3.1 HYPOTHESES

The preliminary data on form-function links in running mammals presented in this chapter have demonstrated that **many osteological features correlate with range of motion** in these species, but that there is some variation between the groups. Findings are summarized in Table 3.3.1.

Table 3.3.1 Summary of morphological features that correlate with range of motion.
DV, dorsoventral; ML, mediolateral; DFL, dorsiflexion; VFL, ventroflexion.

	SAGITTAL	LATERAL	TORSION
CAT	**Joint shape:** Horizontal, ventrally-placed and wide zygapophyses **Linear measurements:** DV tall endplate, tall neural spine (DFL), short neural spine (VFL)	**Joint shape:** Narrow, dorsally-placed zygapophyses **Linear measurements:** Short transverse processes and narrow zygapophyses	No data
SHEEP	**Joint shape:** DV compressed centrum, sagittally-oriented, wide zygapophyses **Linear measurements:** DV short, ML wide endplate, short neural spine	**Joint shape:** DV tall and ML narrow centrum, narrow and horizontal zygapophyses **Linear measurements:** None	**Joint shape:** Horizontal zygapophyses, DV tall but ML narrow centrum **Linear measurements:** tall arch, tall neural spine and narrow transverse processes
HORSE	**Joint shape:** DV compressed centrum, wide and ventrally-placed zygapophyses **Linear measurements:** DV short, ML wide endplate.	**Joint shape:** DV tall and ML narrow centrum, less curved zygapophyses **Linear measurements:** DV tall and ML narrow centrum, short transverse processes and narrow zygapophyses	**Joint shape:** Horizontal zygapophyses **Linear measurements:** tall neural spine and narrow transverse processes

I can now address the specific hypotheses posed at the beginning of the chapter:

H1. Limited sagittal bending is correlated with a tall arch with dorsally-placed zygapophyses, a tall endplate, a strong ventral keel, a tall neural spine and horizontal zygapophyses.

H1 was supported in the sheep and horse, but only partially in the cat. Digital modeling revealed that bony joint interactions seem to play a greater role in restricting dorsiflexion than ventroflexion. Ventroflexion was overestimated in a bone-only model in all species because the proposed mechanisms for restricting ventroflexion involve mostly tensile resistance of ligaments (e.g., supraspinous, ligamenta flava) which were not included in the model. In contrast, impaction of the zygapophyses frequently restricted motion during dorsiflexion in the digital model. Accordingly, modeled dorsiflexion closely matched experimental dorsiflexion (cat) and total sagittal motion (sheep and horse). The importance of joint interactions was supported by the strong correlation of sagittal mobility with dorsoventrally compressed endplates and more sagittally-oriented, wide zygapophyses in the sheep and the horse. There were also negative correlations with endplate shape in both taxa, reflecting a lower height:width ratio, and relatively less resistance of intervertebral discs to sagittal bending. In addition, there was a negative correlation with neural spine height in the sheep but not in the horse, implicating the supraspinous ligament in restricting ventroflexion in this species. Indeed, lesion experiments in mammals have suggested that disc resistance may be important in resisting ventroflexion in some species, whereas ligament tension (particularly of ligamenta flava) is more important in others (Gál, 1993). Additional correlations with transverse process and zygapophyseal width likely reflect the

emphasis on the lumbar region for sagittal mobility in sheep.

In contrast, the cat showed quite different patterns of correlation. This may be because of different methods used to collect mobility data in this taxon. In terms of total sagittal mobility, there was relatively less variation along the column, with high mobility throughout, but especially so in the anterior thoracics which assist in neck movements (Macpherson and Ye, 1998). This reduced craniocaudal variability in total sagittal motions makes correlations with morphology more difficult to detect. However, there were strong craniocaudal variations in dorsiflexion and ventroflexion. They corresponded with the pre-diaphragmatic and post-diaphragmatic region, respectively, and were inversely related. Thus, in the morphological analysis, dorsiflexion was correlated with horizontal zygapophyses, whereas ventroflexion was more related to sagittal zygapophyses. The 'zero' position used in this study was the angle at which the centra of the adjacent vertebrae formed a straight line. Thus a joint which is strongly dorsoflexed in its natural stance (e.g., anterior thoracics), but can bend in both directions, will be capable of more dorsiflexion than ventroflexion when measured from this zero point. In the cat there was a correlation between sagittal mobility/dorsiflexion and a tall neural spine, whereas ventroflexion was linked with a shorter neural spine, suggesting that relatively short spines of the lumbar region may assist in ventroflexion via reduced advantage of the supraspinous ligament. There was also a correlation of dorsiflexion with negative PC1, reflecting wide and ventrally-placed zygapophyses, which supports H1. However, total sagittal mobility in the cat was correlated with increased height:width ratio of the centrum, which contradicts H1.

Both digital modeling and morphological correlations suggest that bony

morphology more closely reflects dorsiflexion than ventroflexion, and that morpho-functional predictions are more closely met in dorsostable than dorsomobile taxa, presumably because there is less reliance on soft-tissues for joint stabilization in the latter taxa. However, the nature of the data available for the cat makes comparisons difficult.

H2. Limited lateroflexion is correlated with a wide transverse process, widely spaced zygapophyses or a wide endplate.

H2 is supported, particularly in the lumbar region. The digital model overestimated lateroflexion throughout the column of the cat and in the thoracic region of the sheep and horse. This suggests that other structures, such as ribs or intercostal muscles are also important in resisting lateroflexion in the thoracic region. This further suggests that zygapophyses may play a more important role in restricting lateroflexion in the sheep and horse than in the cat. Despite this, joint shape was correlated with lateroflexion in all species. High mobility was related to narrower, horizontally-oriented zygapophyses and narrower endplates, meeting the predictions of H2. In addition, the transverse process was negatively correlated with lateral mobility in the cat and the horse, implicating the intertransverse ligament in restricting mobility in the lumbar region.

H3. Limited torsion is correlated with sagittally-oriented or wide zygapophyses.

H3 is partially supported because horizontal zygapophyses relate to increased mobility, but narrowly-spaced zygapophyses do not. Torsional range of motion in the digital model closely resembled that obtained from experimental data. This suggests

that the zygapophyseal interactions noted in the digital model are very important in restricting torsion in intervertebral joints. High torsion was correlated with horizontal, pre-diaphragmatic-type joints in both the sheep and the horse, strongly supporting the predictions of H3. No quantitative data were available for torsion in the cat column, but this is consistent with the qualitative observation that torsion was restricted to the posterior pre-diaphragmatic region. However, torsion did not correlate with zygapophysis width in either sheep or horses, suggesting that this feature relates more to lateroflexion than torsion. Torsion was additionally correlated with a tall neural spine and short transverse processes in both sheep and horse. This reflects the higher neural spines of the withers in the thoracic region of ungulates, but functionally it likely relates more to support of the head via the nuchal ligament than restricting torsion.

3.3.2 INDICATORS OF JOINT MOBILITY IN THE THORACOLUMBAR SPINE

The data presented in this chapter represent only a preliminary consideration of form-function in the thoracolumbar region of running mammals. The major limitation of this study is that literature range of motion data were used, and therefore form and function could only be compared at a species-mean level. Additionally, the variations in measurement techniques prevented direct comparisons between species. To confirm and embellish these findings, future work should characterize both range of motion and morphology in the same individuals, which would provide a more powerful test of form-function relationships. Additionally, combining *in vivo* kinematic data would provide the final link between form, total potential range of motion and actual motion during gaits. However, there is a relative paucity of data available on function of the vertebral column, so even the limited data considered here provide valuable insights

into the types of variation which relate to function.

These results both support and augment previous data on form and function of the thoracolumbar region in mammals. Lesion experiments in a broad range of mammals implicated zygapophyseal impaction as a mechanism for limiting dorsiflexion in the lumbar region, a result which is strongly supported here (Gál, 1993). Further, the same work found that either disc compression or tension in the ligamenta flava could limit ventroflexion and suggested a size-related shift to disc-limiting ventroflexion at larger size. Similarly, here the advantage of the supraspinous ligament (reflected by neural spine height) correlated with reduced sagittal mobility in cats and sheep, but not in horses. The supraspinous ligament also contributes to stiffness in ventroflexion in dolphins (Long et al., 1997). In contrast, centrum dimensions were more important in determining stiffness in crocodiles (Molnar et al., 2014). The data presented here also show that centrum width and height variation relate to sagittal versus lateral range of motion, particularly in sheep and horses, suggesting that disc compression limits mobility.

To summarize the findings of this chapter, osteological features of vertebrae can provide information about range of motion at joints. However, some types of motion are much more strongly correlated with osteological features than others. In particular, dorsiflexion and torsion are closely related to the shape and exact position of the zygapophyses relative to the center of rotation of the joints. This type of morphology is well characterized by the 2D morphometric method presented here because it takes into account not only the shape of the zygapophyses but also their position relative to the endplate (and therefore discs). Hence this method was successful at both separating

different vertebral positions and capturing functionally relevant morphology. Variance was concentrated in the first principal component, which suggests strong integration of joint shape. In all three species PC1, which represented from 57% to 68% of variation, reflected variation from a dorsoventrally compressed, mediolaterally wide joint to a dorsoventrally tall, mediolaterally narrow joint. This correlated with sagittal mobility in the sheep and horse, and specifically dorsiflexion in the cat, and meets functional predictions for the facilitation of dorsiflexion of the column. Further torsion was related to horizontal, pre-diaphragmatic-type joints in both sheep and horses, which would be difficult to capture using linear measures alone. Linear measures demonstrated that transverse processes are important in restricting lateroflexion in cats and sheep, and the neural spine limits ventroflexion. However, these data provide much less information about the morphology and position of the zygapophyses than the landmark data. Therefore, this chapter supports the use of landmark data of joint complex shape as an informative method for studying vertebral functional morphology.

CHAPTER 4: ALLOMETRY OF THE VENTRAL COLUMN

This chapter examines allometry of linear dimensions of the ventral column (centrum and discs) in felids and bovids. Specifically, I compared scaling of the length (craniocaudal), width (mediolateral) and height (dorsoventral) of the thoracolumbar centra against body mass to both geometric and elastic similarity models. Least-squares and reduced major axis regressions on raw and phylogenetically corrected data were used to estimate the relationships between shape and size.

4.1   HYPOTHESES

This chapter asks: **does the ventral column become more robust with increasing size?** To answer this question I address the following specific hypotheses:

H1. Craniocaudal length of the ventral column (regions and individual centra) scales with exponent 0.25 (elastic similarity), indicating that the column becomes relatively shorter with increasing size.

H2. Dorsoventral height of the ventral column scales with exponent 0.375 (elastic similarity), indicating that the column becomes relatively deeper with increasing size.

H3. Mediolateral width of the ventral column scales with exponent 0.33 (geometric similarity), indicating isometry, because major weight-bearing forces are in the sagittal, not mediolateral, plane.

4.2 RESULTS

4.2.1 INTERVERTEBRAL SPACES

Length of the ventral column was estimated from osteological material by summing the lengths of the thoracolumbar centra. A small sample of taxa was used to assess the potential impact of excluding intervertebral spaces on estimating region length allometry. Allometry of the intervertebral spaces relative to centra lengths was measured using radiographs. Analysis of covariance on log intervertebral space length, with log centrum length as a covariate, and family and region as factors, revealed a highly significant effect of centrum length (Table 4.2.1). This indicates that intervertebral spaces become longer as the centra become longer. The effects of family and region were much smaller, with border-line significance at the 95% level, suggesting relative uniformity in the relationship between centra and discs. There were also small effects of the interaction of family and position with centrum length, indicating that slopes were slightly different between groups. However, due to small sample sizes, and since the effect of family was mild, felids and bovids were combined for subsequent allometric analyses. Results indicate that the slopes were not significantly different from one, indicating that discs scaled in a similar way to centra (Table 4.2.2, Figure 4.2.1). On average, length of the intervertebral spaces was around 10% of the length of their associated centra. Since regressions were performed on pooled family data which consist of small felids and large bovids, I cannot rule out the possibility that intra-family regressions might give different results. This can only be tested by acquiring further samples. However, the data presented here provide no evidence for a relationship other than isometry, which indicates that exclusion of discs should not influence allometric analyses based on centra alone.

Table 4.2.1 Results of ANCOVA on log intervertebral space length.
Intervertebral space length is strongly related to centrum length, but other effects are small and marginally-significant.

	Mean Squares	F-ratio	P-value
Centrum length	0.217	93.876	<0.001
Family	0.012	5.027	0.042
Region	0.012	5.014	0.042
Centrum length*Family	0.013	5.758	0.031
Centrum length*Region	0.019	8.235	0.012
Family*Region	0.009	4.793	0.047

Table 4.2.2 Relationship of intervertebral space length (Y) to centrum length (X).
*relationship not significantly different from one. In both thoracic and lumbar regions, intervertebral space length scales isometrically with centrum length. A, intercept; B, slope, yellow column; LCI, lower confidence interval on slope; UCI, upper confidence interval on slope; SEE, standard error of the estimate.

			LEAST SQUARES				RMA					
X	**Y**	**N**	**A**	**B**	**LCI**	**UCI**	**A**	**B**	**LCI**	**UCI**	**R**	**SEE**
Log thoracic centrum length	Log thoracic intervertebral space length	11	-1.004	0.965*	0.891	1.039	-1.007	0.968*	0.895	1.042	0.998	0.045
Log lumbar centrum length	Log lumbar intervertebral space length	9	-1.071	1.04*	0.987	1.093	-1.074	1.042*	0.989	1.095	0.996	0.063
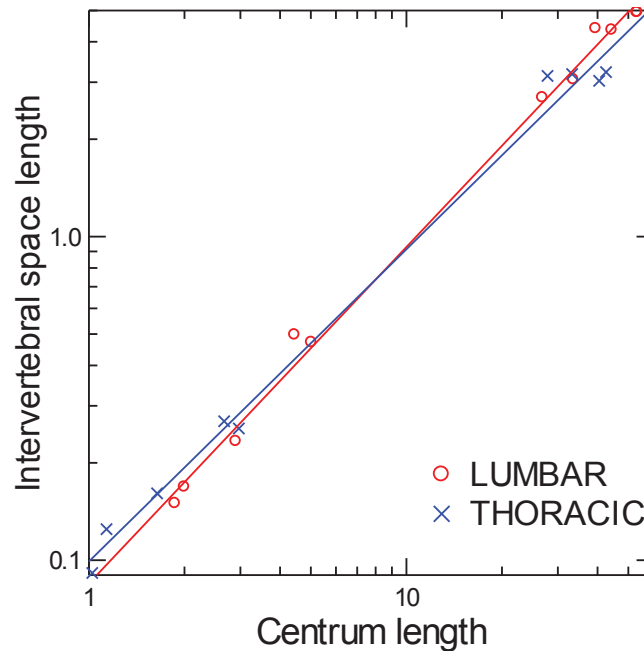
Figure 4.2.1 Relationship of intervertebral space length to centrum length (mm) in felids and bovids.
Scaling is close to isometry in both regions suggesting that excluding discs should not have a large effect on the scaling of region lengths.

4.2.2   LEAST SQUARES AND REDUCED MAJOR-AXIS REGRESSIONS

Linear measurements from the ventral column are provided in Appendix 3. Both least-squares (type 1) and reduced major axis (RMA) regressions were used to test relationships of shape with size. As the correlation coefficients were very high these two methods gave very similar overall results. However, preference is given to RMA, as this method takes into account error on both x and y axis (see Methods section). The results of the RMA on phylogenetically corrected analysis gave mostly similar results, but any contradictions with the RMA analysis are presented in the next section. Slopes (B) are highlighted in yellow in each table and were compared to predictions of elastic and geometric similarity for each measure presented in Table 4.2.3, along with their abbreviations. If shape remains the same with increasing size, under the geometric

139

similarity model, all linear measures will have a slope of 0.33. In contrast, the elastic

similarity model predicts that the ventral column will become more robust, hence there

will be a reduced slope for lengths (0.25) and an increased slope for diameters (0.375).

Examination of residual versus predicted plots for evidence of non-linearity and

normality of the residuals revealed that the data fit well the assumptions of regression.

The only exception was post-diaphragmatic length in bovids, which showed some non-

linearity.

Table 4.2.3 Abbreviations of measurement names and predictions of slopes for geometric similarity and elastic similarity against mass.

Geometric similarity predicts that linear measures should scale against mass with a slope of 0.33, whereas areas should scale with 0.66. Elastic similarity predicts lengths should scale with negative allometry (0.25), but diameters and areas with positive allometry (0.375/0.75).

Measure	Abbreviation	Geometric Similarity	Elastic Similarity
Total thoracolumbar length	TOTTL	0.33	0.25
Total thoracic length	TOTT	0.33	0.25
Total lumbar length	TOTL	0.33	0.25
Pre-diaphragmatic region length	PREDL	0.33	0.25
Post-diaphragmatic region length	PODL	0.33	0.25
Mid-thoracic centrum length	TCL	0.33	0.25
Mid-thoracic centrum height	TCH	0.33	0.375
Mid-thoracic centrum width	TCW	0.33	0.375
Diaphragmatic centrum length	DCL	0.33	0.25
Diaphragmatic centrum height	DCH	0.33	0.375
Diaphragmatic centrum width	DCW	0.33	0.375
Mid-lumbar centrum length	LCL	0.33	0.25
Mid-lumbar centrum height	LCH	0.33	0.375
Mid-lumbar centrum width	LCW	0.33	0.375
Mid-thoracic endplate area	ENDAREAT	0.66	0.75
Diaphragmatic endplate area	ENAREAD	0.66	0.75
Mid-lumbar endplate area	ENDAREAL	0.66	0.75
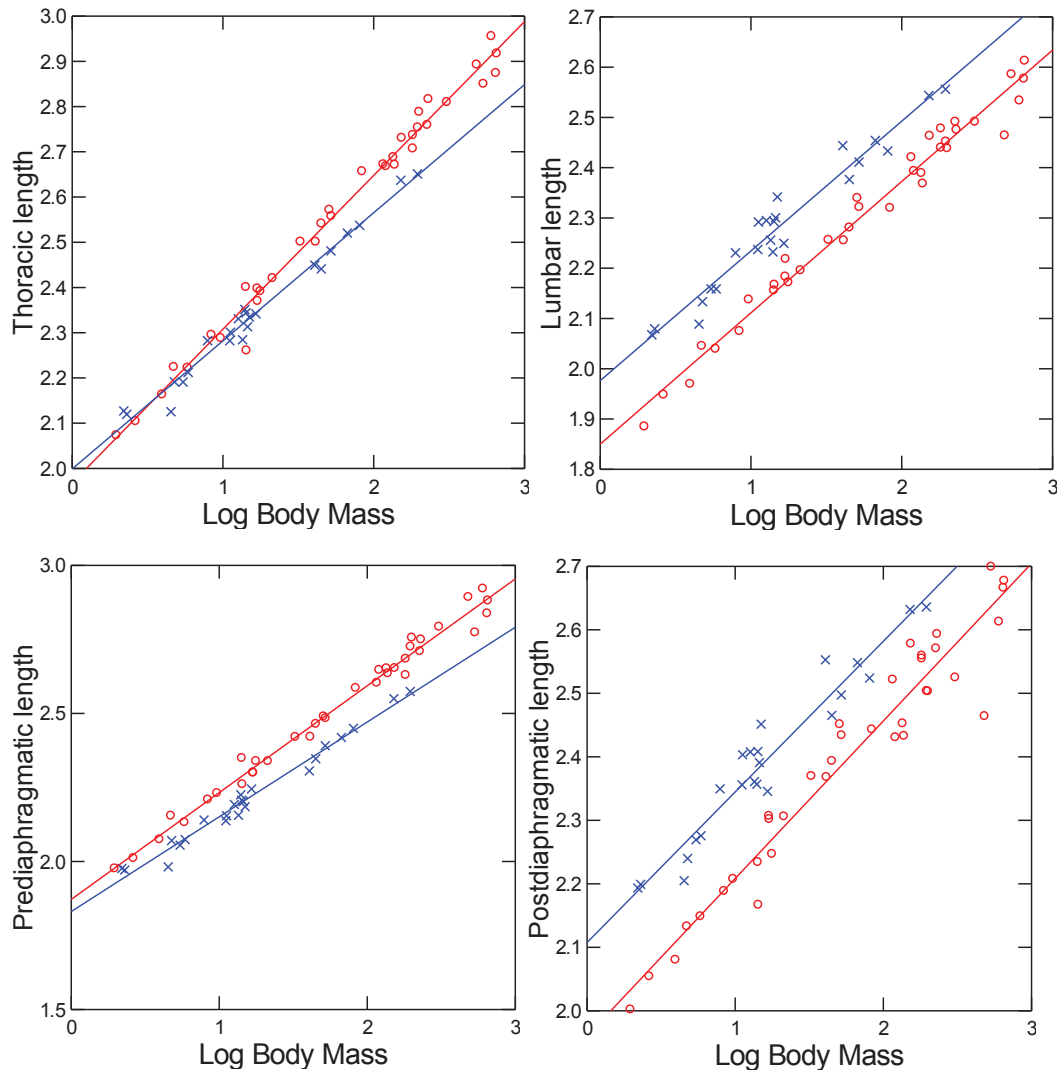
Figure 4.2.2 Bivariate plots of log region lengths against log body mass.
Length in mm, Body Mass in Kg. Red circles, bovids; blue crosses, felids. Note the longer lumbar and post-diaphragmatic regions of felids.

Felidae

Scaling exponents (B) of both least-squares and RMA regressions in felids are presented in Table 4.2.4. Length of the thoracolumbar region in felids scales less steeply than geometric similarity (GS), but more steeply than elastic similarity (ES), suggesting it becomes shorter with increasing size. Examination of regional scaling patterns reveals that this reflects the contrasting scaling patterns of the length of the

thoracic and lumbar regions combined. The thoracic region scales with a steeper slope than the lumbar region (Figure 4.2.2), suggesting that while the lumbar region becomes shorter the thoracic region maintains a more similar length with increasing size. Scaling of lumbar length was not significantly different from ES using both regression models. Further, when the zygapophyseal definition is used to define the regions the contrast becomes even more marked. The length of the pre-diaphragmatic region scales with GS (geometric isometry), whereas the length of the post-diaphragmatic region scales with ES indicating shortening (Figure 4.2.2).

In terms of diameter of the ventral column, interesting craniocaudal patterns are seen (Figure 4.2.3). At the mid-thoracic position, scaling of centrum height exceeds elastic similarity (0.396/0.398), indicating that the thoracic centra become very tall as size increases. In stark contrast, the width of the mid-thoracic centrum scales with GS, indicating that this measure remains similar with increasing size. In the diaphragmatic region height also scales more steeply than width. This time height scales with ES, whereas width scaling slightly exceeds GS. In the mid-lumbar region, height scales with ES, whereas width scales with GS. This indicates a heightening of the centrum with size while the width remains similar. In terms of overall endplate area, the scaling exponents decrease craniocaudally. The mid-thoracic and diaphragmatic positions scale with ES, becoming relatively larger in terms of area with size, whereas mid-lumbar centrum area scales with slightly less than ES.

Table 4.2.4 Scaling exponents of ventral column dimensions with body mass for felids.

All variables were log transformed. Bold values are not significantly different from elastic similarity (ES). Underlined slopes are not significantly different from geometric similarity (GS). All branch lengths were Grafen Rho (0.5) transformed (see Table 4.7 for justification). A, intercept; B, slope; highlighted in yellow; LCI, lower confidence interval on slope; UCI, upper confidence interval on slope; SEE, standard error of the estimate. See Table 4.2.3 for other abbreviations. There is no A (intercept) for PIC slopes because regressions were run through the origin.

FELIDS MEASURE	N	LEAST SQUARES				RMA						INDEPENDENT CONTRASTS				
		A	B	LCI	UCI	A	B	LCI	UCI	R	SEE	B	LCI	UCI	R	SE
TOTTL	23	2.289	0.272	0.253	0.29	2.285	0.275	0.256	0.293	0.989	0.022	0.276	0.254	0.298	0.966	0.011
TOTT	23	1.99	0.282	0.265	0.302	1.995	0.286	0.268	0.305	0.989	0.022	0.288	0.265	0.311	0.964	0.012
TOTL	23	1.976	0.258	0.232	0.284	1.969	0.265	0.238	0.291	0.976	0.032	0.267	0.239	0.294	0.943	0.014
PREDL	23	1.841	0.314	0.296	0.333	1.838	0.317	0.298	0.335	0.992	0.022	0.314	0.289	0.339	0.965	0.013
PODL	23	2.117	0.232	0.204	0.259	2.108	0.239	0.211	0.267	0.969	0.032	0.255	0.226	0.284	0.929	0.015
TCL	23	0.858	0.288	0.272	0.304	0.855	0.29	0.274	0.306	0.993	0.019	0.288	0.267	0.309	0.971	0.011
TCH	23	0.495	0.396	0.382	0.411	0.494	0.398	0.383	0.412	0.997	0.017	0.405	0.385	0.425	0.987	0.010
TCW	23	0.648	0.345	0.32	0.369	0.643	0.349	0.324	0.373	0.989	0.029	0.35	0.317	0.382	0.952	0.017
DCL	23	0.934	0.277	0.264	0.289	0.932	0.278	0.266	0.29	0.996	0.014	0.284	0.260	0.308	0.962	0.012
DCH	22	0.521	0.392	0.372	0.413	0.518	0.395	0.374	0.415	0.994	0.022	0.4	0.373	0.427	0.976	0.014
DCW	22	0.794	0.348	0.334	0.361	0.793	0.349	0.335	0.362	0.997	0.015	0.34	0.324	0.356	0.989	0.008
LCL	23	1.197	0.237	0.209	0.264	1.188	0.244	0.216	0.272	0.97	0.032	0.26	0.228	0.292	0.917	0.016
LCH	23	0.602	0.38	0.362	0.399	0.599	0.382	0.364	0.401	0.994	0.022	0.377	0.356	0.398	0.982	0.011
LCW	23	0.861	0.341	0.326	0.356	0.859	0.342	0.328	0.357	0.996	0.017	0.332	0.315	0.349	0.985	0.009
ENDAREAT	23	1.049	0.734	0.702	0.774	1.045	0.742	0.706	0.778	0.995	0.042	0.748	0.703	0.793	0.979	0.023
ENAREAD	23	1.251	0.73	0.703	0.757	1.248	0.732	0.705	0.759	0.997	0.029	0.724	0.691	0.757	0.989	0.017
ENDAREAL	23	1.395	0.713	0.684	0.742	1.392	0.716	0.687	0.745	0.996	0.034	0.699	0.665	0.733	0.987	0.018
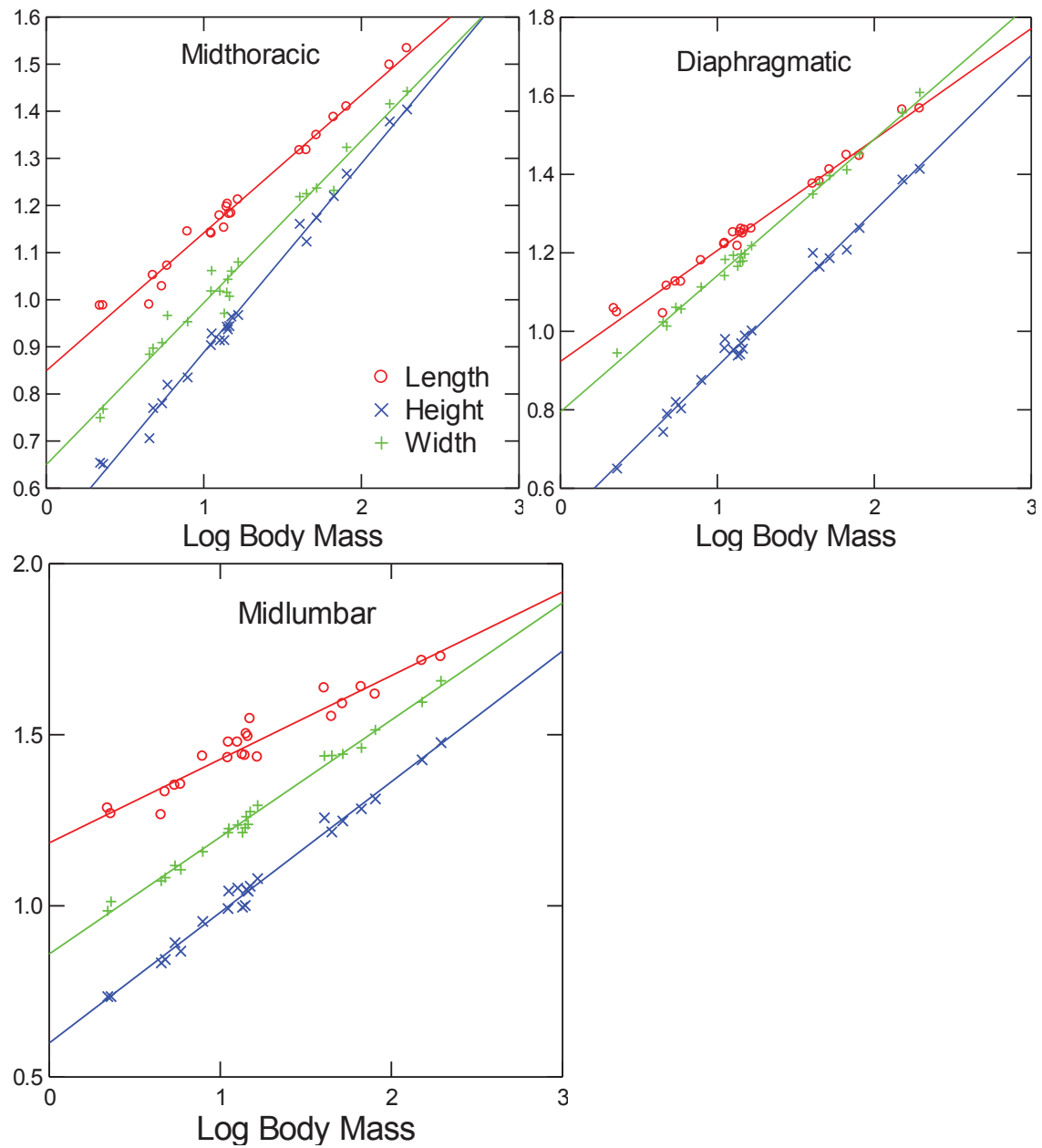
Figure 4.2.3 Scaling of the dimensions of individual vertebrae at three positions for felids.

Y axis: log centrum dimensions in mm, log body mass in Kgs. Red circle, length; blue cross, height; green plus, width. Height scales most steeply, followed by width, then length.

Bovidae

Scaling exponents (B) of both least-squares and RMA regressions in bovids can be found in Table 4.2.5. In bovids, the total thoracolumbar length scales with a slightly lower exponent than GS, indicating slight shortening. As in felids, scaling was stronger in the lumbar than the thoracic region in terms of length (Figure 4.2.2). The thoracic region scales with GS, suggesting length of this region remains similar with size increases. In contrast, the lumbar region scales with ES (least-squares) or slightly steeper (RMA), indicating more extreme shortening. Pre-diaphragmatic length scales more steeply than GS in both models, actually becoming relatively longer as size increases. Conversely post-diaphragmatic length scales with ES in both models representing a shortening with increasing size. *Bison bonasus* was an outlier with a relatively short post-diaphragmatic and lumbar region, and as this species was only represented with one specimen this may represent an anomalous result.

In terms of column diameter, craniocaudal patterns mimic those found in felids and height scales more steeply than width, suggesting the centra tend to become taller than wider (Figure 4.2.4). In the mid-thoracic region, centrum height scales more steeply than ES (0.423/0.425). In contrast, centrum width scales slightly more steeply than GS, but less than ES (0.354/0.355). At the diaphragmatic vertebra, height scales more steeply than ES but width scales less steeply than GS. At the mid-lumbar position, height scales with ES, whereas width scales slightly less steeply than GS, indicating the centra become a little narrower. Endplate area slopes decrease caudally, with mid-thoracic area meeting expectations of ES but diaphragmatic and mid-lumbar area falling between GS and ES (Figure 4.2.5).

Table 4.2.5 Scaling exponents of centrum dimensions with body mass for bovids.

All variables were log transformed. Bold slopes are not significantly different to geometric similarity. Underlined slopes are not significantly different to elastic similarity. All branch lengths were natural log transformed (see table 4.7 for justification). A, intercept; B, slope, yellow column; LCI, lower confidence interval on slope; UCI, upper confidence interval on slope; SEE, standard error of the estimate. There is no A (intercept) for PIC slopes because regressions were run through the origin.

BOVIDS MEASURE	N	LEAST SQUARES				RMA						INDEPENDENT CONTRASTS				
		A	B	LCI	UCI	A	B	LCI	UCI	R	SEE	B	LCI	UCI	R	SE
TOTTL	35	2.21	0.312	0.303	0.321	2.208	0.313	0.304	0.322	0.996	0.019	0.315	0.296	0.334	0.968	0.009
TOTT	35	1.977	0.337	0.326	0.348	1.974	0.338	0.327	0.349	0.996	0.023	0.338	0.315	0.361	0.958	0.012
TOTL	35	1.849	0.262	0.248	0.276	1.843	0.265	0.251	0.279	0.989	0.03	0.282	0.253	0.311	0.905	0.015
PREDL	35	1.874	0.36	0.345	0.375	1.87	0.362	0.348	0.377	0.993	0.031	0.361	0.336	0.386	0.957	0.013
PODL	34	1.957	0.254	0.237	0.272	1.949	0.259	0.241	0.277	0.982	0.036	0.284	0.240	0.328	0.792	0.022
TCL	35	0.835	0.341	0.33	0.351	0.832	0.342	0.332	0.352	0.996	0.022	0.348	0.328	0.368	0.969	0.010
TCH	35	0.471	0.423	0.408	0.438	0.468	0.425	0.41	0.44	0.995	0.031	0.441	0.406	0.476	0.944	0.018
TCW	35	0.663	0.354	0.343	0.364	0.66	0.355	0.344	0.366	0.996	0.022	0.377	0.353	0.402	0.962	0.013
DCL	35	0.923	0.309	0.3	0.318	0.921	0.31	0.301	0.319	0.997	0.018	0.325	0.304	0.346	0.964	0.011
DCH	35	0.508	0.398	0.383	0.412	0.504	0.4	0.385	0.415	0.995	0.031	0.403	0.376	0.430	0.959	0.014
DCW	35	0.78	0.317	0.307	0.327	0.778	0.318	0.308	0.329	0.996	0.022	0.334	0.315	0.353	0.972	0.009
LCL	35	1.072	0.267	0.256	0.278	1.069	0.269	0.258	0.28	0.993	0.023	0.294	0.275	0.313	0.963	0.009
LCH	35	0.577	0.383	0.371	0.395	0.574	0.385	0.373	0.397	0.996	0.025	0.403	0.381	0.425	0.974	0.011
LCW	35	0.844	0.316	0.306	0.327	0.841	0.318	0.307	0.328	0.996	0.022	0.332	0.314	0.350	0.973	0.009
ENDAREAT	35	1.045	0.771	0.749	0.793	1.041	0.773	0.751	0.795	0.997	0.046	0.811	0.757	0.865	0.959	0.028
ENAREAD	35	1.22	0.702	0.681	0.722	1.215	0.704	0.684	0.725	0.997	0.043	0.722	0.687	0.757	0.979	0.018
ENDAREAL	35	1.351	0.688	0.67	0.707	1.348	0.69	0.672	0.708	0.997	0.038	0.722	0.689	0.755	0.981	0.017
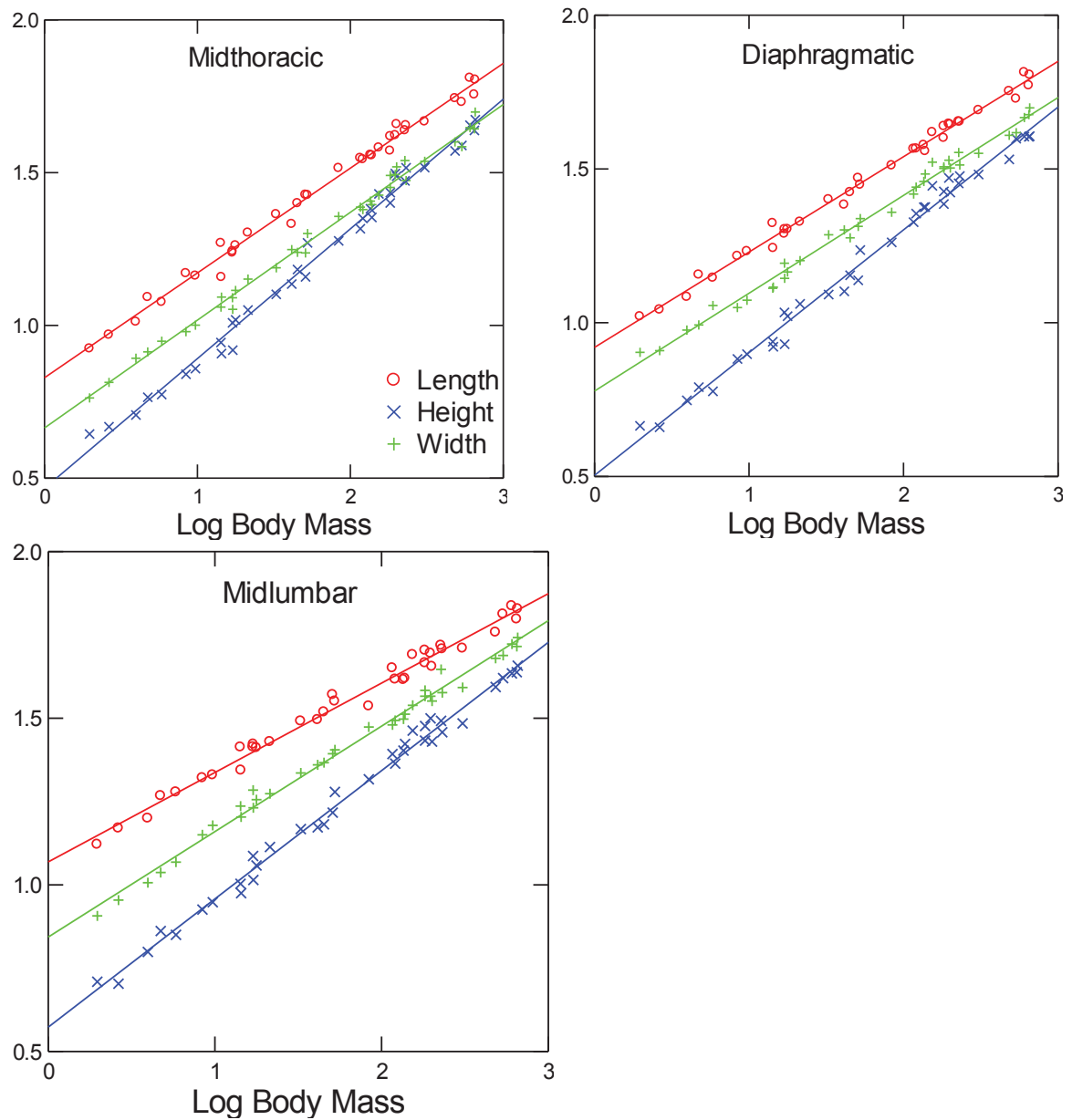
Figure 4.2.4 Scaling of the dimensions of individual vertebrae at three positions for bovids.

Y axis: log centrum dimensions in mm, log body mass in Kgs. Red circle, length; blue cross, height; green plus, width. Height scales most steeply, followed by width, then length.

147

Family differences

ANCOVAs were used to test for family level differences between slopes and elevations (Table 4.2.6). Unsurprisingly, the effect of body mass was highly significant in all the ANCOVAs. In terms of slope differences, bovids scale more steeply than felids in total thoracolumbar length, total thoracic length and total pre-diaphragmatic length (Figure 4.2.2), as well as individual lengths of the mid-thoracic, diaphragmatic and mid-lumbar vertebrae. They also exceed felids in thoracic centrum height scaling. Felid slopes are greater for both diaphragmatic and mid-lumbar widths. In terms of elevation differences, bovids have wider mid-thoracic centra and larger mid-thoracic endplate areas. In contrast, felids have longer lumbar and post-diaphragmatic regions (Figure 4.2.2). They also have slightly taller lumbar centra and larger endplate areas at the diaphragmatic and mid-lumbar positions (Figure 4.2.5).

Table 4.2.6 ANCOVAs on centrum dimensions.

*Differences in slope and intercept between families. Elevation differences were only tested when slopes were similar. Mean squares values are shown. *significant at the 0.05 level. **significant at the 0.01 level. Variable abbreviations are shown in table 4.2.3.*

Variable	N	Body mass	Family	Body mass *Family	Elevation difference?	Slope difference?
TOTTL	57	1.486**	0.014**	0.009**	-	B>F
TOTT	57	1.688**	0.002*	0.016**	-	B>F
TOTL	57	1.184**	0.038**	>0.001	F>B	-
PREDL	57	2.034**	0.002	0.009**	-	B>F
PODL	57	1.018**	0.045**	0.001	F>B	-
TCL	57	1.767**	0.001	0.013**	-	B>F
TCH	57	3.004**	0.001	0.003*	-	B>F
TCW	57	2.99**	0.008**	>0.001	B>F	-
DCL	57	1.534**	>0.001	0.005**	-	B>F
DCH	56	2.485**	>0.001	>0.001	-	-
DCW	56	1.759**	>0.001	0.004**	-	F>B
LCL	57	1.136**	0.031**	0.004*	-	B>F
LCH	57	3.547**	0.005**	>0.001	F>B	-
LCW	57	1.933**	0.001	0.003*	-	F>B
ENDAREAT	57	10.182**	0.019*	0.005	B>F	-
ENAREAD	56	11.721**	0.058**	0.003	F>B	-
ENDAREAL	57	11.673**	0.07**	0.003	F>B	-
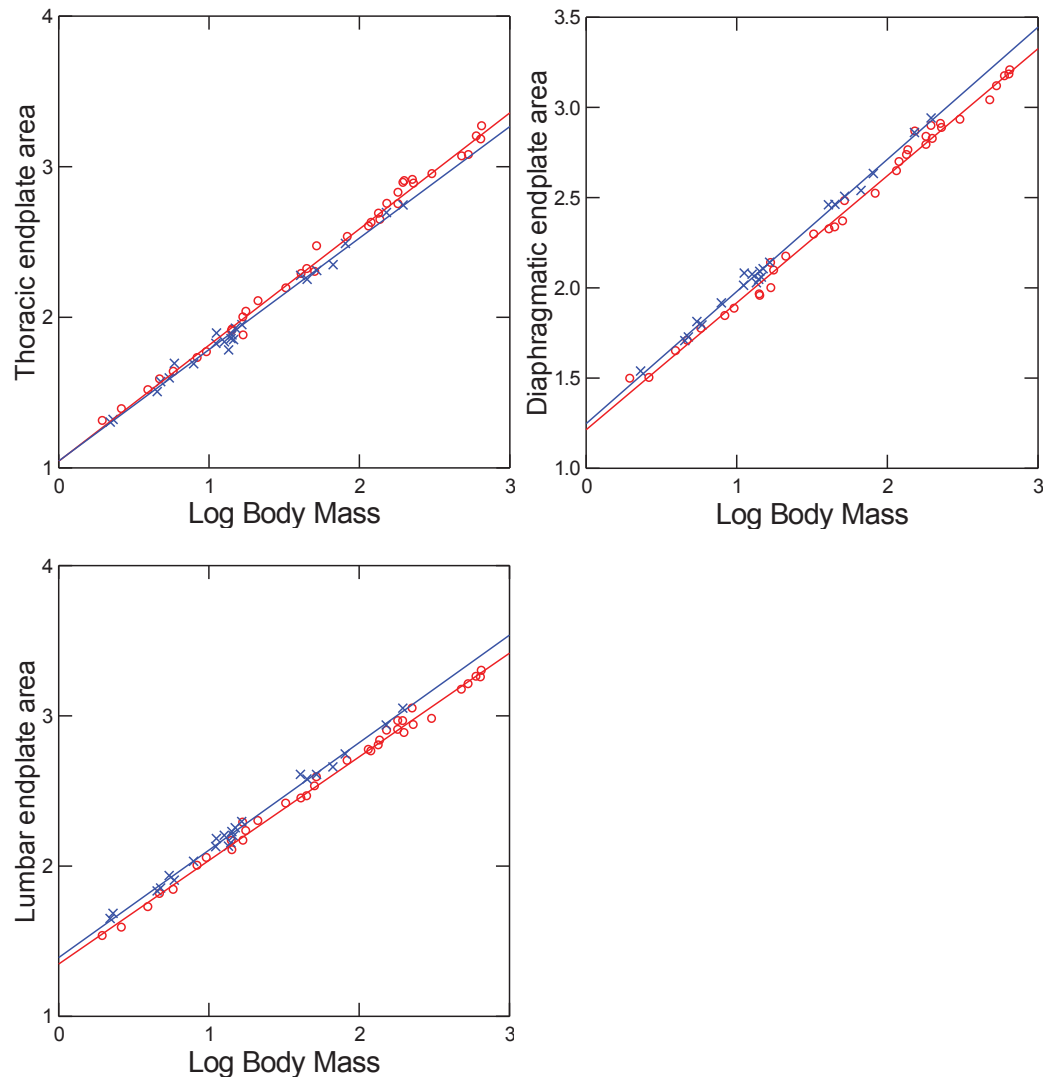
Figure 4.2.5 Bivariate plot of endplate area against body mass.

Area in logged mm². Red circles, bovids; blue crosses, felids. Bovids have slightly larger thoracic centra, whereas felids have slightly larger diaphragmatic and lumbar centra.

4.2.3   PHYLOGENETICALLY INDEPENDENT CONTRASTS REGRESSIONS

Branch length transformations

      To check that the contrasts used in the phylogenetic independent contrasts

(**PIC**) analyses were properly standardized, the regression coefficients for correlations

between the absolute contrasts and their deviations were used (Table 4.2.7). Low

correlations indicate proper standardization. Correlations were compared for raw

branch length data, and branch lengths that had been transformed using natural log and Grafen Rho transform. For felids, the Grafen-Rho transformed branch lengths produced the lowest correlations and were used in the subsequent analyses. For bovids, log-transformed branch length produced the lowest correlations, though the correlation coefficients were higher than those produced for felids. This seemed to be driven by very short branches between species of the same genus -- i.e., *Bos, Bison* and *Connochaetes.*

Table 4.2.7 Testing branch length assumptions for Independent Contrasts analysis. *Correlation values (r-squared) for the absolute value of the standardized contrast against the square root of the sum of the corrected branch lengths, using both raw data and with branch lengths transformed by natural log and Grafen's rho. High correlations indicate that the contrasts are not properly standardized and branch lengths do not meet requirements. Lowest correlations are emboldened, and the transformation which yields the lowest correlations was used in the independent contrasts analysis. For abbreviations see Table 4.2.3.*

Variable	Felidae			Bovidae		
	Raw	Log	Grafen (0.5)	Raw	Log	Grafen (0.5)
BODY MASS	0.1979	0.2585	**0.082**	0.1994	**0.0733**	0.1965
TOTTL	0.2183	0.2471	**0.0907**	0.1577	**0.1202**	0.2324
TOTT	0.2146	0.2386	**0.0971**	0.1429	**0.1107**	0.2335
TOTL	0.2011	0.2333	**0.0719**	0.1858	**0.1111**	0.2176
PREDL	0.2178	0.2421	**0.1088**	0.1396	**0.1248**	0.2291
PODL	0.2234	0.2512	**0.0699**	0.2172	**0.0851**	0.2702
TL	0.1698	0.1901	**0.0722**	0.161	**0.1147**	0.2246
TCH	0.1847	0.231	**0.0600**	0.1736	**0.1429**	0.212
TCW	0.1844	0.2537	**0.0847**	0.225	**0.1898**	0.236
DL	0.1706	0.1755	**0.0539**	0.2038	**0.1788**	0.2512
DCH	0.1057	0.0558	**0.0446**	0.1105	**0.0761**	0.1959
DCW	0.1067	0.0699	**0.0656**	0.2036	**0.1231**	0.2591
LL	0.2229	0.2279	**0.0671**	0.2018	**0.1523**	0.2466
LCH	0.1659	0.1999	**0.0876**	0.1985	**0.1305**	0.2576
LCW	0.1799	0.2182	**0.0757**	0.1513	**0.0847**	0.2149
TAREA	0.1931	0.2524	**0.0772**	0.2031	**0.173**	0.2244

DAREA	0.1089	0.0658	**0.0569**	0.1607	**0.1026**	0.2279
LAREA	0.1796	0.2176	**0.0835**	0.1772	**0.1103**	0.2375

Slope differences with phylogenetic correction

Phylogenetically corrected slopes (RMA) can be compared to slopes using raw data in Table 4.2.4 for felids and Table 4.2.5 for bovids. Phylogenetically corrected slopes for felids were very similar to those produced using raw data. In terms of matching predictions for GS and ES, the patterns for felids are the same except that diaphragmatic centrum width matches GS using contrasts, but slightly exceeds it using the raw data. In contrast, the patterns seen in the bovid data using contrasts are quite different from those using raw data. In general, the contrasts data tended to give steeper slopes than the raw data. Total thoracolumbar length was not significantly different from GS using contrasts, but was less than GS using raw data. Mid-thoracic centrum height was even steeper using this method (0.441), and mid-thoracic centrum width matched ES. Mid-thoracic centrum length, diaphragmatic centrum length, diaphragmatic centrum width and mid-lumbar centrum width were all significantly similar to GS using the contrasts method. In contrast, mid-lumbar centrum height exceeded ES. In terms of endplate areas, diaphragmatic and mid-lumbar endplates matched ES whereas the mid-thoracic endplate exceeded it. In addition, the correlation coefficient for post-diaphragmatic length was much lower for the PIC method (0.792) than the raw data (0.982), indicating a poorer fit of the data. The larger discrepancy in results in the bovid than felid data may result from stronger phylogenetic signal in the bovid data, or because the branch length transformation was less satisfactory.

4.3 DISCUSSION

4.3.1 HYPOTHESES

The centrum, along with the intervertebral discs, forms the ventral column, which is the major weight-bearing portion of the vertebral column. This chapter has demonstrated that **allometry of the ventral column was generally consistent with an elastic similarity model in the craniocaudal and sagittal dimensions, but patterns of allometry vary along the column.** A summary of the findings of this chapter can be found in Table 4.3.1.

Table 4.3.1 Summary of results from allometric analyses.
GS, geometric similarity; ES, elastic similarity.

	THORACIC	TRANSITIONAL	LUMBAR
FELIDS	**Length:** intermediate **Height:** >ES **Width:** GS **Area:** ES	**Length:** intermediate **Height:** ES **Width:** ~GS **Area:** ES	**Length:** ES **Height:** ES **Width:** GS **Area:** intermediate
BOVIDS	**Length:** GS **Height:** >ES **Width:** intermediate **Area:** ES	**Length:** intermediate **Height:** >ES **Width:** <GS **Area:** intermediate	**Length:** ES **Height:** ES **Width:** <GS **Area:** intermediate

I can now address the specific hypotheses posed at the beginning of the chapter as follows:

H1. Craniocaudal length of the ventral column (regions and individual centra) will scale with exponent 0.25 (elastic similarity), indicating that the column becomes relatively shorter with increasing size.

Length scaling varies among vertebral regions. In the thoracic region H1 can be rejected, as thoracic region length scales with GS in bovids and slightly above GS in felids. Therefore the length of the thoracic region remains approximately equivalent

with increasing size. However, H1 is supported in the lumbar region, where length scales with the predicted ES slope of 0.25, or very close to it in bovids. This indicates that the lumbar region is relatively shorter in larger animals. More interesting patterns emerge when we compare the rib-based and zygapophysis-based definitions of the lumbar region. In both groups the slope of the pre-diaphragmatic region exceeds that of the thoracic region, whereas that of the post-diaphragmatic region is less than the lumbar region. This results in an even starker contrast in slopes when the zygapophyseal instead of the rib-based definition is used. Thus the pre-diaphragmatic region meets (felids) or exceeds (bovids) GS, whereas the post-diaphragmatic region meets ES in both groups, using all regression models. This suggests that the transitional region scales with a slope of less than GS (more similar to the lumbar region). This may be due to shortening of individual vertebrae, or to loss of vertebrae if the diaphragmatic vertebra shifts to a more caudal position relative to the first rib with size. In terms of individual centra lengths, there was a reduction in the scaling exponent posteriorly in both felids and bovids, such that the mid-thoracic position exceeded the diaphragmatic, which itself exceeded the mid-lumbar position. Thus, similarly to the region scaling, lumbar centra more closely matched predictions of elastic similarity (0.244/0.269 for felids/bovids) than the more anterior positions.

These data agree with previous studies of bovid lumbar length scaling (Halpert et al., 1987). In comparison to similar data collected on thoracolumbar region lengths in primates, the thoracic region of these quadrupedal mammals scales more steeply than: an all-primates sample (0.27), prosimians (0.29), platyrrhines (0.3) or catarrhines (0.23); whereas the lumbar region scales less steeply than: all-primates (0.29) or

prosimians (0.4); but similarly to: platyrrhines (0.23) and catarrhines (0.25) (Majoral et al., 1997).

H2. Dorsoventral height of the ventral column will scale with exponent 0.375 (elastic similarity), indicating that it becomes relatively deeper with increasing body size.

Scaling exponents of centrum height either exceeded (felid mid-thoracic, bovid mid-thoracic and diaphragmatic) or met (felid diaphragmatic, felid mid-lumbar, bovid mid-lumbar) the elastic similarity prediction. H2 is therefore accepted because these results indicate deepening of the ventral column to an equivalent level, or in excess of, levels that are required to produce similar elastic deformations. In felids, centrum height exponents are relatively similar along the column and only decrease slightly caudally (mid-thoracic = 0.398, diaphragmatic =0.395, mid-lumbar =0.382). In bovids, however, there was a stronger caudal decrease in scaling exponents (mid-thoracic = 0.425, diaphragmatic = 0.4, mid-lumbar = 0.385). Moreover, the slope of the mid-thoracic centrum height was significantly greater in bovids than felids, suggesting that mid-thoracic vertebrae become more robust in the sagittal plane in large bovids than in large felids. This may relate to one of two differences between the families. First, it may relate to the fact that thoracic and pre-diaphragmatic region lengths scale more steeply in bovids, such that large bovids have relatively longer thoracic regions, which may require increased sagittal thickness to resist bending. Alternatively, it may relate to the development of large withers in the thoracic region of large bovids which convey extra load from the head via the nuchal ligament. In the lumbar region the scaling exponents of both groups closely match the predictions for ES, except in bovids with phylogenetic contrasts, which was slightly higher than predicted for ES.

155

H3. Mediolateral width of the ventral column will scale with exponent 0.33 (geometric similarity), indicating isometry, because major weight bearing forces are in the sagittal rather than mediolateral plane.

Mediolateral width scaling exponents were much lower than those of dorsoventral height. In felids, centrum width in all three vertebral positions matches GS when using the phylogenetically-corrected method (diaphragmatic width was slightly steeper than GS using raw data). In bovids, the width of the diaphragmatic and mid-lumbar vertebrae matches GS when using contrasts and scales slightly below GS when using raw data, indicating that there was no reinforcement of the centrum or disc in the mediolateral plane with increasing size. In contrast, the mid-thoracic centrum of bovids scales with a slope exceeding GS when using raw data, and matching elastic similarity when using phylogenetically-corrected data. Therefore H3 is supported for all positions except the mid-thoracic region of bovids, which becomes more robust in both mediolateral and sagittal planes than predicted by the model. Previous data from the lumbar region of bovids found slightly higher width and height slopes for the mid-lumbar position (H=0.41, W=0.33) (Halpert et al., 1987).

4.3.2 ALLOMETRY OF THE VENTRAL COLUMN

Results presented in this chapter have shown that the ventral column of the thoracolumbar region changes shape as size increases. Scaling patterns are quite consistent between these two families. As body size increases, the forces acting on the thoracolumbar spine increase, and if its shape and material properties remained similar, the stresses in the column would increase and might approach the safety limits of the intervertebral discs. Hence, these results suggest that structural allometry of the ventral

column is an important mechanism for resisting these increasing loads. If the ventral column was acting only as a compressive element, one would expect equivalent scaling of dorsoventral and mediolateral dimensions. However, the stronger allometry of sagittal dimensions compared to mediolateral dimensions throughout the column suggests that the ventral column resists at least some sagittal bending.

There were two distinct allometric mechanisms in the anterior and posterior regions of the column. Thoracic and pre-diaphragmatic region length in bovids, and pre-diaphragmatic region length (only) in felids, remain similar, or become slightly longer with increasing size. Sagittal dimensions scale with strong positive allometry here, to compensate for this increasing length. On the other hand, the posterior portion of the column decreases in length with increasing size. Elastic similarity is met in the post-diaphragmatic length of bovids and in both lumbar and post-diaphragmatic lengths of felids, while sagittal dimensions increased to a lesser extent than in the thoracic region. The transitional vertebrae showed an intermediate pattern. Total length of the transitional region shortened with increasing size, but diaphragmatic centrum length scaled close to GS in bovids.

Results of this chapter suggest that while the lumbar region becomes stockier in two dimensions (length and height) with increasing size, the thoracic region responds mostly in terms of height. The thoracic region is intimately involved in respiration and is linked to ventral structures via the ribs (Flower, 1885; Jayne, 1898; Bramble and Jenkins, 1993; Rawls and Fisher, 2010). However, evolution of a muscular diaphragm in mammals has functionally differentiated the lumbar region from the rib cage (Schilling and Hackert, 2006; Buchholtz et al., 2011; Buchholtz, 2014). Association of

the pre-diaphragmatic vertebrae with ribs which articulate with the sternum and respiratory structures may place a mechanical constraint on variation in craniocaudal length of these vertebrae. Further, the rib cage may help to support the thoracic region via dorsoventral deepening or thickening of ribs, which could facilitate relatively long thoracic regions in large running mammals; however, more data are required to test this hypothesis.

Contrasting patterns of length variation between the thoracic and lumbar centra also exist through growth (Jones and German, 2014). In four small mammal species, centra in the pre-diaphragmatic region maintained GS as they grew, whereas post-diaphragmatic centra elongated through the post-natal growth period. Mimicking these patterns, species that are specialized for half-bounding had relatively longer centra in the lumbar and post-diaphragmatic regions, achieved by increased post-natal growth, than did generalists (Jones and German, 2014). Thus, both intra- and inter-specific variations in centrum length were concentrated on the same vertebrae: the post-diaphragmatics, with the exception of the last lumbar. The data presented here show that in a cross-taxonomic sample of mammals, from two relatively distantly-related groups with contrasting function, the same pattern exists. Centrum length scaling matches or exceeds GS in the pre-diaphragmatic region, but deviates more from GS in the post-diaphragmatic region. Thus, these developmental and allometric data together support greater plasticity of post-diaphragmatic centra for evolutionary changes in length in running mammals, which may be controlled by variation in post-natal growth. In the absence of shortening length, increasing size of the sagittal dimension seems to be more important for resisting the loads with increasing size in the pre-diaphragmatic

158

region.

There are also some differences between these two families. Cross-sectional dimensions and area of the thoracic centra scale more steeply in bovids than in felids. This may relate to increased loading in the thoracic region of large bovids from supporting a heavy head, which is transferred to the thoracic withers via the nuchal ligament. In addition, felids have longer lumbar and post-diaphragmatic regions than bovids for a given body size. This may be an adaptation to their enhanced use of sagittal bending to increase stride length during running, or during other behaviors such as climbing or pouncing (Hildebrand, 1959; Harty, 2010; Hudson et al., 2012). Consequently, felids also have relatively taller lumbar centra and larger diaphragmatic and lumbar endplate areas than bovids (despite similar slopes). In fact, felids generally have slightly larger lumbar and post-diaphragmatic centra than bovids, whereas bovids typically have slightly larger thoracic centra than felids, in terms of both length and area.

CHAPTER 5: THREE-DIMENSIONAL ALLOMETRY OF THE PENULTIMATE LUMBAR VERTEBRA

This chapter examines the three-dimensional allometry of the penultimate

lumbar vertebra in felids and bovids. The influence of body size on shape is

characterized using geometric morphometrics and multivariate regression. The scaling

of the centrum, arch and process is assessed and the influence of phylogeny tested using

phylogenetically independent contrasts analysis.

5.1   HYPOTHESES

This chapter asks if **allometry of the penultimate lumbar is consistent with

lumbar stabilization with increasing size**, by testing the following specific

hypotheses:

H1. The centrum becomes craniocaudally shorter and dorsoventrally taller with

increasing size.

H2. The zygapophyses become more interlocking and metapophyses become larger.

H3. The processes (spinous and transverse) become more robust, craniocaudally longer,

dorsoventrally/mediolaterally wider and less inclined from the primary planes of the

vertebra.

5.2 RESULTS

5.2.1 BOVIDAE

Species mean PCA

A principal components analysis of all bovid specimens revealed that specimens from the same species tend to group closely together in morphospace on PC1 and PC2 (Figure 5.2.1). This supports the use of species means in subsequent allometric analyses. Species-mean PC scores for bovids can be found in Appendix 4. The distribution of species-mean shapes in a principal components analysis is shown in Figure 5.2.2, shape changes associated with PC1 are shown in Figure 5.2.3 and the variance explained by each component is shown in Table 5.2.1. PC1 explained most of the variation in the sample (77%) and was closely related to size (r-sq=0.835). Small taxa such as *Madoqua* and *Neotragus* cluster at negative PC1 and large taxa such as *Bison* and *Syncerus* display positive PC1 scores. This is despite the fact that pure size was removed during the GPA step, and suggests that there is a significant portion of shape which is highly correlated with size (as demonstrated below).

Multivariate regression of eight PCs (which represent 95% of shape variation) against log body mass was highly significant (p<0.0001).The correlation of shape with size explains 68.2% of the total variance in the sample, indicating that the effect of allometry was large. In particular, PC1 had the largest r-squared value, indicating that it was most strongly related to size (Table 5.2.1), while subsequent components had very low correlations. Shape changes associated with PC1 are shown in Figure 5.2.3. Species with negative scores have a dorsoventrally compressed, mediolaterally wide endplate with strongly ventrally and cranially inclined transverse processes,

craniocaudally long centra and widely-spaced zygapophyses. Positive scores are associated with mediolaterally wider, craniocaudally longer and less inclined transverse processes with dorsoventrally tall and craniocaudally short centra and narrowly-spaced zygapophyses.
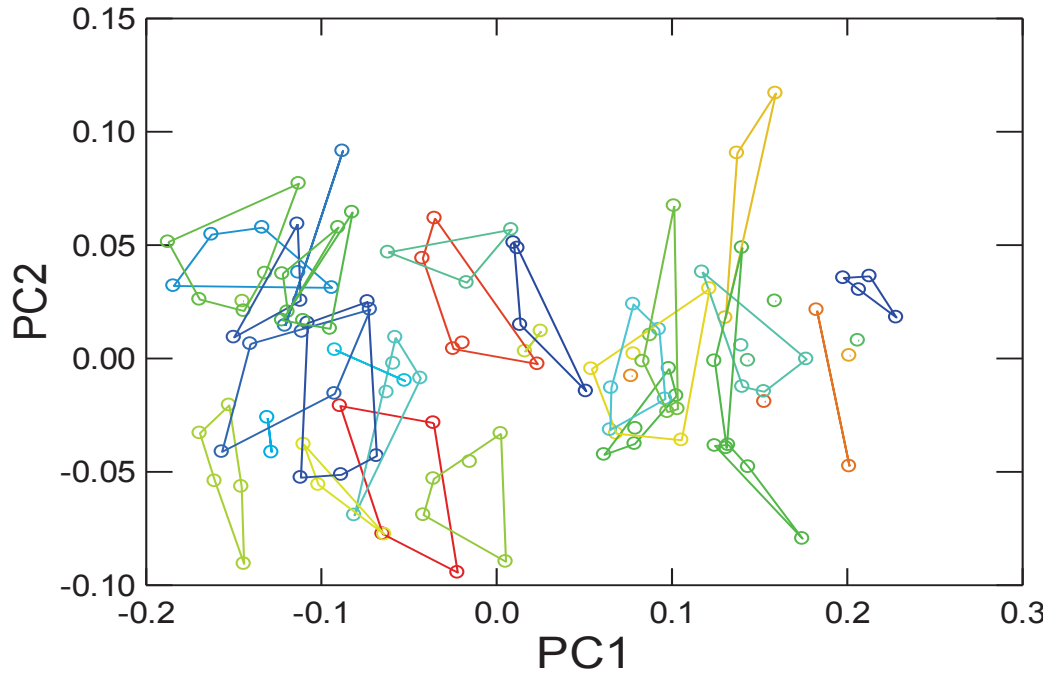
Figure 5.2.1 PC1 against PC2 for all bovid specimens.
Species are grouped by color and connected with polygons. Note the close clustering of specimens from the same species. For taxonomic names and mean values see Figure 5.2.2.
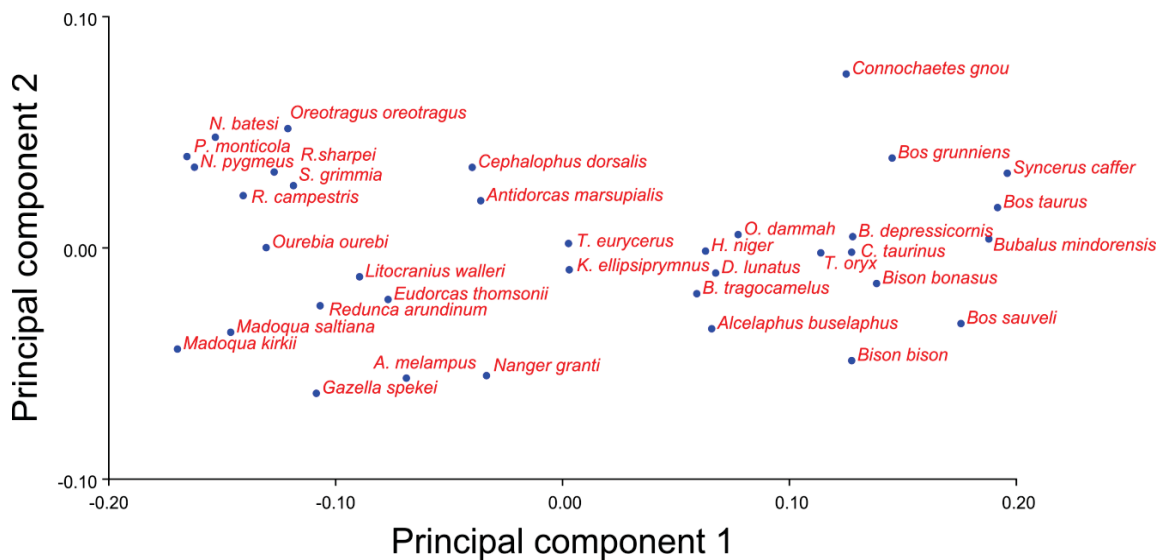
Figure 5.2.2 PC1 against PC2 for a principal components analysis of bovid species-mean shape.
Large species tend to have positive PC1 scores while small species tend to have negative scores. Variance described by each axis shown in Table 5.2.1.
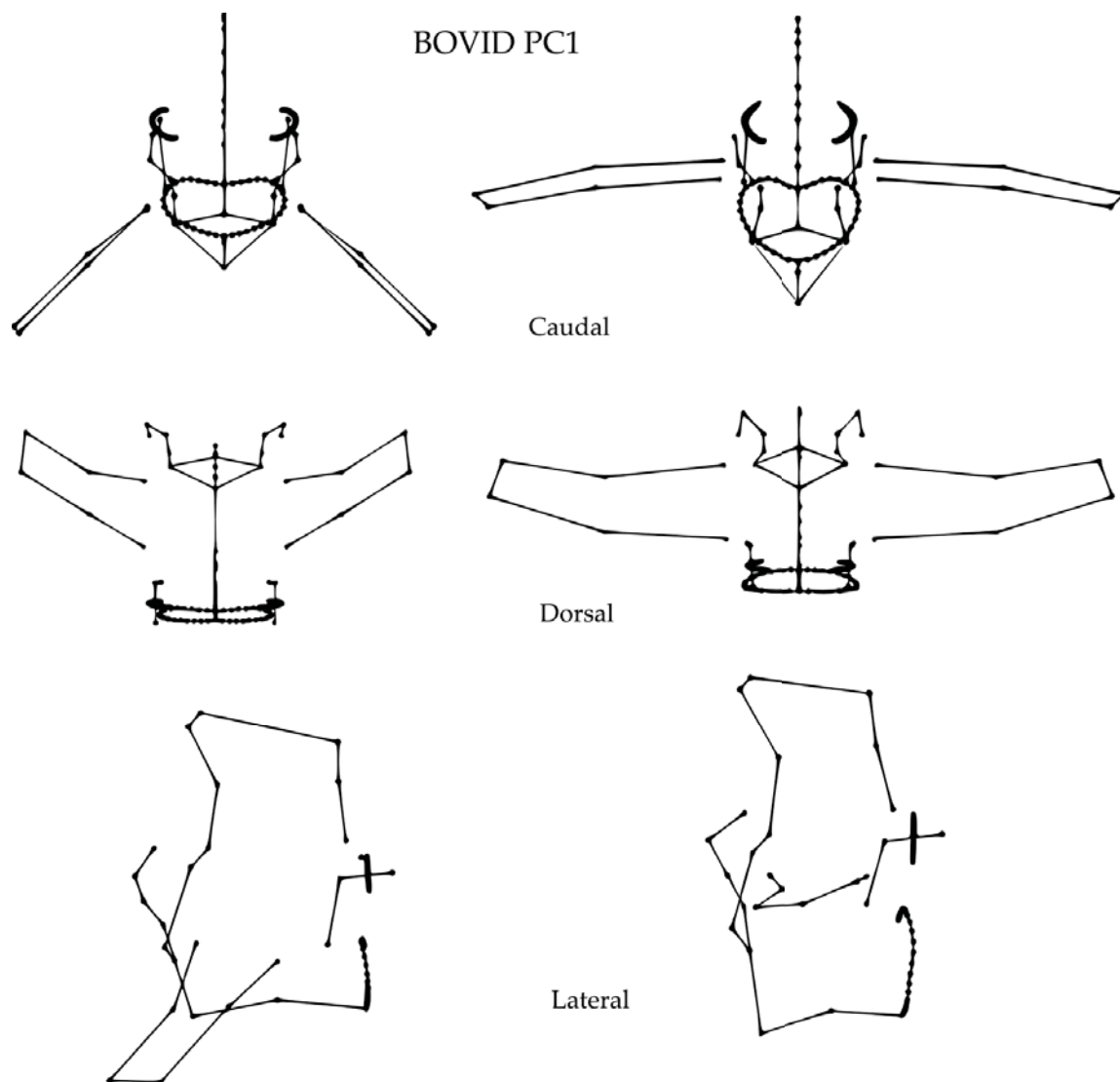
Figure 5.2.3 Shape changes associated with PC1 for the bovid species-mean PCA.
Caudal, dorsal and lateral view. The left side represents negative PC1 scores and the right side positive PC1 scores.

Table 5.2.1 Eigenvalues from principal components analysis of bovid species-mean shape.

Regression coefficients (slope) and r-squared values for multivariate regressions of shape on log body mass using both raw data and phylogenetically-corrected independent contrasts (PIC). r-sq, r-squared value; coeff., coefficient.

PC	Eigenvalues	Variance (%)	Cumulative variance (%)	Regression coeff. (raw)	r-sq	Regression coeff. (PIC)	r-sq
1.	0.0153	77.0	77.0	0.155	0.835	0.130	0.701
2.	0.0012	5.8	82.8	-0.008	<0.001	-0.015	0.036
3.	0.0007	3.8	86.6	0.007	0.003	0.007	0.012
4.	0.0006	3.1	89.7	<0.001	<0.001	0.001	<0.001
5.	0.0005	2.4	92.1	-0.006	0.009	-0.007	0.024
6.	0.0003	1.4	93.5	-0.001	<0.001	0.002	0.002
7.	0.0002	1.1	94.6	0.001	<0.001	0.003	0.009
8.	0.0002	0.8	95.4	0.002	<0.001	0.006	0.040

Phylogeny

To correct for phylogeny, principal components scores for the eight components representing over 95% of variation were subjected to phylogenetically independent contrasts analysis. The appropriateness of branch lengths was assessed using the correlation of absolute contrasts with the branch lengths, and r-squared values are shown in Table 5.2.2. Generally, the Grafen-rho transformation produced the lowest correlations, and therefore the most appropriate branch lengths. Since all variables were considered simultaneously in a multivariate regression, Grafen-rho (0.5) was used to scale all variables even though other transformations were better for some variables. Multivariate regression of standardized contrasts through the origin also revealed a highly significant effect of body mass (p<0.001), with highest correlations on PC1.

Table 5.2.2 Assumptions of independent contrasts analysis for bovids.
Correlation coefficients of absolute contrasts versus square root of sum of corrected branch lengths of raw, log-transformed and Grafen-rho transformed branch lengths. The lowest correlations indicate the best fit of branch lengths and are emboldened.

	Raw	**Log**	**Grafen (0.5)**
PC1	**0.0017**	0.0059	0.108
PC2	0.3536	0.4618	**0.105**
PC3	0.1989	0.0792	**0.0217**
PC4	**<0.0001**	0.0023	0.0106
PC5	0.2807	0.1119	**0.0218**
PC6	0.0269	0.0573	**0.0079**
PC7	0.1308	0.1557	**0.0041**
PC8	0.256	0.2239	**0.0012**
Body Mass	0.118	**0.0721**	0.193

Vertebral regions

A permutation test of 10,000 contiguous partitions of landmarks revealed that centrum, arch and processes vary relatively independently of one-another and thus can be considered semi-autonomous modules (p=0.006). When regressions were performed separately on landmarks from each of these modules the effect of size varied between regions. Size explains 58.8% and 63.3% of shape variation in the processes and centrum, respectively, but only 17.1% of variation in the arch, indicating a smaller influence of allometry in the arch.

Allometric vector

The interspecific allometric vector (shape associated with increasing size) was calculated using the coefficients of a multivariate regression which included all the Procrustes coordinates. Since all the variation was included, the shape changes associated with size could be calculated. This allometric vector is illustrated in Figure 5.2.4 and closely resembles shape changes seen in PC1. The typical small bovid lumbar is relatively elongate with ventrally and cranially inclined transverse processes. The

centrum is dorsoventrally compressed and the zygapophyses are wide-set and revolute. The neural spine is craniocaudally elongate and cranially inclined. As size increases, the shape of the penultimate lumbar changed. There is a noticeable craniocaudal shortening and dorsoventral expansion of the body, which has a more heart-shaped outline. The zygapophyses are relatively closely spaced, tall and slightly sigmoid-revolute. Both the transverse and neural processes are oriented perpendicular to the major planes of the vertebra, and are no longer inclined. Transverse processes are relatively longer.

BOVIDAE

Caudal

Dorsal

Lateral

SMALL   LARGE
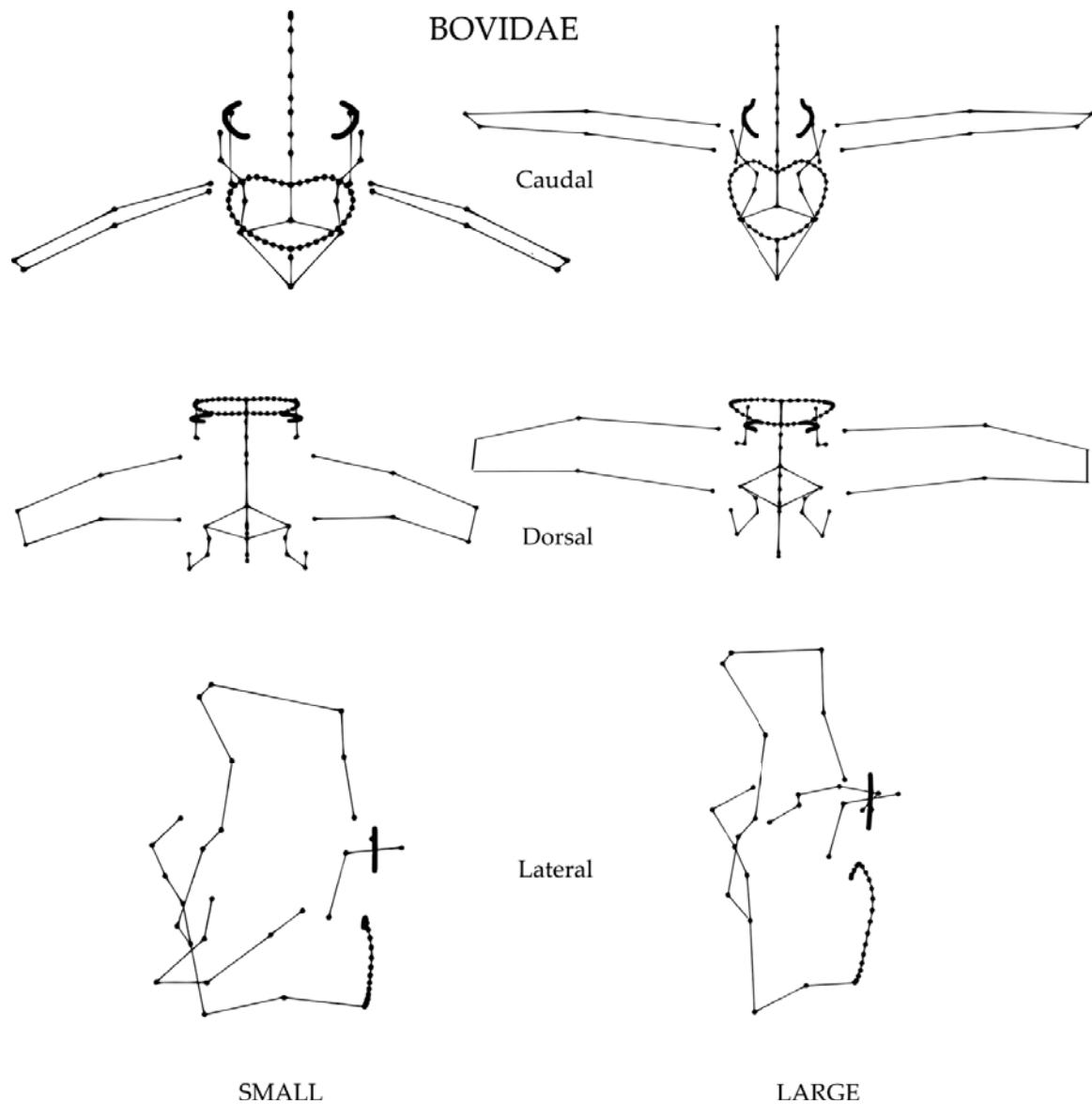
Figure 5.2.4 Allometric vector in bovids.
The allometric vector was calculated from the coefficients of a multivariate regression of all the Procrustes co-ordinates onto log body mass, and represents the portion of shape most correlated with size. Left side is small extreme and right side is the large extreme.

5.2.2 FELIDAE

Species mean PCA

A PCA of Procrustes coordinates from landmarks from all specimens is shown in Figure 5.2.5. When variation across all specimens was considered, specimens tended to cluster together by species, suggesting intraspecific variation is smaller than interspecific variation. Species-mean shape was computed by averaging Procrustes coordinates from specimens and the resulting PCA is shown in Figure 5.2.6, with associated eigenvalues (relative contribution to variance) in Table 5.2.3 and shape changes for PC1 in Figure 5.2.7. Species mean PC scores are provided in Appendix 5.

As observed for bovids, PC1 is strongly related to size. Large species such as the lion and tiger (*Panthera leo* and *Panthera tigris)* have positive PC1 scores, and small species such as *Leopardus tigrinus* tend to have negative values. PC1 contributes 57.3% to the total variance in the sample. The strong relationship of PC1 with body mass was confirmed by a significant slope when ten PCs (constituting over 95% of total variation) were regressed against log body mass using multivariate regression (p<0.001). However, only 40.3% of total variation was attributable to size, suggesting size has less relative influence on shape than for bovids. Examining regressions of individual PCs reveals that PC1 was primarily related to size. It has higher regression coefficients and r-squared values than the other PCs (Table 5.2.3). Shape variation on PC1 is depicted in Figure 5.2.7. Negative PC1 scores represent a vertebra with a craniocaudally long and dorsoventrally-compressed, oval centrum. The zygapophyses were dorsally placed and transverse processes were strongly ventrally inclined. The

neural spine was slender and cranially inclined. In contrast, positive scores indicate a shorter centrum with larger, rounder endplate, more robust transverse processes and a more upright neural spine (Figure 5.2.7).
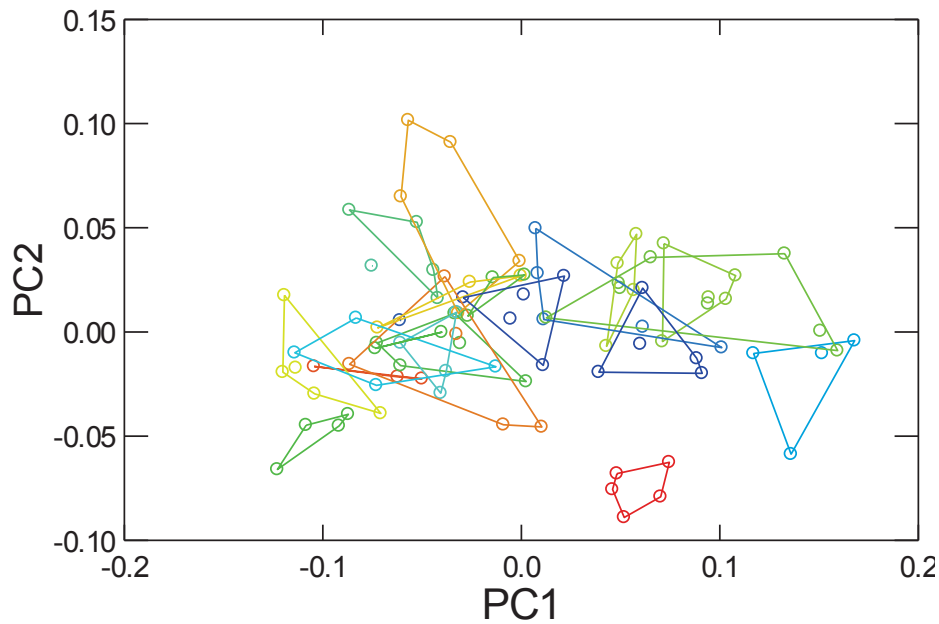
Figure 5.2.5 PC1 and PC2 from a principal components analysis of all felid specimens. *Species are grouped by color and using polygons, and specimens of the same species tend to cluster together. For taxonomic names and mean values see Figure 5.2.6.*
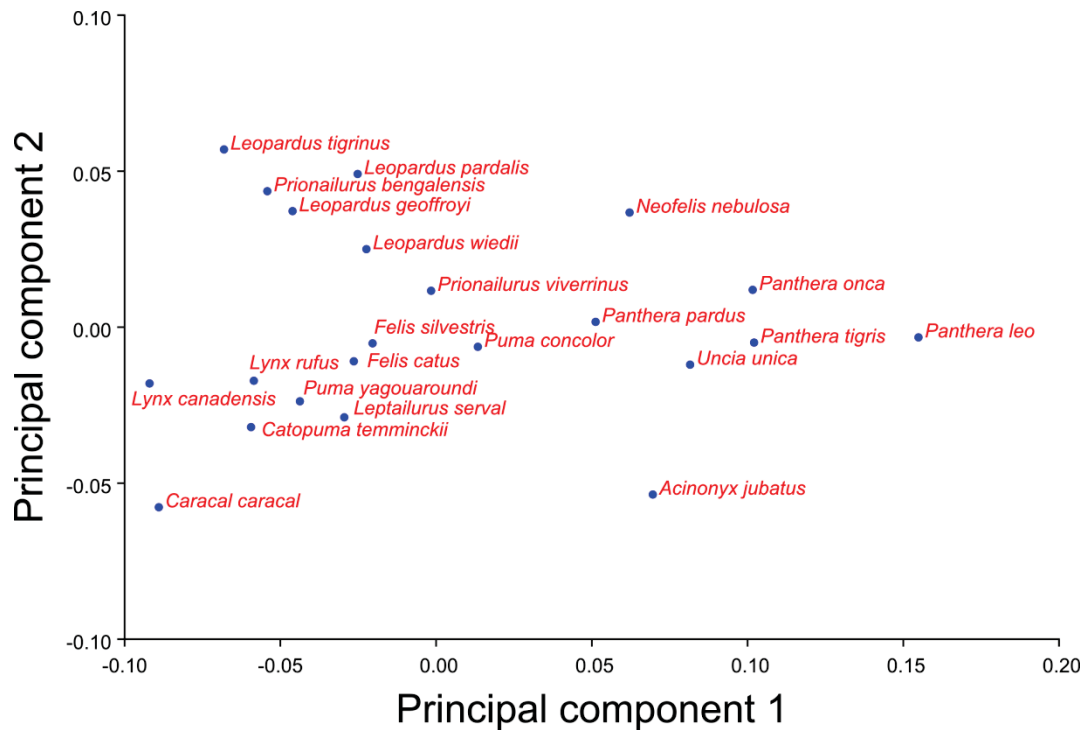
Figure 5.2.6 PC1 and PC2 from a principal components analysis of species-mean shape for felids.
Note that Acinonyx jubatus *has a distinctive lumbar morphology, with low PC2 score.*

FELID PC1

Caudal
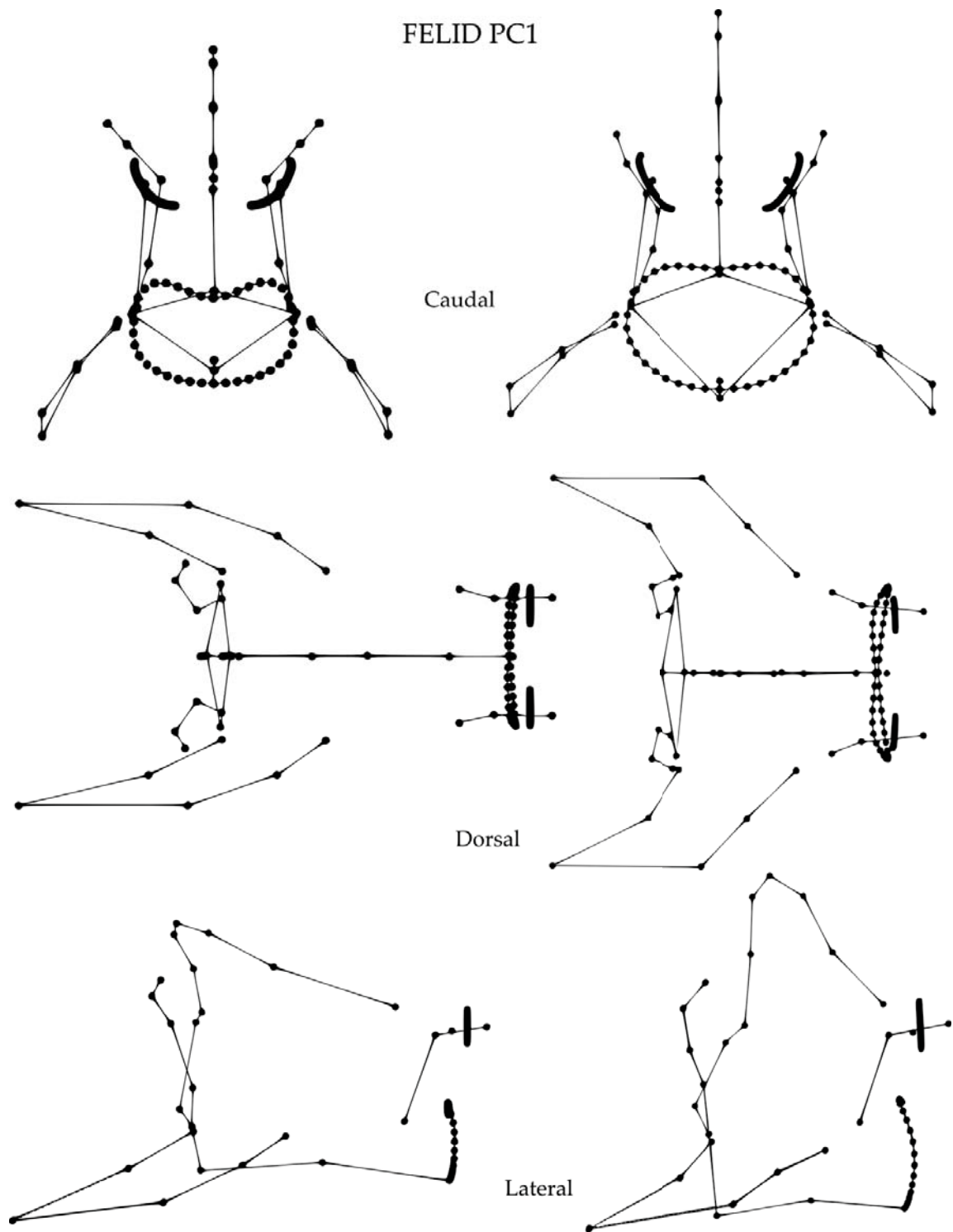
Dorsal

Lateral

Figure 5.2.7 Shape changes associated with PC1 from species-mean PCA.
Caudal, dorsal and lateral views. Left is the negative PC1 whereas right is the positive
PC1, representing 57.3% of total variance.

Table 5.2.3 Eigenvalues from principal components analysis of felid species-mean shape.

Regression coefficients and r-squared values for multivariate regressions of shape on log body mass using both raw data and phylogenetically-corrected independent contrasts. r-sq, r-squared value; coeff., coefficient.

PC	Eigenvalues	Variance (%)	Cumulative variance (%)	Regression coeff. (raw)	r-sq	Regression coeff. (PIC)	r-sq
1.	0.0048	57.3	57.2	0.102	0.620	0.082	0.487
2.	0.0009	11.8	69.1	-0.02	0.075	-0.019	0.1
3.	0.0007	8.3	77.4	0.011	0.006	0.020	0.079
4.	0.0005	5.8	83.2	-0.002	>0.001	-0.006	0.012
5.	0.0004	4.2	87.4	<0.001	>0.001	-0.008	0.033
6.	0.0003	3.0	90.4	0.003	>0.001	0.009	0.036
7.	0.0002	1.9	92.3	-0.003	>0.001	-0.004	0.012
8.	0.0001	1.3	93.6	-0.004	>0.001	-0.002	0.005
9.	0.0001	1.2	94.9	0.002	>0.001	>0.001	>0.001
10.	0.0001	0.9	95.8	-0.001	>0.001	-0.008	0.132

Phylogeny

First, the assumptions of independent contrasts were tested. Correlation of absolute contrasts with branch lengths revealed that the Grafen-rho transformation of branch lengths was most appropriate for the majority of the variables, producing the lowest correlations (Table 5.2.4). A multivariate regression of standardized contrasts of PC scores on log body mass produced a significant correlation (p=0.003). Again, regression coefficients and r-squared values were greatest for PC1. However, they were less than those produced in the analysis of raw PC scores, indicating some correlation between phylogeny and size on PC1. In contrast, r-squared values actually increased in several of the other principal components.

Table 5.2.4 Assumptions of independent contrasts analysis for felids.
Correlation coefficients of absolute contrasts versus square root of sum of corrected branch lengths of raw, log-transformed and Grafen-rho transformed branch lengths. Lowest correlations indicate best fit of branch lengths and are emboldened.

	Raw	**Log**	**Grafen (0.5)**
PC1	**-0.0015**	0.0507	0.0044
PC2	0.0029	0.029	**0.0001**
PC3	0.4012	0.5133	**0.0068**
PC4	**0.0395**	0.0451	0.1095
PC5	0.2178	0.2327	**0.0483**
PC6	0.3472	0.4547	**0.0304**
PC7	0.2707	0.4233	**0.0509**
PC8	0.0881	0.214	**0.001**
PC9	0.3937	0.4704	**0.0314**
PC10	0.1194	0.2267	**0.0012**
Body Mass	-0.5041	-0.5562	**0.0012**

Vertebral regions

There was evidence of three vertebral modules (centrum, arch and processes). Comparison of co-variation patterns to 10,000 random contiguous partitions of landmarks resulted in none with a higher within- to between-module variation ratio than these ($p<0.001$). When regression analyses were conducted separately for landmarks from each of these three regions, different allometric patterns were revealed. The centrum had high correlation with body mass (52.0% variance explained), whereas the arch and processes were much less strongly related to size (25.5% and 9.8% variance explained respectively).

Allometric vector

The allometric vector for felids is shown in Figure 5.2.8. Small felids have relatively elongate, dorsoventrally compressed centra. The transverse processes of small felids are even more inclined ventrally and cranially than those of the bovids, and

the neural spine is tapered and inclined cranially. The zygapophyses are less curved than the bovids, forming a relatively flat surface. They are oriented at less than 45º from vertical. This orientation does not change as size increases. However, the centrum becomes craniocaudally shorter and round in cross-section, with some waisting in the mid-centrum. The transverse process becomes wider and slightly less ventrally inclined, though never reaching the horizontal orientation seen in large bovids. The neural spine reorients with increasing size, becoming vertical.
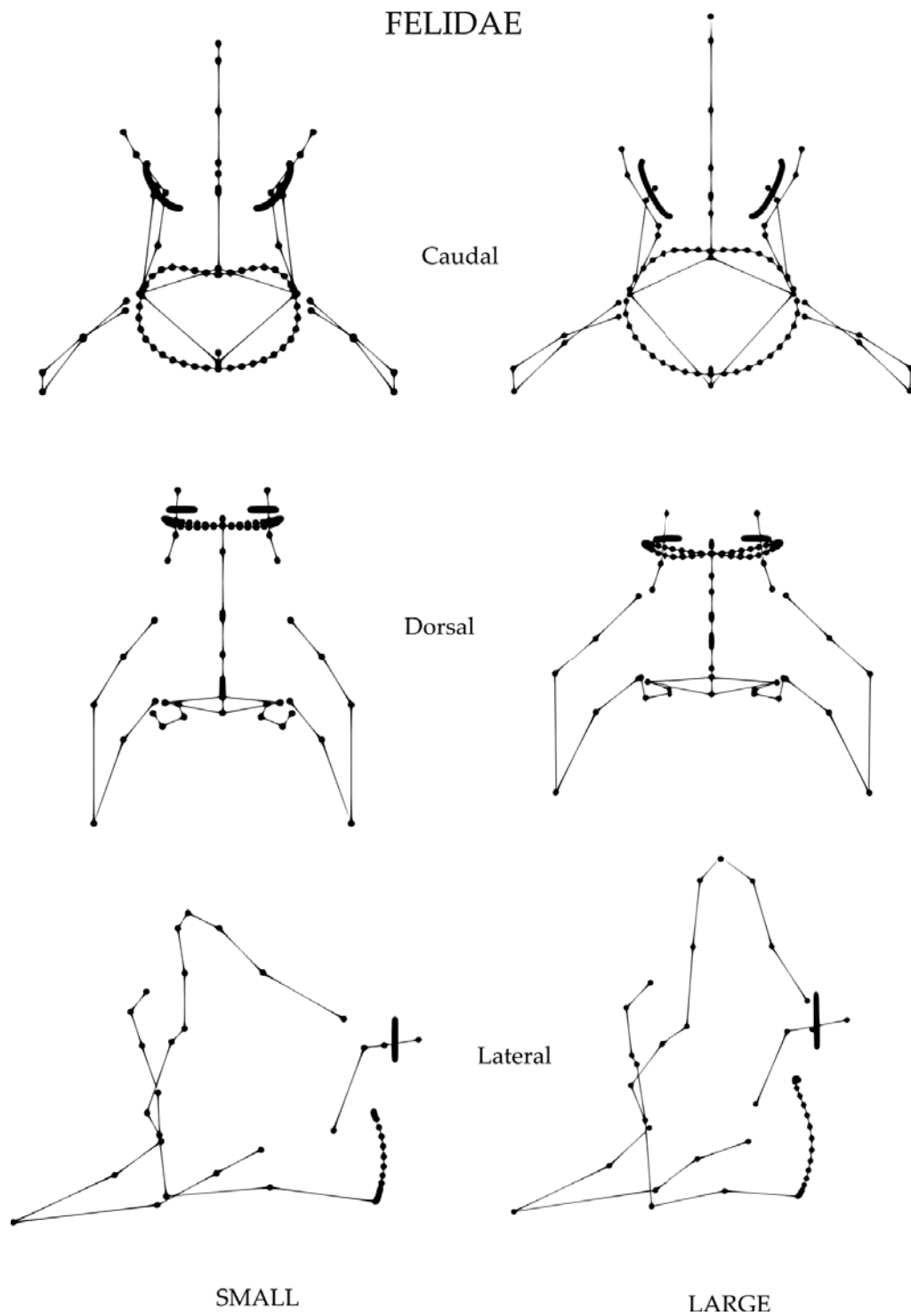
Figure 5.2.8 Allometric vector in felids.

The allometric vector was calculated from the coefficients of a multivariate regression of all the Procrustes co-ordinates onto log body mass, and represents the portion of shape most correlated with size. Left side is small extreme and right side is the large extreme.

5.3 DISCUSSION

5.3.1 HYPOTHESES

This chapter has demonstrated that **3D lumbar shape is strongly influenced by body size, but that allometric vectors vary between felids and bovids.** I can now address the specific hypotheses posed at the beginning of this chapter:

H1. The centrum becomes craniocaudally shorter and dorsoventrally taller with increasing size.

As the centrum is the major weight-bearing portion of the column, it is unsurprising that there is strong allometry of the centrum in both groups (63% and 52% of total variance for bovids and felids respectively). H1 is supported in both groups as the centrum becomes craniocaudally shorter and dorsoventrally taller with increasing size, confirming results from Chapter 4. This shape can better resist increased compressive and sagittal bending loads due to increasing size, in both centra and discs (ventral column). However, the more sophisticated analyses performed here provide a more detailed analysis of shape changes in the centrum. The shape of the endplate changes in both groups, though the nature of this change varies. In bovids the centrum becomes more heart-shaped with increasing size, developing a more marked ventral keel where the ventral longitudinal ligament attaches (Sisson, 1975b, a). This ligament connects adjacent centra and resists dorsiflexion of the column (Denoix, 1999). In addition, the relative size of the anterior or cranial endplate increases in both groups, resulting in a marked waisting at the mid-centrum. This may reflect a relative increase in size of the intervertebral disc (which articulates with the endplate) relative to the vertebral body. The body is made of bone, which is very effective at resisting

177

compressive loads, whereas the fibrocartilagenous disc is relatively weaker. Thus to support the same compressive load throughout the whole column, a larger cross-sectional area of disc than bone may be required, resulting in this waisted effect on the body.

H2. The zygapophyses become more interlocking and metapophyses become larger.

The neural arch supports the synovial zygapophyseal joints, houses the spinal cord and provides attachment for muscles. Generally, there was weak allometry of the arch structures, representing 17% (bovids) and 26% (felids) of the total variance in these regions. The primary size-related variation related to the arch was an overall craniocaudal shortening, in concert with the shortening of the body. In felids H2 is not strongly supported, as the 26% shape associated with size primarily represents a shortening of the arch, and not elaboration of the zygapophyses or metapophyses. However, in bovids there was some support as the zygapophyses vary from revolute to slightly sigmoid-revolute and the metapophysis becomes taller and broader. This may reflect increasing resistance to torsion with increasing size. Further, sigmoid-revolute zygapophyses have been linked with dorsal element loading, where compressive forces are transmitted through the arch and zygapophyses as well as the centrum (Slijper, 1946; Filler, 1986). Zygapophyses also become mediolaterally closer to one another with increasing size. Since widely-spaced zygapophyses have been linked with resisting lateroflexion, this might suggest a relative increase in the importance of intertransverse ligaments over zygapophyses in resisting lateroflexion at large size (Boszczyk et al., 2001).

H3. The processes (spinous and transverse) become more robust, craniocaudally longer, dorsoventrally/mediolaterally wider and less inclined from the primary planes of the vertebra.

The muscular processes provide attachment points for paraxial muscles that act to move the column, those which stabilize the column and a series of stabilizing ligaments. Strongly inclined processes are related to a sagittally mobile column, whereas perpendicular process reflect relative stability (Smeathers, 1981; Shapiro, 1993; Ward and Latimer, 1993; Shapiro, 1995; Sargis, 2001; Argot, 2003, 2012). The response of this anatomical region to increasing size varied between these two families. While size explains 58% of process variation in bovids, only 10% is explained in felids. In bovids, with increasing size the transverse processes become mediolaterally longer, craniocaudally wider and much less ventrally and cranially inclined. While ventrally and cranially inclined transverse processes provide better advantage in the sagittal plane for the epaxial muscles, straight processes indicate a stronger effect of stabilizing intertransverse ligaments. Inclination of the transverse processes has been interpreted as an adaptation for sagittal mobility of the spine because it increases the sagittal component of epaxial action and ensures proper action of the erector spinae through a wide range of joint motion (Smeathers, 1981; Shapiro, 1993; Ward and Latimer, 1993). Therefore, straightening of these processes with increasing size likely reflects a reduction in sagittal mobility with size.

This finding is supported by myological data from a small number of bovids indicating that epaxial muscle mass is relatively smaller in larger species (Grand, 1997). In addition, *in vivo* motion analyses indicated reduced sagittal mobility during

running in larger bovids (Halpert et al., 1987). The effect is less marked in the neural spine, where process height and width relative to the centrum remain similar but there is slightly less cranial inclination. In contrast, in felids the neural spine varies from strongly cranially inclined to almost straight, becoming slightly taller, while the transverse processes retain similar orientation. This trend has been attributed to shifts in the muscle vectors of multifidus associated with craniocaudal shortening of the vertebra (Slijper, 1946).

Results presented in this chapter have shown that body size is an important influencing factor in lumbar vertebral shape variation in cursorial mammals. These data suggest that while the ventral column scaled in a relatively conserved way between mammalian groups, meeting requirements to maintain tolerable levels of stress in the centra and intervertebral discs with increasing size, allometry of other structures is quite variable. In terms of allometry of the muscular processes, allometric patterns were less strong, relative to other sources of variation, in felids than in bovids. The morphology observed suggests relatively greater lumbar stabilization in large bovids than large felids. Felids hunt prey using short bursts of rapid running (Wilson et al., 2013). Hence, sprinting using high-energy back movements may only be sustainable in large animals for short periods of time. In contrast, bovids may favor stamina by exchanging active for passive stabilization of the lumbar region at large body sizes, while maintaining stride-length with relatively longer limbs.

CHAPTER 6: CRANIOCAUDAL PATTERNS OF LUMBAR ALLOMETRY

This chapter examines craniocaudal patterns in the allometry of the lumbar region. Craniocaudal trends in vertebral morphology are characterized using three vertebral positions that are comparable among species with different lumbar counts (first lumbar, mid-lumbar, last lumbar). Lumbar shape is measured from photographs using 2D geometric morphometrics and scaled linear measures. For each family, the influence of size and vertebral position is tested using a MANCOVA design.

6.1 HYPOTHESES

This chapter asks: **how does vertebral allometry vary along the lumbar region, and do craniocaudal patterns vary between families?** These questions are addressed by testing the following specific hypotheses:

H1. There is an effect of size on lumbar shape. Specifically, increasing size is associated with a dorsoventrally taller centrum, increased lever arm of the neural spine and arch, and decreased angle between the neural spine and transverse process.

H2. The effect of size varies among vertebral positions and families. Specifically:

A. Size and position. Allometric slopes vary along the lumbar region.

B. Size and family. Allometric slopes vary between families.

C. Family and position. There is stronger craniocaudal variation in bovids than felids because bovids have enhanced mobility at the lumbosacral joint relative to the rest of the lumbar region. In particular, the last lumbar may have a dorsoventrally shorter

centrum, arch or neural spine.

6.2 RESULTS

6.2.1 LINEAR MEASUREMENTS

Species-position-mean linear dimensions for felids and bovids can be found in Appendix 6. MANCOVA was used to examine the influence of size, vertebral position and family on linear measurements. The results, including effects of family, vertebral position, body mass and interactions between these factors are shown in Table 6.2.1. Size coefficients represent allometric slopes. There are significant effects of all variables on shape of the vertebrae, including significant interactions. This indicates that there was allometry of shape, craniocaudal variation, between-family variation, and that slopes and elevations varied between position and family. As there are slope differences between the families (interaction of size and family), the analysis was rerun on felids and bovids separately (Table 6.2.2 and Table 6.2.3). Bivariate plots of the variables against mass are shown in Figures 6.2.1 to 6.2.8.

When both families are included, centrum height scales positively with body mass in both families at all positions, suggesting that centra universally become taller. However, the effect is greater in bovids, which scale more steeply than felids. There is no effect of vertebral position on centrum height in the felid-only analysis, which suggests that centrum height is similar throughout the lumbar region in felids. However, in the bovid-only analysis there is a strong effect of vertebral position. Specifically, the last lumbar vertebra has a more dorsoventrally compressed centrum than the proximal lumbars. Proximal lumbars of bovids are taller than any of the felid vertebrae, but the bovid last lumbar is relatively shorter than any felid position (Figure 6.2.1). Centrum width has similar trends, but in reverse. With increasing size, lumbar

vertebrae become narrower. Further, bovid last lumbars are wider than the other vertebrae examined (Figure 6.2.2), suggesting that this vertebra is mediolaterally wide but dorsoventrally compressed. The tiny royal antelope (*Neotragus pygmaeus*) was an outlier, with a relatively tall and narrow centrum for its body size.

Height of the neural arch tends to decrease with increasing size; however, slopes vary between families and vertebral positions (Table 6.2.1). Felids scale more strongly than bovids, indicating that larger felids have relatively shorter neural arches. Within felids, the L1 and mid-lumbar positions scale most steeply, suggesting a dramatic reduction in arch height. The last lumbar has a shorter neural arch, but it also scales less strongly in both groups, indicating that this position is less strongly influenced by size (Figure 6.2.3).

Surprisingly, the height of the neural spine scales isometrically in both groups (Table 6.2.2, Figure 6.2.4). However, its height varies among families and along the lumbar region. Bovids have dorsoventrally shorter neural spines on the last lumbar vertebra, whereas felids have a taller spine at the mid-lumbar position. Generally, bovids have taller neural spines than felids (Figure 6.2.4). The Kouprey (*Bos sauveli*) had the tallest neural spine for its size. The transverse process is also wider in bovids than felids, though scaling relationships are quite different between the groups (Table 6.2.1, significant interaction of family and mass). In bovids, the transverse process becomes relatively wider with increasing size. In contrast, the transverse process becomes slightly mediolaterally narrower in felids as size increases (Figure 6.2.5). The cheetah (*Acinonyx jubatus*) had a relatively wide transverse process at L1.

184

The distance between post-zygapophyses decreases relative to endplate area with increasing size, however slopes vary between families and positions (Table 6.2.1). Post-zygapophyses become closer to each other with increasing size in felids than bovids. However, in both groups the last lumbar has more wide-set zygapophyses than the other positions (Figure 6.2.6). The size of the endplate itself becomes slightly larger with increasing size in felids (coefficient=0.056) but remains isometric to body mass in bovids (Table 6.2.2 and Table 6.2.3). In both families the area of the endplate increases caudally, suggesting that vertebrae become larger posteriorly (Figure 6.2.7). Species with relatively large vertebrae compared to their estimated body mass were *Bosephalus tragocamelus, Gazella spekei* and *Felis silvestris.*

The angle between the transverse process and the neural spine diminishes as size increases, but much more strongly so in bovids than felids (Table 6.2.2, Table 6.2.3, Figure 6.2.8). This suggests that the transverse process is less ventrally inclined in larger taxa, particularly in bovids. There is no significant effect of craniocaudal position on transverse process angle, indicating that it is similar throughout the lumbar region.

Table 6.2.1 Results of the MANCOVA on species-mean felid and bovid linear measures.

All linear measures scaled by square root endplate area except square root area itself, which is scaled by cube root of mass, and transverse process angle which is uncorrected. Coefficients are reported, and bold values are variables which are significant in univariate f-tests at the p=0.05 level. For factors, values indicate the elevation difference between cited level and a reference level, either Felidae (family) or the proximal lumbar (position). For interactions between factors and mass, values indicate the slope difference between the cited level and reference level. Multivariate Pillai's trace test statistic reported. Abbreviations: CH, centrum height; CW, centrum width; Arch LA, Arch lever arm; NS LA, neural spine lever arm; TP LA, transverse process lever arm; Zyg width, zygapophysis width; TP angle, transverse process angle with neural spine. LL, last lumbar; ML, mid-lumbar.

Factor	Level	CH	CW	Arch LA	NS LA	TP LA	Zyg width	Endplate area	TP angle	F-ratio (Pillai's)	P-value (Pillai's)
Cube-root Mass		**0.115**	**-0.066**	**-0.105**	-0.016	0.027	**-0.179**	**0.031**	**-0.099**	**58.280**	<0.001
Family	Bovidae	-0.013	**0.006**	-0.006	**0.045**	**0.078**	**0.038**	0.005	0.000	**17.050**	<0.001
Position	LL	**-0.044**	**0.016**	**-0.115**	**-0.077**	**0.021**	**0.083**	**0.046**	**-0.010**	**19.437**	<0.001
Position	ML	**0.020**	**-0.007**	**0.064**	**0.059**	**0.041**	**-0.022**	**-0.009**	0.010	-	-
Family * Mass	Bovidae	0.008	-0.006	**0.060**	0.019	**0.119**	**-0.038**	**-0.025**	**-0.063**	**11.803**	>0.001
Position * Mass	LL	0.003	**0.014**	**0.069**	0.031	-0.017	**0.063**	-0.012	0.003	**7.953**	>0.001
Position * Mass	ML	-0.002	-0.006	-0.034	-0.025	0.027	-0.033	0.004	0.002	-	-
Position * Family	LL* Bovidae	**-0.043**	**0.022**	0.005	**-0.028**	**-0.051**	**-0.019**	**0.014**	**0.011**	**23.963**	>0.001
Position * Family	ML* Bovidae	**0.022**	**-0.011**	**-0.012**	**-0.015**	**0.032**	**0.011**	**-0.008**	**-0.001**	-	-

186

Table 6.2.2 MANCOVA of felids only.

Coefficients are reported, bold values are variables significant in univariate f-tests at the p=0.05 level. For factors, values indicate the elevation difference between cited level and a reference level, either Felidae (family) or the proximal lumbar (position). For interactions between factors and mass, values indicate the slope difference between the cited level and reference level. Multivariate Pillai's trace test statistic reported. For abbreviations see Table 6.2.1. LL, last lumbar; ML, mid-lumbar.

Factor	Level	CH	CW	Arch LA	NS LA	TP LA	Zyg width	Endplate area	TP angle	F-ratio (Pillai's)	P-value (Pillai's)
Cube-root of Mass		**0.107**	**-0.060**	**-0.164**	-0.034	**-0.091**	**-0.142**	**0.056**	**-0.035**	**25.464**	**>0.001**
Position	LL	0.006	-0.003	**-0.146**	**-0.062**	**0.083**	**0.095**	**0.031**	-0.016	**8.932**	**>0.001**
Position	ML	-0.004	0.002	**0.102**	**0.101**	**0.010**	**-0.034**	**0.004**	0.017	-	-
Position * Mass	LL	-0.013	0.008	**0.130**	0.062	-0.042	0.081	-0.009	-0.008	1.995	0.02
Position * Mass	ML	0.002	-0.001	**-0.095**	-0.089	0.025	-0.031	-0.008	-0.010	-	-

Table 6.2.3 MANCOVA of bovids only.

Coefficients are reported, bold values are variables significant in univariate f-tests at the p=0.05 level. For factors, values indicate the elevation difference between cited level and a reference level, either Felidae (family) or the proximal lumbar (position). For interactions between factors and mass, values indicate the slope difference between the cited level and reference level. Multivariate Pillai's trace test statistic reported. For abbreviations see Table 6.2.1. LL, last lumbar; ML, mid-lumbar.

Factor	Level	CH	CW	Arch LA	NS LA	TP LA	Zyg width	Endplate area	TP angle	F-ratio (Pillai's)	P-value (Pillai's)
Cube-root of Mass		**0.124**	**-0.072**	**-0.047**	0.003	**0.147**	**-0.217**	0.006	**-0.161**	**60.306**	**<0.001**
Position	LL	**-0.091**	**0.037**	**-0.098**	**-0.098**	**-0.034**	**0.067**	**0.061**	0.000	**13.589**	**<0.001**
Position	ML	**0.042**	**-0.017**	**0.040**	**0.032**	**0.073**	**-0.011**	**-0.020**	0.008	-	-
Position * Mass	LL	0.009	0.016	**0.049**	0.021	-0.009	0.058	-0.013	0.007	6.334	**<0.001**
Position * Mass	ML	-0.004	-0.007	**-0.014**	-0.005	0.027	-0.033	0.008	0.005	-	-
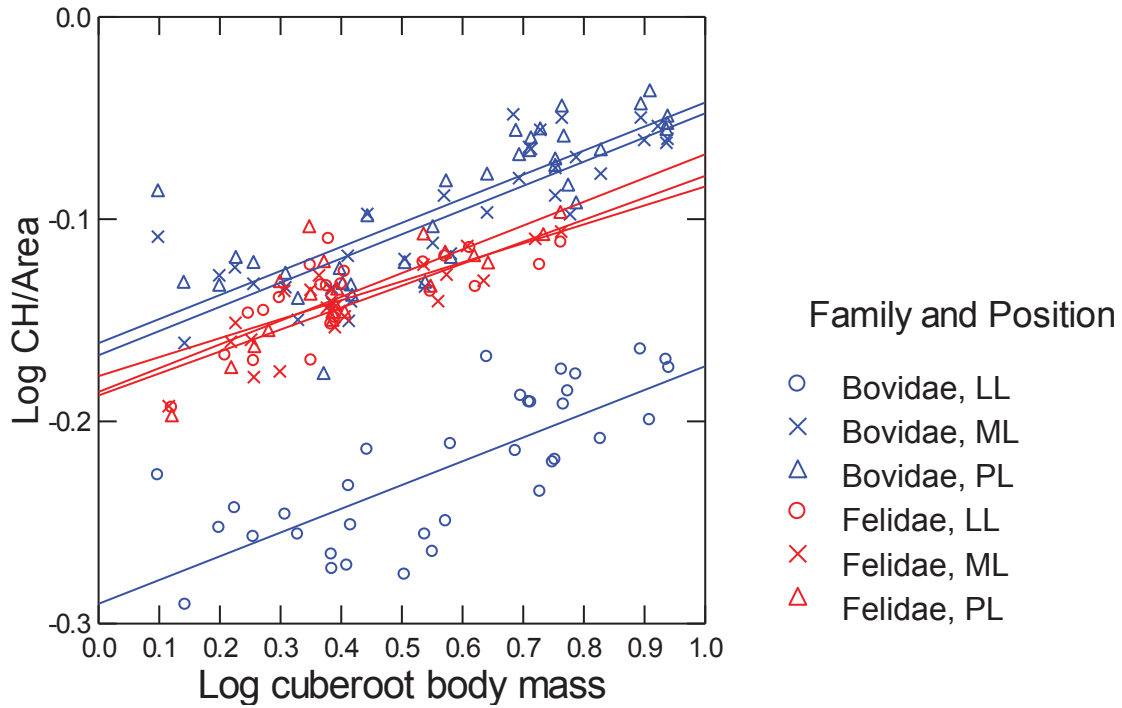
Figure 6.2.1 Centrum height (CH) scaling in felids and bovids.

Linear measurements are scaled by square-root endplate area. LL, last lumbar; ML, mid-lumbar; PL, proximal lumbar (L1).
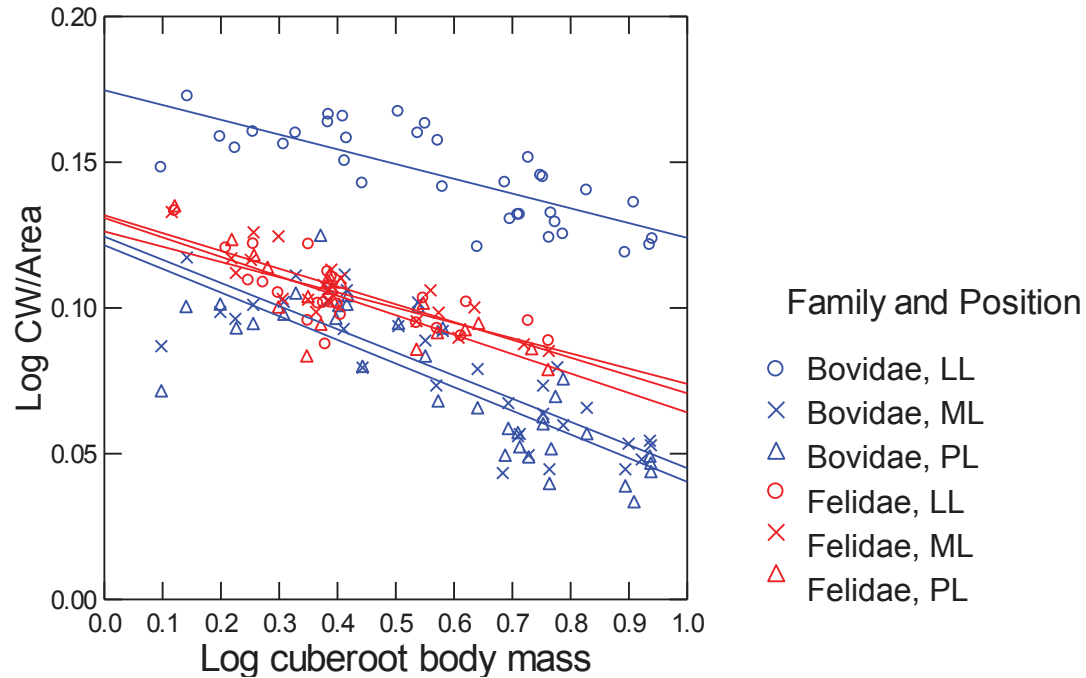
Figure 6.2.2 Scaling of centrum width (CW).

Linear measurements are scaled by square-root endplate area. LL, last lumbar; ML, mid-lumbar; PL, proximal lumbar (L1).
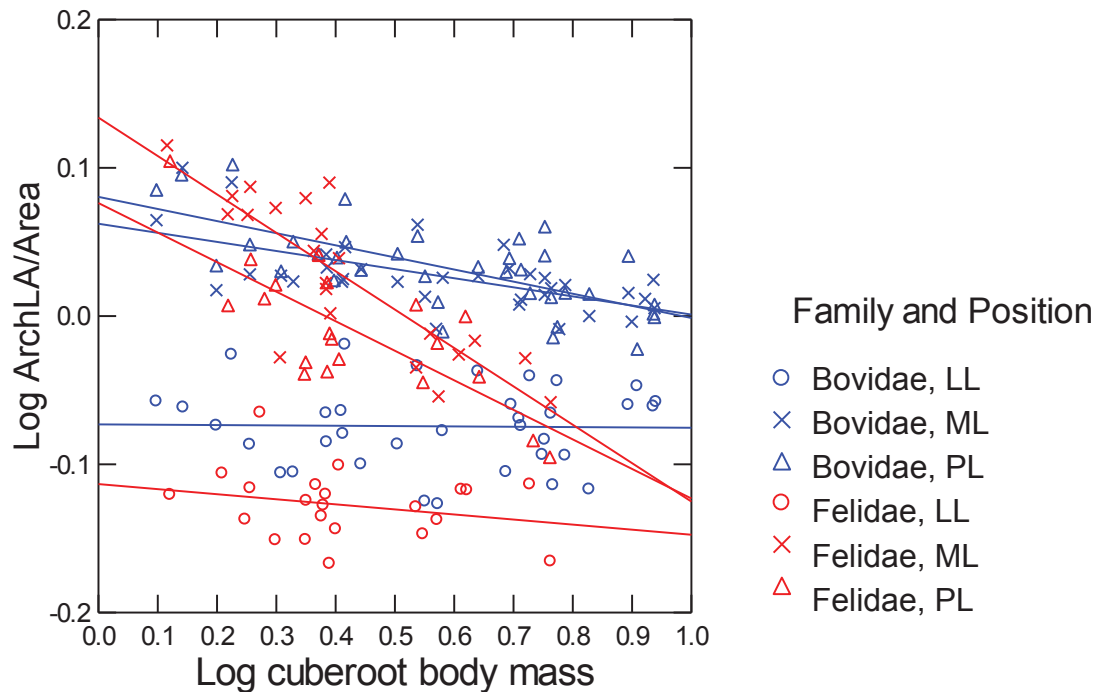
Figure 6.2.3 Scaling of arch lever arm (ArchLA).

Linear measurements are scaled by square-root endplate area. LL, last lumbar; ML, mid-lumbar; PL, proximal lumbar (L1).
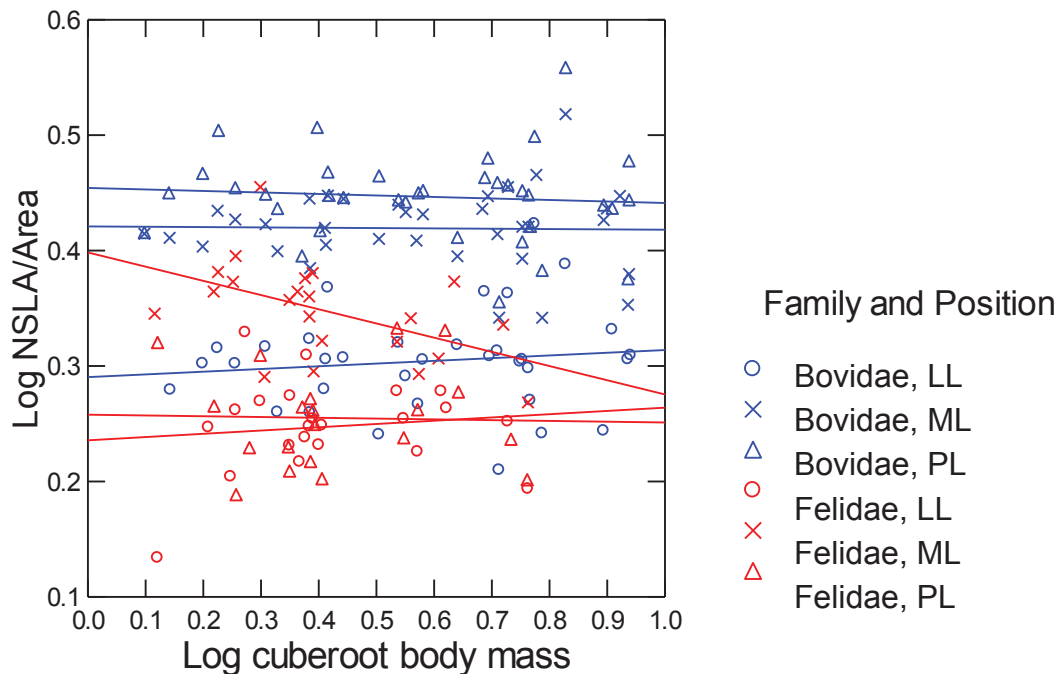
Figure 6.2.4 Scaling of neural spine lever arm (NSLA).

Linear measurements are scaled by square-root endplate area. LL, last lumbar; ML, mid-lumbar; PL, proximal lumbar (L1).
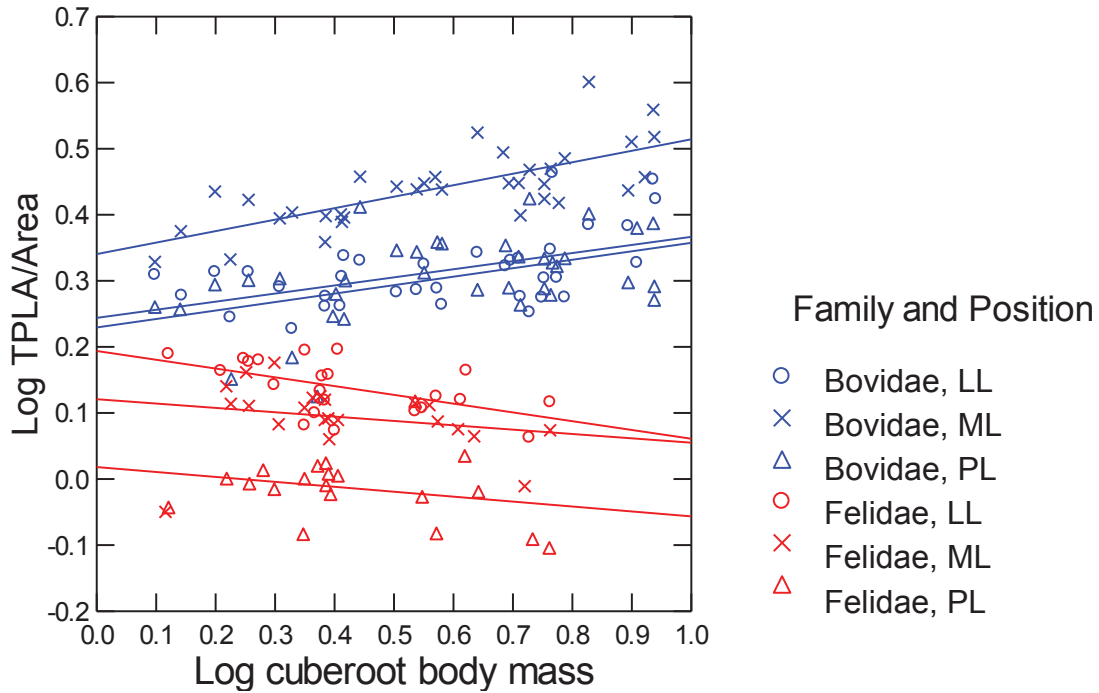
Figure 6.2.5 Scaling of the transverse process lever arm (TPLA).
Linear measurements are scaled by square-root endplate area. LL, last lumbar; ML, mid-lumbar; PL, proximal lumbar (L1).
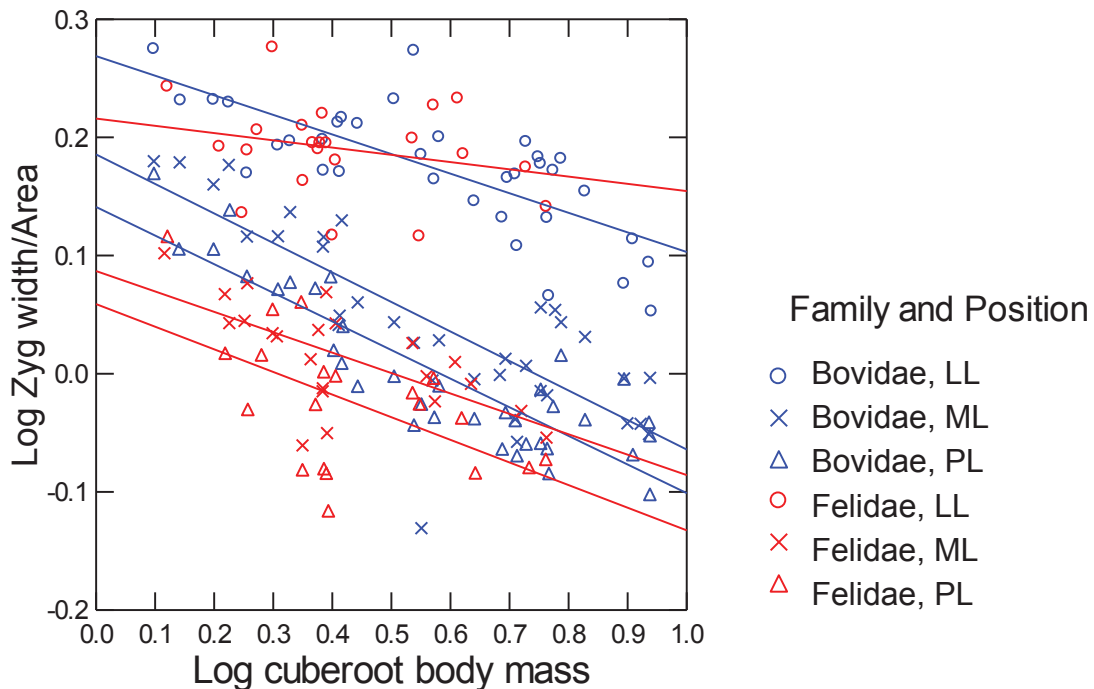
Figure 6.2.6 Scaling of the width of the zygapophyses.
Linear measurements are scaled by square-root endplate area. LL, last lumbar; ML, mid-lumbar; PL, proximal lumbar (L1).
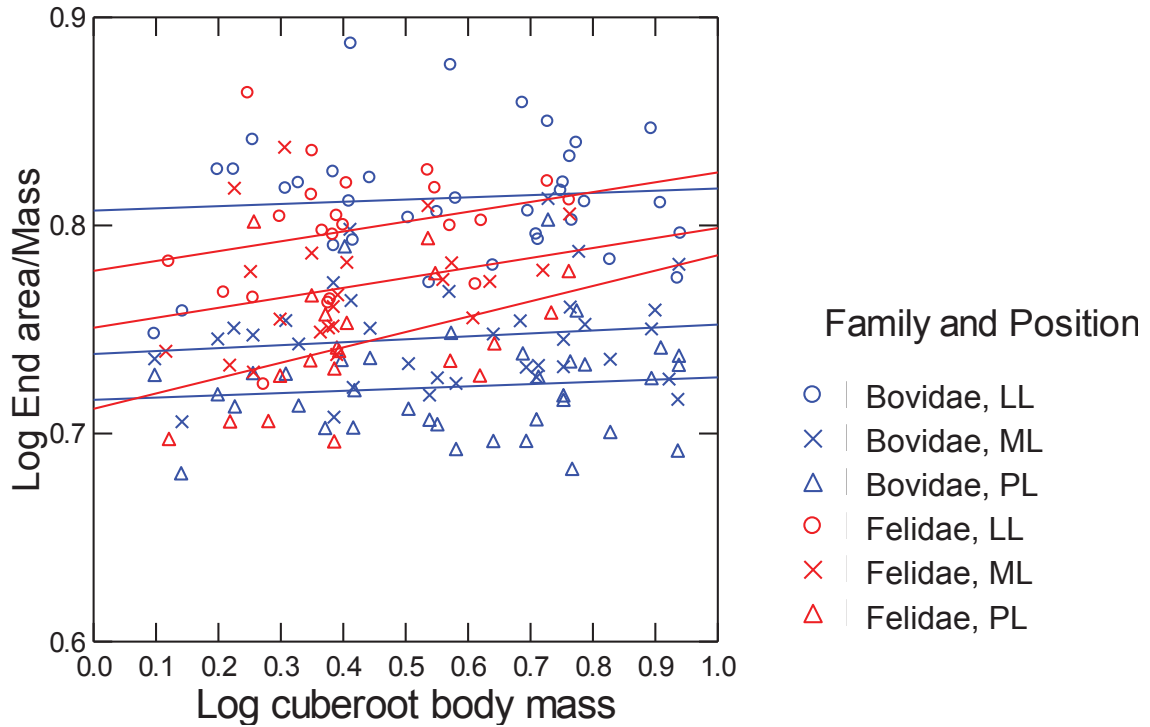
Figure 6.2.7 Scaling of the square root of the area of the endplate.

Linear measurements are scaled by square-root endplate area. LL, last lumbar; ML, midlumbar; PL, proximal lumbar (L1).
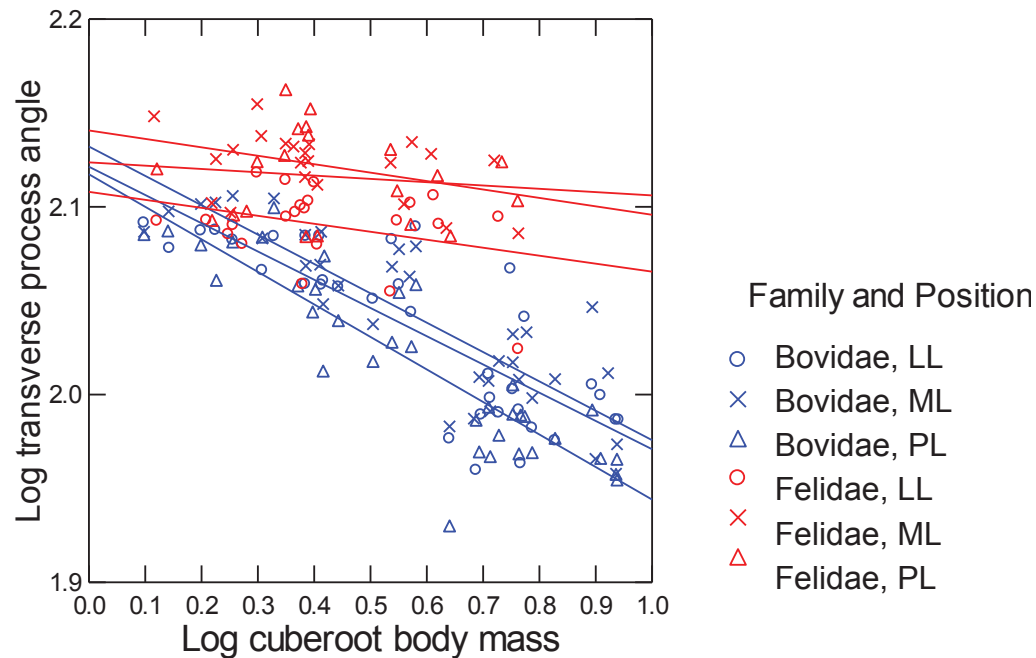
Figure 6.2.8 Scaling of the angle of the transverse process.

Linear measurements are scaled by square-root endplate area. LL, last lumbar; ML, midlumbar; PL, proximal lumbar (L1).

6.2.2 JOINT COMPLEX SHAPE

Principal components analysis was performed on Procrustes co-ordinates of 2D landmarks from the joint complex, which was run on felids and bovids separately. The PC scores from this analysis can be found in Appendix 6. The distribution of specimens on PC1 and PC2 and their associated shape variation are shown in Figure 6.2.9. Table 6.2.4 reports the variation explained by the first three principal components. The high loading of variance on just a few axes suggests that joint complex shape in the lumbar region is highly integrated among loci.

Table 6.2.4 Percentage variance explained by each principal component in the PCA

	FELID	BOVID
PC1	90.1	83.0
PC2	6.4	8.7
PC3	1.4	2.7
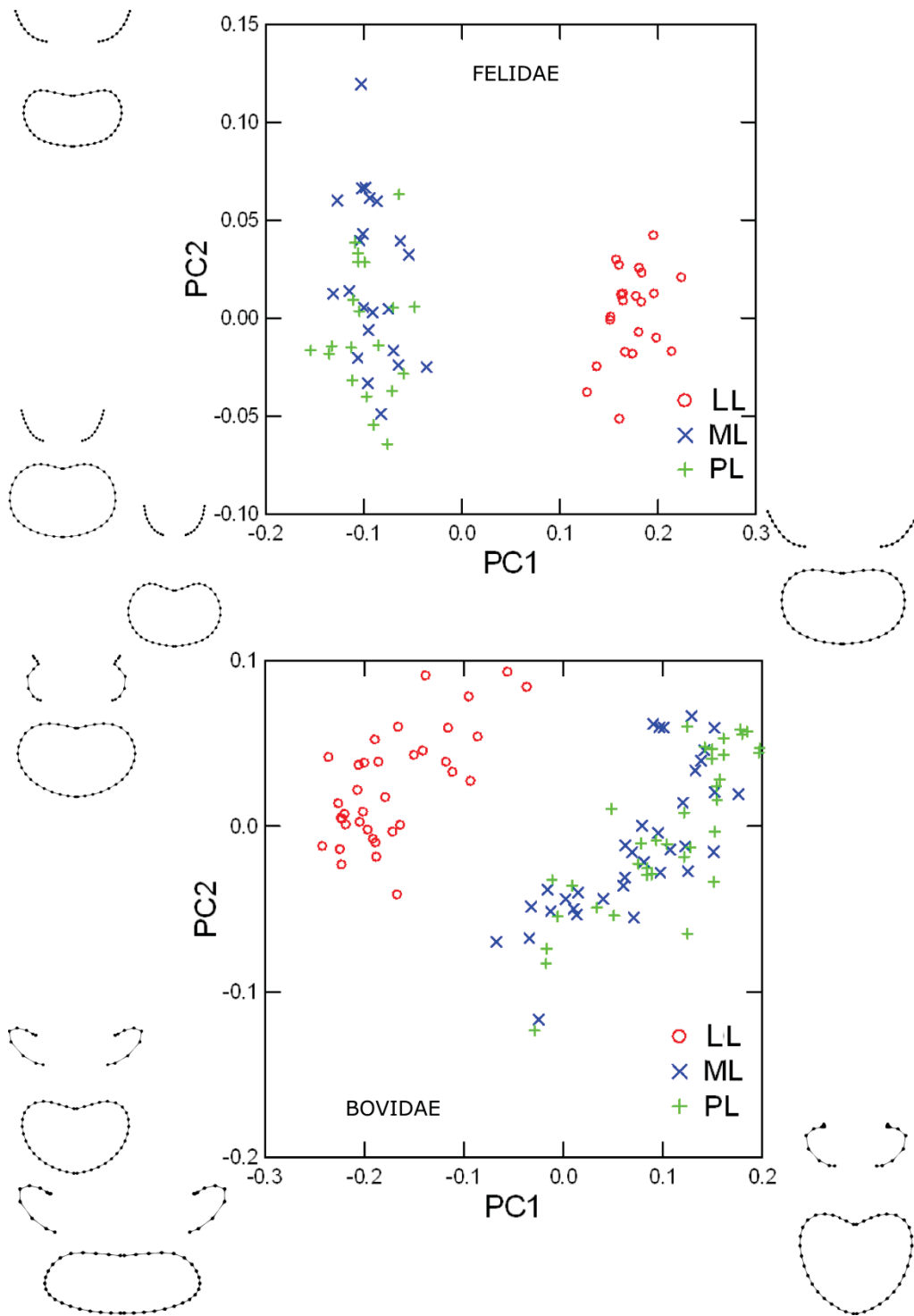
Figure 6.2.9 PC1 against PC2 of principal components analysis of species-mean 2D joint shape in felidae and bovidae.

Wireframes represent extreme shapes. LL, last lumbar; ML, mid-lumbar; PL, proximal lumbar (L1).

In felids, nearly all of the variation (96.5%) is explained in just two PC axes. PC1 separates the last lumbar vertebra from the two more proximal positions due to much more widely-spaced and ventrally placed zygapophyses. PC2 highlights the allometric shape change. Small felids have positive PC2 scores, whereas large felids have more negative PC2 scores. Negative scores represent vertebrae with a larger endplate and relatively shorter arch. In bovids, the first three components explain 94.4% of variation. PC1 also highlights variation between the last lumbar and more proximal lumbars. The last lumbar is typified by very wide centra and wide-set, revolute zygapophyses. PC2 scores reflect variation from revolute (negative) to sigmoid-revolute (positive) zygapophyses.

MANCOVA was used to test for effects of size and vertebral position on joint complex shape. PC scores (representing over 95% of variation) were significantly correlated with body mass and varied craniocaudally (Table 6.2.5 and Table 6.2.6). In felids, PC2 is related to body mass but both PC1 and PC2 are influenced by vertebral position. Specifically, the last lumbar has higher PC1 scores, reflecting its mediolaterally wide but dorsoventrally short shape. Allometric slopes vary between vertebral positions on PC2. Slopes are much steeper for the first and middle lumbars than the last lumbar (Figure 6.2.10 and Figure 6.2.11). This suggests that the last lumbar has wider zygapophyses but varies less strongly with size, whereas the more proximal lumbars have narrower zygapophyses and taller endplates with increasing size.

Table 6.2.5 MANCOVA of joint shape in felids.
Coefficients are reported and bold values are significant in univariate f-tests at the
p=0.05 level. For factors, values indicate the elevation difference between cited level and
a reference level, either Felidae (family) or the proximal lumbar (position). For
interactions between factors and mass, values indicate the slope difference between the
cited level and reference level. Multivariate Pillai's trace test statistic reported. ML,
mid-lumbar; LL, last lumbar.

Factor	Level	PC1	PC2	F-ratio (Pillai's)	P-value (Pillai's)
Cube-root body mass		0.017	**-0.138**	42.03	<0.001
Position	LL	**0.192**	**-0.047**	25.15	<0.001
Position	ML	**-0.098**	**0.045**	-	-
Position * Mass	LL	-0.031	**0.104**	5.84	<0.001
Position * Mass	ML	0.029	**-0.075**	-	-
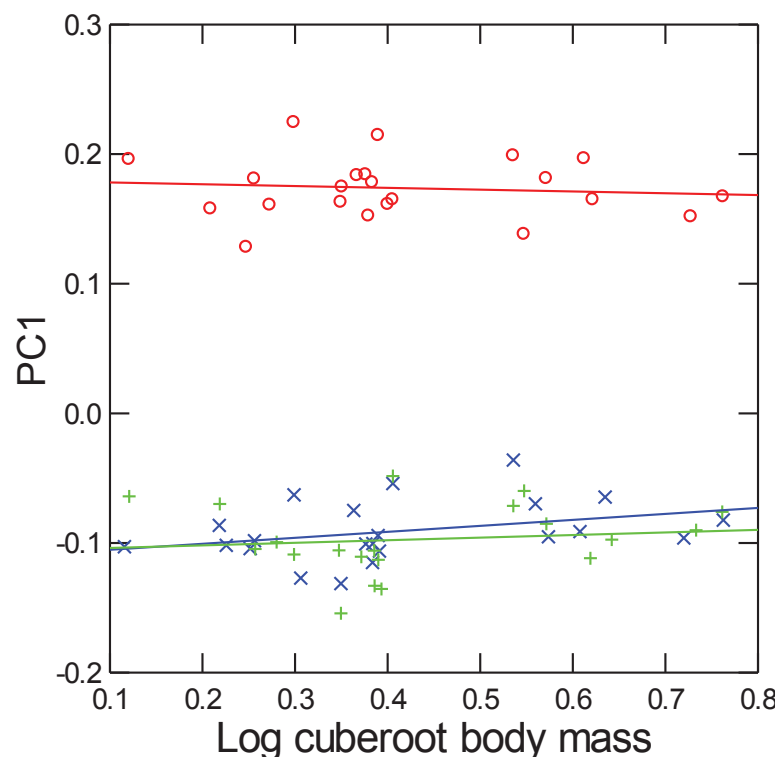
Figure 6.2.10 Scaling of PC1 for felids.
Red circle, last lumbar; blue cross, mid-lumbar; green plus, proximal lumbar (L1). PC1
distinguishes the last lumbar from the more anterior positions.
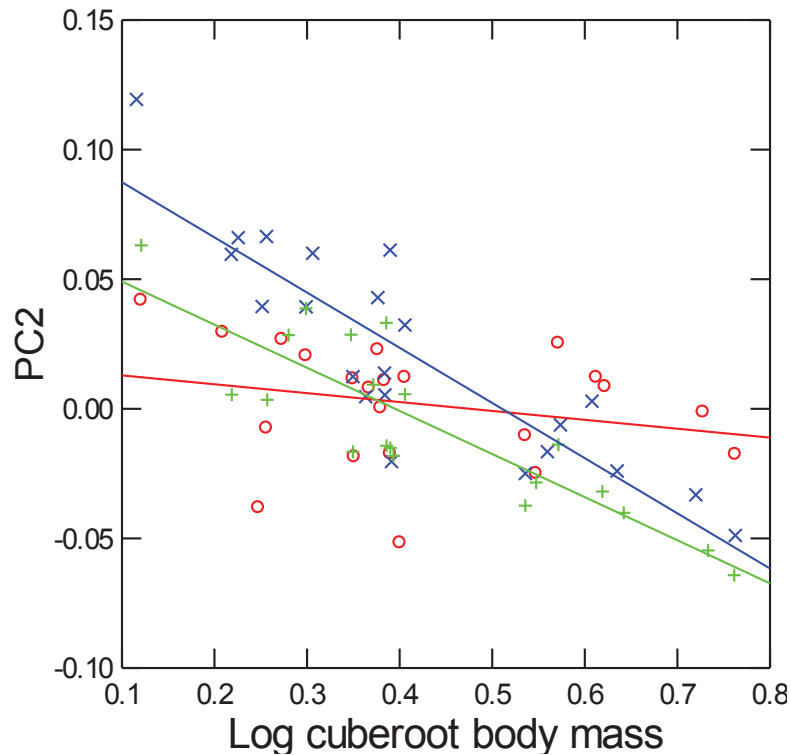
Figure 6.2.11 Scaling of PC2 for felids.
*Red circle, last lumbar; blue cross, mid-lumbar; green plus, proximal lumbar (L1). PC2
is inversely correlated with size.*

In bovids, both PC1 and PC2 are related to both size and position. In contrast,

PC3 is not significantly correlated with any of the variables (Table 6.2.6). The last

lumbar tends to have lower PC1 scores, but all positions are positively correlated with

size (Figure 6.2.12). This suggests that the last lumbar has a wider and shorter endplate

and wider zygapophyses than the proximal lumbars, but that all positions become

dorsoventrally taller and mediolaterally wider with increasing size. All positions are

positively correlated with body size on PC2, though the proximal lumbars scale more

steeply (Figure 6.2.13). This suggests that the zygapophyses become more complex and

interlocking with increasing size, especially in the first and middle lumbar positions.

Table 6.2.6 MANCOVA of joint shape in bovids.

Coefficients are reported and bold values are significant in univariate f-tests at the p=0.05 level. For factors, values indicate the elevation difference between cited level and a reference level, either Felidae (family) or the proximal lumbar (position). For interactions between factors and mass, values indicate the slope difference between the cited level and reference level. Multivariate Pillai's trace test statistic reported. LL, last lumbar; ML, mid-lumbar

Factor	Level	PC1	PC2	PC3	F-ratio (Pillai's)	P-value (Pillai's)
Cube-root body mass		**0.219**	**0.118**	0.018	109.66	<0.001
Position	LL	**-0.148**	**0.050**	-0.013	21.47	<0.001
Position	ML	**0.063**	**-0.026**	0.011	-	-
Position * Mass	LL	**-0.043**	**-0.051**	0.020	1.95	0.075
Position * Mass	ML	**0.013**	**0.021**	-0.012		
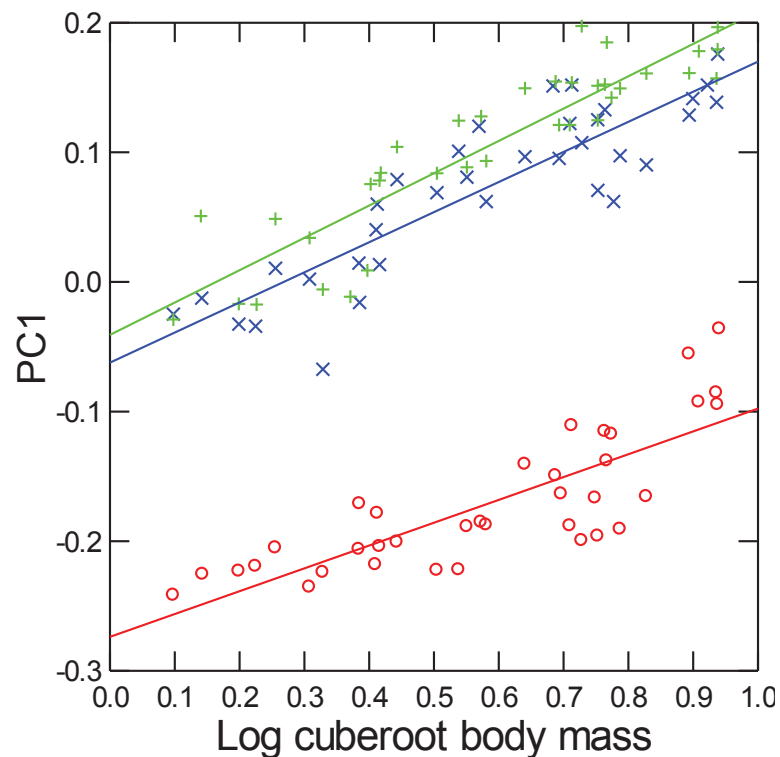
Figure 6.2.12 Scaling of PC1 in bovids.

Red circle, last lumbar; blue cross, mid-lumbar; green plus, proximal lumbar (L1). PC1 is positively correlated with size.
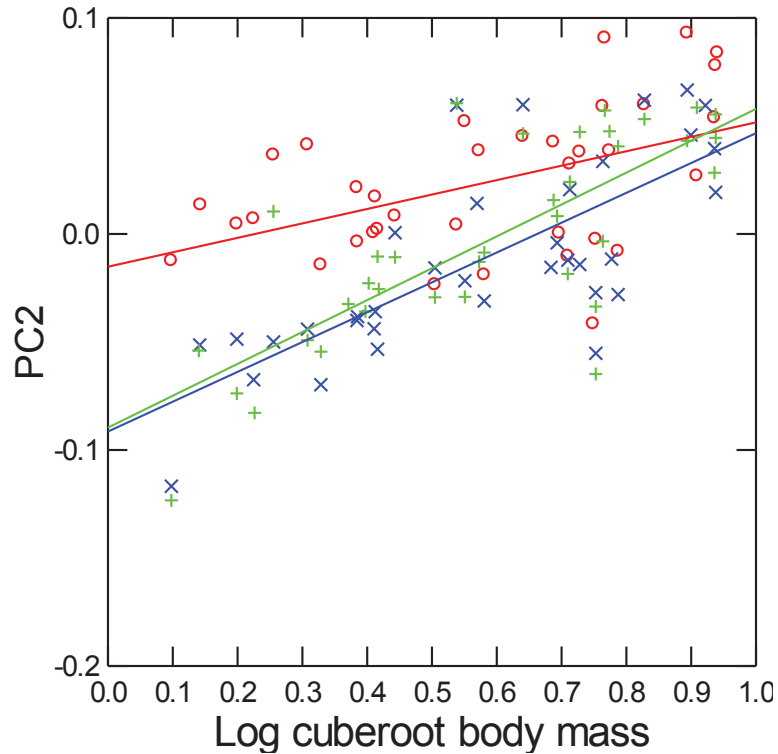
Figure 6.2.13 Scaling of PC2 in bovids.
Red circle, last lumbar; blue cross, mid-lumbar; green plus, proximal lumbar (L1). PC2 is also correlated with size.

6.2.3 PHYLOGENETICALLY-CORRECTED SLOPES

A Grafen-rho transformation was used on branch lengths prior to the calculation of contrasts for both morphometric and linear variables, as this transformation best fit the assumptions of PIC. The same transformation was used for each variable so that they could be included together in a multivariate analysis (Garland et al., 1992). Examination of the correlation between contrasts and branch lengths revealed that on the whole, Grafen-rho transformation produced the most appropriate branch lengths (Table 6.2.7). Correlation coefficients based on regression through the origin of contrast data are shown in Table 6.2.8 for linear measurements and Table 6.2.9 for joint shape axes.

Similar patterns were found using phylogenetically-corrected linear measures to raw data, though there were some differences. When phylogeny is taken into account fewer variables are significantly related to size in felids. Specifically, there is no effect of size on transverse process lever arm, endplate area and transverse process angle. This suggests either that some of the allometric signal was actually driven by phylogenetic similarity, or that size and phylogeny are correlated, such that the effects cannot be separated. The genus *Panthera,* which has the largest body sizes within felids, may be influencing this result. Magnitudes and polarities of correlation were similar for the other variables. For bovids, both linear and morphometric results were unchanged by the phylogenetic correction.

Table 6.2.7 Test of the assumptions of independent contrasts analysis.
Correlation coefficients of absolute contrast with corrected branch lengths. Low correlations indicate a good fit of the branch lengths with the assumptions of the standardization. Grafen-rho (0.5) transformation generally produces the best branch lengths. Variables are combinations of: PL, proximal lumbar (L1); ML, mid-lumbar; LL, last lumbar; CH, centrum height; CW, centrum width; ARCH, arch lever arm; NS, neural spine lever arm; TP, transverse process lever arm; ZYG, zygapophysis width; AREA, endplate area; TPA, transverse process angle; MASS, body mass.

	FELIDAE			BOVIDAE		
	RAW	LOG	GRAFEN-RHO	RAW	LOG	GRAFEN-RHO
PL CH	0.016	**<0.001**	0.030	0.268	0.273	**0.180**
PL CW	0.028	**0.002**	0.035	0.338	0.346	**0.203**
PL ARCH	0.126	0.049	**0.021**	0.047	0.064	**0.002**
PL NS	0.197	0.169	**0.041**	0.468	0.557	**0.124**
PL TP	**<0.001**	0.004	0.003	0.255	**0.139**	**0.139**
PL ZYG	0.007	**<0.001**	0.021	0.105	**0.102**	0.159
PL AREA	0.252	0.259	**0.062**	0.090	**0.018**	0.019
PL TPA	**0.027**	0.081	0.141	0.101	**0.009**	0.234
PL MASS	0.066	**0.020**	0.025	0.128	**0.084**	0.203
ML CH	0.022	0.036	**0.019**	0.158	0.135	**0.116**
ML CW	**0.017**	0.022	0.029	0.217	0.195	**0.139**
ML ARCH	0.001	**<0.001**	0.102	0.003	**<0.001**	**<0.001**
ML NS	0.057	0.106	**0.026**	0.437	0.549	**0.113**
ML TP	0.233	0.333	**0.069**	0.357	0.317	**0.193**
ML ZYG	0.131	0.181	**0.059**	0.069	0.059	**0.041**
ML AREA	0.190	0.226	**0.022**	0.329	0.357	**0.084**
ML TPA	0.093	0.114	**<0.001**	0.219	**0.104**	0.183
ML MASS	0.177	0.257	**0.062**	0.106	**0.058**	0.174
LL CH	0.166	0.174	**0.066**	0.084	**0.079**	0.147
LL CW	0.192	0.194	**0.076**	0.106	**0.102**	0.156
LL ARCH	0.347	0.428	**0.013**	0.069	0.076	**<0.001**
LL NS	0.208	0.230	**0.052**	0.274	0.389	**0.019**
LL TP	0.029	**0.006**	0.007	0.212	0.371	**0.071**
LL ZYG	0.419	0.347	**0.043**	0.218	0.318	**0.096**
LL AREA	0.264	0.356	**0.106**	0.108	0.238	**0.001**
LL TPA	0.105	0.074	**0.009**	**<0.001**	0.005	0.093
LL MASS	0.073	0.025	**0.019**	**0.069**	0.081	0.210
PL PC1	0.211	**0.120**	0.207	0.108	**0.022**	0.174
PL PC2	0.005	**0.003**	0.051	**0.008**	0.019	0.011

PL PC3	0.013	**0.002**	0.138	0.230	0.133	**0.033**
ML PC1	**<0.001**	0.009	0.083	0.298	**0.195**	0.264
ML PC2	0.179	0.251	**0.138**	0.299	0.254	**0.157**
ML PC3	0.013	**0.008**	0.151	0.281	0.299	**0.012**
LL PC1	0.091	0.045	**0.014**	0.319	0.273	**0.204**
LL PC2	0.524	0.562	**0.057**	0.279	0.339	**0.068**
LL PC3	0.254	0.231	**0.034**	0.306	0.324	**0.036**

Table 6.2.8 Coefficients of linear measures against log cube-root body mass using phylogenetically independent contrasts.

Multivariate regression through the origin used, coefficients reported. CH, centrum height; CW, centrum width; Arch LA, arch lever arm; NS LA, neural spine lever arm; Zyg width, zygapophysis width; End area, endplate area; TP angle, transverse process angle. Bold values are significant in univariate f-tests at the p=0.05 level

Factor	CH	CW	Arch LA	NS LA	TP LA	Zyg width	End. area	TP angle	F-ratio (Pillai's)	P-value (Pillai's)
Felidae	**0.111**	**-0.063**	**-0.134**	-0.033	-0.058	**-0.156**	0.043	-0.036	16.8	<0.001
Bovidae	**0.105**	**-0.064**	**-0.05**	0.011	**0.141**	**-0.245**	0.016	**-0.136**	**30.91**	<0.001

Table 6.2.9 Coefficients of PC scores against log cube-root body mass using phylogenetically independent contrasts.

Multivariate regression through the origin used, coefficients reported. Bold values are significant in univariate f-tests at the p=0.05 level

Factor	PC1	PC2	PC3	F-ratio (Pillai's)	P-value (Pillai's)
Felidae	-0.014	**-0.153**	-	23.96	<0.001
Bovidae	**0.23**	**0.102**	0.013	45.66	<0.001

6.3 DISCUSSION

6.3.1 HYPOTHESES

This chapter has demonstrated that **craniocaudal and allometric patterns vary between the felids and bovids.** Results are summarized in Table 6.3.1. I can now address the specific hypotheses posed at the beginning of this chapter:

H1. There is an effect of size on lumbar shape.

There are significant effects of body size on many variables, though not all match the predictions of H1. The predictions regarding endplate shape are supported. With increasing size the endplate becomes taller, indicating increasing resistance to sagittal bending, and supporting findings of Chapters 4 and 5. In contrast, H1 is not supported with regard to the increase in the height of the neural spine. This suggests either that the supraspinous ligament does not play a role in resisting the extra load with increasing size, or that changing material properties of the ligament (such as elasticity) are more important than lever arm. The lever arm of the arch had the opposite to the expected pattern, becoming shorter with increasing size, which may reflect relatively conservative scaling of the spinal cord. The angle between the transverse process and spinous process diminishes with increasing size. However, when phylogeny is taken into account, this relationship holds true in bovids but not in felids. Straighter transverse processes are associated with more stabilized lumbar regions (Smeathers, 1981; Shapiro, 1993; Ward and Latimer, 1993; Shapiro, 1995; Sargis, 2001; Argot, 2003, 2012). Interestingly, the zygapophyses become more closely spaced with increasing size in both groups. The transverse processes become longer in bovids but shorter in felids (though non-significantly when phylogeny is considered).

Hence, centrum shape changes, shortening of the arch and narrowing of the zygapophyses seem to be consistent scaling patterns between families. Bovids have additional lengthening and straightening of the transverse processes and increased complexity of the zygapophyseal joint.

Table 6.3.1 Summary of the significant effects.
TPs, transverse processes; NS, neural spine.

	FELIDAE	BOVIDAE
SIZE	Taller and narrower centrum, Shorter arch, Narrower zygapophyses	Taller and narrower centrum, Shorter arch, Longer TPs, Narrower zygapophyses Straighter TPs, Sigmoid zygapophyses
POSITION (Last lumbar)	Larger endplate Wider zygapophyses Shorter arch Long TPs	Wider, shorter endplate Larger endplate Wider zygapophyses Shorter arch Shorter NS
INTERACTIONS: **Slope between family** **Slope between position** **Position between family**	Arch height, TP length, Zygapophysis width, Area Arch height All variables	

H2. The effect of size varies among vertebral positions and families.

There were significant interactions between all the variables, supporting H2. These can be broken down into three main types of interaction. First, interactions between mass and position indicate craniocaudal variation in the allometric slope (H2A). This type of interaction was only found in one variable: height of the arch, which indicated weaker allometry of the arch at the last lumbar position. Therefore H2A is not strongly supported.

Second, interactions between mass and family indicate variable allometries between felids and bovids (H2B). Specifically, the height of the arch has a steeper negative slope in felids than bovids, the length of the transverse processes becomes shorter in felids but longer in bovids, the width of the zygapophyses scales more steeply in bovids, and the endplate area scales more steeply in felids. This suggests that as they become larger bovids have more closely-set zygapophyses but wider and straighter transverse processes. It is not surprising that the two traits of the transverse processes show similar patterns, as they are geometrically linked.

Third, interactions between family and position indicate differences in the magnitude of craniocaudal variation within the group and were significant for every variable (H2C). In particular, bovids have much stronger craniocaudal variation in endplate shape than felids, due to the dorsoventrally compressed but mediolaterally wide last lumbar joint. In bovids, the centrum, arch and neural spine are shorter at the last lumbar position, reflecting the increased sagittal mobility there. In addition the endplate and zygapophyses are wider, also suggesting reduced lateroflexion and torsion. In felids, there is no decrease in centrum or neural spine height at the last lumbar; however, there was still a reduction in arch height. There is also an increase in zygapophyseal width, which may limit lateroflexion at this joint. Hence these results support the predictions of H2C that bovids will show greater craniocaudal variation than felids in features related to sagittal mobility, due to specialization of the last lumbar joint.

6.3.2 CRANIOCAUDAL ALLOMETRY PATTERNS IN THE LUMBAR REGION

The data from this chapter have shown considerable variation in craniocaudal

and allometric patterns between families but remarkable consistency of allometric trends along the lumbar region. They support the results of previous chapters in emphasizing the strong relationship between endplate shape and size in both families. However, these data provide additional information about the centrum because they highlight the contrasting craniocaudal patterns in felids and bovids. In particular, felid endplate shape is relatively constant along the lumbar region, whereas bovids have strong dorsoventral compression at the lumbosacral joint. Moreover, this shape disparity is maintained at all sizes, suggesting that bovids of all sizes have a differentiated last lumbar joint. This also demonstrates that the ventral column at all points along the lumbar region responds to increasing size in relatively similar ways, as would be predicted by a hypothesis of a homogeneous static loading on the column with increasing body size.

Apart from the centrum, allometric patterns are more variable between families. The reduced height of the arch with increasing size in both groups (but especially felids) was somewhat surprising. However, it may reflect relative conservatism of the structures housing the spinal cord to isometric scaling relative to the endplate, which is under stronger mechanical influence. Further, there was both a reduction of absolute height and slope of the arch at the last lumbar position. If the spinal cord itself is important in determining diameter of the arch, this might reflect the caudal reduction of the cord diameter, as the end of the cauda equina is reached at the posterior extent of the spinal cord. Also surprising is the lack of significant scaling of the neural spine, suggesting a similar advantage for the supraspinous ligament in small and large animals. This suggests that either the neural spine does not help to resist additional

sagittal loading, or that supraspinous ligament composition account for increasing its strength. However, the neural spine is reduced in height near the lumbosacral joint in bovids, supporting increased sagittal mobility there. Zygapophysis spacing width decreased with size in both families, suggesting a reduction in the resistance of the joints to lateroflexion. In bovids, where the trend is strongest, this is compensated for by a simultaneous increase in the lever arm of the transverse process, which may be more important for lateral stabilization at large sizes. Finally, the angle of the transverse process is significantly reduced in bovids of increasing size, supporting findings from Chapter 5, which revealed strong allometry of transverse processes in bovids.

Data from this chapter demonstrate that some craniocaudal vertebral patterns are common to felids and bovids, whereas some that vary between them. In particular, bovids have strong morphological differentiation of the last lumbar vertebra at all sizes. If anatomy reflects function, this indicates that both small and large bovids have increased sagittal mobility and decreased lateral mobility, at the lumbosacral joint relative to the more cranial joints (as illustrated in the sheep and horse in Chapter 3). There are some advantages to this arrangement. First, maintaining sagittal mobility primarily in one joint is less energetically costly than supporting the whole lumbar region actively, but still facilitates some flexion for locomotor-respiratory coupling. Second, as sagging moments are greatest at the mid-trunk, situating the mobile joint near the sacrum where moments are lower may also reduce costs (Smit, 2002). Thus, this mobility pattern may reflect adaptation for increased efficiency of running in ungulates.

CHAPTER 7: ALLOMETRY OF THE LUMBOSACRAL REGION IN FOSSIL AND EXTANT EQUIDAE

This chapter examines the influence of size in the evolution of the lumbar region in Equidae. Modern horses are extremely efficient runners which have a stable lumbar spine and a hinge-like lumbosacral joint that flexes and extends during asymmetric gaits, such as the canter and transverse gallop. However, the vertebral anatomy of small-bodied equids is poorly understood. I examined a large sample of equid lumbars from genera at key stages in the evolution of the Equidae. In this Chapter, I compare morphology of small-bodied fossil horses to that of *Equus* and bovids (extant ungulates of similar size range) in order to assess the influence of size on stabilization of the lumbar region in Equidae.

7.1 HYPOTHESES

This chapter asks **when in equid evolution did specialization of the lumbar region for dorsostable running first appear, and were they related to size increases?** Specifically, I hypothesize:

H1. Dorsostable running evolved in Miocene horses, in association with increased body size in the Equinae. Dorsostable running is indicated by:

A. Lumbar joints: Dorsoventrally tall centra, with a strong ventral keel and pitched-interlocking zygapophyses.

B. Processes: Tall neural spines and wide transverse processes which are not ventrally or cranially inclined.

C. Lumbosacral joint: A hinge-like lumbosacral joint which is dorsoventrally

compressed, but mediolaterally wide, with lateral joints to resist lateroflexion and torsion.

7.2 RESULTS

7.2.1 FEATURES RELATED TO EQUID VERTEBRAL FUNCTION

A summary of features associated with vertebral function in horses from the

literature can be found in Table 7.2.1 (Townsend and Leach, 1984; Denoix, 1999). The

thoracolumbar column of *Equus caballus* is shown in Figure 7.2.1, with important

functional features labeled.

At the inter-lumbar joints sagittal motion is limited (Townsend et al., 1983).

Dorsiflexion is restricted by the strong ventral longitudinal ligament (indicated by the

ventral keel) and interlocking, pitched zygapophyses (see also Chapter 3). This type of

zygapophysis, which was described in more detail in the Introduction, consists of a J-

shaped facet in caudal view. On the post-zygapophysis, there is both a laterally and

ventrally facing surface, and the whole joint is inclined dorsally away from the

horizontal (see Figure 7.2.1). This post-zygapophysis fits tightly into the associated pre-

zygapophysis, limiting motion. The pre- and post-zygapophyseal facets on each joint

are directly opposed during dorsiflexion, while the lateral facets resist torsion.

Ventroflexion is limited by a strong supraspinous ligament, indicated by closely-

spaced, craniocaudally long neural spines with a dorsal ridge or thickened region for

the attachment of the ligament (Figure 7.2.1). The spinous processes are robust and

vertically oriented. The diaphragmatic vertebra is relatively caudally-placed, such that

it is coincident with the last thoracic or thereabouts, resulting in a shortened post-

diaphragmatic region, which is associated with stabilization in other mammalian groups

(Williams, 2012a).

In contrast, the lumbosacral joint is capable of over 20º of sagittal motion *ex*

vivo. Dorsiflexion is permitted here by smaller, sagittally oriented post-zygapophyses on the last lumbar that may slide past their opposing facet on S1. The centrum is dorsoventrally compressed; facilitating increased sagittal mobility by reducing the lever arm of the disc and longitudinal ligaments. Mobility is also promoted by a thicker disc here, though this is not preserved in fossils. Ventroflexion is permitted at the lumbosacral joint because the supraspinous ligament is much less well-developed and more elastic (Denoix, 1999). This is reflected in the divergence and slenderness of the neural spines at the lumbosacral joint (Figure 7.2.1). Finally, there are well-developed lateral transverse process joints which greatly restrict lateroflexion and torsion at this joint. However, they still permit flexion and extension because they are hinged; forming a roughly cylindrical shape whose long axis runs mediolaterally (Figure 7.2.1).

Figure 7.2.2 shows the craniocaudal variation in centrum shape, scaled by endplate area, in *Equus caballus*. This figure demonstrates that the centrum becomes dorsoventrally compressed and mediolaterally wider approaching the last lumbar joint, especially in the last three lumbars. This reflects a relative increase in mediolateral stiffness and decrease in sagittal stiffness of the intervertebral discs posteriorly. The penultimate one or two lumbar joints are frequently fused, preventing all movement, whereas the lumbosacral joint never fuses (Townsend and Leach, 1984). Centrum length (scaled by mid-thoracic) increases only slightly in the anterior lumbar region, before decreasing rapidly toward the lumbosacral joint.

Table 7.2.1 Anatomical features associated with patterns of mobility in **Equus.**

Anatomy	Function	Reference
<u>Lumbar-Lumbar Joints</u>		
Pitched, interlocking zygapophyses	Limit axial rotation and dorsiflexion	Townsend and Leach (1984)
Long (craniocaudal) and tall (dorsal) spinous process	Limit ventroflexion	Denoix (1999)
Ventral longitudinal ligament well developed (forming keel)	Limit dorsiflexion	Denoix (1999)
Tall (dorsoventral) centra	Limit sagittal motion	This study
<u>Lumbosacral Joint</u>		
Zygapophyses flat, small and sagittally oriented	Permit dorsiflexion	Townsend and Leach (1984)
Divergence of the neural spines at the lumbosacral joint	Permit sagittal motion	Townsend and Leach (1984)
Decreased height and increased thickness of discs (and centra)	Permit sagittal motion	Denoix (1999)
Lateral joints	Limit lateroflexion and rotation	Townsend and Leach (1984)
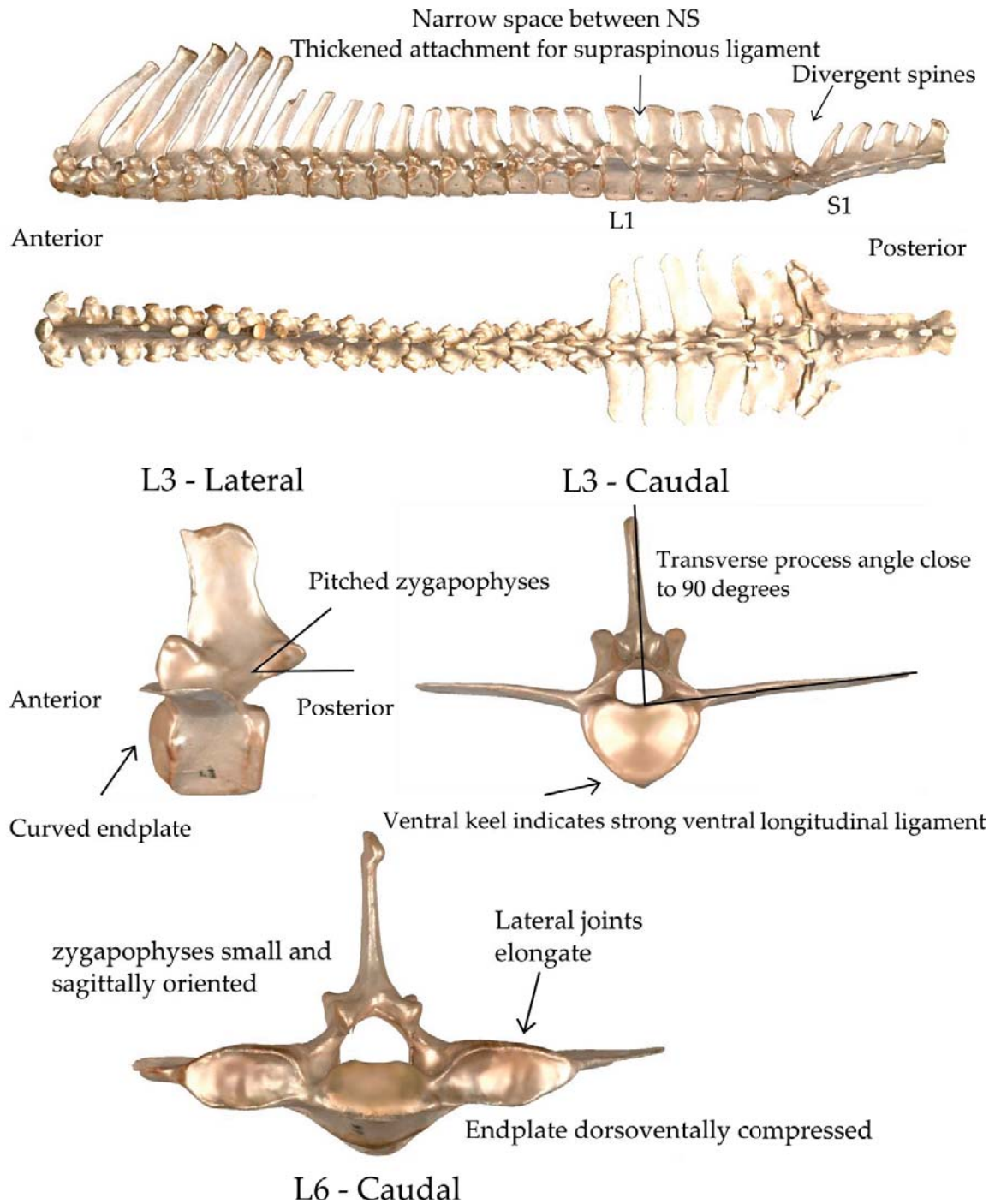
***Figure 7.2.1 Illustration of anatomical features associated with function in the
lumbosacral region of* Equus caballus.**

*Upper images are complete thoracolumbar region in lateral and dorsal view. Lower
images show features on L3 (lateral and caudal) and the last lumbar vertebra (caudal).
L3 length: 45.5mm, L6 centrum width: 46.9mm.*
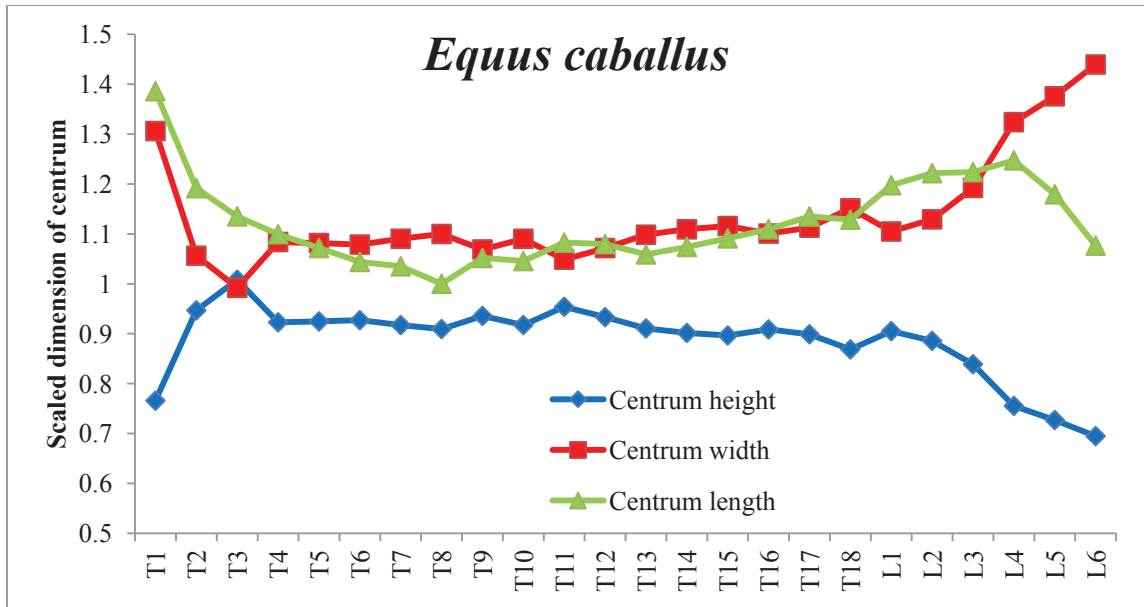
***Figure 7.2.2 Craniocaudal variation in centrum shape in* Equus caballus.**
Centrum width and centrum height were scaled by the endplate area (width multiplied by height) of the same vertebra. Centrum length was scaled by the length of the middle thoracic vertebra (T8). Note the changing shape of the centrum approaching the lumbosacral joint. Data can be found in Appendix 9.

7.2.2 **VERTEBRAL MORPHOLOGY OF FOSSIL EQUIDS**

Phenacodus vortmani

Phenacodontid condylarths have been considered closely related to

perissodactyls (Radinsky, 1966) and are used here to represent an outgroup to Equidae.

Specifically, I examined *Phenacodus vortmani* as a model for the vertebral column in

the precursors of Equidae. *P. vortmani* was studied using the column of AMNH FM

4378 (Figure 7.2.3). This specimen, from the Bighorn Basin of Wyoming, is dated from

the Early Eocene. This specimen has been partially restored, so this description uses

only portions of the vertebral column which were considered original by Otts (1991). In

addition, one specimen of *Phenacodus primeavus* from the USNM collection at Johns

Hopkins (USNM 27589) with isolated lumbars was also examined and compared to *P.*

vortmani to support inferences based on this specimen. Phenacodontid locomotion was

likely ambulatory, with incipient specialization for running. Primitive characters

include pentadactyl feet and a less-grooved astragalus with a rounded head (Radinsky,

1966). Its body mass has been estimated at 11.5kg (Damuth, 1990).

AMNH FM 4378 likely has the vertebral formula 15T:6L (Otts, 1991), which is

the same as the vertebral formula assigned to *P. primaevus* by Osborn (Osborn, 1923) .

The diaphragmatic vertebra in *P. vortmani* is around T13, and in *P. primaevus* it seems

to be at T12 or T13 (based on the illustration), resulting in two post-diaphragmatic

thoracic vertebrae. The centra of *P. vortmani* are more craniocaudally elongate in the

lumbar region than the thoracic region, reaching a peak around L3 (Figure 7.2.4). These

data matched the pattern shown in Osborn's illustration of *P. primaevus* where the mid-

lumbar (L3) was approximately 1.7 times the length of the mid-thoracic (L7). However,

there was little craniocaudal variation in the shape (width and height) of the centra along the lumbar region. In particular, there was no evidence of dorsoventral compression in the last few lumbars, although the centrum of L6 in AMNH FM 4378 is partially restored and cannot be relied upon.

Centra have a ventral keel indicating a moderately-developed ventral longitudinal ligament. There is a slight opisthocoelous curvature to the endplates in the lumbar region. Transverse processes on this specimen were reconstructed in the lumbar region and so were unavailable for study. The neural spines are preserved in the caudal thoracics and lumbar L3. In the caudal thoracic region, the spines are square and relatively short, with blunt ends, whereas in the lumbar region they appear a little longer and more cranially inclined. The ends of the lumbar neural spines are blunt and not very tapering, but lack a strong ridge.

The zygapophyses of AMNH FM 4378 were mostly reconstructed in the lumbar region, but post-zygapophyses are preserved in L1 and L6. They are flat to slightly convex, but not revolute. The post-zygapophysis on L6 is oriented at about 55º to the mid-sagittal plane and slightly caudally (Otts, 1991). *P. primaevus* (USNM 27589) preserves some disarticulated lumbars, including one with post-zygapophyses intact. These joints are very widely-spaced and ventrally-placed, suggesting this vertebra is from the posterior portion of the series. They are flat to convex, and rather horizontal in orientation, forming an angle of around 60º to the vertical. In contrast, Otts noted that *P. primaevus* (PU 14684) tended to have more sagittally oriented lumbar post-zygapophyses than *P. vortmani,* and thus inferred that the larger species had greater dorsoventral flexibility (Otts, 1991). The endplate of the USNM specimen is large, oval

and around 1.4 times wider than it is tall.

The lumbar region of *Phenacodus* lacks a number of lumbar specializations of equids. In the posterior lumbar region, there is no evidence of lateral transverse joints, and centra are not strongly dorsoventrally compressed or mediolaterally wide. This suggests that *Phenacodus* was not specialized for flexion-extension of the lumbosacral joint, and did not have reinforcement of that region against mediolateral bending from hindlimb muscles. The diaphragmatic vertebra is cranially displaced from the first lumbar, and the lumbars are relatively elongate, suggesting some sagittal mobility in the lumbar and posterior thoracic region. However, these features are not as extreme as in specialist dorsomobile runners such as carnivores. Hence, *Phenacodus* represents a relatively generalized primitive condition for ungulates, neither specialized for mobility nor stability.

Neural spines flat at tip

Zygapophyses flat-convex

T14

L1

L5
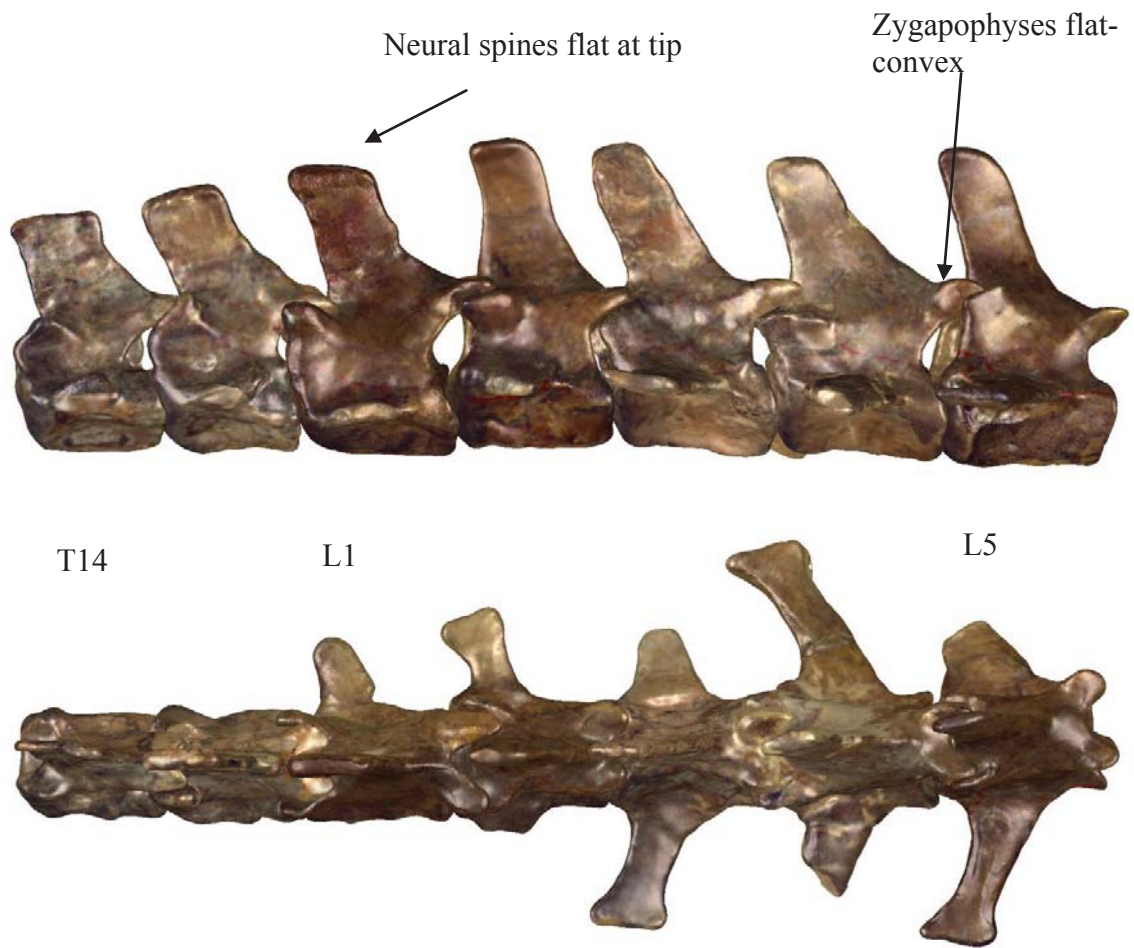
Figure 7.2.3 The lumbar region of **Phenacodus vortmani** *AMNH FM 4378.*
From T14 to L5, lateral and dorsal views. T14 length: 18.7mm.
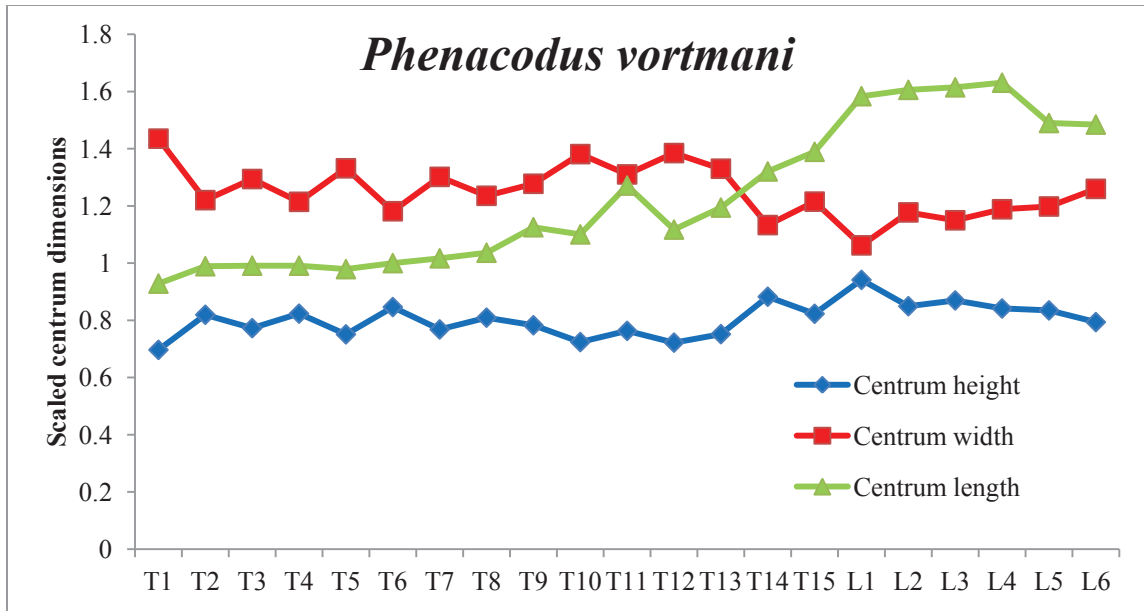
***Figure 7.2.4 Craniocaudal variation of centrum dimensions in* Phenacodus vortmani**
AMNH FM 4378.
Centrum width and centrum height were scaled by the endplate area (width multiplied by
height) of the same vertebra. Centrum length was scaled by the length of the middle
thoracic vertebra. Centrum shape in the lumbar region is relatively constant. Data can
be found in Appendix 9.

Hyracotherium grangeri

  Hyracotherium is a primitive equid genus in the subfamily Hyracotheriinae

from the early Eocene of North America. For simplicity, I use the name

Hyracotherium, sensu lato, following Wood et al. (2011), although some authors argue

that *Hyracotherium* should not be used for early equids and replace it with numerous

other genera, as this genus is likely paraphyletic (Hooker, 1994; Froehlich, 2002).

Hyracotherium was a primitive, small-bodied equid with a tetradactyl manus and

tridactyl pes, and was relatively more specialized for cursoriality than *Phenacodus*

(Radinsky, 1966).

The vertebral morphology of *Hyracotherium* was studied using an exceptionally preserved specimen of *Hyracotherium grangeri* (UM115547) with an almost complete vertebral column, from the early Eocene of the Clarks Fork Basin of Wyoming (Wood et al., 2011). Its mass was estimated at 9 kg (Wood et al., 2011). The specimen was preserved with most of the lumbar region in articulation, forming a distinctly curved profile (Figure 7.2.5). The vertebral formula of this specimen was 17T:7L, hence it displays the elevated thoracolumbar counts typical of perissodactyls. The last three thoracics are post-diaphragmatic. Examination of the craniocaudal variation in centrum shape shows an interesting combination of traits (Figure 7.2.6). There was a peak in centrum length in the lumbar region similar to, but more exaggerated than, that of *Phenacodus*. However, there was also a strong dorsoventral compression of the centrum toward the lumbosacral joint. Specifically, the last two lumbars had wider and more sagittally compressed centra than the more cranial lumbars.

The neural spines are cranially inclined in the anterior lumbar region, but more vertical in the posterior lumbar region. They are similar to *Phenacodus* in that they have relatively square, blunt tips. The posterior lumbar spines are taller than those located more anteriorly. The neural spine on the last lumbar of *Hyracotherium* was shorter than that of the penultimate lumbar. Transverse processes are relatively wide (mediolaterally) and are inclined, both cranially and ventrally (see 7.2.5 for measurements). The ends are blunt, not tapering. The ventral keel is less developed than in *Phenacodus* and is present only in the proximal lumbars.

The joint morphology of the articulated section was visualized using CT scan slices in its original description (Figure 7.2.7). Overall, the centra tend to be oval in

cross section, not heart-shaped, with a greater mediolateral than dorsoventral diameter.
Zygapophyses are relatively widely spaced and the spacing increases posteriorly along
the column. The post-zygapophyses of L1-L3 and posterior thoracics are shallowly
curved in the convex direction, similar to those described for *Phenacodus*. In contrast,
L4-L7 are revolute, displaying an additional dorsal surface on the postzygapophysis to
form a 'c' shaped joint. The zygapophyses on the last lumbar joint are much more
widely-spaced and more ventrally placed than the joints of the anterior lumbars. There
is no evidence of lateral transverse joints at the lumbosacral joint, neither in this
specimen, nor in multiple other Bighorn Basin specimens from the USGS and USNM
collections housed at Johns Hopkins.

Hyracotherium grangeri has a mixture of primitive and derived traits. The
anterior lumbar and posterior thoracics are similar to those of *Phenacodus,* whereas the
posterior lumbars are more specialized. These derived traits include long neural spines,
revolute zygapophyses and dorsoventral compression of the posterior centra. Further,
the neural spine of the last lumbar is shorter and slightly cranially inclined, suggesting
that it may have diverged with that of the first sacral. However, there was no evidence
of lateral transverse joints. Thus the lumbosacral joint of *Hyracotherium* is 'incipiently
hinged', which I define as dorsoventrally compressed but lacking lateral joints to
further stabilize the joint against torsion and lateroflexion. Zygapophyses in the
posterior lumbar region are revolute, which could provide resistance to torsion from the
hindlimb.

Neural spines cranially
inclined

Neural spines more vertical

Transverse process
wide and square

L1

T15

L1

S1
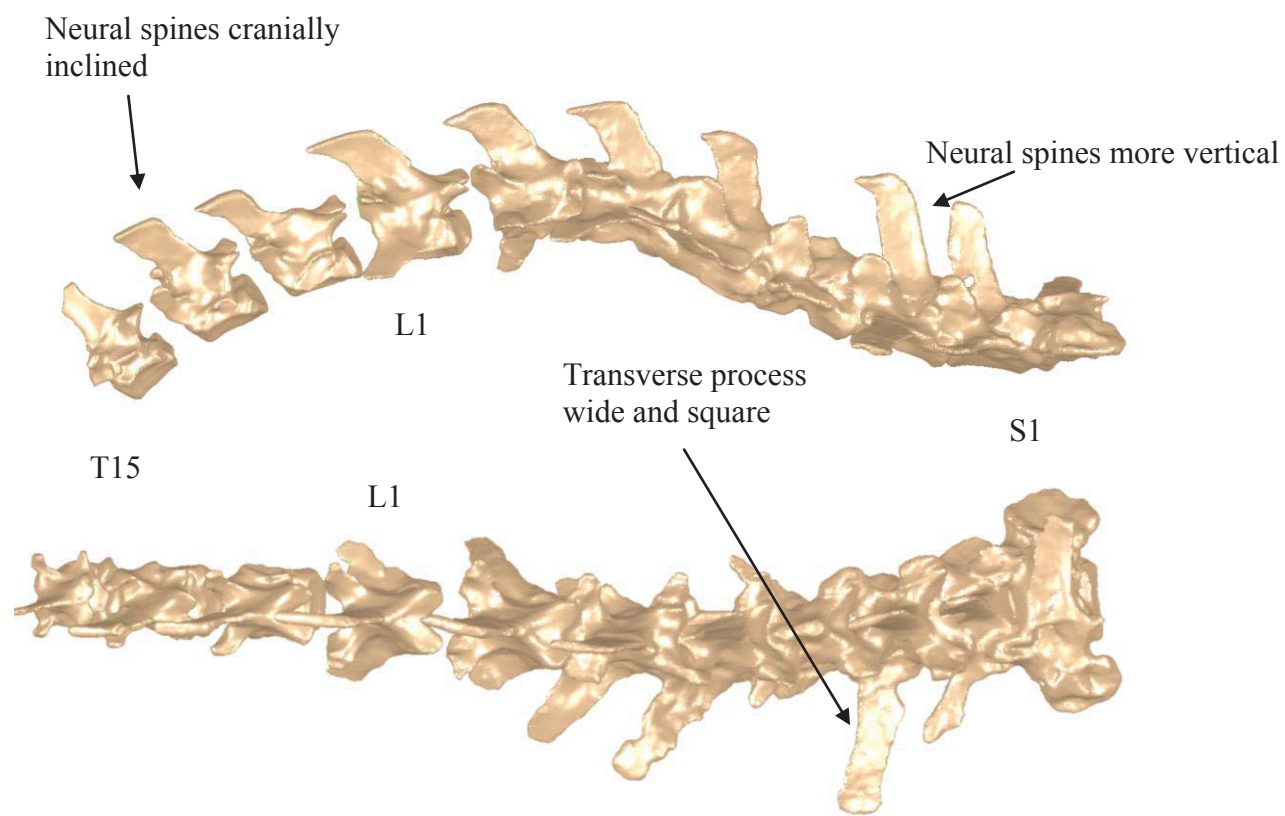
Figure 7.2.5 Post-diaphragmatic region of **Hyracotherium grangeri** *UM 115547.*
T15-S1. T15 length: 12.3mm.
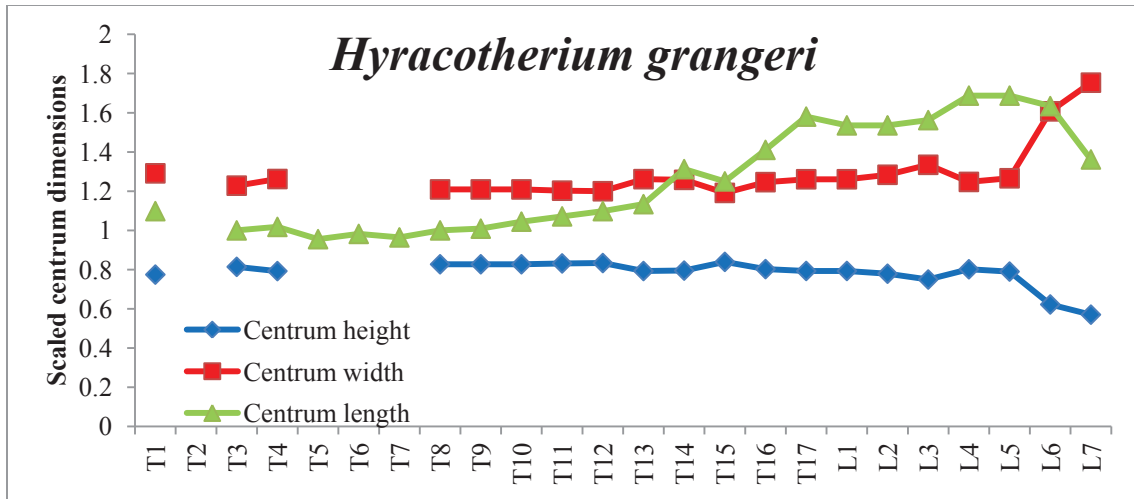
Figure 7.2.6 Craniocaudal variation in centrum dimensions of **Hyracotherium grangeri.**

Centrum width and centrum height were scaled by the endplate area (width multiplied by height) of the same vertebra. Centrum length was scaled by the length of the middle thoracic vertebra. Note the change in centrum shape just prior to the lumbosacral joint. Some thoracic vertebrae which were preserved in articulation could not be measured. Data can be found in Appendix 9.
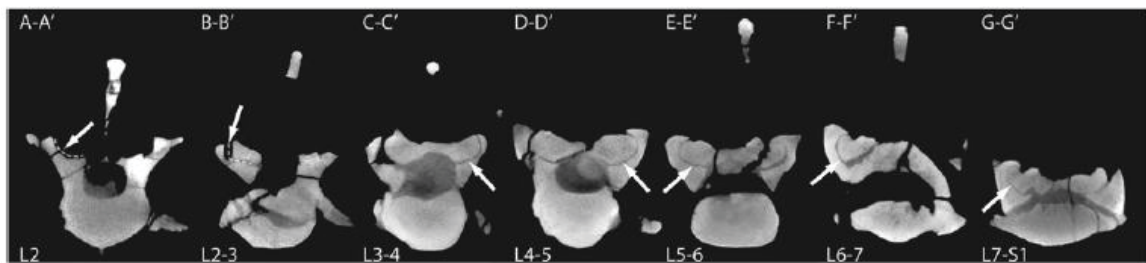
Figure 7.2.7 CT slices through the lumbar joints of **Hyracotherium grangeri.**
From Wood et al. (2011), illustrating changes in zygapophyseal shape along the lumbar region. Note that revolute zygapophyses are present from L4-5 caudad, and that the centrum at L7-S1is extremely dorsoventrally compressed.

Mesohippus bairdii

Mesohippus bairdii is the most primitive member of the subfamily

Anchitheriinae and is common in the Oligocene White River deposits of Nebraska,

South Dakota, and Wyoming. *Mesohippus* was larger and had more cursorial specializations of the limbs than *Hyracotherium,* including a tridactyl manus and subunguligrade foot posture. Mass estimates for this species range from 25kg to 42kg (MacFadden, 1986; Damuth, 1990; Janis, 1990). Complete specimens were difficult to access because of their popular use as exhibit mounts. Two partially complete lumbar regions were examined: YPM 13791 preserves T17 to L6 (excluding L7), and YPM 11376 preserves L3 to S5. These two specimens are shown in Figure 7.2.8 and Figure 7.2.9. The vertebral formula for *Mesohippus* has been interpreted as 17T:7L, with 2-3 transitional thoracics, based on Sinclair (1925) and the mounted specimen AMNH 1492 (Sinclair, 1925).

Craniocaudal patterns of mean centrum shape calculated from YPM 13791 and 11376 reveal that there is some dorsoventral compression of the centra toward posterior lumbar region (Figure 7.2.10). Similar to *Hyracotherium,* the last two lumbar vertebrae have relatively compressed centra, indicating reduced stiffness of the disc in the sagittal plane relative to the mediolateral plane. However, there is relatively less variation in centrum length along the lumbar region than *Hyracotherium.*

Few examples of vertebral processes were available for study. YPM 11376 preserves the neural spine of L6, which is tall but relatively craniocaudally slender, and slightly cranially sloping. The S1 neural spine also seems to have been cranially inclined in this specimen; however, examination of the fossil suggested that this process may have been deformed and therefore this orientation cannot be trusted. Transverse processes are only preserved in one specimen (excluding those with lateral joints), USNM 74048, and they suggest a moderate ventral inclination. There is a weakly

223

developed ventral keel along the anterior lumbar region.

Morphology of the zygapophyses is relatively well preserved in both these specimens, and they are revolute from L2 caudad. L1 and the post-diaphragmatic thoracics have curved zygapophyses similar to those in the anterior column of *Hyracotherium*. *Mesohippus* also had well-developed lateral transverse joints between L6-L7 and L7-S1. The lumbosacral lateral joints are oval in shape and mediolaterally elongate (Figure 7.2.8). In YPM 11376, L6-L7 are articulated and may or may not be fused.

The lumbar region of *Mesohippus* is more derived than that of *Hyracotherium* because of the presence of lateral joints between the transverse processes on the last two presacral joints. These joints are similar in morphology to those found in *Equus caballus*. Combined with the dorsoventrally compressed centrum on the last lumbar vertebra, these joints form a hinge-like lumbosacral joint capable of flexion and extension but resistant to lateroflexion or torsion. In *Equus caballus* sagittal motion at this joint is important during asymmetric gaits, thus it is interpreted as an adaptation to cursoriality. The lumbar region of *Mesohippus* is similar to that of *Hyracotherium* in that the zygapophyses are flatter in the transitional and anterior lumbar region but revolute in the posterior lumbar region, suggesting resistance to axial torsion in the posterior column.

Transverse process tall and craniocaudally slender

Fused?

Lateral joints

L3

Sacrum

Lateral joints,
Mediolaterally elongate
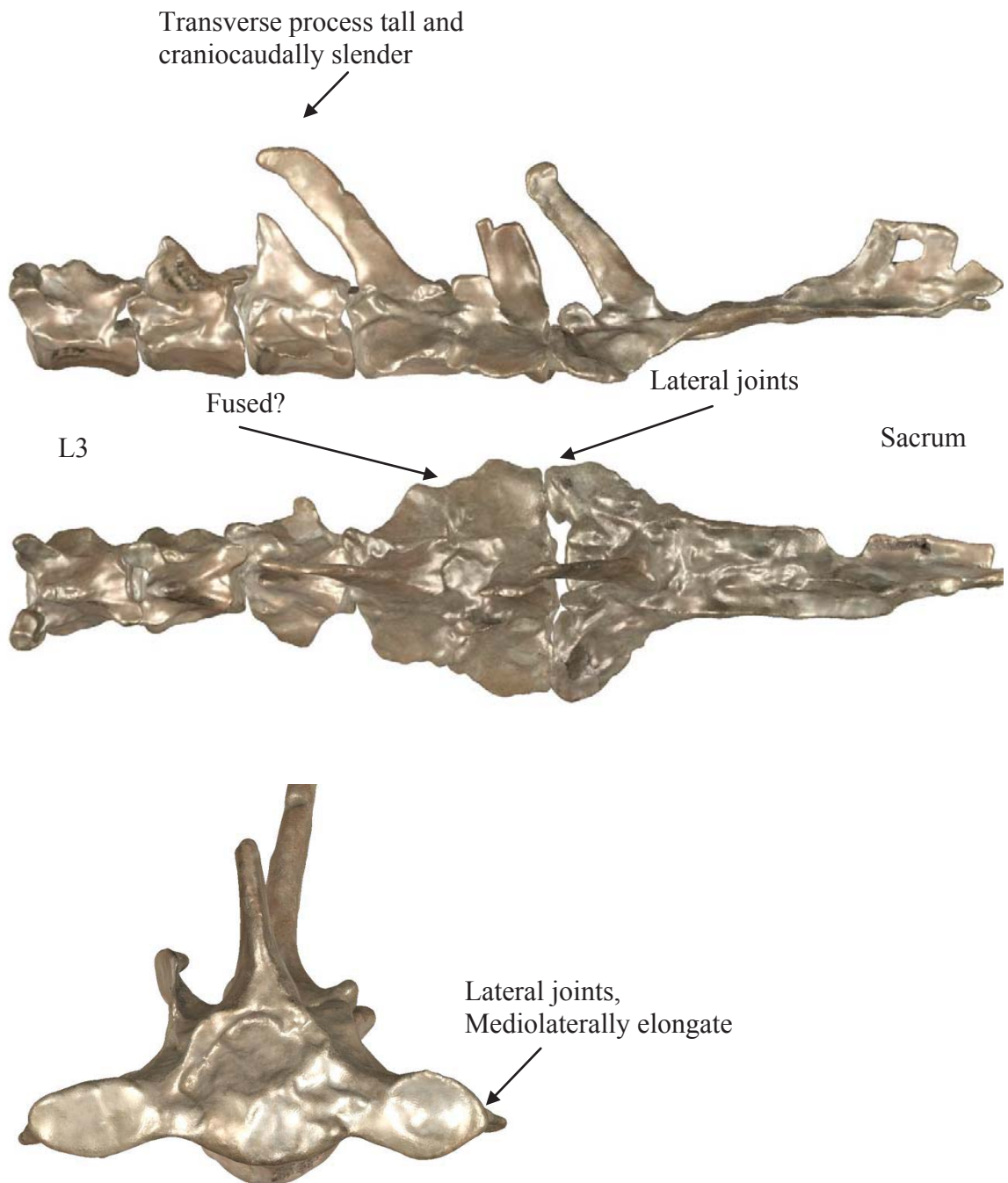
Figure 7.2.8 **Mesohippus bairdii** *YPM 11376.*
L3-S3, lateral and dorsal views. L6 caudal view below. L3 length: 21.37mm.
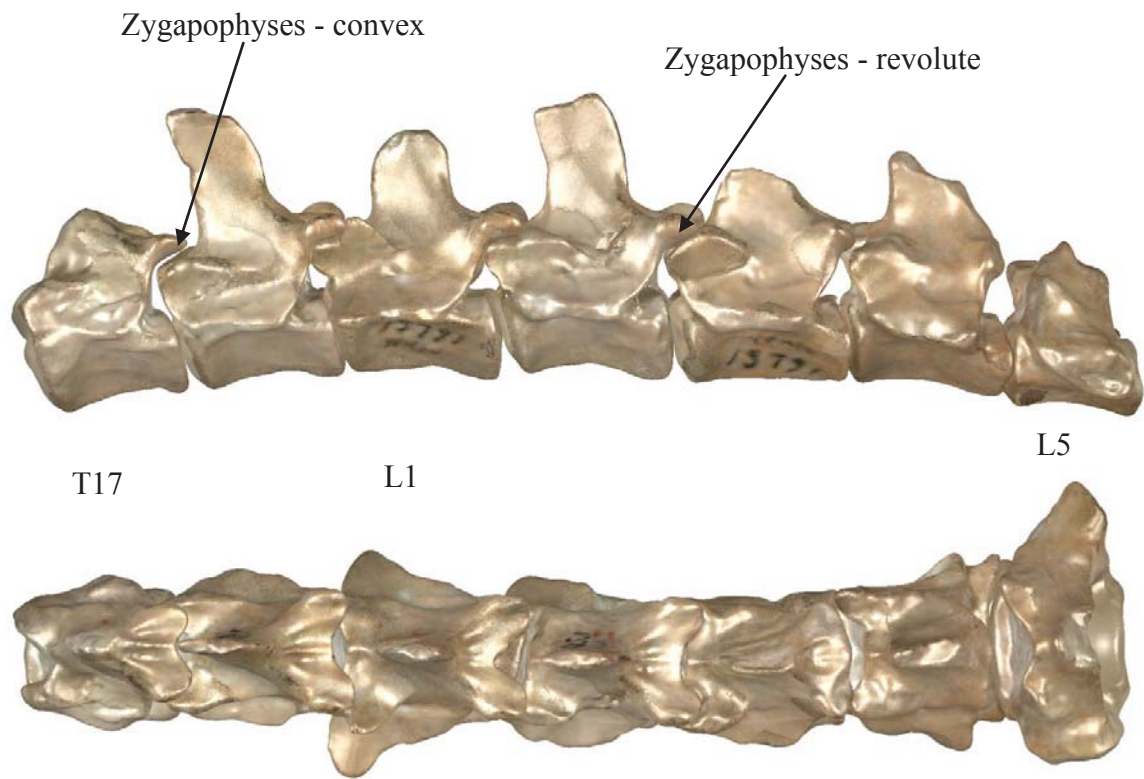
Figure 7.2.9 **Mesohippus bairdii** *YPM 13791.*

T17-L5, lateral and dorsal views. T17 length: 20.8mm. L3 length: 20.94mm
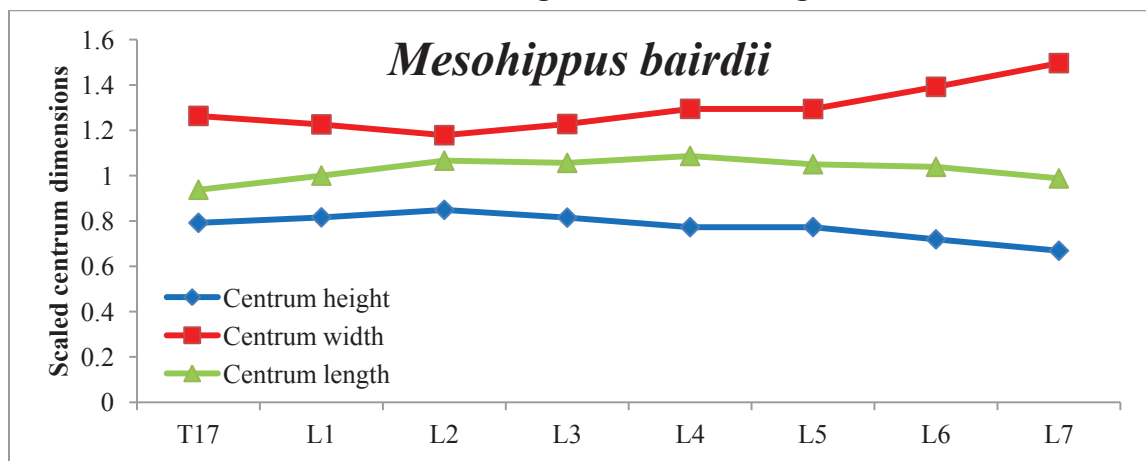
Figure 7.2.10 Craniocaudal variation in the lumbar region of **Mesohippus bairdii.**
Based on mean values from YPM 11376 and YPM 13791. Centrum width and centrum height were scaled by the endplate area (width multiplied by height) of the same vertebra. Centrum length was scaled by the length of the first lumbar vertebra. Data can be found in Appendix 9.

Archaeohippus blackbergii & Parahippus leonensis

Isolated vertebrae were available for study from the Thomas Farm locality of
the Hemingfordian (middle Miocene) of Florida representing two sympatric anchithere
species: *Archaeohippus blackbergi* and *Parahippus leonensis* (Figure 7.2.11, Figure
7.2.12). These taxa were tridactyl like *Mesohippus,* but the lateral digits were greatly
reduced. Though the isolated vertebrae were well preserved, no complete columns were
available for study, so the vertebral formulae of these species cannot be confirmed.
Based on the vertebral counts of *Mesohippus* and *Merychippus* they likely had 6-7
lumbars (Simpson, 1932). *Archaeohippus blackbergi* likely weighed between 23kg and
44kg, whereas *Parahippus leonensis* weighed between 69kg and 77kg (MacFadden,
1986; Janis, 1990).

By assessing variation among the isolated lumbars of *Parahippus* in the Florida
collection, and comparing them with *Mesohippus*, I was able to assign most vertebrae
to either proximal lumbar, middle lumbar, penultimate or last lumbar. Based on these
assignments I constructed a composite column for *Parahippus leonensis* shown in
Figure 7.2.12. Centra were dorsoventrally compressed and wider in the posterior
lumbars, relative to the more anterior vertebrae (Figure 7.2.13). There was little
craniocaudal elongation in the mid-lumbar region. *Archaeohippus* had similar lumbar
morphology to *Parahippus*, where equivalent elements were preserved.

There are transverse process joints on at least the last two presacral joints in
both species. The lateral joints on the last lumbar are wider mediolaterally, whereas the
penultimate lumbar ones are much rounder (Figure 7.2.11, Figure 7.2.14). No
specimens indicated fused lumbars. Processes are not preserved in these specimens so I

am unable to comment on the morphology of the neural spine or transverse process. There is a moderate keel which is absent on the last two lumbars. Revolute zygapophyses are only present in the posterior lumbars and not the anterior lumbars or transitional thoracics. Thus, the morphology of the lumbar region of these species seems congruent with that of *Mesohippus*.
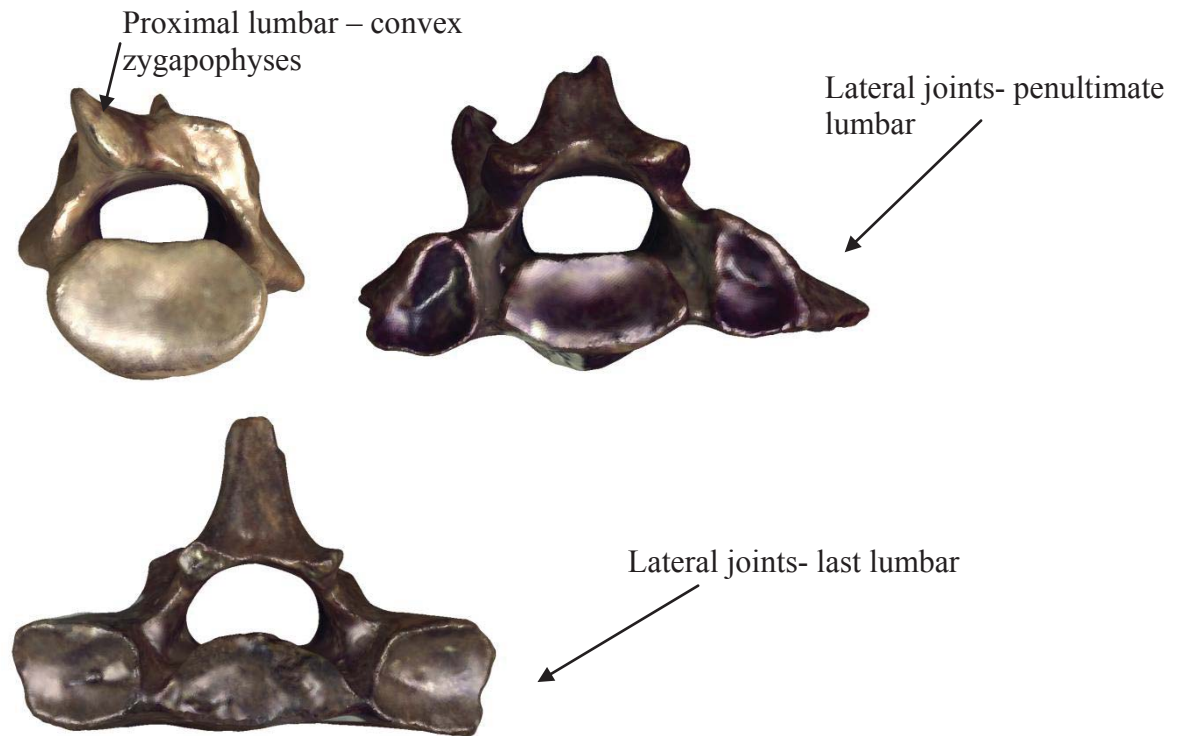
Figure 7.2.11 **Archaeohippus blackbergi** *lumbars.*
Proximal lumbar, UF 276606, centrum width:16.7mm; penultimate lumbar, UF 259127, centrum width:16.5mm; last lumbar, UF 258551, centrum width: 20.9mm.

L1

L7

Figure 7.2.12 **Parahippus leonensis** *composite.*
Using: UF 163493, 199217, 205530, 255585, 256115, 260245, 273270; L1-L7
approximately. L1 length: 28.3mm.
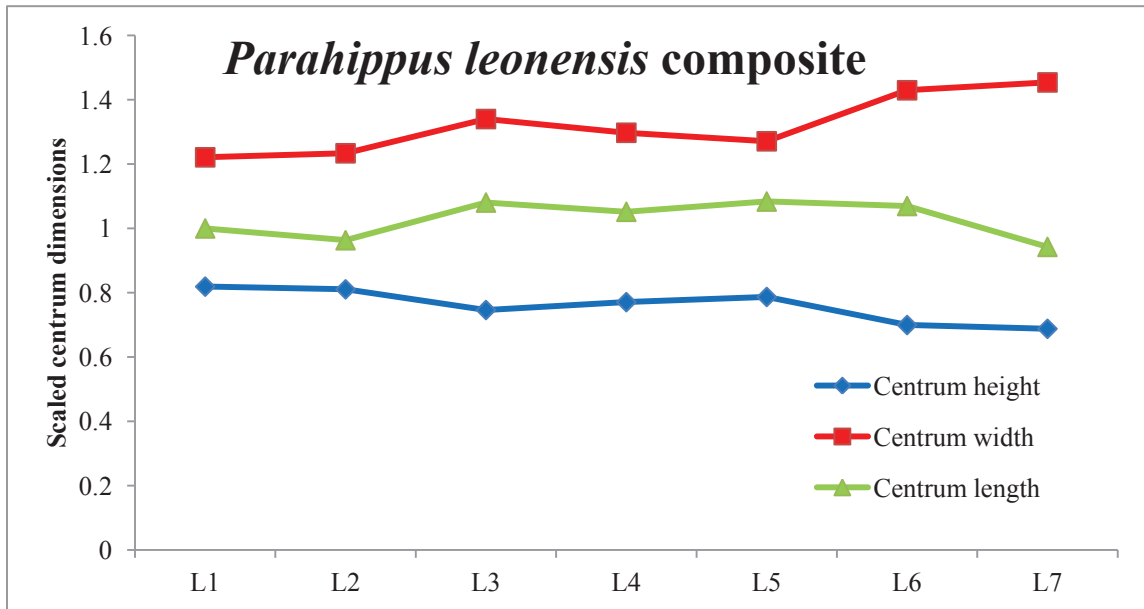
Figure 7.2.13 Craniocaudal variation in **Parahippus leonensis** *based on the composite.*
Centrum width and centrum height were scaled by the endplate area (width multiplied by
height) of the same vertebra. Centrum length was scaled by the length of the first lumbar
vertebra. Data can be found in Appendix 9.

229

***Figure 7.2.14 Last lumbar joint of* Parahippus leonensis.**
Showing lateral transverse articulations. UF 199217, centrum width: 20.0mm.

"Merychippus"

The genus *"Merychippus"* is a paraphyletic grouping that includes multiple, relatively primitive species from the subfamily Equinae. The hypsodont teeth, unguligrade foot posture and larger body size of these equids suggests that they were open-plains grazers, more specialized for cursoriality than anchitheres (MacFadden, 1992). *Merychippus* likely weighed between 85kg and 111kg (MacFadden, 1986; Damuth, 1990). Although *Merychippus* is generally well known, little vertebral material was available for study, primarily because of its use in exhibits or collection bias. Most of the material I found came from the holotype collections at AMNH, and thus represents multiple species. Therefore it was not possible to get an accurate idea of the craniocaudal patterns in any one species.

Merychippus quintus likely had the vertebral formula T18:L6 (Simpson, 1932). This specimen, on exhibit in the Mammal Hall at the American Museum of Natural History (F:AM 14185 and 71173), is shown in Figure 7.2.15. Though a significant portion of the column is reconstructed, the neural spines of L4 and L5 are original.

They are craniocaudally long and vertically oriented, with a strong dorsal ridge. The posterior thoracics T17 and T18 are also original, and are a little shorter dorsoventrally, but similarly robust and vertically oriented.

Morphology of the last lumbar of *M. republicanus* and the penultimate lumbar of *M. proparvulus* can be seen in Figure 7.2.16. These vertebrae indicate that both species had lateral joints on the last and penultimate lumbar joints. *M. republicanus* (upper image) has facets for joints on both cranial and caudal edges of the transverse processes indicating it is likely the last lumbar, though the cranial pair is very small. The caudal pair is wide in a similar fashion to *Parahippus*. Zygapophyses on the last lumbar joint are small and sagittally oriented, without being revolute, though they may have been revolute more anteriorly. The specimen of *M. proparvulus* (AMNH 9394, lower image) has only a caudal lateral joint facet, which is small and round, suggesting that it is the penultimate lumbar vertebra. An unprepared specimen of *M. isonesus* AMNH F:AM 69512 (Figure 7.2.17) suggests that the neural spines of *Merychippus* at the last lumbar and first sacral diverged, as in *Equus caballus,* implying higher sagittal mobility at the lumbosacral joint.

Examination of further specimens will help to clarify the craniocaudal variation in lumbar morphology in *Merychippus.* However, the data presented here support a lumbosacral joint which is similar in morphology and function to that of the anchitheres. However, morphology of the neural spines, particularly in the transitional region, suggests greater stabilization of the lumbar region in *Merychippus.*
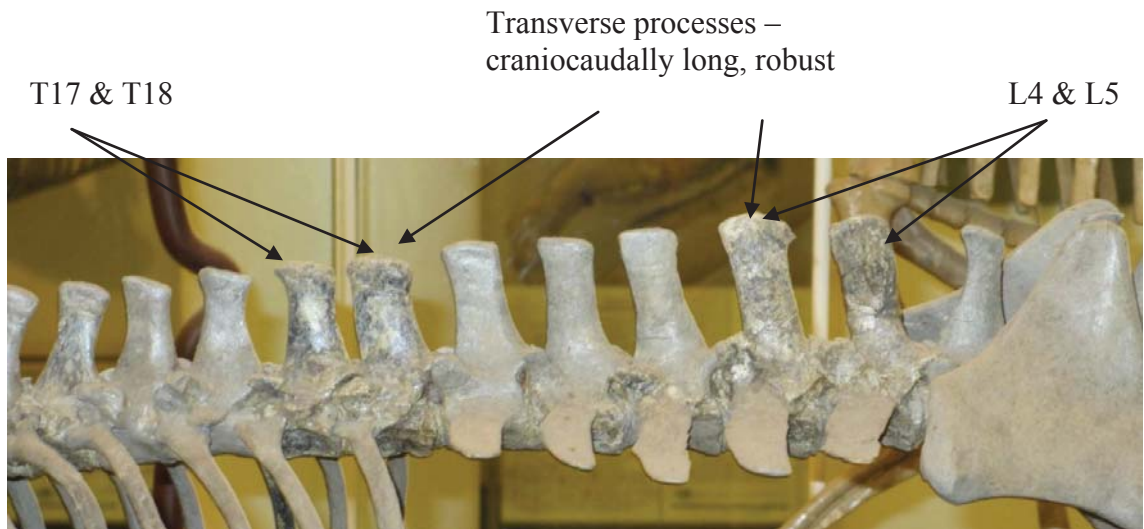
Figure 7.2.15 Mounted specimen of Merychippus quintus *AMNH FM 14185/FM 71173*.

On display in fossil mammal hall, lateral view. The last two thoracics and lumbar L4 and L5 seem to be original except for the transverse processes.
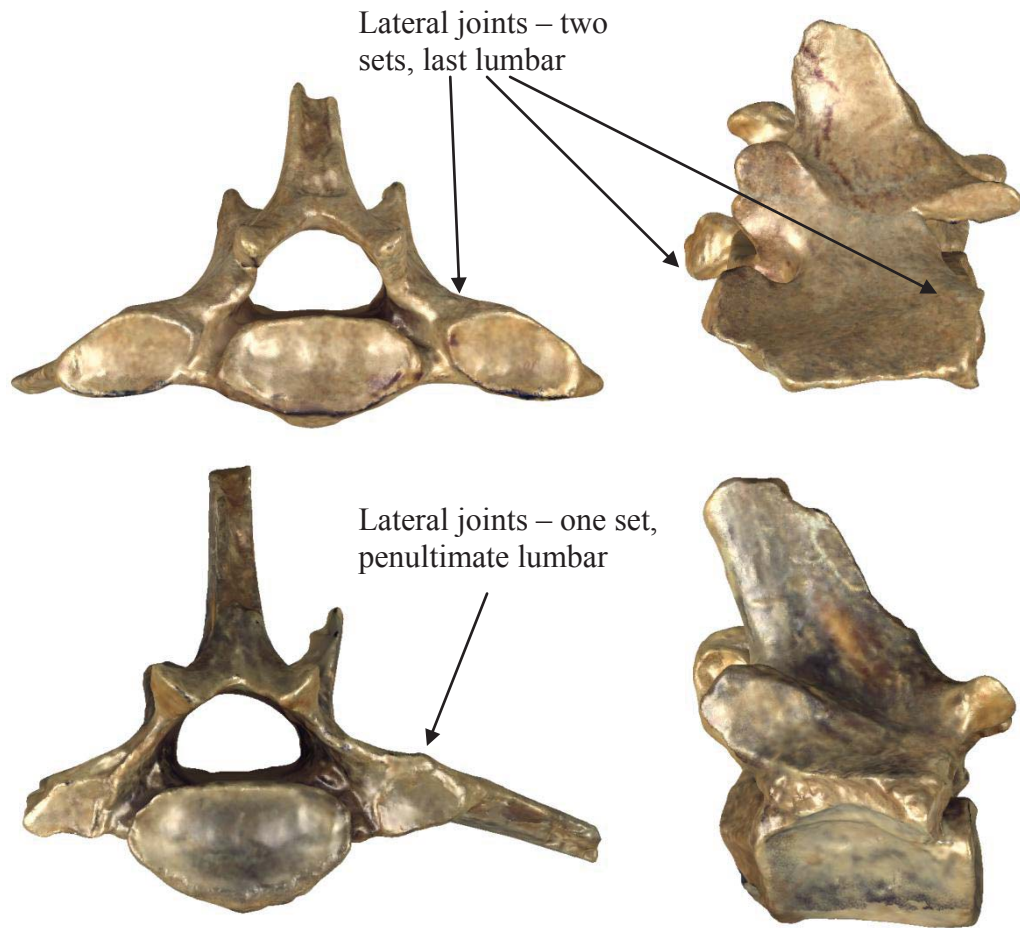
Figure 7.2.16 **Merychippus** *lumbars.*

Top: Merychippus republicanus FM AMNH 8347, centrum width: 25.6mm; bottom: Merychippus proparvulus AMNH FM 9394, centrum width: 29.7mm. Both are shown in caudal and lateral views.
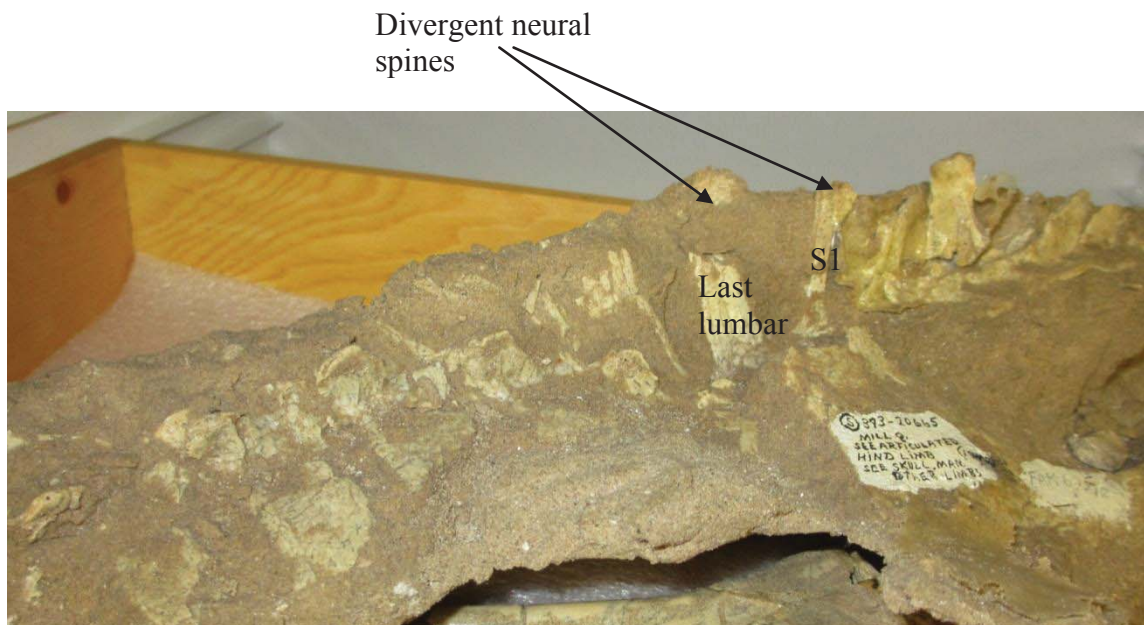
Figure 7.2.17 Unprepared specimen of **Merychippus isonesus** *AMNH F:AM 69512.*
Note divergent neural spines at lumbosacral joint.

Nannippus minor

    Nannippus minor represents the tribe Hipparionini (subfamily Equinae). It was

relatively small for this subfamily, with an estimated body mass between 60kg and

89kg, which is thought to represent secondary size reduction (MacFadden, 1986;

Alberdi et al., 1995). It was strongly hypsodont and had a functionally monodactyl foot

structure (Sondaar, 1968). Specimens examined were from the Tyler Farm locality,

early Hemphillian (late Miocene) of Florida.

    Four associated vertebrae (L1-L4, UF 69933) and multiple isolated vertebrae

were examined (Figure 7.2.18). These vertebrae have robust, craniocaudally long

neural spines with a thickened dorsal ridge, indicating the presence of a strong

supraspinous ligament. Moreover, the ventral keel is better developed than in

Mesohippus, suggesting a strong ventral longitudinal ligament, too. Endplates are

curved and slightly opisthocoelous, which suggests a caudally displaced center of

rotation for the joint, as in *Equus caballus* (Denoix, 1999). Figure 7.2.19 shows the L3-L4 joint of UF 69933 to illustrate how the joint locks together. This demonstrates that *Nannippus* had pitched interlocking zygapophyses and not revolute joints. Note that the ventral surface of the post-zygapophysis is inclined caudally so that it abuts the dorsal surface of the pre-zygapophysis, and that the two surfaces fit together tightly.

In contrast, the lumbosacral joint has small, sagittally oriented zygapophyses as in *Equus caballus*, with ovoid lateral transverse joints (Figure 7.2.20). The presence of much smaller lateral processes on other vertebrae suggests these joints occurred on at least the last two presacral joints. These specimens suggest that, despite its relatively dimunitive size, *Nannippus* had a lumbar region that was relatively similar to that of *Equus caballus*.

Neural spine – craniocaudally long, robust

T18

Pitched-interlocking zygapophyses

L3
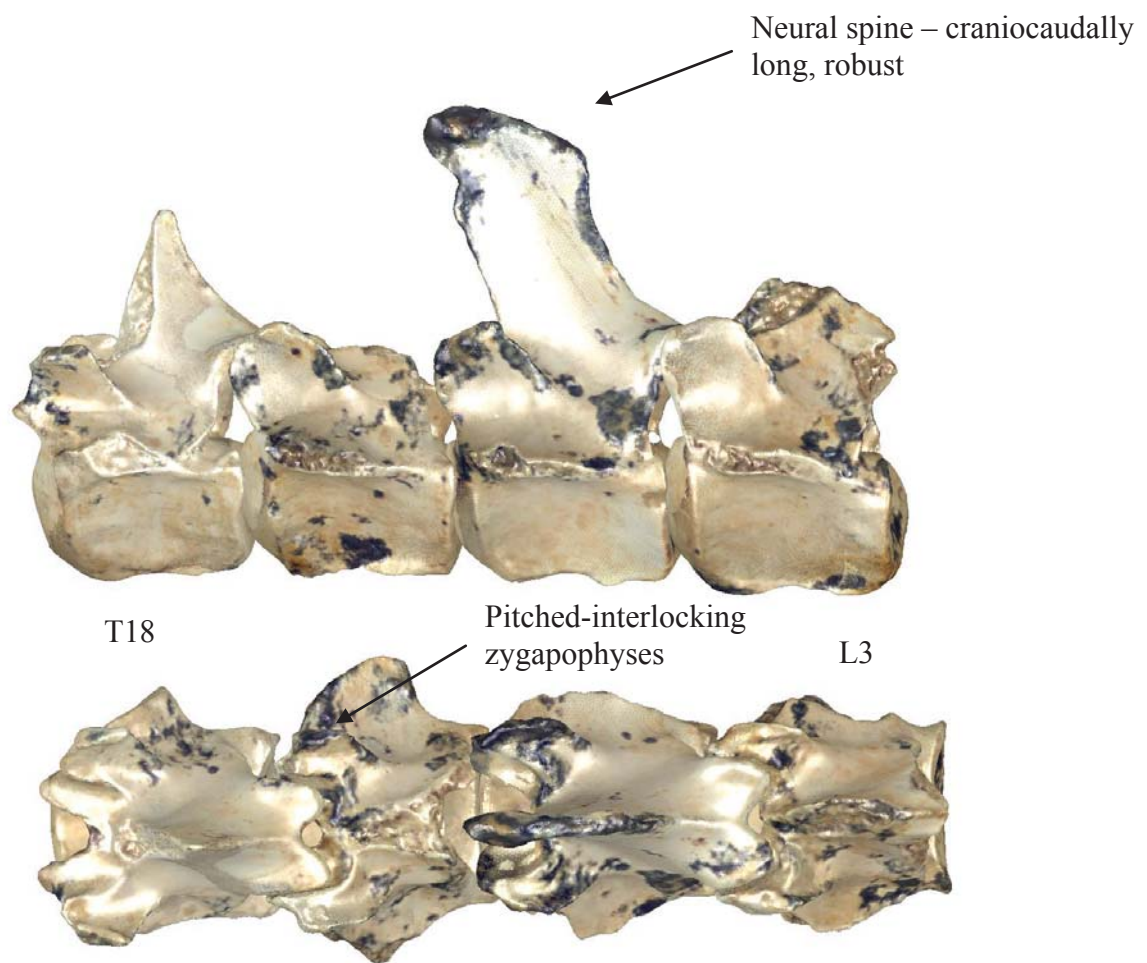
Figure 7.2.18 **Nannippus minor *UF 69933*.**
Probably T18-L3. Lateral and dorsal view. T18 length: 28.5mm.

Post-zygapophysis   Pre-zygapophysis
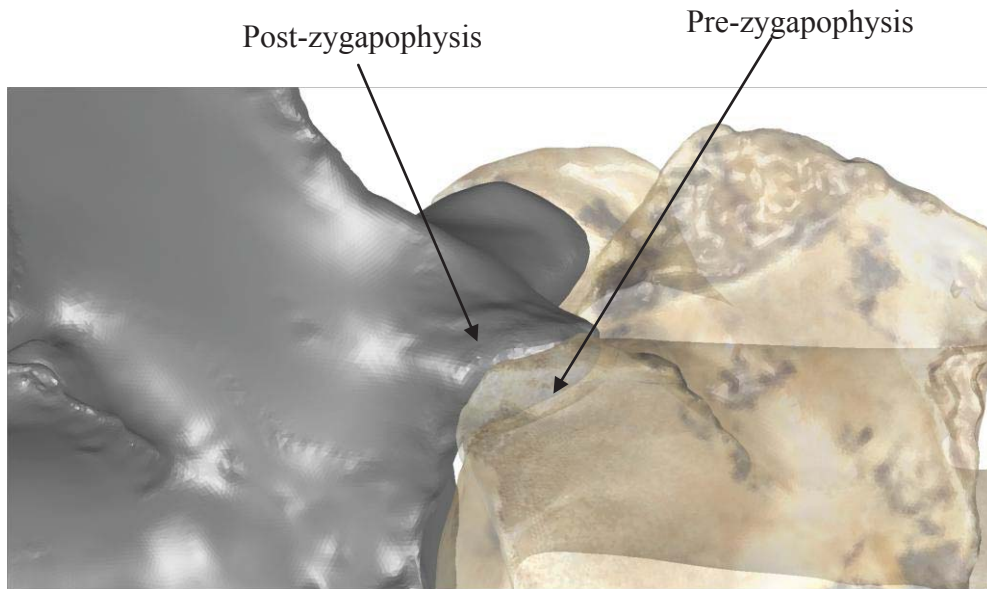
Figure 7.2.19 L3-L4 joint of* Nannippus minor *UF 69933.

L3 is in gray and L4 is partially transparent. Note the pitched-interlocking zygapophyses. Dorsolateral view.

Figure 7.2.20* Nannippus minor *lumbars.

Left: last lumbar, caudal view, UF 224208, width: 25.3mm; Right: proximal lumbar, lateral view, UF 224215, length: 30.2mm.

Pliohippus pernix

      Pliohippus pernix (subfamily Equinae, tribe Equini), from the Miocene, is a

close relative of modern *Equus*, weighing 155-182kg (MacFadden, 1986; Alberdi et al., 1995). The morphology of this species is characterized by AMNH F:AM 60803 which has a complete lumbosacral region, though some of the processes are partially reconstructed (Figure 7.2.21). It is from the June Quarry, Nebraska, and is middle Miocene in age. This specimen is unusual as it has a developmental asymmetry. L6 is sacralized on the right side so that the last lumbar is fused into the sacrum unilaterally.

Craniocaudal patterns in scaled centrum dimensions are shown in Figure 7.2.22. The pattern for *Pliohippus pernix* is similar to that of *Equus caballus*. There is a gradual dorsoventral compression and widening of the centra that took place over the last three lumbars, but little elongation of the vertebrae in the mid-lumbar region. The neural spines are original on all lumbars except L3. The anterior lumbars had robust, craniocaudally elongate neural spines with a well-developed dorsal ridge similar to that seen in *Nannippus*. However, the more distal neural spines were slightly more gracile than those of *Equus caballus*. The transverse processes are almost entirely reconstructed, with the exception of around the lateral joints, therefore I cannot comment on their morphology. Judging by the angle of their bases, they would have likely been quite horizontal. The ventral keel was moderately well developed in the anterior lumbar region, but less so than in *Equus*.

Lumbar joints in this species had pitched-interlocking zygapophyses. At the lumbosacral joint, strongly divergent neural spines suggest sagittal mobility, as do the more sagittally oriented zygapophyses, which are not tightly interlocking. There are lateral joints on the last two or three presacral joints, depending on whether the sacralized lumbar is considered as L6 or S1. The vertebral morphology of *Pliohippus* is

238

generally very similar to that of *Equus caballus*, though slightly more gracile.
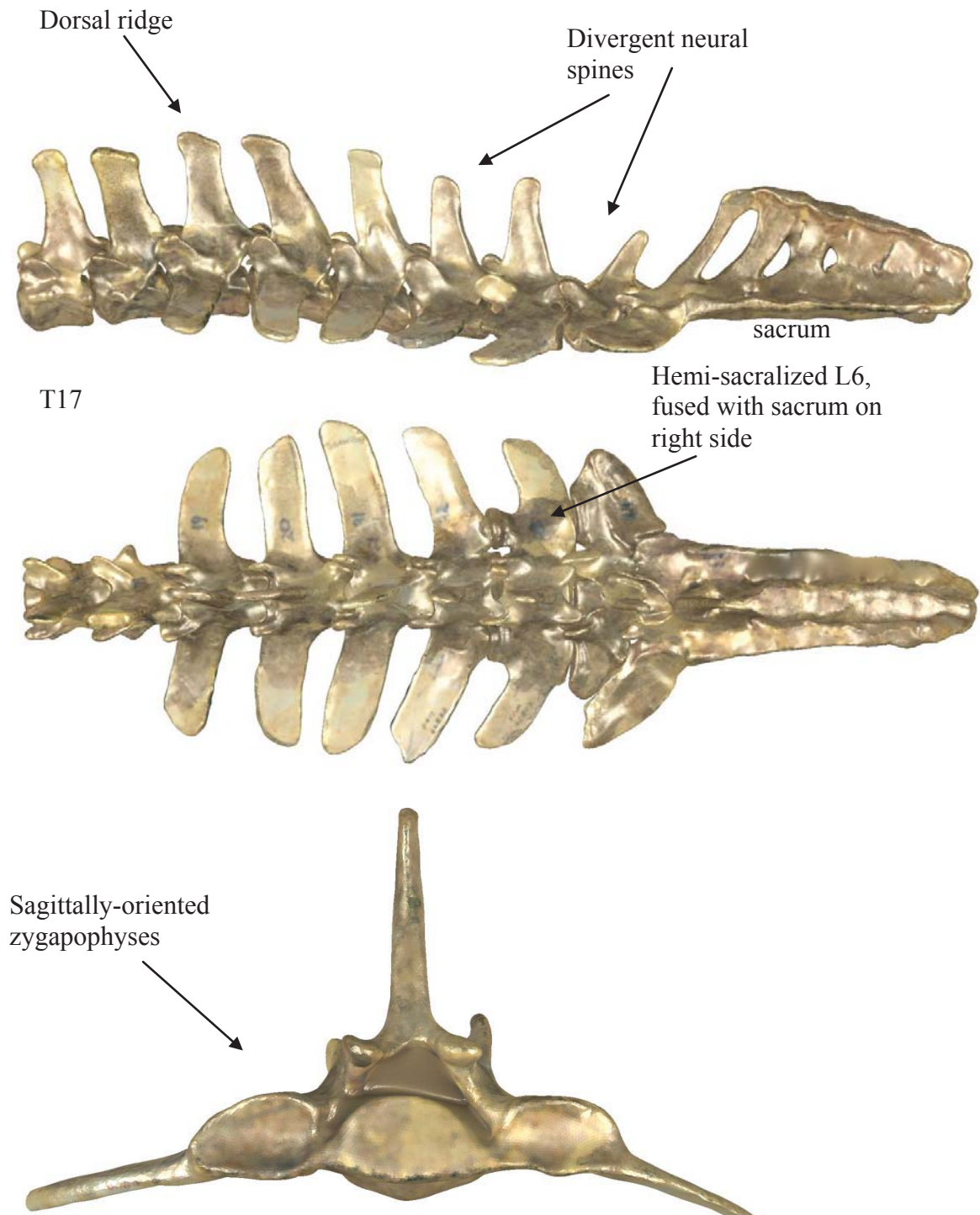
Figure 7.2.21 Pliohippus pernix *AMNH F:AM 60803.*
T17-S5. Partially sacralized last lumbar. T17 length: 34.5mm.
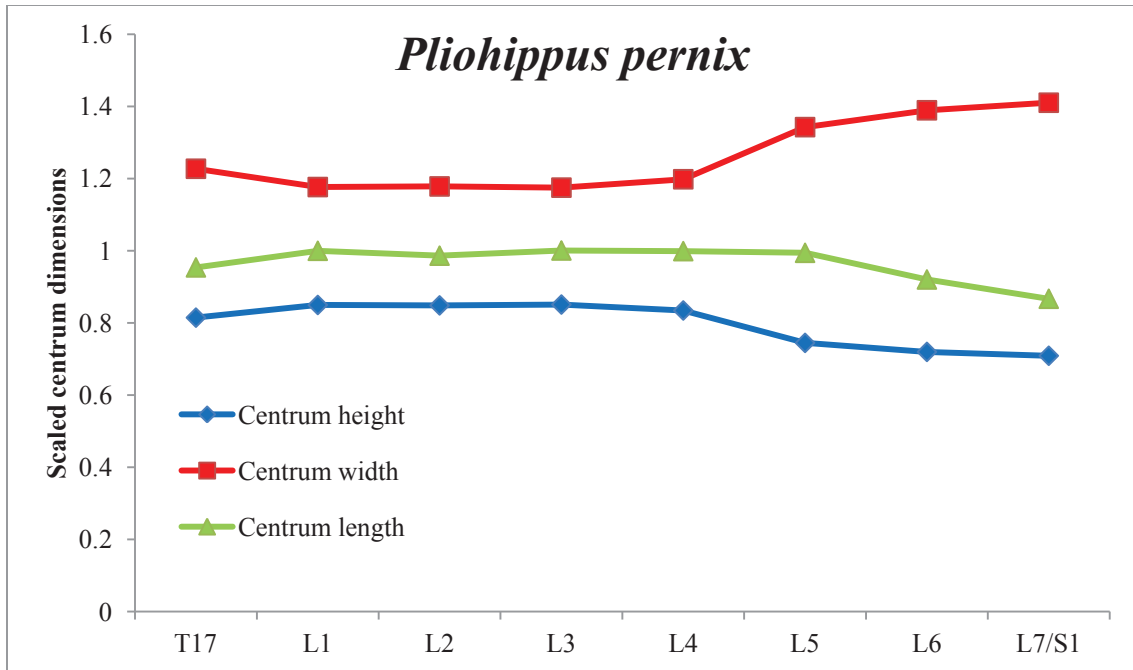
Figure 7.2.22 Craniocaudal variation in centrum dimensions of* Pliohippus pernix*,
AMNH F:AM 60803.

Centrum width and centrum height were scaled by the endplate area (width multiplied by
height) of the same vertebra. Centrum length was scaled by the length of the first lumbar
vertebra. Data can be found in Appendix 9.

7.2.3   SHAPE OF THE JOINT COMPLEX (CENTRUM AND ZYGAPOPHYSES)

PCA of equids and bovids

Principal components analysis was used to quantitatively compare joint shape in
modern and fossil equids with that of bovids, an extant artiodactyl family spanning a
similar size range. PC scores from this analysis can be found in Appendix 7. PC1 and
PC2, based on species-position mean joint shapes, are shown in Figure 7.2.23, with
extreme joint shapes figured as wireframes on the axes. Beneath the graph is a picture
of a *Pliohippus* lumbar vertebra with the joint complex curves marked in red to
illustrate the origin of the landmarks. The variance explained by each component is

documented in Table 7.2.2. Specimens were rescaled prior to analysis using generalized Procrustes analysis (GPA).

PC1 explains 76% of the variation in joint shape. PC1 reflects variation from a dorsoventrally compressed joint complex (centrum and zygapophyses) to a dorsoventrally tall joint complex. This type of variation is associated with decreasing sagittal mobility. Specifically, negative scores represent a dorsoventrally compressed, mediolaterally wide endplate. Zygapophyses are widely-spaced and have a ventral position, relatively near to the centrum. These features suggest relatively higher stiffness of the joint in the mediolateral plane, and relatively lower stiffness of the joint in the dorsoventral plane. Positive PC1 scores represent a dorsoventrally tall, heart-shaped endplate, with narrowly-spaced, dorsally-positioned zygapophyses. This type of joint complex suggests relatively lower stiffness in the mediolateral plane, but higher stiffness in the dorsoventral plane. PC2 reflects only 7% of variation and represents variation in zygapophyseal morphology. Negative scores represent larger, revolute zygapophyses, whereas positive scores represent a larger endplate and a J-shaped zygapophysis with a ventral facet, typical of the perissodactyl-type pitched interlocking zygapophyses.

PC1 highlights craniocaudal variation, whereas PC2 mostly separates equids and bovids. The last lumbar vertebra of both equids and bovids is distinguished from the other positions mostly by lower PC1 scores, reflecting its dorsoventrally compressed centrum. This suggests that there are similarities in the craniocaudal patterns in the two groups. Within the proximal and middle positions, the smaller taxa of both equids and bovids tend to have lower PC1 scores, as will be explained in more

241

detail in the next section. The proximal and middle joints of equids and bovids are distinguished from one another on PC2, with bovids generally displaying a lower score than equids.
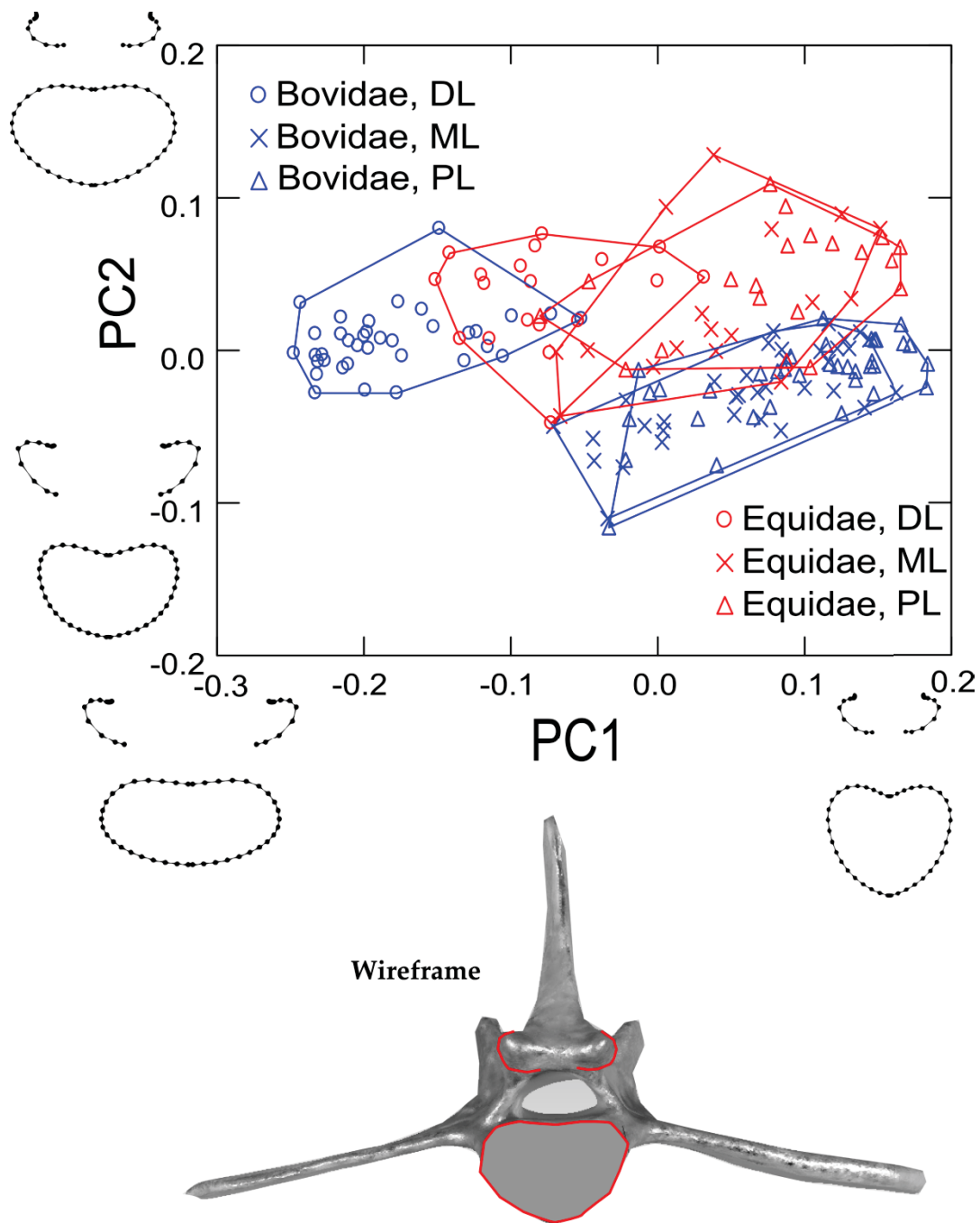
Figure 7.2.23 PCA of species-position mean joint shape for equids and bovids.
PL, proximal lumbar; ML, mid-lumbar; DL, distal lumbar. Wireframes represent shape at the extreme of each axis and show the endplate and zygapophyses in caudal view, as illustrated in red on a lumbar of Pliohippus pernix. *Note that PC1 separates distal lumbars from more proximal ones, whereas PC2 distinguishes proximal and mid-lumbars of equids and bovids.*

Table 7.2.2 Eigenvalues from the PCA of equids and bovids.

PC	Eigenvalues	% Variance	Cumulative %
1	0.016899	75.87	75.87
2	0.00164	7.36	83.23
3	0.001356	6.09	89.32
4	0.00064	2.87	92.19
5	0.000634	2.85	95.04

MANCOVA

Results of a MANCOVA of joint shape (PC scores) on family, vertebral position and vertebral size (represented by centroid size from Procrustes fit, see Methods) are shown in Table 7.2.3. A scatter plot showing the relationship of PC1 with centroid size is shown in Figure 7.2.24, with shape variation on PC1 illustrated on the Y axis. There were significant effects of all factors and interactions in a multivariate Pillai's Trace test. In terms of the univariate effects on specific PCs, size has a significant effect on the first three PCs. There were positive correlations on PC1 and PC2 and a negative correlation with PC3. This suggests that larger animals have dorsoventrally taller centra and more narrowly-spaced zygapophyses (see Figure 7.2.24). The significant differences in allometric slope among the positions (indicated by a significant interaction of position and slope) prevented the model from being able to detect differences in elevation between vertebral positions on PC1. However, examination of the graph (Figure 7.2.24), and a Tukey's HSD post-hoc test showed that distal lumbars tend to have a lower PC1 score than proximal or middle lumbars ($p<0.001$). Figure 7.2.24 demonstrates that while all vertebrae scale positively with size on PC1, proximal and middle lumbars tend to scale more strongly than last lumbars, suggesting they are more strongly influenced by size on this axis. This reflects the

significant interaction of size and position in the MANCOVA. The significant

interactions between family and position on PC1 indicate a stronger craniocaudal shape

contrast between the last and more proximal lumbars in the bovids than in equids.

While proximal and middle lumbars of bovids and equids have comparable joint

complex shape in the PCA, bovid last lumbars are more strongly dorsoventrally

compressed than equid last lumbars.

Individual lumbar positions are examined in Figure 7.2.25, Figure 7.2.26 and

Figure 7.2.27, with shape variation illustrated on the Y axis. At the most proximal

position, equids scale more steeply than bovids such that large bovids and equids have

similar PC1 scores for their size, but some small, fossil equids have relatively lower

scores. *Hyracotherium* and *Mesohippus* have particularly low scores indicating that

they have a very dorsoventrally compressed joint complex for this vertebral position. At

the middle lumbar position equids scale more steeply than bovids again, but there is

more overlap between the groups. Though *Hyracotherium* and some *Mesohippus* have

relatively low scores, they overlap with small bovids. Thus for the more anterior lumbar

positions, hyracotheres and primitive anchitheres have joint complex morphology that

indicates relatively low sagittal stiffness compared to extant bovids of a similar size.

At the last lumbar joint a different pattern is seen. Bovids have lower PC1

scores than equids at all sizes. There is more variation in equids in this joint, and the

relationship with size is weaker. These results suggest that bovids have more

dorsoventrally compressed, mediolaterally wider joint complexes than equids.

However, bear in mind that this analysis only takes into account the zygapophyses and

centrum, when most equids have an additional pair of lateral joints here, which are not

considered.

Table 7.2.3 MANCOVA on PC scores from 2D landmarks on equids and bovids.

Factor	Level	PC1	PC2	PC3	PC4	PC5	F-ratio (Pillai's)	P-value (Pillai's)
Log CS		**0.234**	**0.104**	**-0.060**	0.010	0.007	68.191	<0.001
Position	DL	0.001	**0.100**	**-0.059**	0.059	-0.031	3.788	<0.001
Position	ML	0.000	**-0.093**	**-0.003**	-0.021	0.028	-	-
Family	Bovidae	0.017	**0.062**	-0.025	-0.032	**-0.109**	8.134	<0.001
Position * CS	DL	**-0.066**	**-0.044**	**0.026**	**-0.033**	0.017	4.967	<0.001
Position * CS	ML	**0.023**	**0.039**	**0.005**	**0.012**	-0.014	-	-
Family * CS	Bovidae	-0.015	**-0.043**	-0.001	0.018	**0.052**	10.637	<0.001
Position * Family	DL * Bovidae	**-0.045**	**0.010**	-0.001	**0.011**	-0.005	11.927	<0.001
Position * Family	ML * Bovidae	**0.023**	**-0.003**	0.002	**0.000**	0.002	-	-

Bold values indicate significance at the p=0.05 level. CS, centroid size; Pos, position; fam, family. Pillai's trace is the multivariate test statistic. Univariate values quoted are the model coefficients, beta, which are estimates of the effect of each factor. DL, distal lumbar; ML, middle lumbar.
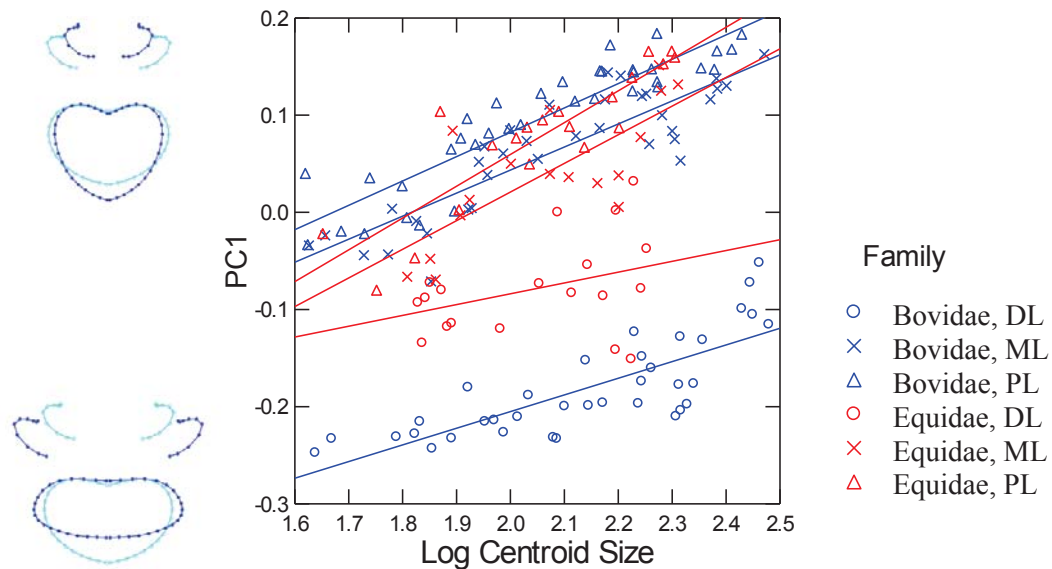
Figure 7.2.24 PC1 against log centroid size (proxy for vertebral size) for equids and bovids.

PL, proximal lumbar; ML, mid-lumbar; DL, distal lumbar. Shape variation on PC1 illustrated on Y axis. In models at left, dark blue denotes shape extremes, light blue signifies mean shape. PC1 is positively correlated with size, but slopes are steeper at more proximal positions.
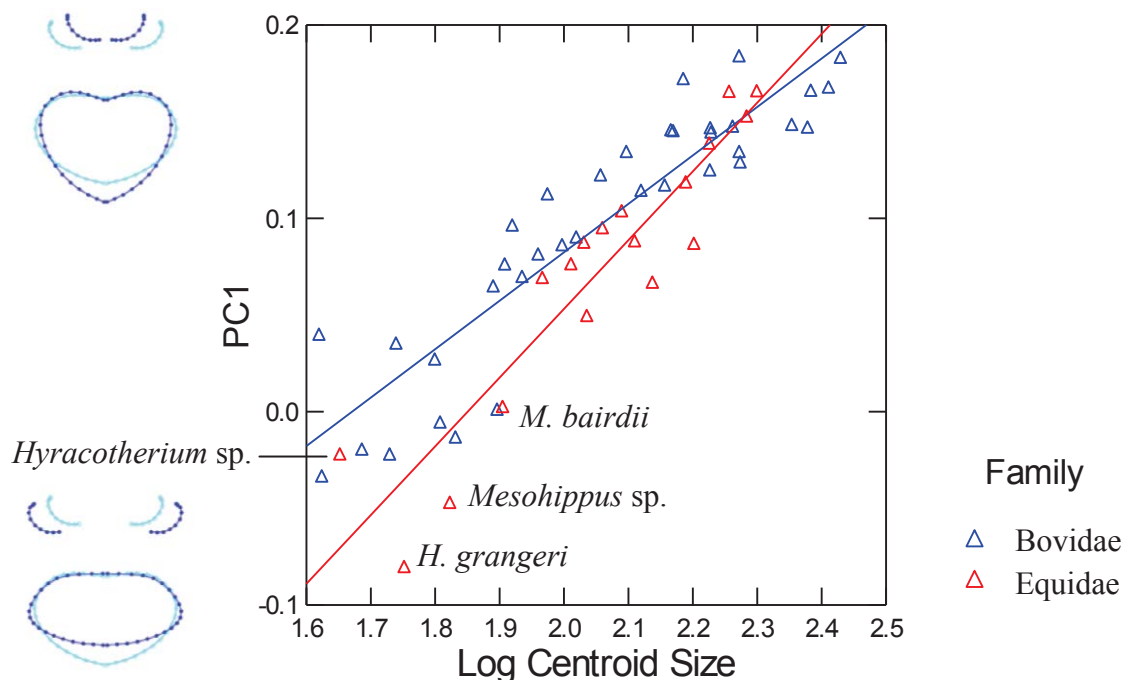
Figure 7.2.25 PC1 against centroid size for proximal lumbars only.
Shape variation on PC1 illustrated on Y axis. Dark blue, shape extremes; light blue, mean shape. Small equids have lower scores than small bovids at the proximal lumbar
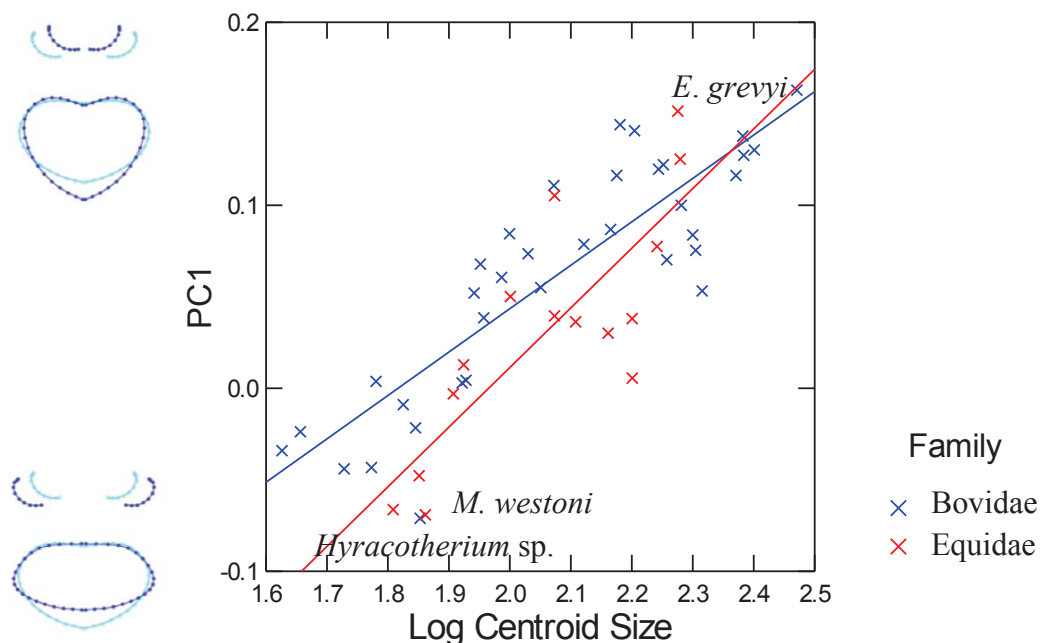
Figure 7.2.26 PC1 against centroid size for middle lumbars only.
Shape variation on PC1 illustrated on Y axis. Dark blue, shape extremes; light blue, mean shape. Small equids have lower scores than small bovids at the middle lumbar.
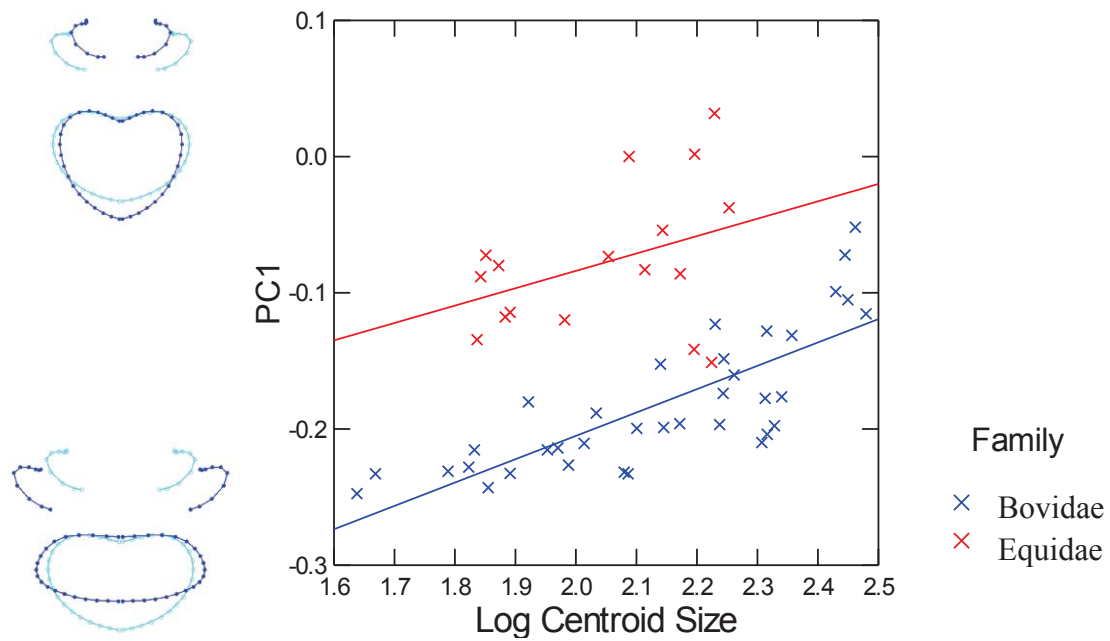
Figure 7.2.27 PC1 against centroid size for distal lumbars only.
Shape variation on PC1 illustrated on Y axis. Dark blue, shape extremes; light blue,
mean shape. Bovids have a lower score than equids at all sizes.

Genus-level comparison of fossil equids

        Craniocaudal variation in joint complex shape among genera of fossil equids is

shown in Figure 7.2.28. PC1 here is from an equid-only analysis of joint shape and

accounts for 69.8% of variation, though the types of morphological variation were

extremely similar between the two analyses. Craniocaudal patterns vary among the

subfamilies. *Hyracotherium* has a lower score for the last lumbar than for the proximal

lumbars, but generally low scores throughout the lumbar region. This suggests that all the

lumbars have relatively dorsoventrally compressed joint complexes, and therefore likely

lower sagittal stiffness. Within the anchitheres, PC1 scores for the proximal vertebrae

gradually increase, resulting in increased craniocaudal disparity. This suggests that the

proximal and middle lumbars are becoming taller. This trend continues into the Equinae.

Here there is a clear distinction between the last lumbar and the others, reflecting sagittal

mobility at the lumbosacral joint versus stability more anteriorly. To test for allometry and craniocaudal morphology patterns, a MANCOVA was run on the top five PCs (accounting for more than 95% of variation). There were significant effects of size, position and interactions (

Table 7.2.4). Specifically, PC1 is positively correlated with size, indicating that joint complexes become taller with increasing size. The last lumbar joints scale less strongly than other vertebral positions, suggesting that they remain more constant with increasing size.

Table 7.2.4 MANCOVA on PC scores from 2D landmarks on equids.

Factor	Level	PC1	PC2	PC3	PC4	PC5	F-ratio (Pillai's)	P-value (Pillai's)
Log CS		**0.244**	**0.152**	**-0.059**	-0.011	**-0.042**	26.100	<0.001
Position	DL	0.184	**0.079**	-0.059	0.092	**-0.139**	2.974	0.003
Position	ML	-0.079	**-0.167**	-0.009	-0.018	**0.089**	-	-
Position * CS	DL	**-0.133**	-0.038	0.026	-0.054	**0.072**	3.662	<0.001
Position * CS	ML	**0.050**	0.076	0.006	0.010	**-0.045**	-	-

Bold values indicate significance at the p=0.05 level. CS, centroid size; Pos, position; fam, family. Pillai's trace is the multivariate test statistic. Univariate values quoted are the model coefficients (beta) which are estimates of the effect of each factor.
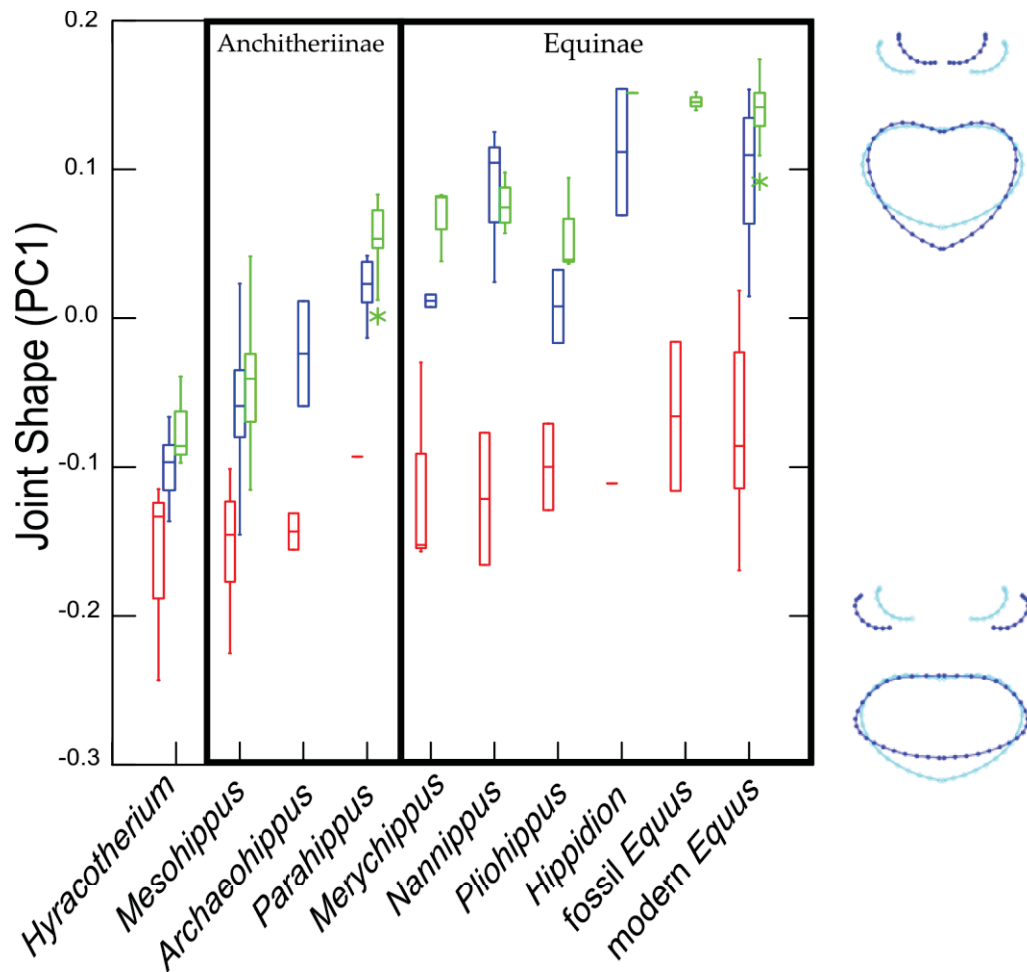
Figure 7.2.28 Equid-only PC1 scores by genus and position.
Green, proximal lumbar; blue, middle lumbar; red, last lumbar. Shape variation on PC1 illustrated on Y axis. Dark blue, shape extremes; light blue, mean shape. Box indicates inter-quartile range, whiskers indicate range, dashes are single points.

7.2.4 LATERAL TRANSVERSE JOINTS

Lateral transverse process joints are found in extant horses, tapirs and rhinos. However, *Hyracotherium* did not have transverse joints. The earliest definite lateral joints observed in this study were in the anchithere *Mesohippus bairdii*.

Table 7.2.5 shows the mean transverse process joint shape (joint height/joint width) for each species, for both last and penultimate joints. Data for each specimen examined can

be found in Appendix 8. Last lumbar joints vary from 0.46 to 0.5, indicating that they are

approximately twice as wide as they are tall. Penultimate joints vary from totally round 1

to 0.60 in *Equus*, but are always rounder than the last joint. There was no shape trend

within fossil horses through time, and intraspecific variation in this feature was quite

high. In *Equus caballus* the lateral joints are fused in the penultimate joint in 60% of

cases (Townsend and Leach, 1984). However, no unequivocal cases of lateral joint fusion

were found in my fossil sample. One possible case is in the *Mesohippus bairdii* specimen,

YPM 11376. However, it was unclear whether the two vertebrae were held together by

matrix or by fusion of the joints. In addition, of the modern equid specimens examined,

only specimens of *Equus caballus* had fused joints, specifically the largest specimens,

suggesting it may relate only to domesticated horses.

Table 7.2.5 Variation in the shape of the lateral transverse joints

Genus	species	LL shape	PL shape	N
Equus	*burchellii*	0.48	0.60	4
Equus	*caballus*	0.58	0.88	3
Equus	*grevyi*	0.46	0.69	3
Hippidion	*neogaeus*	0.54		1
Pliohippus	*pernix*		0.62	1
Nannippus	*minor*	0.58	1.06	2
Merychippus spp.		0.52	0.72	3
Parahippus	*leonensis*	0.51	0.67	5
Archaeohippus	*blackbergii*	0.42	1.02	3
Mesohippus	*bairdii*	0.57	0.86	9

Shape = height/width. LL, last lumbar; PL, penultimate lumbar.

7.2.5   SPINOUS AND TRANSVERSE PROCESSES

The processes are the least-well preserved portion of the vertebra, and are

frequently missing or distorted. Therefore, the sampling of processes is considerably

less than for the joints. Neural spine and transverse process angle for each specimen can be found in Appendix 8. Box plots showing the orientation of the muscular processes in each genus (pooled across all vertebral positions) are presented in Figure 7.2.29. Muscular processes became more perpendicularly oriented through equid evolution (closer to 90º). The neural spines were generally quite inclined in hyracothere and anchithere equids, but became increasingly vertical in the equines. Similarly, the anteroposterior transverse process angle approached 90º only in the equines. The dorsoventral angle of the transverse process was greatest in *Hyracotherium*, then somewhat reduced in anchitheres, and then further reduced only in the Equini. Length of the transverse processes was also greater in equines than in more primitive equids.
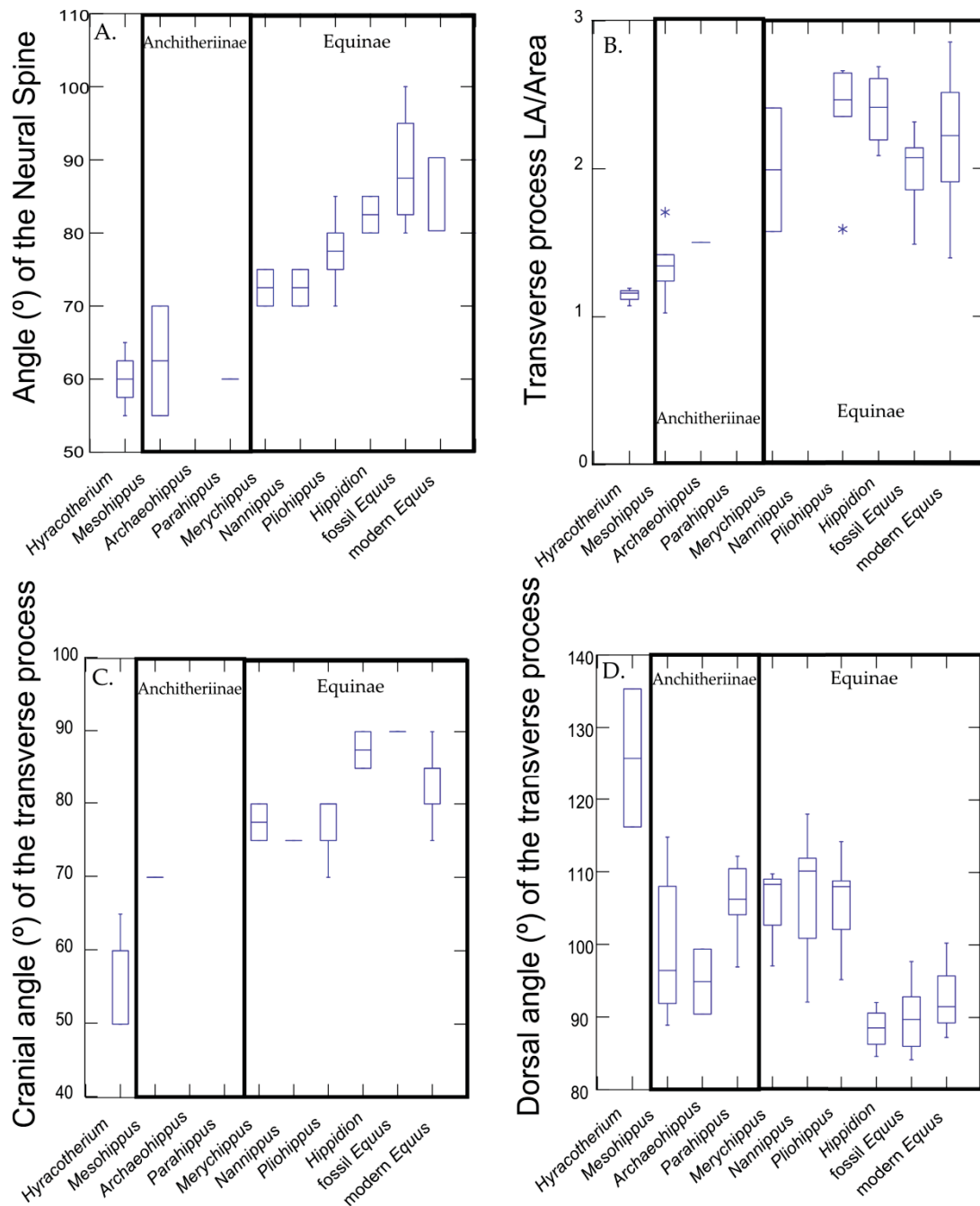
Figure 7.2.29 Variation in length and angle of the transverse processes and neural spine by genus.

All positions are pooled due to rarity of preservation of these features. A. Angle of the neural spine from caudal to cranial in the sagittal plane. B. Transverse process lever arm (LA) scaled by endplate area. C. Angle of the transverse process in the craniocaudal plane, measured from caudal. D. Angle of the transverse process in the dorsoventral plane, measured from dorsal. Box, interquartile range; whiskers, range; dash, individual point; star, outlier.

7.3 DISCUSSION

7.3.1 EQUID LUMBAR EVOLUTION

The ancestral thoracolumbar vertebral count for mammals is 19 vertebrae (Narita and Kuratani, 2005). However, perissodactyls are unusual in having an elevated thoracolumbar count of 22-24 vertebrae (Narita and Kuratani, 2005). *Equus caballus* has 18-19 thoracics and 5-6 lumbars, making a total count of 23-25 vertebrae. The primitive equid *Hyracotherium grangeri* had 24 thoracolumbar vertebrae, displaying an elevated count relative to *Phenacodus* which had 21 vertebrae. The thoracolumbar region of *Hyracotherium* constituted 17 thoracics and 7 lumbars, meaning it had a slightly longer lumbar region than *Equus*. Further, the diaphragmatic vertebra in *Equus* is located coincident with, or one to two vertebrae cranial to, the thoracolumbar transition, resulting in a very short transitional region. In contrast, the diaphragmatic vertebra of *Hyracotherium grangeri* was positioned four vertebrae cranial to the first lumbar, resulting in a relatively long transitional region. This equates to a post-diaphragmatic region that was 10 vertebrae long. This relatively long post-diaphragmatic region suggests that *Hyracotherium* had relatively more lumbar mobility than *Equus* because sagittal mobility is typically facilitated by post-diaphragmatic joints and is correlated with cranial diaphragmatic placement in other mammalian groups (Williams, 2012a). This also supports findings from previous chapters which suggest that the post-diaphragmatic region tends to decrease in length with increasing size in running mammals.

Length of the post-diaphragmatic region depends not only on vertebral count but on the length of individual vertebrae. In highly dorsomobile species, such as

carnivores, there tends to be a gradient of increasing craniocaudal length of the centra posteriorly, which reaches a peak in the mid-caudal lumbar region, then decreases again at the last lumbar. In contrast, when examining the craniocaudal profile of *Equus caballus* (Figure 7.2.2), length of the centra remain more constant along the series. In the lumbar region there is a slight increase in length, followed by a sharp decrease prior to the lumbosacral joint. This flatter profile is typical of large ungulates and dorsostable taxa (Slijper, 1946). *Hyracotherium grangeri* has relatively more elongation of the lumbar vertebrae than *Equus*. The mid-lumbar is around 1.6 times the length of the mid-thoracic (Figure 7.2.6), whereas it is only 1.2 times as long in *Equus caballus*. This further suggests elongation of the post-diaphragmatic region in early equids.

Cross-sectional dimensions of the centra also have distinctive craniocaudal patterns in equids. In *Equus caballus* there is a strong decrease in dorsoventral dimension and increase in mediolateral dimension in the posterior lumbar region up to the lumbosacral joint. The resulting lumbosacral joint is wide and compressed, and can facilitate sagittal bending but restrict lateroflexion. This pattern is also typical of artiodactyls such as bovids, which also have more mobility at the lumbosacral joint than in the relatively stiff lumbar region. *Hyracotherium grangeri* has a similar pattern, but to a lesser degree. This suggests there was reduced dorsoventral stiffness of the lumbosacral joint relative to the other lumbar joints, even in very primitive horses.
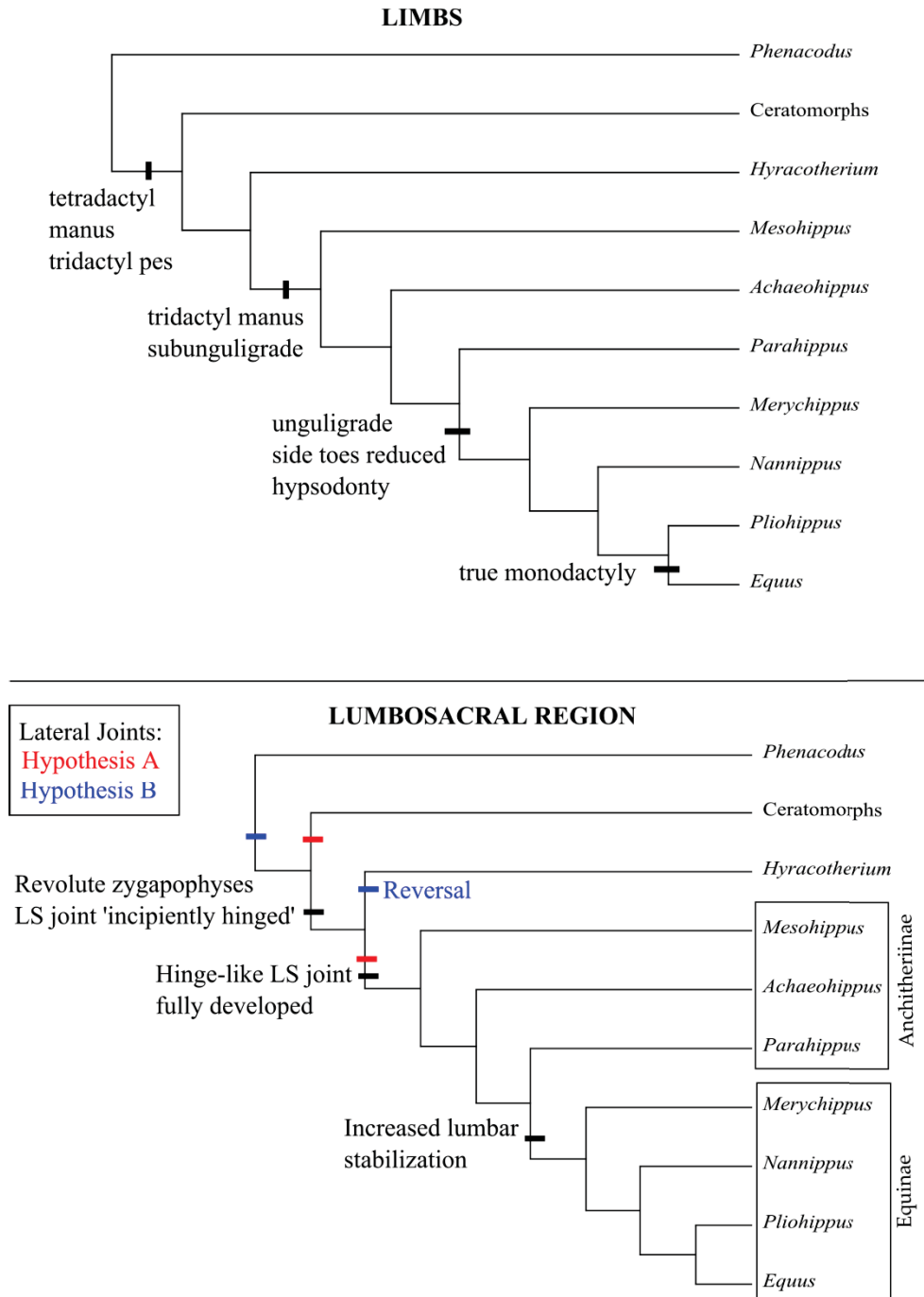
Figure 7.3.1 Summary of the evolution of limb and vertebral features in equids.
Two opposing hypotheses for the evolution of lateral joints are shown: A, they evolve at the red ticks, B, they evolve or are lost at the blue ticks. Limb features taken from literature (Sondaar, 1968; Thomason, 1986; MacFadden, 1992; Stromberg, 2006). LS, lumbosacral.

In addition to a dorsoventrally compressed centrum, the hinge-like lumbosacral joint of *Equus* is supported against lateroflexion and torsion by lateral joints. These joints form on the last two (100%) to three (88%) presacral joints in *Equus caballus,* and are fused in 59% and 23% of cases respectively (Townsend and Leach, 1984). Lateral joints were not present in *Hyracotherium grangeri*. There were well-developed lateral joints in *Mesohippus* and all subsequent equids, of a similar morphology to that of *Equus.* However, it is unclear exactly when this morphology evolved as appropriate material was not available for taxa intermediate between *Hyracotherium* and *Mesohippus,* such as *Orohippus.* The interpretation of the evolution of these joints is further complicated by the fact that they are also present in both living rhinos and tapirs (Figure 7.3.2). They are somewhat different from those of *Equus* because they are rounder in shape, less mediolaterally wide, and have a relatively flat surface that is not concavo-convex dorsoventrally. This morphology suggests that these joints would restrict lateroflexion but are not specialized to permit flexion and extension, compared to those of *Equus*. Therefore, two hypotheses may be proposed for the evolution of lateral joints in perissodactyls (Figure 7.3.1). Hypothesis A suggests that these joints evolved twice in perissodactyls, once on the branch leading to *Mesohippus* and independently on the branch leading to ceratomorphs. The alternative hypothesis (B) is that the lateral transverse joints are primitive for perissodactyls but were secondarily lost in *Hyracotherium,* perhaps related to its small size.

Figure 7.3.2 Last lumbar vertebra in caudal view of a rhino (left, Rhinoceros, USNM 336953) and tapir (right, Tapirus, USNM 155410).
Showing lateral joints, which are rounder and flatter than those of Equus.

Several other fossils have bearing on the question of the evolution of lateral

joints. First, there is no evidence of these joints in either *Phenacodus* confirming that

they are likely restricted to within Perissodactyla. Second, the rhino *Hyrachyus eximius*

(AMNH 11652); and tapiromorphs *Colodon sp.* (AMNH 1197) and *Isectolophus*

latidens (AMNH 12222) all have lateral joints (Holbrook, pers. comm.), as does

Heptodon (Radinsky, 1965), the oldest ceratomorph. However, these joints are lacking

in *Lambdotherium* (UW 1883). This suggests that many early tapiromorphs have this

joint and indicates that it may be primitive for ceratomorphs. Information from

primitive perissodactyls such as *Homogalax* would be useful in this regard.

In *Equus caballus,* lateral joints help to stabilize the posterior lumbar region

against lateroflexion. Lateroflexion and torsion moments are generated in the axial

skeleton near the girdles due to the action of muscles that retract and protract the limb

(Schilling and Carrier, 2010). Specifically, at the hind limb, lateroflexion forces on the

pelvis may be generated by protractors ipsilateral to, and retractors contralateral to, the

supporting limb. In the dog these forces are resisted using unilateral contraction of

longissimus and multifidus (Schilling and Carrier, 2010). These forces may be greater in the horse due to a well-developed expansion of the middle gluteal, known as the gluteal tongue, which originates from the thoracolumbar fascia as far cranial as L1 (Jeffcott and Dalin, 1980; Ritruechai, 2009). Therefore, the lateral transverse joints likely evolved to stabilize the posterior lumbar region against these lateroflexion moments produced by hind limb movements. It seems likely that the evolution of lateral joints in *Mesohippus* relates to increasing lateral and torsional forces in the posterior lumbar region, potentially related to the expansion of the gluteal tongue and more generally expansion of the hindlimb musculature for running. The absence of lateral joints in *Hyracotherium* could relate to a reduction in the lateral and torsional forces generated by hind limb muscles in this very small equid. Cases of extreme lateroflexion or torsional forces may lead to fusion. Fusion of lateral joints has only been definitively recorded in *Equus caballus.* Of those examined in this study, the two largest specimens had fused joints, suggesting size or ontogeny may be a factor, though samples were too small to test this idea. Fusion of the lateral joints may be a response to extremely high *in vivo* lateroflexion or torsion forces generated in very large individuals. There was no evidence of fusion of lateral joints in the smaller-bodied fossil equids examined here.

Torsion in the lumbar region is also effectively resisted by the zygapophyses. In *Phenacodus* and many other mammal species the post-diaphragmatic zygapophyses have a flat to convex transverse profile. In contrast, *Equus caballus* has unusual zygapophyses which tightly interlock with both a lateral and ventral surface, and are slightly pitched caudally. While the lateral surface restricts torsion, the pitched ventral

surface comes into contact to resist dorsiflexion. Interestingly, the zygapophyseal morphology of fossil equids is quite different from that of *Equus.* In *Hyracotherium grangeri,* the transitional and anterior lumbar vertebrae have the convex type of zygapophysis. However, the posterior lumbar zygapophyses are revolute, with an additional facet forming on the dorsal portion of the post-zygapophysis. This morphology strongly resists torsion by preventing dorsal shear, and is shared convergently with many other mammal groups including artiodactyls, pangolins, mesonychids, creodonts and arctocyonids (Wortman, 1894; Slijper, 1946; Zhou et al., 1992; Argot, 2012). It tends to be associated with dorsostable ungulates and taxa with large heads, which may generate increased axial torsion (Howell, 1944). This morphology therefore suggests that torsional forces were higher in the posterior portion of the lumbar column of *Hyracotherium,* again implicating increased development of hind limb retractors and protractors in generating these forces.

7.3.2 CURSORIALITY, BODY SIZE AND VERTEBRAL EVOLUTION

The lumbosacral region in *Equus caballus* is highly specialized for dorsostable running. The specialization of the appendicular skeleton for cursoriality through equid evolution has been well documented (Simpson, 1951; Sondaar, 1968; Hussain, 1975; Thomason, 1986; Hermanson and MacFadden, 1996). Data presented here have shown that the axial skeleton was also undergoing functional shifts through the evolution of the group. The incipiently hinge-like lumbosacral joint was an early adaptation to cursoriality in equids, and arose in concert with stabilization of the posterior lumbar region against axial torsion, likely reflecting expansion of hind limb muscles associated with powerful extension there. Extreme stabilization against sagittal flexion in the

lumbar region likely evolved later in the Equinae.

What influence did increasing size have on lumbosacral evolution? As body size increases, the stresses on the axial skeleton associated with locomotion will necessarily increase (McMahon, 1975b; Biewener, 1983; Steudel and Beattie, 1993; Bertram and Gutmann, 2009). Therefore specializations that resist stresses and reduce the energetic cost of running will be selected for at large size. Data presented in this chapter have provided support for a link between stabilization of the lumbar region in equids and increasing size. In particular, joint complexes become taller, neural and transverse processes become less inclined and more robust, and zygapophysis morphology changes. Thus morphological adaptations associated with dorsostable running seem to correlate with size. These may represent size-dependent cursorial specializations, which evolved because running at large body size requires stronger adaptation than running at small sizes (Steudel and Beattie, 1993).

A more flexible lumbar region in small-bodied fossil equids may indicate they could have used a wider range of gaits. *Equus caballus* is restricted to the transverse gallop and uses only hind limb-initiated transitions in center of mass motions (Bertram and Gutmann, 2009). This gait has no extended flight phase and involves limited sagittal motion of the lumbar region. In contrast, small equids such as *Hyracotherium,* with greater sagittal mobility, may have been able to employ extended flight phases, and rotary gallops using forelimb-initiated transitions in center of mass motions. Many mammals use a speed-dependent gait, in which the transverse gallop is preferred at slower speeds but the rotary gallop is used at higher speeds, e.g., small artiodactyls (Bertram and Gutmann, 2009; Biancardi and Minetti, 2013). Further, the specialization

of the lumbosacral joint to permit flexion-extension but restrict lateroflexion suggests there was strong development of muscles around the hip and sacrum in primitive equids. This supports data from the hind limb of *Hyracotherium,* which indicate it was relatively specialized for antero-posterior motion, with a strong semitendinosus muscle for extending the habitually flexed hip (Hussain, 1975). Therefore the incipiently hinge-like lumbosacral joint constitutes an early adaptation of equids to cursoriality, predating unguligrady or extreme digit loss.

CHAPTER 8: DISCUSSION

This dissertation investigated structural allometry of the thoracolumbar region in running mammals using one-, two- and three-dimensional morphometric data from vertebrae. There was strong allometry in the length of the regions, shape of the centra, morphology of muscular processes and zygapophyses. These findings have implications both for static support of the trunk against body mass, and for function of the thoracolumbar region during locomotion.

8.1   STATIC SUPPORT OF THE VERTEBRAL COLUMN

The function of the thoracolumbar region is two-fold: to provide support for the trunk against gravity and to facilitate movement during locomotion (Thompson, 1917; Slijper, 1946; Hildebrand, 1995). The ventral column, consisting of centra and discs, provides the primary strength under axial compression and so is vital to body support (Denis, 1983). In Chapter 4, I measured the allometry of the ventral column in Felidae and Bovidae and compared it to predictions of geometric and elastic similarity. Results revealed that the ventral column becomes more robust with increasing body size and that allometric patterns are fairly consistent between the two groups despite differences in spinal mobility. In particular, with increasing size the post-diaphragmatic region becomes both shorter craniocaudally and dorsoventrally deeper, whereas the pre-diaphragmatic region enlarges only in the sagittal diameter. The mediolateral diameter tends to remain geometrically similar at all body sizes. These patterns suggest that as size increases the ventral column adapts not only to cope with increasing axial compression (cross-sectional area increase) but also to resist some bending in the sagittal plane (increased sagittal dimension). Further, it indicates that structural

modifications of the ventral column do play a role in coping with allometric stresses in the thoracolumbar region.

The role of structural allometry in the limbs is thought to depend upon size (Biewener, 2005). Data from a wide array of mammals suggest that structural changes only become important at larger sizes and that small mammals primarily adapt through postural changes (Bertram and Biewener, 1990; Biewener, 2000). The data presented here show no evidence of non-linearity of the scaling of the vertebral measures, and thus no indication of a size-related change in any skeletal coping mechanism. Further, bovids tend to have stronger limb allometry than felids, whereas in the axial skeleton allometric scaling was found in both families. Allometric scaling exponents frequently match those predicted under an elastic similarity model, particularly in lumbar length and height. This suggests that the lumbar region meets the predictions of the elastic similarity model better than the limbs typically do.

How does this fit the current concept of the role of the vertebral column in static support? Simple modeling of the trunk as a beam, with load distributed between the limbs, provides two key predictions about static loading of the thoracolumbar region (Figure 8.1.1) (Slijper, 1946; Macpherson and Ye, 1998; Smit, 2002). First, there should be a net ventroflexion moment in the anterior thoracic region caused by the reaction to the anterior support limb, which forms a peak over the ground reaction force. Second, there should be a net dorsiflexion moment in the mid-trunk caused by the tendency to sag between the support pillars, which reaches a maximum around 40-50% of the distance from the pelvis; i.e., at the cranial lumbar region. As the thoracolumbar region is mostly held in a constant posture, these respective bending

moments must be overcome by a combination of passive supports (bones and ligaments, including the ventral column) and active supports (muscles).

The suspension bridge model proposes that the ventroflexion moment from the forelimb is distributed along the thoracic region via suspension of the column from the scapula, using the trapezius and rhomboid muscles (Macpherson and Ye, 1998). This arrangement, combined with a strongly dorsoflexed posture in the upper thoracic region, distributes support of forelimb loads as axial compression in the vertebral bodies. At the mid-trunk two main mechanisms are proposed. First, ventral elements are subject to tension. The abdominal muscles and linea alba connect the sternum and ribs to the pelvis and have a strong lever arm for action on the lumbar spine. Contraction of these muscles or tension in ligaments such as linea alba or connective tissues could produce a ventroflexion moment which would counter sagging, in a similar manner to a strung bow (Slijper, 1946). Additionally, contraction of the hypaxial muscles may fulfill a similar function in the cat (Macpherson and Ye, 1998). Second, there must be compression in the dorsal elements, which is accommodated by the vertebral column (Smit, 2002). Axial compression is mostly facilitated by the ventral column, although there is evidence that the dorsal arch and joints can transmit significant loads, especially in certain postures (e.g., extreme extension in humans) (Shirazi-Adl and Drouin, 1987; Shirazi-Adl, 1994).
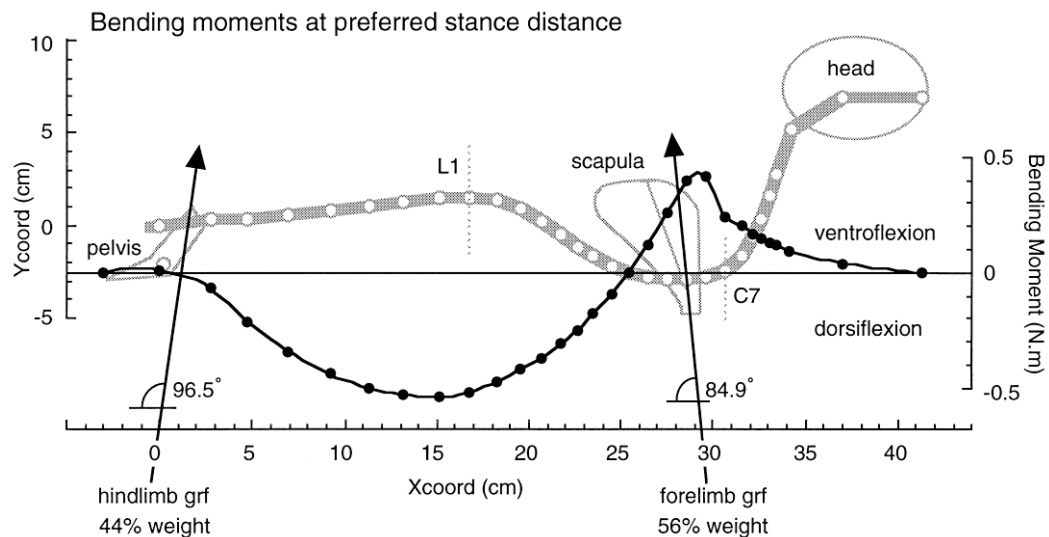
Figure 8.1.1 Static support of the vertebral column.
From Macpherson and Ye (1998); Fig 8. Figure depicts the hypothetical bending moments at each position along the vertebral column of a cat. White circles and grey line indicate the position of the intervertebral joints and centra (left Y axis). The dark circles and black line indicate the calculated bending moments (right Y axis), with positive values representing ventroflexion and negative values representing dorsiflexion. Arrows indicate the ground reaction force from the limbs. Note the strong sagging moment at the mid-trunk.

The results of Chapter 4 fit well with a model of the ventral column as the dorsal compression member in supporting static loads. The change in cross-sectional shape also suggests that there may be some sagittal bending moment or eccentric axial loading component in addition to pure axial compression. Estimated dorsiflexion moment from a static model far exceeds measured *ex vivo* bending strength of sheep lumbar joints (Wilke et al., 1997a; Smit, 2002). This suggests that the vertebral column plays a rather limited role in resisting sagittal bending, and that this moment must be resisted using soft tissue support. Similarly, human lumbar spines loaded vertically *ex*

vivo cannot resist the forces that have been recorded during life. However, if those same forces are applied as a 'follower load' (i.e., a load which follows the vertebral curvatures producing pure axial compression), the *in vivo* loading can be reproduced (Patwardhan et al., 1999). This suggests that one important role of the paraxial musculature may be to convert eccentric axial loads into pure axial loads, against which the ventral column is strongest. The sagging moments of a quadrupedal mammal may be resisted in a similar way. However, as size increases the ventral column becomes stiffer in the sagittal plane in these groups, suggesting some resistance to sagittal bending.

The above data agree with previously published allometric data on bovids, which also found elastic scaling in the lumbar region (Halpert et al., 1987). However, they expand upon the previous study by presenting data on the thoracic region, including felids (a group with contrasting locomotor function) and verifying the scaling relationships in a phylogenetically corrected analysis. These new data have shed light on contrasting allometric patterns between the thoracic and lumbar regions, which may relate to functional constraints on the thoracic region for respiration (see Chapter 4 for further discussion). Further, demonstrating allometric patterns in another group of mammals than bovids was important because bovid limb scaling is not typical of that of other mammal groups (Bertram and Biewener, 1990). However, felids showed similar patterns of shortening and deepening of the ventral column with size, suggesting generality of these patterns in running mammals.

Collecting further data on intervertebral disc morphology will test and augment the results presented here. A preliminary study of intervertebral spacing, using a small

number of radiographs, did not suggest that the discs scaled differently to the centra, but a more comprehensive study is required to test this finding. Region length calculated from centra alone provides only an approximation, but radiographs or cadaveric specimens could be used to directly measure this distance. Further, the composition of the intervertebral discs also affects their mechanical function. For example, the proportions of proteoglycans in the nucleus pulposus or the distribution of type 1 and type 2 collagen fibers in the annulus fibrosus can influence the flexibility of an intervertebral motion segment (Koob and Long, 2000). Data of this type are rare outside of *Homo sapiens* but could contribute to our understanding of how the ventral column deals with loadings associated with increasing size.

8.2   SAGITTAL BENDING DURING RUNNING

The second key function of the thoracolumbar region is to provide dynamic support and enable mobility during locomotion. Traditionally cursorial mammals have been divided into 'dorsostable' and 'dorsomobile' running modes based on their use of vertebral flexion during running. Dorsostable running is characterized by the horse and dorsomobile by the cheetah (Slijper, 1946; Hildebrand, 1959; Gambaryan, 1974; Filler, 1986). Cheetah-type dorsomobile species use large thoracolumbar flexion-extension to increase stride length, whereas horse-like dorsostable taxa (such as ungulates) maintain a stiff back but increase stride length using long limbs.

Recent *in vivo* kinematic data on small mammals and horses have provided a new perspective on the use of sagittal flexion in running (Faber et al., 2001a; Haussler et al., 2001; Schilling and Hackert, 2006; Zaneb et al., 2013). These data indicate that

sagittal flexion and extension motions in the lumbosacral region are important during asymmetric gaits in both types of runners (see Figure 8.2.1, Figure 8.2.2). During symmetric gaits there are small biphasic sagittal motions of the thoracolumbar column; however, epaxial muscles act to stabilize the column against vertical motions due to oscillations in the center of mass (Schilling and Carrier, 2010). In contrast, during asymmetric gaits there is a single flexion-extension cycle which is synchronized with both limb movements and breathing patterns (Carrier, 1987; Bramble and Jenkins, 1993). In small mammals, sagittal motions of the thoracolumbar region produce very large pelvic displacements (29-45º), which are achieved by the combined movement of the last seven presacral vertebrae. Amplitude of intervertebral motions increases caudally (Schilling and Hackert, 2006). Maximal ventroflexion occurs slightly before touchdown of the hind limbs, and dorsiflexion begins during the hind limb stance phase (Figure 8.2.1). Maximum dorsiflexion is achieved shortly after lift-off of the hind limbs during the extended flight phase. In cantering horses, similar motions were recorded but they were limited to the lumbosacral joint (Figure 8.2.2) (Haussler et al., 2001). Ventroflexion of the lumbosacral region is high during the right forelimb stance phase and short gathered flight phase. Again, dorsiflexion begins once the left hind limb touches down then becomes more extreme as the right hind limb touches down. Maximum dorsiflexion is reached as the right forelimb touches down, as there is no extended flight phase in a canter.
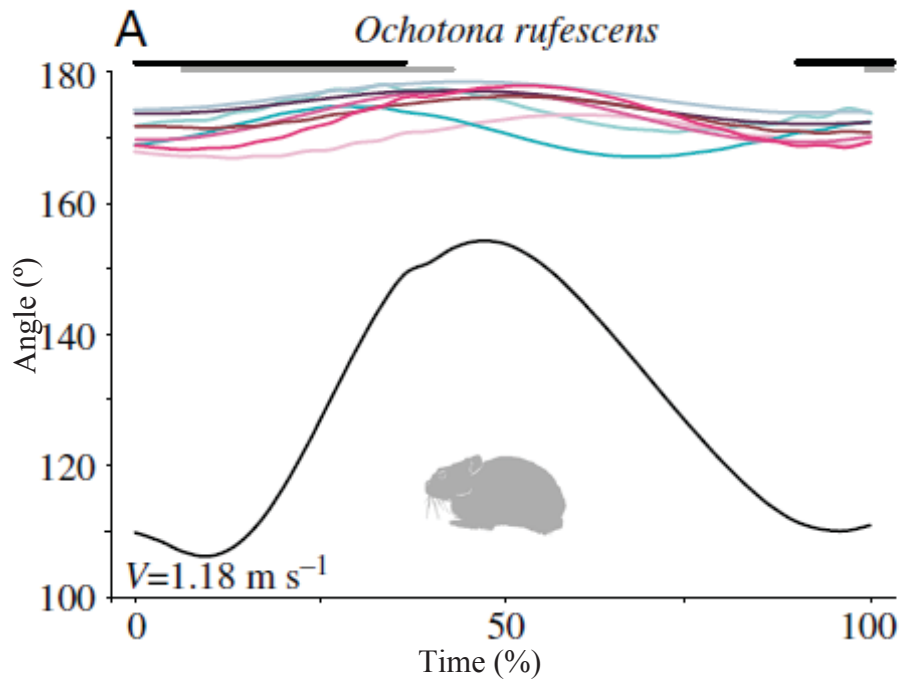
Figure 8.2.1 Sagittal vertebral motions of the pika during gallop.

From Schilling and Hackert (2006). Angular movements during a single stride. Colored lines indicate angles of last eight individual presacral joints, where 180° indicates a straight line between centra. Higher values represent dorsiflexion (extension) and lower values representing ventroflexion (flexion). The black curve indicates the angle of the pelvis to the horizontal. Lines at the top indicate footfall patterns of the hind limb, with grey indicating the leading hind limb and black the trailing hind limb. V is the velocity at which the animal was running when the data were recorded.
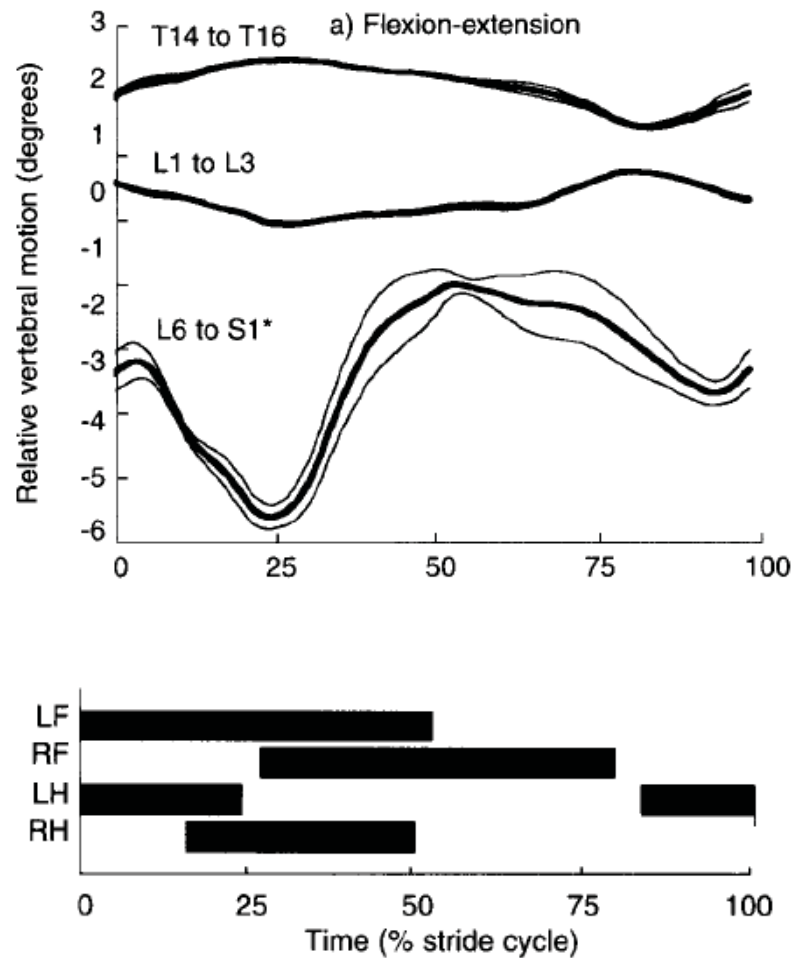
Figure 8.2.2 Sagittal vertebral motions of the cantering horse.
Graph shows degrees of motion at three vertebral positions over the stride cycle, footfall
patterns of which are shown below (Haussler et al., 2001). LF. Left forelimb; RF, right
forelimb; LH, left hind limb; RH, right hind limb. Positive angles indicate ventroflexion
(flexion) and negative angles indicate dorsiflexion (extension) relative to a straight line
between vertebrae. The lumbosacral joint is held in an extended posture, but has
relatively large flexion and extension bending about the neutral position during canter.

The nature of the sagittal motions experienced by the thoracolumbar region

during running are therefore broadly comparable in both horses (dorsostable) and

various small bounding mammals (dorsomobile). The similar connection between

sagittal motions and limb movements during asymmetric gaits in different types of mammals may reflect the importance of these movements in producing locomotor-respiratory coupling (Bramble and Carrier, 1979; Bramble and Jenkins, 1993; Daley et al., 2013).The major difference between vertebral kinematics in the small mammal and horse studies was the recruitment of more cranial lumbars into flexion-extension motions for increasing stride length in small mammals. This mobility has been associated with certain gait types. Dorsomobile taxa, such as felids, tend to use an extended flight phase (Bertram and Gutmann, 2009). This is when the time between lift-off of the hind limbs and touch-down of the forelimbs is prolonged, resulting in the leaping-type suspended phase, typical of rotary galloping gaits. Horses, on the other hand, tend to employ only a gathered flight phase. This is when the time between lift-off of the forelimbs and touch-down of the hind limbs is prolonged. Thus, instead of discrete categories, it may be more useful to think of the use of sagittal bending in running as a continuum, in which the contribution of the vertebral column to stride length varies along with gait use.

This dissertation gathered preliminary data about the connection between craniocaudal mobility patterns and vertebral morphology in dorsostable and dorsomobile mammals, including the horse and cat. In agreement with the above described kinematic data, the craniocaudal range of motion data from the literature confirmed contrasting craniocaudal patterns between these two species. In particular, sagittal mobility was relatively high throughout the thoracolumbar region of cats but was isolated to the lumbosacral joint in horses (Townsend et al., 1983; Macpherson and Ye, 1998). A similar pattern was also found in the sheep, which presumably represents

a convergent adaptation to dorsostable running in artiodactyls and perissodactyls. Further, the increase in sagittal range of motion at the lumbosacral joint in both sheep and horses was correlated with a similar change in vertebral morphology at the last lumbar. In particular, this vertebra had a shorter centrum and neural spine, suggesting reduced sagittal stiffness from the disc and supraspinous ligament. Dorsoventral height of the joint complex also correlated with sagittal range of motion, suggesting that the disc and zygapophyses are important in determining vertebral flexibility. This indicates that craniocaudal joint morphology patterns may provide a means to infer vertebral function in fossil ungulate species. Further data linking mobility and morphology from the same individuals will help to test these findings. Clarification of relationships between form and function in the vertebral column represent an important future research direction as they provide a means of testing the role of the axial skeleton in locomotor evolution.

Craniocaudal morphology patterns reflecting dorsostable versus dorsomobile mobility patterns in bovids and felids were also detected in Chapter 6. In bovids, the last lumbar has a sagittally compressed centrum and shorter neural spine, both of which indicate reduced rigidity in the sagittal plane, relative to the more cranial lumbars. Both felids and bovids have a mediolaterally wider centrum and more widely spaced zygapophyses at the lumbosacral joint than at more cranial lumbar joints. This suggests that the lumbosacral joint is also reinforced against lateroflexion. This likely provides support against lateroflexion and torsion moments produced by the action of protractors and retractors of the hind limb on the pelvis (Schilling and Hackert, 2006; Schilling and Carrier, 2010; Schilling, 2011). Data from this dissertation indicate that morphological

data from the axial skeleton can provide useful information about the relative distribution of sagittal flexibility during in running in mammals.

8.3   LUMBAR ALLOMETRY AND CURSORIALITY

Both static and dynamic loadings on the vertebral column will increase as body size increases (Slijper, 1946; Smeathers, 1981). In the introduction to this dissertation I presented the hypothesis that stabilization of the lumbar region would be energetically favored at large size, and predicted there should be strong allometry in lumbar morphology. In Chapters 5 and 6 I tested allometry of the lumbar region in both felids and bovids, and in Chapter 7 I tested lumbar allometry in equids. There is strong allometry of lumbar shape in all three families indicating that size is a very important influencing factor on morphological variation. Further, some features associated with stabilization of the lumbar region are correlated with body size, particularly in bovids and equids. These results indicate that some of the morphologic features that typify a dorsostable-type lumbar region are correlated with size and may reflect a size-related specialization to cursoriality.

Structural allometry accounted for around 70% and 40% of total morphological variation in the penultimate lumbar of bovids and felids respectively, suggesting that size is a strong determinant of lumbar shape in these groups. Allometric patterns varied among the centrum and other vertebral features. With regard to the centrum, craniocaudal shortening and dorsoventral deepening of the centrum with size were found in all three mammal groups examined, suggesting this allometric pattern is widespread. As mentioned above, this result suggests that the ventral column becomes

increasingly stiff in the sagittal plane, assuming disc properties remain similar. Consistent scaling patterns of the centrum across clades may reflect the importance of the ventral column in resisting static loads, and suggest that cross-sectional dimensions of the lumbar centra may be the best vertebral indicator of body size. In particular, centrum width tended to scale close to geometric similarity, and therefore could be a useful addition into allometric equations for body size estimation. Centra would be particularly useful for estimating body mass in fossils because they are most frequently preserved. However, craniocaudal variation in allometry means that the position of the vertebra, down to vertebral region, should be determined to reduce error in estimations from fossil taxa. This idea could be tested on a broader range of mammals to assess the potential of vertebral centra to provide new information to predictive body size equations.

Other vertebral features varied more widely among families. In particular, reorientation of the transverse processes, from inclined to horizontal, was correlated with size in bovids and equids, but changed less in felids. These results support the findings of Halpert et al. (1987), who found a correlation between transverse process angle and size in bovids. Horizontal, wide and robust transverse processes have been linked to dorsostability, as they are thought to reflect reduced influence of mobilizing epaxial muscles and increased ligament support in the lumbar region (Slijper, 1946; Shapiro, 1993; Argot, 2003). However, this pattern could be further explored by investigation of the soft-tissue anatomy of small and large mammals. Indeed, muscle mass measurements from a small sample of bovids have shown that epaxial muscle mass (as a proportion of total muscle mass) does decrease with size, supporting these

inferences (Grand, 1997).

Zygapophyseal morphology correlated with size in bovids but not felids. Specifically, larger bovids were more likely to have sigmoid-revolute zygapophyses than small bovids, while felids of all sizes had flat to convex joints. In humans, lumbar zygapophyses are linked to resisting torsion and hyperextension (Shirazi-Adl, 1994). The presence of revolute zygapophyses in even small bovids may suggest that these joints play a greater role in resisting torsion than in felids, where deep epaxials (e.g., multifidus and rotatores) may be more important. Enhancement of zygapophyses with size may reflect increasing torsional forces in large bovids. The functional implications of variations in zygapophyseal morphology represent an interesting avenue of future research because they vary widely across mammals, and revolute joints are known from a diverse range of fossil taxa.

The morphological data presented in this dissertation provide support for the idea that passive support mechanisms correlate with size in the lumbar region of running mammals. This may be because increased energetic costs of running with size require large animals to become more specialized than small animals (Garland, 1983; Hildebrand, 1995). Leaping gaits which involve large vertical changes in center of mass become mechanically challenging at larger size. Thus transverse galloping, which involves minimal vertical movements are most efficient for large ungulates such as horses (Bertram and Gutmann, 2009). In contrast, running in small ungulates is less constrained, and may involve a larger contribution of axial bending to stride length. This effect may be exaggerated in herbivorous mammals due to the additional weight of the enlarged digestive tract, which would increase both sagging and torsional loads in

the thoracolumbar spine. Allometric patterns were weaker in the dorsomobile felids than the ungulates. Lumbar mobility may be more important to facilitate sprinting and pouncing during hunting in felids of all sizes, despite its increasing energetic cost with size. An interesting future line of inquiry would be to examine soft-tissue adaptations to increasing size in felids. In particular, soft tissue changes such as in the muscle-fiber pinnation or fiber-type composition may play a role in resisting loads in dorsomobile mammals. Collecting *in vivo* and *ex vivo* experimental data on vertebral function in a broader range of taxa will be key to understanding variation in vertebral function in running mammals.

Fast, efficient and prolonged running is an essential component of mammalian diversity and success. Adaptations of the appendicular skeleton to cursoriality are well known, but features of the vertebral column, though qualitatively discussed, have rarely been systematically and quantitatively examined (Thompson, 1917; Slijper, 1946; Gambaryan, 1974; Steudel and Beattie, 1993; Hildebrand, 1995). This dissertation has quantified vertebral morphology and variation in three families of cursorial mammals, identified craniocaudal morphology patterns associated with particular running modes and found evidence of strong allometry in traits associated with stabilization. Understanding vertebral morphology and function can shed new light on mammalian locomotor evolution, and particularly cursoriality, because sagittal spinal flexion is most important during asymmetric gaits, which are the fastest mammalian gaits (Schilling and Hackert, 2006; Schilling, 2011). The lumbosacral region provides interesting new insights not provided by limb morphology alone, because its use varies between symmetric and asymmetric gaits. In particular, limb elongation provides

increased locomotor efficiency at all speeds, whereas sagittal bending of the lumbar region is only important in the fastest asymmetric gaits, particularly rotary gallops or those with forelimb-initiated transitions in center of mass motions (Slijper, 1946; Smith and Savage, 1956; Hildebrand, 1995; Bertram and Gutmann, 2009). Axial skeletal morphology could be used to help to differentiate gait usage in extinct taxa and study the evolution of gait. This idea could be tested by collecting more data on a broader cross-taxonomic sample of mammals that prefer different gaits.

8.4   CONCLUSIONS

1. **Scaling of the ventral column is consistent with its perceived role in body support as a dorsal compressive element.** Specifically, the pre-diaphragmatic region increased in the sagittal dimension with increasing size, whereas the post-diaphragmatic region became craniocaudally shortened and sagittally deeper.

2. **Features associated with lumbar stability are correlated with size.** There is strong allometry of the lumbar region in felids, bovids and equids. While allometry of the centrum was similar across groups, allometry of the processes was stronger in the dorsostable families.

3. **Passive stabilization of the lumbar region in dorsostable groups may be a size-dependent cursorial specialization.** The correlation of stabilizing features with size suggests that the degree of specialization of the lumbar region for dorsostability is a response to the energetic cost of running at large size.

4. Preliminary data suggest that **the shape of the intervertebral joint complex reflects range of motion.** There is a strong relationship between morphology and mobility in both dorsiflexion and torsion and, to a lesser extent, lateroflexion in cats, sheep and horses.

5. **Craniocaudal patterns of lumbar morphology reflect differences in craniocaudal mobility between dorsostable and dorsomobile groups**. Bovids and equids have strong differentiation of the morphology of the last lumbar vertebra and lumbosacral joint for permitting sagittal mobility and restricting lateroflexion. This hinge-like lumbosacral joint appears to be characteristic of both bovids and equids of

all sizes, and it reflects a convergent adaptation to cursoriality.

6. **The hinge-like lumbosacral joint may have been an early adaptation to cursoriality in the Equidae**. Small-bodied fossil equids, such as *Hyracotherium grangeri,* likely had more flexibility of the anterior lumbar region than modern horses, and therefore may have been able to utilize a more diverse range of leaping gaits, such as rotary gallops.

APPENDIX 1. Bovid and felid specimens

AMNH, Department of Mammalogy, American Museum of Natural History, New York;

NHM, Natural History Museum London; USNM, Department of Mammalogy, United

States National Museum of Natural History, Smithsonian Institution, Washington, D.C..

Body masses were estimated from limb dimensions as described in the methods.

SPECIES	BM (Kg)	N	Specimen numbers
Bovidae			
Neotragus pygmaeus	2	1	USNM 429835
Neotragus batesi	2.6	5	AMNH 53180, 53946; NHM 1936.10.28.36, 1937.8.4.26, 1937.8.4.27
Madoqua saltia	4	2	NHM 1936.3.28.6, 1935.12.12.5
Philantomba monticola	4.7	5	NHM 1901.8.9.132, 1936.10.28.28, 1936.10.28.29, 1936.10.28.31, 1936.10.28.30
Madoqua kirkii	5.8	5	AMNH 87218; NHM 1936.5.28.1, 62.129; USNM 538106, 541419
Raphicerus sharpei	8.4	3	USNM 367433, 367445, 367434
Raphicerus campestris	9.7	3	AMNH 34728, 80538; USNM 586524
Sylvicapra grimmia	14.2	4	NHM 1934.4.1.194, 1936.3.30.7, 1966.8.5.1, 1966.10.17.1
Oreotragus oreotragus	14.4	2	AMNH 82074, 80553
Gazella spekei	17	3	NHM 1935.12.13.2, 1935.12.13.4, 1935.12.13.3
Ourebia ourebi	17	5	AMNH 80258, 82070; NHM 1934.5.1.3, 1936.3.28.7, 1928.8.2.4
Cephalophus dorsalis	17.8	3	AMNH 52924, 52928, 52898
Eudorcas thomsonii	21.4	5	AMNH 82058, 82059; USNM 164538, 172903, 163067
Antidorcas marsupialis	32.8	5	AMNH 233055, 35864, 81739, 83549; USNM 173040
Litocranius walleri	41.3	2	AMNH 88409, 81170
Aepyceros melampus	45.1	4	AMNH 216393, 82050; USNM 261111, 241588,
Redunca arundinum	50.9	5	AMNH 80505, 80506, 80507, 80508; USNM 469909

Nanger granti	52.5	5	AMNH 85152, 85153; NHM 1976.4.18.1; USNM 163080, 163083
Bubalus depressicornis	83.8	1	USNM 219297
Oryx dammah	116.2	5	AMNH 113804; USNM 449934, A35256, 464515, 575162
Damaliscus lutus	120.7	5	AMNH 113781, 83526; USNM 163009, 163010, 163008
Alcelaphus buselaphus	135.3	5	AMNH 17276, 82033; USNM 162996, 172905, 162994
Connochaetes gnou	138.2	3	AMNH 35183, 81722, 80020
Boselaphus tragocamelus	153.6	1	USNM 269127
Hippotragus niger	182.2	5	AMNH 189374, 216381, 83476; USNM 218780, 396597
Kobus ellipsiprymnus	182.4	3	AMNH 53492, 53494, 53458
Connochaetes taurinus	196.6	5	AMNH 216386, 81789; NHM 1932.6.6.27; USNM 163019, 163012
Bubalus mindorensis	200.7	1	USNM 219049
Tragelaphus eurycerus	227.4	3	NHM 1959.1.2.2, 34.11.9.1; USNM 542466, 449524
Bos grunniens	231.3	1	USNMA14328
Bos sauveli	306.3	2	USNM 399379, 361392
Bison bonasus	483.4	1	USNM310690
Taurotragus oryx	536	3	NHM 1960.11.10.3, 647.1; USNM 162985
Bison bison	605.2	5	USNM 175783, 113934, 114032, 141896, 22377
Syncerus caffer	647.2	5	AMNH 216373, 53566, 82004, 82006, 82007
Bos Taurus	655.5	1	USNM 277262
Felidae			
Leopardus tigrinus	2.2	1	USNM 395090
Prionailurus bengalensis	2.3	1	USNM 317283
Felis catus	4.5	5	NHM 1936.5.11.1, 80.2566, 80.2567, 80.2570, 1952.10.20.4
Leopardus wiedii	4.8	3	NHM 1846.4.21.8, 1849.11.7.2; USNM 305072

Felis silvestris	5.4	5	NHM 1929.2.27.2, 1953.6.11.1, 1953.8.5.1, 1953.8.5.2
Leopardus geoffroyi	5.9	4	AMNH 205903, 205907, 205910; USNM 574136
Puma yagouaroundi	7.9	2	AMNH 215137; USNM 124336
Prionailurus viverrinus	11.1	3	AMNH 70128; NHM 75.2284, 1860.7.22.22
Lynx lynx	11.2	1	AMNH 19692
Caracal caracal	12.7	4	USNM 384162, 396160, 520686; NHM 1855.9.17.2
Catopuma temminckii	13.5	3	USNM 362188, 395758, 395843
Leopardus pardalis	14	5	AMNH 248728; NHM 1846.4.21.8, 1952.1083; USNM 012182, 271094
Leptailurus serval	14.2	4	AMNH 34767; USNM 521039, 548666; NHM 1966.7.11.1
Lynx rufus	14.5	5	AMNH 255663; USNM 271310, 292037, 188754, 282369
Lynx canadensis	15	5	AMNH 120950, 147218, 147755, 15662; USNM 188731
Neofelis nebulosa	16.5	4	USNM 399290, 399291, 545387; NHM 1965.1.18.1
Acinonyx jubatus	40.6	5	AMNH 119654, 119655; USNM 398031, 521037, 395137
Uncia uncia	44.9	4	AMNH 166952; NHM 1962.12.11.1, 1963.2.25.1, 1967.6.29.1; USNM 241212
Panthera pardus	52	5	AMNH 54854; USNM 155454, 156284, 396948; NHM 1880.2.16.1
Puma concolor	66.8	5	USNM 21527, A01385, A21526, A21528, 262132
Panthera onca	80.7	5	AMNH 139959, 214738, 35571, 80063; USNM A49393
Panthera tigris	151.3	7	AMNH 135846, 14030, 35482; NHM 1884.1.22.6, 1937.1.2.1; USNM 49773, A49799
Panthera leo	195	5	AMNH 54995, 54996; USNM 172677, A22705, A12319

APPENDIX 2. Equid specimens

AMNH, Division of Paleontology, American Museum of Natural History, New York;

MCZ, Museum of Comparative Zoology, Harvard University, Cambridge,

Massachusetts; F:AM, Frick Collection; FM, fossil mammals. USNM, Department of

Paleobiology, United States National Museum of Natural History, Smithsonian

Institution, Washington, D.C. (except genus *Equus*, which are from the Department of

Mammalogy); UF, University of Florida Museum of Natural History, Gainesville; UM,

University of Michigan Museum of Paleontology, Ann Arbor; YPM, Peabody Museum

of Natural History, Yale University, New Haven, Connecticut.

SPECIES	GROUP	N	Specimen no
Phenacodus vortmani	Phenacodontidae	1	AMNH FM 4378, USNM 27589
Hyracotherium grangeri	Hyracotheriinae	1	UM 115547
Hyracotherium sp.	Hyracotheriinae	4	AMNH FM 144323, 88338, 88339, 144322
Mesohippus sp.	Anchitheriinae	11	AMNH FM 12459, 12454; USNM 15960, 16104, 16815, 16817, 16818, 16819, 16830; YPM 13791, 16876
Mesohippus westoni	Anchitheriinae	1	AMNH F:AM 74048
Mesohippus bairdii	Anchitheriinae	6	AMNH F:AM 74026, 74082, 74025; AMNH FM 1492; YPM 10927, 11376
Archaeohippus blackbergi	Anchitheriinae	5	UF 211479, 258551, 276606, 528584, 259127
Parahippus leonensis	Anchitheriinae	18	AMNH F:AM 109857; UF 12621, 163493, 186578, 189958, 193046, 199217, 205530, 255585, 255764, 256115, 258364, 259137, 260245, 273270, 299538, 205668, 276766
Merychippus republicanus	Equinae	1	AMNH FM 8347
Merychippus quartus	Equinae	1	AMNH FM 14184
Merychippus proparvulus	Equinae	1	AMNH FM 9394
Merychippus campestris	Equinae	1	AMNH FM 9096
Merychippus isoneus	Equinae	1	AMNH F:AM 143273
Merychippus sp.	Equinae	1	AMNH F:AM 144326

Nannippus minor	Equinae	5	UF 201426, 224207, 224208, 224215, 69933
Pliohippus pernix	Equinae	1	AMNH F:AM 60803
Hippidion neogaeus	Equinae	1	AMNH FM 11872
Equus sp.	Equinae	1	AMNH FM 90887
Equus burchellii	Equinae	4	USNM 162954, 162955, 259848, 162960
Equus zebra	Equinae	1	USNM 270125
Equus caballus	Equinae	4	USNM 172454, USNM 302898, USNM 396016, USNM 582088
Equus grevyi	Equinae	2	USNM 163338, USNM 152231, USNM A49944

APPENDIX 3. Linear dimensions of the ventral column

Dimensions in mm.Body mass calculated from limb dimensions (Kg). LogBM, log body mass; Tott, total thoracic region length; Totl, total lumbar region length; Tottl, total thoracolumbar region length; Predl, total pre-diaphragmatic region length; Podl, total post-diaphragmatic region length; Tch, mid-thoracic centrum height; Tcw, mid-thoracic centrum width; Dch, diaphragmatic centrum height; Dcw, diaphragmatic centrum width; Lch, mid-lumbar centrum height; Lcw, mid-lumbar centrum width; Areat, mid-thoracic centrum area; Aread, diaphragmatic centrum area; Areal, mid-lumbar centrum area.

Family	Species	LogBM	Tott	Totl	Tottl	Predl	Podl	Tch	Tcw	Dch	Dcw	Lch	Lcw	Areat	Aread	Areal
Bovidae	*Aepyceros melampus*	1.65	347.7	190.9	538.6	291.3	247.3	15.2	17.3	14.3	18.9	15.2	23.3	208.6	215.9	290.6
Bovidae	*Alcelaphus buselaphus*	2.13	487.5	244.9	732.4	448.8	283.5	24.1	25.5	23.7	28.8	25.3	31.4	486.1	543.7	633.7
Bovidae	*Antidorcas marsupialis*	1.51	317.0	180.3	497.4	263.2	234.2	12.6	15.4	12.3	19.3	14.7	21.7	155.3	197.1	260.0
Bovidae	*Bison bison*	2.77	902.6	341.6	1244.2	834.2	409.9	45.2	44.4	40.3	46.5	43.1	52.8	1584.4	1485.6	1815.7
Bovidae	*Bison bonasus*	2.68	781.1	291.0	1072.1	781.1	291.0	37.3	39.9	34.0	40.7	39.2	47.8	1167.8	1093.3	1487.9
Bovidae	*Bos grunniens*	2.36	655.1	298.7	953.8	561.9	392.0	32.8	29.8	30.0	32.6	28.7	37.7	769.6	768.1	865.8
Bovidae	*Bos sauveli*	2.49	645.1	309.9	955.0	620.3	334.8	32.9	34.5	30.3	35.5	30.5	39.1	890.0	852.4	951.4
Bovidae	*Bos taurus*	2.82	826.4	409.8	1236.2	760.5	475.7	47.2	49.9	40.4	49.9	45.5	55.2	1851.1	1602.5	1989.5
Bovidae	*Bosephalus tragocamelus*	2.19	537.7	290.5	828.2	449.7	378.4	26.9	26.7	27.9	33.3	29.0	34.6	565.1	733.5	794.0
Bovidae	*Bubalus depressicornis*	1.92	453.8	208.9	662.6	385.3	277.4	18.9	22.7	18.2	22.9	20.7	29.8	340.6	331.7	500.4
Bovidae	*Bubalus mindorensis*	2.30	613.8	274.5	888.3	569.9	318.4	30.8	33.0	26.5	31.8	26.9	35.6	800.0	668.1	766.6
Bovidae	*Cephalophus dorsalis*	1.24	246.3	148.5	394.8	218.2	176.6	10.4	13.0	10.5	14.6	11.4	18.0	108.5	124.5	170.5
Bovidae	*Connochaetes gnou*	2.13	468.9	233.4	702.4	431.5	270.9	22.6	24.8	23.8	30.4	26.5	32.5	442.1	577.5	682.9
Bovidae	*Connochaetes taurinus*	2.29	567.0	283.0	850.0	531.1	318.9	31.4	31.2	29.6	33.7	31.6	36.8	779.4	788.0	919.6

286

Family	Species															
Bovidae	*Damaliscus lunatus*	2.08	465.4	247.4	712.8	443.2	269.6	22.4	24.0	22.6	27.6	23.1	31.1	422.6	496.9	578.6
Bovidae	*Eudorcas thomsonii*	1.32	263.3	157.0	420.3	218.0	202.3	11.2	14.2	11.5	15.9	13.0	18.8	127.6	148.5	199.1
Bovidae	*Gazella spekei*	1.23	249.8	152.4	402.2	199.5	202.7	10.2	12.3	10.8	15.6	12.2	19.2	99.7	137.0	194.1
Bovidae	*Hippotragus niger*	2.26	509.6	275.2	784.8	426.1	358.7	25.2	28.3	24.3	31.7	27.1	36.8	561.7	618.1	803.6
Bovidae	*Kobus ellipsiprymnus*	2.26	545.4	300.5	845.9	483.4	362.4	27.2	31.0	26.7	32.1	30.0	38.3	669.1	685.3	920.2
Bovidae	*Litocranius walleri*	1.61	316.8	180.0	496.8	263.5	233.4	13.7	17.7	12.6	20.0	14.9	22.9	193.5	210.4	280.7
Bovidae	*Madoqua kirkii*	0.76	166.9	109.5	276.4	135.5	140.9	5.9	8.9	6.0	11.4	7.1	11.7	43.3	59.2	69.3
Bovidae	*Madoqua saltia*	0.60	145.6	93.3	238.9	118.6	120.3	5.1	7.8	5.6	9.5	6.3	10.2	32.7	44.5	53.1
Bovidae	*Nanger granti*	1.71	361.0	209.6	570.6	304.4	271.5	18.6	20.0	17.2	21.8	19.0	25.4	295.3	301.7	389.2
Bovidae	*Neotragus batesi*	0.42	127.1	88.7	215.9	102.6	113.3	4.7	6.5	4.6	8.1	5.1	9.0	24.5	31.6	38.8
Bovidae	*Neotragus pygmaeus*	0.29	118.4	76.7	195.1	94.7	100.4	4.4	5.8	4.6	8.0	5.1	8.1	20.4	31.3	34.1
Bovidae	*Oreotragus oreotragus*	1.16	182.2	146.8	329.0	182.2	146.8	8.1	12.4	8.3	13.0	9.4	16.0	82.7	90.0	127.1
Bovidae	*Oryx dammah*	2.06	470.0	263.3	733.4	401.1	332.3	20.7	24.4	21.2	26.2	24.7	30.2	399.6	441.8	592.3
Bovidae	*Ourebia ourebi*	1.23	234.5	165.3	399.8	199.4	200.4	8.3	11.3	8.5	13.9	10.3	17.0	75.6	99.4	147.2
Bovidae	*Philantomba monticola*	0.67	167.5	110.9	278.4	142.7	135.8	5.8	8.2	6.2	9.8	7.3	10.9	38.6	50.8	65.0
Bovidae	*Raphicerus campestris*	0.98	194.1	137.3	331.3	170.0	161.3	7.2	10.0	7.9	11.8	8.9	15.1	58.5	76.4	112.9
Bovidae	*Raphicerus sharpei*	0.92	197.3	118.8	316.0	161.7	154.4	6.9	9.5	7.6	11.2	8.4	14.1	53.4	69.7	100.2
Bovidae	*Redunca arundinum*	1.70	372.8	218.6	591.3	308.7	282.7	14.4	17.3	13.7	20.6	16.5	24.7	199.5	232.9	338.7
Bovidae	*Sylvicapra grimmia*	1.15	251.6	143.1	394.7	223.3	171.4	8.8	11.5	8.7	12.9	10.1	17.2	80.8	91.8	146.7
Bovidae	*Syncerus caffer*	2.81	748.0	377.4	1125.4	687.9	463.5	43.5	44.0	40.2	47.5	43.5	51.9	1512.3	1519.0	1798.6
Bovidae	*Taurotragus oryx*	2.72	708.3	385.1	1093.4	593.0	500.4	38.8	38.5	39.7	41.5	41.7	48.8	1192.7	1306.8	1619.8
Bovidae	*Tragelaphus eurycerus*	2.36	574.5	309.9	884.4	512.3	372.1	29.7	34.6	28.4	35.8	31.1	44.3	814.5	808.0	1115.2
Felidae	*Acinonyx jubatus*	1.60	281.4	277.9	559.3	202.2	357.1	14.5	16.5	15.8	22.4	18.1	27.4	189.8	288.8	408.0
Felidae	*Caracal caracal*	1.10	214.3	197.2	411.4	155.7	255.7	8.2	10.4	9.0	15.6	11.3	17.2	68.7	119.0	160.1
Felidae	*Catopuma temminckii*	1.13	192.6	180.2	372.8	143.2	229.6	8.2	9.4	8.7	14.6	9.9	16.4	60.7	106.8	135.7
Felidae	*Felis catus*	0.64	133.5	122.7	256.2	95.9	160.3	5.1	7.7	5.5	10.6	6.8	11.8	32.1	51.0	68.3
Felidae	*Felis silvestris*	0.73	155.2	144.1	299.4	113.5	185.9	6.0	8.1	6.6	11.5	7.8	13.1	39.6	65.0	86.5
Felidae	*Leopardus geoffroyi*	0.74	163.0	144.1	307.2	118.5	188.6	6.6	9.3	6.4	11.4	7.4	12.7	49.5	62.3	80.6

287

Felidae	*Leopardus pardalis*	1.13	224.6	170.7	395.4	167.9	227.4	8.8	10.4	8.7	15.0	10.0	16.9	72.2	111.6	143.3
Felidae	*Leopardus tigrinus*	0.35	134.0	116.8	250.8	94.7	156.1	4.5	5.6	.	.	5.4	9.7	20.1	.	44.8
Felidae	*Leopardus wiedii*	0.67	155.4	136.0	291.3	117.6	173.7	5.9	7.9	6.2	10.3	7.0	12.1	37.4	53.4	71.4
Felidae	*Leptailurus serval*	1.14	220.8	196.3	417.0	161.0	256.1	8.7	11.1	9.3	15.7	11.2	18.2	76.4	123.5	169.6
Felidae	*Lynx canadensis*	1.17	216.1	219.6	435.8	153.1	282.7	9.2	11.5	9.8	15.7	11.4	18.8	84.6	127.8	180.0
Felidae	*Lynx lynx*	1.05	200.0	195.8	395.8	142.7	253.1	8.5	11.5	9.6	15.2	11.1	16.8	78.6	120.8	152.5
Felidae	*Lynx rufus*	1.15	205.7	199.7	405.4	159.3	246.0	8.8	10.2	9.0	15.1	11.0	17.3	71.0	114.7	158.7
Felidae	*Neofelis nebulosa*	1.21	219.7	177.6	397.3	175.7	221.6	9.3	12.0	10.0	16.5	12.0	19.7	89.3	138.7	197.8
Felidae	*Panthera leo*	2.28	447.9	359.8	807.7	375.2	432.5	25.3	27.7	25.9	40.6	30.0	45.4	557.1	873.5	1124.6
Felidae	*Panthera onca*	1.90	344.6	271.2	615.8	281.6	334.2	18.5	21.1	18.3	28.4	20.5	32.7	309.3	430.4	557.8
Felidae	*Panthera pardus*	1.71	302.6	257.7	560.4	246.0	314.4	14.9	17.3	15.4	24.9	17.7	27.8	204.5	321.5	407.2
Felidae	*Panthera tigris*	2.16	433.7	349.6	783.2	354.6	428.6	23.9	26.0	24.4	36.1	26.7	39.4	495.8	726.0	868.8
Felidae	*Prionailurus bengalensis*	0.36	131.7	120.0	251.8	93.6	158.2	4.5	5.9	4.5	8.8	5.4	10.3	21.0	34.6	48.5
Felidae	*Prionailurus viverrinus*	1.04	191.5	172.6	364.2	137.2	227.0	8.0	10.4	9.1	13.9	9.8	16.4	67.1	103.3	134.7
Felidae	*Puma concolor*	1.80	331.3	284.4	615.8	262.3	353.5	16.6	17.1	16.1	25.8	19.2	29.0	223.5	346.5	457.2
Felidae	*Puma yagouaroundi*	0.90	191.6	170.1	361.7	138.1	223.6	6.8	9.0	7.5	13.0	9.0	14.4	49.1	82.5	107.5
Felidae	*Uncia uncia*	1.64	276.2	237.9	514.1	222.2	291.9	13.3	16.8	14.6	23.8	16.4	27.5	178.7	290.6	380.0

APPENDIX 4. PC scores from 3D landmarks on the penultimate lumbar of Bovidae

Log BM, log body mass (Kg). Top eight PCs account for 95.4% of the total variation, see Table 5.2.1 for eigenvalues.

Species	PC1	PC2	PC3	PC4	PC5	PC6	PC7	PC8	Log BM
Aepyceros melampus	-0.06884	-0.05632	-0.00785	-0.02845	-0.00977	-0.0095	-0.00727	0.009374	1.65
Alcelaphus buselaphus	0.065743	-0.03496	0.004061	0.043949	0.01394	0.02242	0.007318	0.007075	2.13
Antidorcas marsupialis	-0.03605	0.020409	-0.01023	0.023342	0.027769	1.18E-04	0.019087	0.011179	1.51
Bison bison	0.127442	-0.04874	-0.01154	-0.02343	-0.02454	0.0033	-0.00585	-0.0089	2.76
Bison bonasus	0.138417	-0.01539	0.01013	-0.04313	-0.0076	-0.01382	0.004608	0.014958	2.68
Bos grunniens	0.145274	0.038864	-0.03469	0.02519	-0.03473	-0.0307	0.003551	-8.16E-04	2.36
Bos sauveli	0.175611	-0.03271	0.053354	-0.01719	0.038603	-0.01528	0.017484	-0.02987	2.49
Bos taurus	0.191742	0.017449	-0.03074	-0.02052	0.001105	-0.00829	0.011201	-9.92E-04	2.82
Bosephalus tragocamelus	0.059176	-0.0198	0.024727	0.054003	-0.00387	-0.01482	0.01916	0.002398	2.19
Bubalus depressicornis	0.127889	0.004876	0.03587	0.03509	0.006577	-6.83E-04	-0.02435	0.005474	1.92
Bubalus mindorensis	0.187884	0.003866	-0.0246	-0.03121	0.06504	0.00978	-0.03276	-0.00558	2.30
Cephalophus dorsalis	-0.03981	0.034836	0.034998	-0.01891	0.024823	-0.00842	-0.01199	-0.01829	1.24
Connochaetes gnou	0.125037	0.07522	0.00325	0.014503	-0.00798	0.018115	0.030584	0.012568	2.13
Connochaetes taurinus	0.127421	-0.00187	0.006747	0.014425	0.003917	0.028114	0.0163	-0.00505	2.29
Damaliscus lunatus	0.067489	-0.01086	-0.00689	0.037928	0.001517	0.016826	0.005787	-0.00563	2.08
Eudorcas thomsonii	-0.0769	-0.02231	-0.00248	0.014815	0.006239	-0.01034	-0.01429	0.009524	1.32
Gazella spekei	-0.10853	-0.06289	0.00133	-0.01299	-0.00832	0.01234	-0.00943	0.005981	1.23
Hippotragus niger	0.063034	-0.00138	-0.01541	0.005359	-0.01703	-0.01102	0.009036	-5.69E-04	2.26
Kobus ellipsiprymnus	0.002959	-0.00945	0.048262	0.02306	2.12E-04	-0.00744	0.009263	0.005739	2.30
Litocranius walleri	-0.08948	-0.01249	0.025741	0.003325	0.001488	-0.00939	0.001779	0.014969	1.61
Madoqua kirkii	-0.16974	-0.04376	0.03606	-0.02139	-0.00208	-0.00246	0.00202	0.001913	0.76
Madoqua saltiana	-0.14627	-0.0365	-0.01336	6.65E-04	0.044551	0.008064	0.021123	-0.00602	0.60
Nanger granti	-0.03353	-0.05524	-0.02241	-0.00991	-0.01651	0.010392	0.015933	0.004117	1.71
Neotragus batesi	-0.15303	0.047864	-0.0289	0.014212	0.01867	-0.00327	-0.01868	0.010329	0.42
Neotragus pygmaeus	-0.16224	0.034893	-0.03598	0.00711	-0.01949	0.044042	-0.01375	-0.02914	0.29
Oreotragus oreotragus	-0.12108	0.051594	0.009284	-0.00992	-0.00998	0.010587	-0.00703	0.004705	1.16

289

Oryx dammah	0.077389	0.005753	-0.00735	0.052009	-0.02864	-0.03523	-0.01634	-0.02186	2.06
Ourebia ourebi	-0.13063	1.19E-04	-0.0179	-0.00338	-0.01892	-0.00963	0.026486	-0.00726	1.23
Philantomba monticola	-0.16554	0.039523	0.008329	-0.00493	-0.00212	-0.00618	-0.00389	-0.00937	0.67
Raphicerus campestris	-0.14076	0.022617	0.02123	-0.00567	0.023306	-0.01482	-0.00422	0.0288	0.98
Raphicerus sharpei	-0.12711	0.03282	0.024252	-0.02279	-0.00344	-0.01111	0.01163	-0.00839	0.92
Redunca arundinum	-0.10684	-0.02501	-0.00459	0.017036	-0.00488	-0.00595	0.003169	-0.00751	1.70
Sylvicapra grimmia	-0.11861	0.026931	-0.00461	0.001076	0.003804	-0.00948	0.007037	-0.01041	1.15
Syncerus caffer	0.196013	0.032288	-0.00487	-0.02804	0.005919	0.009605	-0.00197	0.015651	2.81
Taurotragus oryx	0.113823	-0.00214	0.015836	0.007882	-0.03361	0.022976	-0.00813	0.008316	2.72
Tragelaphus eurycerus	0.002629	0.001911	0.087685	-0.0285	-0.03397	0.021159	-0.02027	0.002583	2.33

APPENDIX 5. PC scores from 3D landmarks on the penultimate lumbar of Felidae

Log BM, log body mass (Kg). Top ten PCs account for 95.8% of the total variation, see Table 5.2.3 for eigenvalues.

Species	PC1	PC2	PC3	PC4	PC5	PC6	PC7	PC8	PC9	PC10	Log BM
Acinonyx jubatus	0.0696	-0.0536	-0.0629	-0.0320	-0.0136	-0.0287	-0.0071	0.0056	0.0014	-0.0088	1.60
Caracal caracal	-0.0890	-0.0577	0.0052	0.0347	-0.0063	0.0073	-0.0273	0.0122	0.0116	-0.0002	1.10
Catopuma temminckii	-0.0594	-0.0320	0.0273	0.0484	-0.0089	-0.0218	0.0092	-0.0146	0.0011	0.0069	1.13
Felis catus	-0.0264	-0.0109	0.0045	0.0150	-0.0004	-0.0124	0.0166	-0.0026	-0.0175	-0.0162	0.64
Felis silvestris	-0.0204	-0.0052	-0.0216	0.0135	-0.0134	0.0217	0.0230	0.0000	0.0068	0.0017	0.73
Leopardus geoffroyi	-0.0461	0.0372	0.0138	-0.0136	-0.0149	0.0036	0.0045	0.0052	-0.0040	-0.0022	0.74
Leopardus pardalis	-0.0252	0.0491	0.0282	-0.0060	0.0049	0.0155	-0.0177	-0.0024	-0.0007	-0.0119	1.13
Leopardus tigrinus	-0.0681	0.0570	-0.0217	-0.0034	-0.0327	-0.0183	-0.0169	-0.0155	0.0063	0.0104	0.35
Leopardus wiedii	-0.0224	0.0250	-0.0053	0.0043	0.0148	0.0022	0.0137	0.0058	0.0097	-0.0103	0.67
Leptailurus serval	-0.0295	-0.0289	0.0141	-0.0254	-0.0036	0.0055	-0.0012	0.0064	-0.0114	0.0081	1.14
Lynx canadensis	-0.0920	-0.0180	-0.0265	-0.0285	0.0360	0.0115	0.0010	-0.0268	-0.0003	-0.0003	1.17
Lynx rufus	-0.0585	-0.0172	-0.0035	-0.0106	0.0121	0.0128	0.0047	0.0057	0.0135	-0.0037	1.17
Neofelis nebulosa	0.0621	0.0367	-0.0122	0.0141	0.0308	-0.0037	-0.0164	0.0095	0.0022	-0.0051	1.21
Panthera leo	0.1549	-0.0033	-0.0290	0.0277	-0.0229	0.0376	-0.0057	-0.0095	-0.0126	0.0017	2.28
Panthera onca	0.1016	0.0120	0.0153	-0.0135	-0.0075	-0.0044	0.0023	-0.0054	0.0189	0.0044	1.90
Panthera pardus	0.0512	0.0017	0.0192	-0.0163	0.0063	-0.0130	-0.0008	-0.0106	-0.0079	0.0037	1.71
Panthera tigris	0.1021	-0.0049	0.0349	-0.0117	-0.0038	-0.0046	0.0157	0.0049	0.0161	0.0051	2.16
Prionailurus bengalensis	-0.0542	0.0436	-0.0511	0.0189	0.0037	-0.0062	0.0135	0.0153	-0.0041	0.0082	0.36
Prionailurus viverrinus	-0.0016	0.0117	0.0216	-0.0069	0.0020	-0.0148	-0.0026	0.0143	-0.0163	0.0090	1.04
Puma concolor	0.0134	-0.0063	0.0274	0.0009	-0.0186	-0.0047	-0.0027	-0.0029	-0.0026	-0.0210	1.80
Puma yagouaroundi	-0.0437	-0.0238	0.0170	-0.0318	-0.0080	0.0218	-0.0010	0.0079	-0.0065	0.0107	0.90
Uncia uncia	0.0815	-0.0120	0.0054	0.0222	0.0440	-0.0070	-0.0049	-0.0024	-0.0037	0.0098	1.63

APPENDIX 6. Linear measures and PC scores from 2D landmarks of Felidae and Bovidae

PL, proximal lumbar (L1); ML, middle lumbar; DL, distal lumbar (last lumbar); BM, body mass; CH, centrum height; CW, centrum width; ARCHLA, arch lever arm; NSLA, neural spine lever arm; TPLA, transverse process lever arm; ZW, zygapophysis width; TPA, transverse process angle; AREA, endplate area. PC scores are from 2D landmarks and come from separate Procrustes fits for felidae and bovidae. Top 3 PCs account for 97.9% and 94.4% of total variation for felids and bovids respectively, eigenvalues can be found in

Table 6.2.4.

Family	Position	Species	BM	CH	CW	ARCHLA	NSLA	TPLA	ZW	TPA	AREA	PC1	PC2	PC3
Felidae	PL	Acinonyx jubatus	40.6	16.7	26.0	21.7	46.0	28.0	20.6	135.1	21.4	-0.0714	-0.0374	0.0231
Felidae	PL	Caracal caracal	13.1	10.2	16.7	14.8	24.7	14.1	12.7	138.6	13.5	-0.1107	0.0093	0.0102
Felidae	PL	Leopardus geoffroyi	6.9	6.8	12.6	10.0	16.4	10.0	10.0	125.2	9.7	-0.0993	0.0284	-0.0153
Felidae	PL	Puma yagouaroundi	7.9	7.9	13.4	11.2	21.7	10.3	12.1	133.1	10.6	-0.1089	0.0387	0.0081
Felidae	PL	Leopardus pardalis	14.4	8.6	15.5	12.7	22.6	12.8	12.1	121.4	12.1	-0.1059	0.0332	-0.0062
Felidae	PL	Felis silvestris	5.9	7.9	15.0	12.5	17.7	11.3	10.7	124.6	11.5	-0.1046	0.0035	-0.0224
Felidae	PL	Leptailurus serval	14.8	9.8	17.3	13.2	24.7	13.8	11.1	137.5	13.5	-0.1130	-0.0151	-0.0090
Felidae	PL	Prionailurus viverrinus	11.0	9.5	14.7	11.1	20.5	10.0	13.9	134.1	12.1	-0.1057	0.0286	0.0414
Felidae	PL	Felis catus	4.5	5.6	11.2	8.5	15.5	8.4	8.7	123.8	8.4	-0.0699	0.0055	-0.0190
Felidae	PL	Lynx canadensis	14.4	9.3	16.9	12.0	21.6	12.8	10.9	138.9	13.1	-0.1330	-0.0142	-0.0152
Felidae	PL	Lynx lynx	11.2	9.5	16.6	12.2	21.1	13.1	10.8	145.3	13.1	-0.1543	-0.0166	-0.0112
Felidae	PL	Lynx rufus	15.2	10.0	17.2	13.1	24.1	12.9	10.4	142.0	13.6	-0.1355	-0.0181	-0.0211
Felidae	PL	Neofelis nebulosa	16.5	10.3	18.5	13.5	23.0	14.6	14.4	121.5	14.4	-0.0484	0.0056	-0.0217
Felidae	PL	Panthera tigris	159.2	24.2	37.8	25.5	53.4	25.1	25.8	133.0	31.0	-0.0901	-0.0546	0.0158

Felidae	PL	*Panthera onca*	84.8	18.4	30.2	22.1	46.0	23.2	20.0	121.5	24.3	-0.0974	-0.0401	-0.0059
Felidae	PL	*Panthera pardus*	52.0	15.5	25.0	19.4	37.0	16.8	20.1	123.2	20.3	-0.0852	-0.0138	0.0065
Felidae	PL	*Panthera leo*	193.4	27.7	41.5	27.8	55.1	27.2	29.3	126.8	34.6	-0.0760	-0.0642	0.0221
Felidae	PL	*Uncia uncia*	44.1	15.5	26.7	19.0	36.5	19.9	19.9	128.4	21.1	-0.0598	-0.0284	-0.0111
Felidae	PL	*Prionailurus bengalensis*	2.3	4.2	9.0	8.4	13.8	6.0	8.6	131.9	6.6	-0.0640	0.0631	-0.0140
Felidae	PL	*Puma concolor*	72.3	16.9	27.5	22.2	47.6	24.1	20.4	130.8	22.2	-0.1118	-0.0319	0.0129
Felidae	ML	*Acinonyx jubatus*	40.6	16.7	27.6	20.4	46.4	28.8	23.5	132.9	22.1	-0.0360	-0.0250	0.0153
Felidae	ML	*Caracal caracal*	12.3	9.6	16.2	14.3	30.0	17.2	13.3	135.5	12.9	-0.0749	0.0047	0.0075
Felidae	ML	*Catopuma temminckii*	13.5	9.6	17.2	15.2	31.9	17.9	14.6	132.9	13.4	-0.1008	0.0429	0.0008
Felidae	ML	*Leopardus wiedii*	4.8	7.8	14.3	13.3	26.6	14.4	12.2	133.5	11.1	-0.1018	0.0660	-0.0050
Felidae	ML	*Felis catus*	4.5	6.2	11.7	10.5	20.7	12.3	10.4	126.5	8.9	-0.0865	0.0596	0.0029
Felidae	ML	*Leopardus pardalis*	14.8	9.4	17.4	16.5	32.2	16.6	15.7	133.2	13.4	-0.0942	0.0612	-0.0062
Felidae	ML	*Felis silvestris*	5.7	7.4	14.0	12.5	25.3	15.5	11.9	125.0	10.7	-0.1043	0.0395	-0.0019
Felidae	ML	*Leopardus geoffroyi*	5.9	6.4	12.9	11.8	24.0	12.5	11.5	135.0	9.7	-0.0983	0.0665	-0.0108
Felidae	ML	*Puma yagouaroundi*	7.9	7.6	15.1	13.4	32.3	17.0	12.3	142.8	11.3	-0.0629	0.0393	-0.0225
Felidae	ML	*Leptailurus serval*	14.2	10.2	17.7	14.6	30.8	18.4	13.6	134.5	14.0	-0.1004	0.0054	-0.0016
Felidae	ML	*Leopardus tigrinus*	2.2	4.6	9.7	9.3	15.9	6.4	9.1	140.7	7.2	-0.1029	0.1194	-0.0178
Felidae	ML	*Lynx canadensis*	15.0	10.3	18.4	14.4	28.4	16.5	12.8	135.9	14.4	-0.1063	-0.0204	-0.0125
Felidae	ML	*Lynx lynx*	11.2	10.0	17.3	16.4	31.2	17.6	11.9	136.0	13.7	-0.1314	0.0124	-0.0061
Felidae	ML	*Lynx rufus*	14.2	9.9	17.4	14.4	31.3	16.8	13.2	130.6	13.7	-0.1151	0.0138	-0.0030
Felidae	ML	*Neofelis nebulosa*	16.5	11.0	19.9	16.9	32.3	18.9	17.0	129.3	15.4	-0.0541	0.0323	-0.0072
Felidae	ML	*Panthera tigris*	145.1	24.5	38.5	29.5	68.2	30.7	29.3	133.3	31.5	-0.0962	-0.0332	0.0121
Felidae	ML	*Panthera onca*	80.7	18.9	32.2	24.6	60.4	29.7	25.1	122.7	25.6	-0.0646	-0.0240	-0.0042
Felidae	ML	*Panthera pardus*	52.8	16.9	28.5	20.0	44.5	27.7	21.5	136.3	22.7	-0.0952	-0.0062	0.0024
Felidae	ML	*Panthera leo*	195.0	29.0	45.0	32.4	68.6	43.8	32.7	121.9	37.0	-0.0823	-0.0489	0.0136
Felidae	ML	*Uncia uncia*	47.9	15.6	27.5	21.0	47.3	27.9	21.5	126.3	21.6	-0.0698	-0.0166	-0.0096
Felidae	ML	*Prionailurus viverrinus*	8.3	10.2	17.7	13.1	27.2	16.9	15.0	137.3	13.9	-0.1271	0.0600	0.0247
Felidae	ML	*Puma concolor*	66.8	17.8	28.4	21.7	46.8	27.5	23.6	134.3	23.1	-0.0913	0.0029	0.0142

Family		Species												
Felidae	DL	*Acinonyx jubatus*	40.6	17.4	28.6	17.1	43.7	29.2	36.4	113.4	23.0	0.1988	-0.0103	0.0137
Felidae	DL	*Caracal caracal*	12.7	10.8	18.5	11.2	24.1	18.4	22.9	125.1	14.6	0.1835	0.0080	0.0012
Felidae	DL	*Catopuma temminckii*	13.5	10.1	17.4	10.1	23.8	18.7	21.3	126.1	13.8	0.1841	0.0228	-0.0147
Felidae	DL	*Leopardus wiedii*	6.6	7.1	12.7	8.5	21.2	15.0	15.9	120.3	9.9	0.1607	0.0268	-0.0055
Felidae	DL	*Leopardus pardalis*	11.3	10.4	20.3	11.5	28.9	24.1	22.4	124.3	15.4	0.1747	-0.0185	-0.0252
Felidae	DL	*Felis catus*	4.2	6.4	12.5	7.4	16.7	13.8	14.8	123.8	9.5	0.1578	0.0295	-0.0166
Felidae	DL	*Felis silvestris*	5.5	9.2	16.6	9.4	20.7	19.6	17.7	121.7	12.9	0.1281	-0.0381	-0.0200
Felidae	DL	*Leopardus geoffroyi*	5.9	7.1	13.9	8.0	19.2	15.8	16.2	123.1	10.5	0.1809	-0.0074	-0.0268
Felidae	DL	*Puma yagouaroundi*	7.9	9.2	16.2	9.0	23.6	17.6	24.0	131.3	12.7	0.2244	0.0205	0.0143
Felidae	DL	*Leptailurus serval*	14.8	11.1	20.2	10.7	28.1	22.5	24.5	126.8	15.6	0.2144	-0.0172	-0.0140
Felidae	DL	*Prionailurus viverrinus*	13.8	10.8	17.0	10.4	28.4	19.9	21.8	114.5	13.9	0.1523	0.0004	0.0242
Felidae	DL	*Lynx canadensis*	15.9	11.7	20.0	11.4	27.0	18.8	20.8	129.7	15.9	0.1612	-0.0517	-0.0095
Felidae	DL	*Lynx lynx*	11.2	11.0	18.2	10.3	24.9	17.6	23.7	130.1	14.6	0.1628	0.0116	0.0209
Felidae	DL	*Lynx rufus*	14.2	10.6	19.6	11.5	26.7	19.9	25.1	125.6	15.1	0.1781	0.0109	0.0039
Felidae	DL	*Neofelis nebulosa*	16.5	12.6	21.1	13.3	29.8	26.4	25.5	120.2	16.8	0.1648	0.0121	-0.0020
Felidae	DL	*Panthera tigris*	153.3	26.7	44.1	27.2	63.2	40.9	52.9	124.3	35.4	0.1517	-0.0012	0.0102
Felidae	DL	*Panthera onca*	73.7	19.5	33.6	20.3	48.7	38.7	40.7	123.2	26.5	0.1649	0.0086	-0.0056
Felidae	DL	*Panthera pardus*	52.0	17.9	29.1	17.1	39.5	31.4	39.7	126.5	23.5	0.1813	0.0253	0.0228
Felidae	DL	*Panthera leo*	195.0	29.1	46.1	25.7	58.7	49.1	52.0	105.7	37.6	0.1671	-0.0176	0.0099
Felidae	DL	*Uncia uncia*	44.1	17.0	29.4	16.5	41.7	29.7	30.3	123.8	23.2	0.1381	-0.0249	-0.0161
Felidae	DL	*Prionailurus bengalensis*	2.3	5.1	10.9	6.1	10.9	12.4	14.0	123.7	8.0	0.1959	0.0419	-0.0330
Felidae	DL	*Puma concolor*	69.0	18.6	29.8	18.5	45.9	31.9	41.4	127.6	24.2	0.1965	0.0122	0.0312
Bovidae	PL	*Aepyceros melampus*	45.1	14.2	21.8	19.2	49.8	37.0	17.0	113.3	18.0	0.0885	-0.0291	-0.0239
Bovidae	PL	*Alcelaphus buselaphus*	135.3	22.4	29.8	29.4	75.1	56.7	23.8	98.5	26.1	0.1212	-0.0185	-0.0084
Bovidae	PL	*Antidorcas marsupialis*	32.8	12.5	20.5	18.1	48.0	36.5	16.4	104.1	16.5	0.0838	-0.0294	-0.0165
Bovidae	PL	*Bison bison*	654.4	41.5	52.2	46.8	140.8	87.5	37.0	92.4	46.9	0.1794	0.0553	0.0357
Bovidae	PL	*Bison bonasus*	483.4	37.8	45.7	45.8	114.8	82.8	41.3	98.1	41.7	0.1612	0.0431	0.0229
Bovidae	PL	*Bos taurus*	655.5	42.3	52.4	48.2	131.6	92.7	42.0	90.1	47.4	0.1965	0.0445	0.0592

294

Bovidae	PL	*Bos sauveli*	306.3	29.1	38.5	35.0	122.2	85.1	30.9	94.8	33.8	0.1609	0.0531	-0.0015
Bovidae	PL	*Bos grunniens*	231.3	26.8	39.5	34.4	80.1	71.6	34.4	93.1	33.2	0.1494	0.0405	0.0255
Bovidae	PL	*Bosephalus tragocamelus*	153.6	29.9	38.0	35.2	97.2	90.3	29.6	95.1	34.0	0.1974	0.0472	0.0055
Bovidae	PL	*Bubalus mindorensis*	200.7	24.6	31.7	27.2	74.3	59.9	23.2	97.5	28.2	0.1848	0.0572	-0.0341
Bovidae	PL	*Bubalus depressicornis*	83.8	18.2	25.3	23.4	56.0	42.0	19.9	85.1	21.7	0.1494	0.0464	0.0238
Bovidae	PL	*Philantomba monticola*	4.8	6.6	10.8	11.0	27.8	12.3	12.0	115.0	8.7	-0.0174	-0.0829	0.0351
Bovidae	PL	*Cephalophus dorsalis*	17.8	9.7	16.6	15.8	38.6	23.0	13.4	102.9	13.2	0.0783	-0.0105	0.0033
Bovidae	PL	*Connochaetes taurinus*	196.6	28.5	34.5	32.4	88.4	59.9	27.2	93.0	31.5	0.1524	-0.0034	-0.0085
Bovidae	PL	*Connochaetes gnou*	138.2	24.0	31.1	29.6	62.5	50.6	23.5	92.7	27.5	0.1538	0.0241	-0.0210
Bovidae	PL	*Damaliscus lunatus*	120.7	21.0	28.1	26.8	74.1	47.8	22.7	93.2	24.5	0.1211	0.0083	-0.0189
Bovidae	PL	*Eudorcas thomsonii*	21.4	12.1	18.2	16.2	42.2	39.0	14.8	109.5	15.1	0.1042	-0.0108	-0.0192
Bovidae	PL	*Nanger granti*	52.5	17.4	24.5	21.4	59.1	47.9	19.2	106.1	20.9	0.1278	-0.0129	-0.0312
Bovidae	PL	*Gazella spekei*	16.2	11.5	19.6	17.1	40.7	29.7	16.3	113.8	15.6	0.0755	-0.0228	-0.0434
Bovidae	PL	*Hippotragus niger*	182.2	25.0	34.2	32.5	75.6	63.8	25.8	97.6	29.6	0.1514	-0.0336	-0.0257
Bovidae	PL	*Kobus ellipsiprymnus*	182.4	25.1	33.8	33.8	83.4	57.2	28.6	101.2	29.4	0.1248	-0.0649	-0.0181
Bovidae	PL	*Litocranius walleri*	41.3	13.0	22.2	19.9	48.9	38.8	15.9	106.6	17.6	0.1245	0.0605	-0.0298
Bovidae	PL	*Madoqua kirkii*	5.9	7.3	12.0	10.8	27.5	19.3	11.7	120.6	9.7	0.0486	0.0104	0.0214
Bovidae	PL	*Madoqua saltia*	4.0	6.1	10.5	9.0	24.3	16.3	10.6	120.1	8.3	-0.0169	-0.0739	-0.0117
Bovidae	PL	*Neotragus batesi*	2.6	4.9	8.4	8.3	18.7	12.0	8.5	122.2	6.6	0.0509	-0.0540	0.0092
Bovidae	PL	*Neotragus pygmaeus*	2.0	5.5	7.9	8.2	17.5	12.2	9.9	121.7	6.7	-0.0290	-0.1234	0.0681
Bovidae	PL	*Oreotragus oreotragus*	13.0	7.9	15.8	13.1	29.5	15.8	14.0	114.3	11.9	-0.0114	-0.0324	0.0008
Bovidae	PL	*Oryx dammah*	116.2	23.5	29.9	28.6	77.6	60.2	23.0	96.9	26.7	0.1547	0.0157	-0.0053
Bovidae	PL	*Ourebia ourebi*	18.0	10.0	17.5	15.4	38.6	27.5	15.1	118.5	13.8	0.0842	-0.0256	-0.0287
Bovidae	PL	*Raphicerus campestris*	9.7	8.0	14.0	12.4	30.1	16.8	13.2	125.8	11.0	-0.0058	-0.0545	0.0135
Bovidae	PL	*Raphicerus sharpei*	8.4	8.1	13.6	11.7	30.6	21.9	12.8	121.3	10.9	0.0340	-0.0492	-0.0146
Bovidae	PL	*Redunca arundinum*	55.5	14.3	23.3	18.3	53.1	42.6	18.3	114.4	18.8	0.0933	-0.0086	-0.0235
Bovidae	PL	*Sylvicapra grimmia*	15.6	10.2	17.0	14.4	43.6	24.0	16.4	110.7	13.6	0.0089	-0.0359	-0.0307
Bovidae	PL	*Syncerus caffer*	647.2	37.4	47.5	42.6	100.8	103.5	38.6	90.7	42.5	0.1571	0.0283	0.0345

Bovidae	PL	*Taurotragus oryx*	536.0	41.1	48.3	42.5	122.1	107.2	38.2	92.5	44.7	0.1780	0.0585	0.0246
Bovidae	PL	*Tragelaphus eurycerus*	211.1	28.2	40.1	33.6	107.7	71.7	32.0	97.3	34.1	0.1422	0.0475	0.0132
Bovidae	ML	*Aepyceros melampus*	45.1	14.7	23.3	19.5	51.4	53.1	14.0	119.5	19.0	0.0808	-0.0217	-0.0342
Bovidae	ML	*Alcelaphus buselaphus*	135.3	23.6	31.1	27.8	71.0	76.7	25.0	101.7	27.3	0.1223	-0.0121	-0.0215
Bovidae	ML	*Antidorcas marsupialis*	32.8	13.1	21.5	18.3	44.5	48.0	19.1	109.0	17.3	0.0689	-0.0157	-0.0199
Bovidae	ML	*Bison bison*	587.1	39.3	49.7	45.7	124.6	127.4	40.3	102.7	44.5	0.1519	0.0595	0.0419
Bovidae	ML	*Bison bonasus*	483.4	39.3	48.8	45.7	117.7	120.5	43.7	111.3	44.1	0.1287	0.0666	0.0320
Bovidae	ML	*Bos taurus*	655.5	45.6	59.2	53.0	125.6	172.6	52.0	94.1	52.4	0.1758	0.0192	0.0497
Bovidae	ML	*Bos sauveli*	306.3	30.6	42.6	36.6	120.7	146.1	39.3	101.9	36.6	0.0903	0.0619	0.0020
Bovidae	ML	*Bos grunniens*	231.3	29.5	39.8	36.4	76.1	106.0	38.3	99.6	34.7	0.0974	-0.0281	0.0071
Bovidae	ML	*Bosephalus tragocamelus*	153.6	30.6	39.0	37.1	99.1	102.1	35.3	104.2	34.8	0.1074	-0.0142	0.0031
Bovidae	ML	*Bubalus depressicornis*	83.8	19.6	29.3	26.0	60.7	81.8	24.2	96.2	24.5	0.0966	0.0598	0.0277
Bovidae	ML	*Cephalophus dorsalis*	17.8	9.9	17.6	15.3	38.5	34.2	18.5	111.7	13.7	0.0134	-0.0534	0.0026
Bovidae	ML	*Philantomba monticola*	4.7	7.1	11.8	11.6	25.7	20.3	14.2	126.6	9.5	-0.0342	-0.0675	0.0470
Bovidae	ML	*Connochaetes taurinus*	196.6	29.8	37.1	34.9	88.1	98.7	32.1	101.8	33.5	0.1329	0.0336	0.0059
Bovidae	ML	*Connochaetes gnou*	138.2	24.0	31.8	28.6	61.3	69.9	24.4	98.0	27.9	0.1519	0.0205	-0.0166
Bovidae	ML	*Damaliscus lunatus*	120.7	22.1	31.1	28.6	74.5	74.6	27.4	102.2	26.6	0.0953	-0.0041	-0.0077
Bovidae	ML	*Eudorcas thomsonii*	21.4	12.5	18.8	16.8	43.5	44.8	17.9	114.3	15.6	0.0790	0.0005	0.0192
Bovidae	ML	*Nanger granti*	51.3	17.8	25.8	21.3	55.8	62.4	21.5	115.6	21.8	0.1202	0.0141	-0.0177
Bovidae	ML	*Gazella spekei*	17.1	12.3	20.0	17.1	42.5	40.7	17.8	117.3	16.2	0.0402	-0.0439	-0.0193
Bovidae	ML	*Hippotragus niger*	182.2	24.9	36.2	31.6	75.5	85.4	29.5	104.0	30.5	0.1252	-0.0272	-0.0129
Bovidae	ML	*Kobus ellipsiprymnus*	182.4	26.5	36.5	33.4	82.9	83.6	35.8	107.7	31.5	0.0707	-0.0553	0.0259
Bovidae	ML	*Litocranius walleri*	41.3	13.3	22.8	20.8	49.7	49.6	19.2	117.0	18.1	0.1008	0.0596	-0.0072
Bovidae	ML	*Madoqua kirkii*	5.9	7.4	12.7	10.7	26.9	26.6	13.1	127.6	10.1	0.0105	-0.0500	0.0186
Bovidae	ML	*Madoqua saltia*	4.0	6.6	11.0	9.2	22.3	24.0	12.7	126.3	8.8	-0.0326	-0.0487	0.0080
Bovidae	ML	*Neotragus batesi*	2.7	4.9	9.2	8.9	18.1	16.7	10.6	125.2	7.0	-0.0125	-0.0514	0.0362
Bovidae	ML	*Neotragus pygmaeus*	2.0	5.3	8.3	7.9	17.7	14.5	10.3	122.1	6.8	-0.0248	-0.1168	0.0223
Bovidae	ML	*Oreotragus oreotragus*	14.4	8.9	15.8	13.4	30.1	31.0	16.2	117.1	12.4	-0.0158	-0.0383	0.0083

Bovidae														
Bovidae	Oryx dammah	ML	113.0	24.5	30.3	30.6	74.8	85.5	27.3	97.1	27.4	0.1512	-0.0155	0.0143
Bovidae	Ourebia ourebi	ML	17.3	10.6	19.4	15.9	38.1	36.8	16.8	122.1	15.0	0.0601	-0.0360	-0.0145
Bovidae	Raphicerus campestris	ML	9.7	8.4	15.2	12.4	29.6	29.9	16.2	127.2	11.8	-0.0674	-0.0698	0.0250
Bovidae	Raphicerus sharpei	ML	8.4	8.5	14.6	12.3	30.6	28.6	15.1	121.1	11.5	0.0022	-0.0441	-0.0101
Bovidae	Redunca arundinum	ML	55.5	15.4	24.9	21.4	54.5	55.3	21.5	119.9	20.2	0.0620	-0.0310	-0.0199
Bovidae	Sylvicapra grimmia	ML	14.2	10.5	18.2	15.8	40.0	32.8	18.4	121.6	14.3	0.0145	-0.0401	-0.0050
Bovidae	Syncerus caffer	ML	647.2	38.9	50.9	47.5	101.3	162.7	39.9	90.7	44.9	0.1387	0.0395	-0.0024
Bovidae	Taurotragus oryx	ML	502.9	39.6	51.6	45.2	124.6	147.7	41.4	92.4	45.6	0.1415	0.0458	0.0460
Bovidae	Tragelaphus eurycerus	ML	215.9	29.3	44.1	36.0	107.3	96.1	41.6	107.9	36.7	0.0620	-0.0116	0.0239
Bovidae	Aepyceros melampus	DL	45.1	12.4	33.1	17.1	44.5	48.1	34.9	114.4	22.8	-0.1887	0.0520	-0.0099
Bovidae	Alcelaphus buselaphus	DL	135.3	20.7	43.4	27.3	65.8	69.1	47.2	102.5	32.0	-0.1881	-0.0103	0.0066
Bovidae	Antidorcas marsupialis	DL	32.8	10.8	29.9	16.7	35.4	39.0	34.7	112.4	20.3	-0.2224	-0.0235	0.0102
Bovidae	Bison bison	DL	667.9	36.6	72.5	47.7	111.2	144.7	61.6	96.9	54.5	-0.0362	0.0838	0.0588
Bovidae	Bison bonasus	DL	483.4	37.7	72.3	47.9	96.4	132.9	65.5	101.2	55.0	-0.0556	0.0930	0.0375
Bovidae	Bos sauveli	DL	306.3	25.3	56.5	31.2	99.9	99.1	58.3	94.5	40.9	-0.1656	0.0598	0.0192
Bovidae	Bos grunniens	DL	231.3	26.4	52.9	31.9	69.2	74.7	60.3	96.0	39.7	-0.1907	-0.0080	0.0037
Bovidae	Boselaphus tragocamelus	DL	153.6	22.0	53.6	34.5	87.3	67.7	59.5	97.8	37.8	-0.1995	0.0379	-0.0078
Bovidae	Bubalus mindorensis	DL	200.7	23.9	50.3	28.5	69.1	107.8	43.2	91.9	37.1	-0.1380	0.0907	-0.0361
Bovidae	Bubalus depressicornis	DL	83.8	17.9	34.8	24.2	54.9	58.1	36.9	94.7	26.4	-0.1406	0.0451	0.0072
Bovidae	Philantomba monticola	DL	4.7	6.4	16.1	10.6	23.3	19.8	19.1	122.3	11.3	-0.2193	0.0070	0.0196
Bovidae	Cephalophus dorsalis	DL	17.8	9.1	23.3	15.5	37.7	35.2	26.6	115.0	16.2	-0.2041	0.0021	-0.0077
Bovidae	Connochaetes taurinus	DL	196.6	26.5	52.6	34.0	78.5	87.9	53.6	98.1	39.5	-0.1153	0.0591	0.0091
Bovidae	Connochaetes gnou	DL	138.2	20.7	43.4	27.0	52.0	60.5	41.1	99.6	32.1	-0.1108	0.0324	-0.0139
Bovidae	Damaliscus lunatus	DL	123.5	20.7	43.0	27.8	64.8	68.2	46.7	97.5	31.9	-0.1635	0.0004	0.0054
Bovidae	Nanger granti	DL	52.5	15.9	40.5	21.0	52.1	54.7	41.1	110.6	28.2	-0.1853	0.0385	-0.0260
Bovidae	Eudorcas thomsonii	DL	21.4	11.3	25.6	14.7	37.4	39.5	30.0	114.1	18.4	-0.2007	0.0083	0.0057
Bovidae	Gazella spekei	DL	17.4	11.7	28.2	16.6	40.3	40.4	29.6	114.4	20.0	-0.1785	0.0171	-0.0238
Bovidae	Hippotragus niger	DL	182.2	22.6	52.3	30.9	75.7	75.4	56.4	100.6	37.4	-0.1960	-0.0024	0.0047

Bovidae	DL	*Kobus ellipsiprymnus*	177.4	22.1	51.4	29.6	74.0	69.2	56.1	116.7	36.8	-0.1667	-0.0416	-0.0157
Bovidae	DL	*Litocranius walleri*	41.3	11.3	29.6	18.9	42.7	39.5	38.4	121.0	20.5	-0.2220	0.0041	0.0160
Bovidae	DL	*Madoqua kirkii*	5.9	6.9	18.1	10.2	25.0	25.7	18.5	120.9	12.5	-0.2051	0.0366	-0.0307
Bovidae	DL	*Madoqua saltia*	4.0	5.9	15.3	9.0	21.3	21.8	18.1	122.3	10.6	-0.2231	0.0046	0.0039
Bovidae	DL	*Neotragus batesi*	2.7	4.1	11.9	6.9	15.2	15.1	13.6	119.7	8.0	-0.2256	0.0134	-0.0297
Bovidae	DL	*Neotragus pygmaeus*	2.0	4.2	9.9	6.1	.	14.3	13.2	123.4	7.0	-0.2416	-0.0124	0.0446
Bovidae	DL	*Oreotragus oreotragus*	14.4	8.0	22.0	12.3	27.2	28.3	22.3	121.4	15.0	-0.1711	-0.0037	-0.0358
Bovidae	DL	*Oryx dammah*	116.2	21.5	48.9	27.6	81.5	74.0	47.7	91.2	35.2	-0.1494	0.0426	-0.0273
Bovidae	DL	*Ourebia ourebi*	17.0	8.9	24.4	14.4	31.7	30.4	27.2	121.5	16.6	-0.2180	0.0006	-0.0029
Bovidae	DL	*Raphicerus campestris*	9.7	7.8	20.4	11.1	25.6	23.8	22.2	121.4	14.1	-0.2241	-0.0143	-0.0088
Bovidae	DL	*Raphicerus sharpei*	8.4	7.6	19.1	10.5	27.7	26.1	20.8	116.5	13.4	-0.2354	0.0413	-0.0251
Bovidae	DL	*Redunca arundinum*	55.5	15.2	34.3	20.7	50.0	45.5	39.3	122.9	24.8	-0.1874	-0.0189	-0.0056
Bovidae	DL	*Sylvicapra grimmia*	14.2	8.8	23.6	13.9	34.1	29.6	25.6	114.5	16.2	-0.2063	0.0214	-0.0116
Bovidae	DL	*Syncerus caffer*	647.2	34.8	68.0	44.6	103.9	145.9	63.8	97.0	51.4	-0.0855	0.0538	0.0020
Bovidae	DL	*Taurotragus oryx*	536.0	33.1	71.7	47.0	112.5	111.4	68.1	99.9	52.4	-0.0926	0.0269	0.0175
Bovidae	DL	*Tragelaphus eurycerus*	211.1	26.8	55.3	37.1	108.9	82.9	61.0	110.0	41.1	-0.1174	0.0385	0.0469

298

APPENDIX 7. PC scores from 2D landmarks of Equidae and Bovidae pooled

CS, centroid size. PL, proximal lumbar; ML, middle lumbar; DL, distal lumbar.

Family	Position	Species	CS	PC1	PC2	PC3	PC4	PC5	PC6	PC7	PC8	PC9	PC10
Bovidae	PL	Aepyceros melampus	99.29	0.0864	-0.0122	-0.0005	-0.0049	-0.0294	0.0180	0.0085	-0.0024	0.0039	-0.0001
Bovidae	PL	Alcelaphus buselaphus	143.26	0.1172	-0.0089	-0.0002	0.0231	-0.0143	-0.0062	0.0094	-0.0061	0.0035	0.0042
Bovidae	PL	Antidorcas marsupialis	91.12	0.0816	-0.0137	0.0084	-0.0082	-0.0246	0.0207	0.0016	0.0050	-0.0089	0.0099
Bovidae	PL	Bison bison	257.37	0.1679	0.0045	-0.0484	0.0061	0.0546	0.0143	0.0187	-0.0169	0.0024	0.0014
Bovidae	PL	Bison bonasus	225.73	0.1486	0.0069	-0.0046	0.0236	0.0202	0.0063	-0.0187	0.0181	0.0002	0.0028
Bovidae	PL	Bos taurus	268.59	0.1833	-0.0245	-0.0489	-0.0177	0.0827	0.0111	-0.0049	-0.0230	0.0023	0.0024
Bovidae	PL	Bos sauveli	182.69	0.1476	0.0069	-0.0478	0.0070	0.0130	-0.0039	-0.0077	0.0101	0.0053	0.0049
Bovidae	PL	Bos grunniens	187.04	0.1346	-0.0137	-0.0415	-0.0163	0.0415	0.0046	-0.0098	0.0078	0.0017	0.0154
Bovidae	PL	Bosephalus tragocamelus	186.94	0.1841	-0.0090	-0.0576	0.0106	0.0167	0.0007	0.0019	0.0190	-0.0040	0.0021
Bovidae	PL	Bubalus mindorensis	153.12	0.1723	0.0033	-0.0766	0.0019	-0.0108	-0.0275	-0.0106	0.0081	0.0011	0.0021
Bovidae	PL	Bubalus depressicornis	124.94	0.1346	-0.0193	-0.0592	0.0029	0.0359	0.0034	0.0045	0.0112	0.0043	-0.0033
Bovidae	PL	Philantomba monticola	53.60	-0.0219	-0.0718	0.0437	0.0029	0.0023	-0.0058	-0.0005	0.0126	0.0013	0.0053
Bovidae	PL	Cephalophus dorsalis	77.61	0.0651	-0.0437	-0.0185	-0.0058	-0.0074	0.0050	0.0032	0.0251	-0.0083	0.0123
Bovidae	PL	Connochaetes taurinus	169.13	0.1446	-0.0102	-0.0186	0.0278	-0.0041	-0.0223	-0.0091	-0.0137	-0.0028	-0.0027
Bovidae	PL	Connochaetes gnou	147.68	0.1454	0.0075	-0.0354	0.0216	-0.0118	-0.0187	0.0071	-0.0012	-0.0003	0.0014
Bovidae	PL	Damaliscus lunatus	131.68	0.1145	0.0037	-0.0166	0.0233	-0.0174	-0.0186	-0.0028	0.0023	0.0061	0.0010
Bovidae	PL	Eudorcas thomsonii	83.09	0.0965	-0.0162	-0.0109	-0.0083	-0.0207	0.0078	-0.0042	0.0080	-0.0043	-0.0091
Bovidae	PL	Nanger granti	113.93	0.1224	-0.0102	-0.0191	0.0006	-0.0250	-0.0018	-0.0124	-0.0109	0.0026	0.0007
Bovidae	PL	Gazella spekei	86.07	0.0699	-0.0151	-0.0107	-0.0440	-0.0369	0.0105	-0.0198	0.0057	0.0240	-0.0080
Bovidae	PL	Hippotragus niger	168.65	0.1469	-0.0283	-0.0137	-0.0045	-0.0257	-0.0031	0.0098	-0.0142	0.0005	0.0016
Bovidae	PL	Kobus ellipsiprymnus	168.37	0.1250	-0.0412	0.0048	0.0053	-0.0248	0.0093	-0.0090	-0.0212	-0.0029	0.0052
Bovidae	PL	Litocranius walleri	94.21	0.1127	0.0209	-0.0494	-0.0333	-0.0114	0.0256	0.0005	0.0237	0.0050	-0.0021

Family	Code	Species											
Bovidae	PL	*Madoqua kirkii*	54.83	0.0355	-0.0263	-0.0075	-0.0215	0.0163	0.0059	0.0024	0.0269	0.0067	-0.0081
Bovidae	PL	*Madoqua saltia*	48.53	-0.0194	-0.0450	0.0243	-0.0302	-0.0207	0.0112	-0.0306	-0.0091	0.0273	-0.0222
Bovidae	PL	*Neotragus batesi*	41.64	0.0401	-0.0753	-0.0006	-0.0396	-0.0030	-0.0072	0.0060	0.0086	0.0098	-0.0135
Bovidae	PL	*Neotragus pygmaeus*	42.05	-0.0333	-0.1161	0.0598	0.0320	0.0097	0.0096	0.0391	0.0100	-0.0104	-0.0062
Bovidae	PL	*Oreotragus oreotragus*	67.81	-0.0131	-0.0129	0.0242	-0.0263	-0.0073	0.0079	-0.0040	0.0103	0.0060	-0.0020
Bovidae	PL	*Oryx dammah*	146.47	0.1458	-0.0072	-0.0253	0.0062	0.0004	-0.0093	-0.0008	0.0038	0.0082	-0.0090
Bovidae	PL	*Ourebia ourebi*	80.87	0.0764	-0.0371	-0.0239	-0.0393	-0.0251	0.0005	-0.0023	0.0068	0.0018	-0.0042
Bovidae	PL	*Raphicerus campestris*	64.20	-0.0054	-0.0277	0.0398	-0.0162	-0.0063	0.0184	0.0116	0.0090	-0.0094	-0.0019
Bovidae	PL	*Raphicerus sharpei*	62.97	0.0273	-0.0448	0.0007	-0.0243	-0.0235	0.0111	-0.0057	0.0033	0.0041	-0.0184
Bovidae	PL	*Redunca arundinum*	104.42	0.0904	-0.0040	-0.0049	-0.0225	-0.0231	0.0048	0.0087	0.0118	0.0046	-0.0026
Bovidae	PL	*Sylvicapra grimmia*	78.71	0.0013	-0.0256	-0.0094	0.0106	-0.0437	0.0308	-0.0109	0.0024	0.0102	-0.0017
Bovidae	PL	*Syncerus caffer*	238.79	0.1472	-0.0100	-0.0277	0.0134	0.0412	0.0010	0.0140	-0.0101	-0.0006	-0.0037
Bovidae	PL	*Taurotragus oryx*	241.57	0.1662	0.0168	-0.0350	0.0320	0.0356	0.0055	0.0039	-0.0043	0.0100	-0.0021
Bovidae	PL	*Tragelaphus eurycerus*	187.65	0.1292	-0.0108	-0.0567	-0.0101	0.0294	0.0207	-0.0029	-0.0001	-0.0044	-0.0054
Bovidae	ML	*Aepyceros melampus*	107.12	0.0735	-0.0240	-0.0220	-0.0128	-0.0328	0.0093	-0.0069	-0.0112	0.0075	-0.0009
Bovidae	ML	*Alcelaphus buselaphus*	149.75	0.1163	-0.0076	-0.0138	0.0240	-0.0234	-0.0115	0.0070	-0.0080	0.0059	0.0043
Bovidae	ML	*Antidorcas marsupialis*	96.95	0.0606	-0.0163	-0.0077	-0.0053	-0.0228	0.0018	-0.0025	0.0021	-0.0008	0.0104
Bovidae	ML	*Bison bison*	241.08	0.1378	0.0119	-0.0347	0.0199	0.0558	0.0079	0.0006	-0.0008	0.0081	0.0023
Bovidae	ML	*Bison bonasus*	234.91	0.1163	0.0176	-0.0172	0.0349	0.0320	0.0031	-0.0139	0.0168	0.0028	0.0056
Bovidae	ML	*Bos taurus*	295.70	0.1628	-0.0279	-0.0072	-0.0041	0.0591	-0.0014	-0.0510	0.0042	-0.0028	0.0071
Bovidae	ML	*Bos sauveli*	201.76	0.0754	0.0048	-0.0528	0.0350	0.0039	-0.0035	0.0027	0.0213	0.0162	0.0104
Bovidae	ML	*Bos grunniens*	199.50	0.0837	-0.0526	-0.0130	0.0173	-0.0048	-0.0056	-0.0083	-0.0078	0.0001	0.0038
Bovidae	ML	*Bosephalus tragocamelus*	191.08	0.1000	-0.0246	-0.0084	0.0387	-0.0083	-0.0005	-0.0092	0.0061	0.0046	-0.0098
Bovidae	ML	*Bubalus depressicornis*	132.27	0.0787	0.0126	-0.0392	0.0008	0.0429	0.0211	-0.0077	0.0202	0.0058	0.0075
Bovidae	ML	*Cephalophus dorsalis*	83.51	0.0029	-0.0602	-0.0001	0.0089	-0.0189	0.0164	-0.0002	-0.0016	0.0043	0.0083
Bovidae	ML	*Philantomba monticola*	59.28	-0.0433	-0.0724	0.0338	0.0164	0.0140	-0.0114	0.0081	0.0070	0.0099	0.0078
Bovidae	ML	*Connochaetes taurinus*	178.61	0.1221	0.0012	-0.0241	0.0379	0.0070	-0.0225	-0.0136	0.0019	-0.0012	-0.0030
Bovidae	ML	*Connochaetes gnou*	151.62	0.1440	0.0071	-0.0230	0.0223	-0.0115	-0.0206	0.0038	0.0005	0.0021	0.0057

Family		Species											
Bovidae	ML	*Damaliscus lunatus*	146.35	0.0868	-0.0060	-0.0041	0.0245	-0.0148	-0.0036	-0.0028	0.0060	0.0061	0.0067
Bovidae	ML	*Eudorcas thomsonii*	89.47	0.0678	-0.0276	-0.0071	0.0117	0.0096	0.0031	-0.0088	0.0152	0.0000	0.0009
Bovidae	ML	*Nanger granti*	118.09	0.1108	-0.0006	-0.0213	0.0068	-0.0105	-0.0091	-0.0170	-0.0003	0.0038	0.0041
Bovidae	ML	*Gazella spekei*	90.60	0.0385	-0.0204	0.0112	-0.0030	-0.0291	0.0134	-0.0160	0.0040	0.0007	-0.0079
Bovidae	ML	*Hippotragus niger*	175.37	0.1197	-0.0264	-0.0097	0.0009	-0.0154	0.0051	0.0049	-0.0075	-0.0008	0.0028
Bovidae	ML	*Kobus ellipsiprymnus*	180.92	0.0702	-0.0453	0.0335	0.0253	0.0002	0.0110	-0.0101	-0.0029	0.0002	0.0066
Bovidae	ML	*Litocranius walleri*	99.88	0.0844	0.0005	-0.0537	-0.0215	0.0080	0.0154	-0.0083	0.0240	0.0119	0.0008
Bovidae	ML	*Madoqua kirkii*	60.32	0.0037	-0.0525	0.0149	-0.0123	0.0030	-0.0114	0.0077	0.0075	-0.0053	0.0070
Bovidae	ML	*Madoqua saltia*	53.48	-0.0441	-0.0578	0.0082	-0.0047	-0.0107	-0.0058	-0.0066	0.0061	0.0039	-0.0016
Bovidae	ML	*Neotragus batesi*	45.34	-0.0237	-0.0766	0.0172	-0.0199	0.0107	-0.0072	0.0053	0.0180	0.0063	0.0058
Bovidae	ML	*Neotragus pygmaeus*	42.30	-0.0341	-0.1102	0.0309	0.0157	-0.0220	0.0070	0.0127	0.0017	-0.0097	-0.0063
Bovidae	ML	*Oreotragus oreotragus*	70.03	-0.0217	-0.0328	0.0172	-0.0001	-0.0092	0.0143	-0.0124	0.0196	-0.0072	0.0013
Bovidae	ML	*Oryx dammah*	160.15	0.1407	-0.0375	-0.0075	0.0140	0.0080	-0.0162	0.0014	-0.0001	0.0049	0.0033
Bovidae	ML	*Ourebia ourebi*	87.39	0.0520	-0.0423	-0.0087	-0.0361	-0.0158	0.0024	-0.0024	-0.0005	-0.0050	0.0063
Bovidae	ML	*Raphicerus campestris*	71.25	-0.0711	-0.0496	0.0400	0.0077	-0.0042	0.0085	0.0030	0.0022	0.0147	0.0061
Bovidae	ML	*Raphicerus sharpei*	66.87	-0.0090	-0.0494	-0.0049	-0.0044	-0.0243	0.0001	0.0009	0.0009	-0.0022	-0.0027
Bovidae	ML	*Redunca arundinum*	112.39	0.0550	-0.0292	-0.0084	-0.0069	-0.0246	-0.0070	0.0030	-0.0002	-0.0009	0.0007
Bovidae	ML	*Sylvicapra grimmia*	84.74	0.0043	-0.0467	-0.0048	-0.0028	-0.0200	0.0111	0.0044	0.0043	0.0057	0.0088
Bovidae	ML	*Syncerus caffer*	241.92	0.1273	0.0070	-0.0380	0.0182	0.0094	-0.0116	-0.0005	-0.0045	0.0040	-0.0021
Bovidae	ML	*Taurotragus oryx*	251.73	0.1302	0.0013	-0.0196	0.0172	0.0490	0.0166	0.0192	-0.0095	0.0024	0.0027
Bovidae	ML	*Tragelaphus eurycerus*	206.78	0.0532	-0.0304	-0.0079	0.0144	0.0174	0.0288	-0.0159	-0.0050	-0.0052	0.0007
Bovidae	DL	*Aepyceros melampus*	126.08	-0.1996	0.0093	-0.0531	-0.0077	0.0002	-0.0035	0.0057	0.0064	0.0033	0.0034
Bovidae	DL	*Alcelaphus buselaphus*	172.77	-0.1968	0.0012	0.0032	0.0302	-0.0042	-0.0024	0.0043	-0.0109	0.0050	-0.0069
Bovidae	DL	*Antidorcas marsupialis*	120.19	-0.2317	-0.0160	0.0054	-0.0020	0.0006	0.0080	-0.0055	-0.0068	-0.0049	0.0047
Bovidae	DL	*Bison bison*	289.67	-0.0519	0.0207	-0.0516	-0.0187	0.0813	0.0323	0.0285	-0.0230	-0.0098	0.0025
Bovidae	DL	*Bison bonasus*	278.47	-0.0723	0.0236	-0.0723	0.0101	0.0558	0.0303	0.0217	-0.0044	-0.0015	0.0008
Bovidae	DL	*Bos taurus*	301.73	-0.1155	0.0023	-0.0432	0.0168	0.0623	0.0119	-0.0255	0.0297	-0.0075	-0.0034
Bovidae	DL	*Bos sauveli*	218.85	-0.1764	0.0316	-0.0288	0.0131	0.0277	0.0057	0.0002	0.0018	-0.0044	0.0021

Bovidae	DL	Bos grunniens	212.86	-0.1977	0.0118	0.0095	0.0266	-0.0027	-0.0135	-0.0109	-0.0096	0.0040	-0.0058
Bovidae	DL	Bosephalus tragocamelus	202.90	-0.2100	0.0060	-0.0410	0.0136	-0.0080	0.0036	-0.0024	0.0109	-0.0002	0.0030
Bovidae	DL	Bubalus mindorensis	175.59	-0.1485	0.0797	-0.0469	0.0143	-0.0133	0.0104	-0.0155	0.0169	-0.0136	-0.0009
Bovidae	DL	Bubalus depressicornis	138.00	-0.1524	0.0153	-0.0297	0.0315	0.0063	-0.0097	-0.0074	0.0172	-0.0126	-0.0086
Bovidae	DL	Philantomba monticola	66.50	-0.2281	-0.0032	-0.0010	0.0106	0.0077	-0.0066	0.0146	0.0041	0.0127	0.0085
Bovidae	DL	Cephalophus dorsalis	93.37	-0.2139	-0.0117	-0.0242	0.0072	-0.0150	-0.0042	0.0123	0.0062	-0.0019	0.0041
Bovidae	DL	Connochaetes taurinus	206.78	-0.1282	0.0110	-0.0520	0.0200	0.0171	-0.0107	0.0003	0.0039	-0.0055	-0.0066
Bovidae	DL	Connochaetes gnou	169.90	-0.1231	0.0120	-0.0408	0.0055	-0.0049	-0.0135	0.0142	-0.0031	-0.0083	0.0029
Bovidae	DL	Damaliscus lunatus	175.14	-0.1739	-0.0039	-0.0117	0.0156	0.0012	-0.0080	0.0030	-0.0074	0.0018	-0.0086
Bovidae	DL	Nanger granti	148.43	-0.1961	0.0186	-0.0413	-0.0095	-0.0127	-0.0044	-0.0111	-0.0016	-0.0062	-0.0021
Bovidae	DL	Eudorcas thomsonii	103.18	-0.2106	-0.0093	-0.0210	0.0206	-0.0011	-0.0090	-0.0032	0.0036	-0.0095	-0.0098
Bovidae	DL	Gazella spekei	108.06	-0.1883	0.0077	-0.0298	-0.0061	-0.0168	-0.0067	-0.0049	-0.0086	0.0053	0.0029
Bovidae	DL	Hippotragus niger	207.10	-0.2039	0.0028	0.0010	0.0064	-0.0037	-0.0004	0.0173	-0.0028	-0.0061	-0.0010
Bovidae	DL	Kobus ellipsiprymnus	205.51	-0.1775	-0.0281	-0.0066	0.0147	-0.0249	-0.0019	-0.0089	-0.0278	-0.0045	0.0095
Bovidae	DL	Litocranius walleri	121.97	-0.2329	-0.0281	-0.0266	0.0180	0.0050	0.0079	-0.0111	0.0095	-0.0037	-0.0022
Bovidae	DL	Madoqua kirkii	67.95	-0.2154	0.0216	-0.0450	-0.0063	-0.0191	0.0024	0.0031	-0.0034	0.0033	0.0089
Bovidae	DL	Madoqua saltia	61.46	-0.2311	-0.0075	-0.0114	0.0097	-0.0083	-0.0065	0.0133	0.0135	0.0006	0.0079
Bovidae	DL	Neotragus batesi	46.62	-0.2329	0.0108	-0.0291	-0.0070	-0.0288	0.0151	0.0035	0.0036	0.0043	0.0065
Bovidae	DL	Neotragus pygmaeus	43.45	-0.2475	-0.0020	0.0347	0.0263	0.0217	-0.0029	-0.0014	0.0101	0.0190	0.0142
Bovidae	DL	Oreotragus oreotragus	83.46	-0.1802	0.0059	-0.0257	-0.0241	-0.0251	0.0016	-0.0093	-0.0167	0.0096	0.0102
Bovidae	DL	Oryx dammah	182.62	-0.1603	0.0267	-0.0389	-0.0064	-0.0135	-0.0015	-0.0074	0.0028	-0.0049	-0.0078
Bovidae	DL	Ourebia ourebi	97.21	-0.2265	-0.0069	-0.0155	-0.0020	-0.0091	0.0029	0.0097	0.0008	0.0077	0.0012
Bovidae	DL	Raphicerus campestris	77.85	-0.2327	-0.0035	-0.0087	0.0034	-0.0130	-0.0027	0.0017	-0.0084	-0.0119	0.0008
Bovidae	DL	Raphicerus sharpei	71.62	-0.2431	0.0311	-0.0369	0.0161	-0.0183	-0.0120	0.0024	-0.0025	0.0030	0.0069
Bovidae	DL	Redunca arundinum	139.63	-0.1989	-0.0263	-0.0184	0.0106	-0.0135	-0.0064	0.0037	-0.0151	-0.0056	-0.0059
Bovidae	DL	Sylvicapra grimmia	89.72	-0.2154	0.0104	-0.0252	-0.0022	-0.0080	-0.0040	-0.0040	0.0032	-0.0045	0.0066
Bovidae	DL	Syncerus caffer	268.89	-0.0991	0.0224	-0.0445	-0.0098	0.0230	0.0030	-0.0191	-0.0045	-0.0073	-0.0003
Bovidae	DL	Taurotragus oryx	281.53	-0.1052	-0.0042	-0.0289	-0.0127	0.0213	0.0161	0.0115	-0.0031	-0.0062	-0.0002

Family	Code	Species											
Bovidae	DL	*Tragelaphus euryceros*	227.43	-0.1313	-0.0071	-0.0180	0.0051	0.0443	0.0330	-0.0188	0.0111	-0.0045	0.0025
Equidae	PL	*Equus grevyi*	192.04	0.1529	0.0742	0.0442	0.0275	0.0015	-0.0090	0.0022	-0.0024	-0.0069	0.0060
Equidae	PL	*Equus burchellii*	168.01	0.1389	0.0644	0.0416	0.0151	-0.0072	-0.0047	0.0118	0.0072	-0.0024	-0.0015
Equidae	PL	*Equus caballus*	180.39	0.1657	0.0676	0.0034	-0.0003	-0.0280	0.0070	0.0189	0.0021	-0.0160	-0.0039
Equidae	PL	*Equus zebra*	159.05	0.0871	0.0945	0.0327	0.0333	-0.0330	0.0128	0.0157	0.0172	-0.0135	-0.0078
Equidae	PL	*Equus kiang*	154.44	0.1188	0.0702	0.0173	0.0120	-0.0211	0.0142	0.0046	-0.0003	-0.0017	0.0074
Equidae	ML	*Equus grevyi*	188.61	0.1514	0.0797	0.0363	-0.0091	-0.0136	-0.0117	-0.0013	0.0002	0.0015	0.0148
Equidae	ML	*Equus burchellii*	174.32	0.0774	0.0794	0.0551	-0.0081	-0.0065	0.0062	-0.0017	0.0163	0.0053	0.0011
Equidae	ML	*Equus caballus*	190.32	0.1252	0.0893	0.0185	-0.0039	-0.0335	0.0034	0.0218	0.0117	-0.0042	0.0016
Equidae	ML	*Equus zebra*	158.80	0.0055	0.0941	0.0561	0.0241	-0.0235	-0.0005	0.0097	0.0221	0.0071	0.0166
Equidae	ML	*Equus kiang*	158.74	0.0380	0.1281	0.0212	-0.0327	-0.0210	-0.0019	0.0008	0.0200	0.0133	0.0257
Equidae	DL	*Equus grevyi*	157.13	0.0017	0.0675	0.0353	-0.0459	0.0206	-0.0258	-0.0099	-0.0139	0.0067	0.0100
Equidae	DL	*Equus burchellii*	148.78	-0.0861	0.0448	0.0506	-0.0059	0.0318	-0.0183	-0.0031	-0.0068	0.0002	0.0122
Equidae	DL	*Equus zebra*	167.61	-0.1511	0.0462	0.0466	0.0121	0.0072	-0.0113	0.0038	-0.0156	0.0166	-0.0061
Equidae	DL	*Equus caballus*	169.48	0.0317	0.0478	0.0129	-0.0435	0.0128	-0.0097	0.0050	-0.0206	-0.0086	0.0093
Equidae	DL	*Equus kiang*	139.10	-0.0541	0.0192	0.0627	-0.0219	0.0357	0.0061	-0.0081	-0.0350	0.0076	0.0110
Equidae	DL	*Equus sp.*	179.12	-0.0376	0.0593	0.0267	-0.0373	0.0244	-0.0248	-0.0104	-0.0239	0.0022	0.0046
Equidae	PL	*Equus sp.*	199.14	0.1660	0.0405	0.0028	0.0136	-0.0150	0.0062	0.0151	-0.0139	-0.0132	-0.0082
Equidae	DL	*Hippidion neogaeus*	174.86	-0.0785	0.0762	-0.0238	-0.0660	-0.0062	-0.0396	0.0256	-0.0230	-0.0140	0.0085
Equidae	ML	*Hippidion neogaeus*	204.59	0.1316	0.0339	0.0233	0.0087	-0.0136	-0.0069	0.0338	0.0021	-0.0016	0.0001
Equidae	PL	*Hippidion neogaeus*	201.72	0.1596	0.0589	0.0214	0.0300	-0.0177	0.0022	0.0084	-0.0053	-0.0019	-0.0017
Equidae	DL	*Hyracotherium sp.*	70.99	-0.0725	-0.0478	0.0153	-0.0742	0.0170	-0.0154	0.0312	0.0144	-0.0083	-0.0011
Equidae	ML	*Hyracotherium sp.*	64.35	-0.0663	-0.0431	0.0914	0.0285	0.0311	0.0065	0.0233	0.0170	0.0073	0.0011
Equidae	PL	*Hyracotherium grangeri*	56.45	-0.0801	0.0226	0.0546	-0.0111	-0.0068	0.0233	-0.0023	0.0056	0.0206	-0.0022
Equidae	PL	*Hyracotherium sp.*	44.86	-0.0219	-0.0126	0.1084	0.0314	0.0460	0.0058	-0.0160	0.0068	0.0152	0.0115
Equidae	ML	*Merychippus quartus*	118.39	0.0395	-0.0005	0.0554	-0.0065	0.0293	-0.0332	0.0124	0.0070	-0.0058	0.0118
Equidae	PL	*Merychippus quartus*	108.46	0.0498	0.0466	0.0690	-0.0408	0.0069	0.0237	-0.0078	-0.0358	0.0198	-0.0004
Equidae	PL	*Merychippus isoneus*	128.67	0.0884	0.0688	0.0455	0.0212	0.0049	0.0062	-0.0011	-0.0056	-0.0139	-0.0009

Family		Species											
Equidae	DL	Merychippus sp.	156.77	-0.1416	0.0636	0.0490	-0.0697	0.0221	-0.0214	0.0093	0.0179	-0.0038	-0.0009
Equidae	DL	Merychippus republicanus	95.80	-0.1199	0.0492	0.0003	-0.0277	0.0100	-0.0183	0.0163	-0.0010	0.0002	-0.0038
Equidae	ML	Merychippus campestris	128.20	0.0363	0.0138	0.0437	-0.0344	0.0031	0.0148	-0.0094	-0.0146	-0.0188	0.0063
Equidae	DL	Merychippus proparvulus	122.43	0.0000	0.0453	0.0172	-0.0457	0.0050	-0.0067	0.0134	-0.0175	-0.0055	-0.0044
Equidae	PL	Merychippus proparvulus	122.86	0.1039	0.0755	0.0045	0.0419	-0.0009	0.0059	-0.0063	-0.0348	-0.0031	-0.0051
Equidae	ML	Mesohippus bairdii	80.77	-0.0031	-0.0107	0.0532	-0.0100	0.0091	-0.0057	0.0124	0.0078	-0.0057	-0.0077
Equidae	PL	Mesohippus bairdii	80.28	0.0027	0.0001	0.0743	0.0050	0.0096	0.0081	0.0091	0.0176	-0.0135	-0.0111
Equidae	DL	Mesohippus bairdii	76.41	-0.1178	0.0436	0.0302	-0.0159	0.0101	-0.0073	-0.0109	-0.0027	-0.0028	0.0006
Equidae	DL	Mesohippus sp.	68.64	-0.1345	0.0075	0.0211	-0.0297	0.0126	-0.0013	-0.0025	0.0044	-0.0047	-0.0077
Equidae	ML	Mesohippus sp.	71.00	-0.0478	0.0001	0.0271	-0.0102	0.0164	-0.0030	-0.0094	-0.0078	0.0001	-0.0073
Equidae	PL	Mesohippus sp.	66.45	-0.0469	0.0452	0.0400	0.0319	0.0081	0.0169	-0.0175	-0.0072	-0.0113	-0.0127
Equidae	ML	Mesohippus westoni	72.68	-0.0692	-0.0010	0.0505	0.0352	-0.0093	0.0150	-0.0083	0.0143	-0.0070	-0.0020
Equidae	DL	Mesohippus westoni	69.58	-0.0882	0.0195	0.0045	0.0213	-0.0214	-0.0037	0.0024	-0.0078	-0.0240	-0.0161
Equidae	PL	Parahippus leonensis	92.51	0.0694	0.0345	0.0387	-0.0043	0.0055	0.0054	0.0006	0.0001	-0.0044	-0.0038
Equidae	PL	Parahippus sp.	102.48	0.0765	0.1090	0.0444	-0.0174	-0.0058	0.0105	-0.0217	-0.0137	0.0039	0.0118
Equidae	PL	Parahippus pawniensis	107.33	0.0876	-0.0069	0.0287	0.0049	0.0198	0.0212	0.0018	-0.0220	-0.0104	-0.0005
Equidae	DL	Parahippus leonensis	74.54	-0.0800	0.0164	0.0768	-0.0562	0.0165	0.0122	-0.0074	0.0219	-0.0067	-0.0071
Equidae	ML	Parahippus leonensis	100.20	0.0501	0.0097	0.0262	-0.0263	0.0050	0.0043	-0.0143	-0.0070	-0.0093	-0.0011
Equidae	PL	Pliohippus pernix	137.15	0.0670	0.0425	0.0417	0.0268	-0.0080	0.0032	-0.0138	0.0100	-0.0105	-0.0083
Equidae	ML	Pliohippus pernix	144.98	0.0301	0.0241	0.0280	0.0333	-0.0096	0.0175	-0.0333	-0.0074	-0.0064	-0.0055
Equidae	DL	Pliohippus pernix	129.98	-0.0831	0.0682	0.0362	-0.0131	0.0160	-0.0296	-0.0368	-0.0200	0.0150	-0.0020
Equidae	DL	Archaeohippus blackbergi	77.84	-0.1143	0.0075	0.0576	-0.0282	0.0338	-0.0290	-0.0017	-0.0036	0.0114	-0.0019
Equidae	ML	Archaeohippus blackbergi	83.98	0.0128	0.0013	0.0451	-0.0197	0.0376	0.0266	-0.0165	-0.0345	0.0047	0.0061
Equidae	PL	Nannippus sp.	114.69	0.0951	0.0254	0.0343	-0.0013	-0.0119	-0.0060	0.0030	0.0050	0.0034	-0.0112
Equidae	DL	Nannippus sp.	113.19	-0.0734	-0.0017	0.0242	-0.0402	0.0312	-0.0242	0.0000	-0.0209	0.0139	0.0009

| Equidae | ML | _Nannippus sp._ | 118.44 | 0.1053 | 0.0316 | 0.0339 | -0.0105 | 0.0017 | -0.0013 | 0.0053 | -0.0023 | 0.0024 | -0.0095 |

APPENDIX 8. Process angles and lateral joint shape of Equidae

Pos., vertebral position; PL, proximal lumbar; ML, middle lumbar; PNL, penultimate lumbar; LL, last lumbar; NS, neural spine; TPAP, transverse process anteroposterior angle; TPDV, transverse process dorsoventral angle; LJH, lateral joint height; LJW, lateral joint width; H/W, height/width=shape of the lateral joint. AMNH, Division of Paleontology, American Museum of Natural History, New York; MCZ, Museum of Comparative Zoology, Harvard University, Cambridge, Massachusetts; F:AM, Frick Collection; FM, fossil mammals. USNM, Department of Paleobiology, United States National Museum of Natural History, Smithsonian Institution, Washington, D.C. (except genus *Equus*, which are from the Department of Mammalogy); UF, University of Florida Museum of Natural History, Gainesville; UM, University of Michigan Museum of Paleontology, Ann Arbor; YPM, Peabody Museum of Natural History, Yale University, New Haven, Connecticut.

Genus	Species	Specimen Number	Pos.	NS angle	TP AP	TP DV	LJ H	LJ W	H/W
Archaeohippus	*blackbergii*	UF 211479	LL				10.82	25.34	0.43
Archaeohippus	*blackbergii*	UF 258551	PNL				11.73	14.15	0.83
Archaeohippus	*blackbergii*	UF 259127	PNL				9.43	7.77	1.21
Equus	*burchellii*	USNM 162954	LL				20.13	37.36	0.54
Equus	*burchellii*	USNM 162954	PNL	90	85	90	12.12	22.68	0.53
Equus	*burchellii*	USNM 162955	LL				16.44	41.74	0.39
Equus	*burchellii*	USNM 162955	PNL	80	85	90	16.12	20.82	0.77
Equus	*burchellii*	USNM 162960	LL				19.39	36.75	0.53
Equus	*burchellii*	USNM 162960	PNL	90	75	90	11.50	24.55	0.47
Equus	*burchellii*	USNM 259848	LL				17.47	37.81	0.46
Equus	*burchellii*	USNM 259848	PNL	85	80	90	17.60	27.94	0.63
Equus	*caballus*	USNM 172454	PNL	90	90	90			
Equus	*caballus*	USNM 302898	LL				11.24	11.65	0.97
Equus	*caballus*	USNM 302898	PNL	80	85	90	12.75	13.51	0.94
Equus	*caballus*	USNM 396016	LL				13.16	34.85	0.38
Equus	*caballus*	USNM 396016	PNL	80	80	90	12.89	18.22	0.71

Genus	species	specimen							
Equus	*caballus*	USNM 582088	LL				16.44	40.46	0.41
Equus	*caballus*	USNM 582088	PNL	90	85	90	20.19	19.86	1.02
Equus	*grevyi*	USNM 152231	LL				19.65	33.94	0.58
Equus	*grevyi*	USNM 152231	PNL	90	85	90	17.47	20.12	0.87
Equus	*grevyi*	USNM 163338	PNL	90	80	90	16.20	31.59	0.51
Equus	*grevyi*	USNM A49944	LL				15.59	45.04	0.35
Equus	*grevyi*	USNM A49944	PNL	90	85	90	17.90	25.09	0.71
Equus	*kiang*	USNM 49493	PNL	80	80	90	13.05	19.56	0.67
Equus	*zebra*	USNM 270125	LL				17.06	25.92	0.66
Equus	*zebra*	USNM 270125	PNL	90	85	90			
Equus	sp.	AMNH FM 90887	LL	100	90	90	17.28	51.05	0.34
Equus	sp.	AMNH FM 90887	ML	90	90	90			
Equus	sp.	AMNH FM 90887	PL	85	90	85			
Equus	sp.	AMNH FM 90887	PL		90	85			
Equus	sp.	AMNH FM 90887	PNL	80	90	90	24.96	33.51	0.74
Hippidion	*neogaeus*	AMNH FM 11872	LL	80	85	90	21.32	39.51	0.54
Hippidion	*neogaeus*	AMNH FM 11872	ML	85	85	90			
Hippidion	*neogaeus*	AMNH FM 11872	PL	80	90	90			
Hippidion	*neogaeus*	AMNH FM 11872	PL	85	90	90			
Hyracotherium	*grangeri*	UM 115547	DL	60	65	70			
Hyracotherium	*grangeri*	UM 115547	DL	65	60	70			
Hyracotherium	*grangeri*	UM 115547	ML	60	60				
Hyracotherium	*grangeri*	UM 115547	ML	55	50				
Hyracotherium	*grangeri*	UM 115547	PL	55	50	45			
Hyracotherium	*grangeri*	UM 115547	PL	60	60				
Hyracotherium	sp.	AMNH FM 88338	ML	60					
Hyracotherium	sp.	AMNH FM 144322	PL	65	50	55			
Merychippus	*campestris*	AMNH FM 9096	ML			70			
Merychippus	*proparvulus*	AMNH FM 9394	PNL	70	80	80	9.99	13.80	0.72
Merychippus	*quartus*	AMNH FM 14184	ML	75	75	75			
Merychippus	*republicanus*	AMNH FM 8347	LL				9.90	17.96	0.55
Merychippus	sp.	AMNH F:AM 144325	LL				9.51	18.87	0.50
Mesohippus	sp.	MCZ uncat.	LL				6.35	10.96	0.58
Mesohippus	sp.	MCZ uncat.	LL				5.41	8.24	0.66
Mesohippus	sp.	MCZ uncat.	LL	60			3.90	7.67	0.51
Mesohippus	*bairdii*	YPM 11376	LL	55			8.95	12.43	0.72
Mesohippus	*bairdii*	YPM 13791	PL	70					
Mesohippus	*bairdii*	YPM 13791	PNL				7.52	10.94	0.69
Mesohippus	*bairdii*	USNM 16876	LL				7.28	12.11	0.60
Mesohippus	sp.	USNM 15960	LL	70		80	4.09	8.67	0.47
Mesohippus	sp.	USNM 15960	LL				7.52	15.83	0.48
Mesohippus	sp.	USNM 16815	ML	70		75			
Mesohippus	sp.	USNM 16830	PNL				6.61	6.31	1.05
Mesohippus	*westoni*	AMNH F:AM 74048	ML		70	65			

Mesohippus	*westoni*	AMNH F:AM 74048	ML	65					
Mesohippus	*westoni*	AMNH F:AM 74048	PL	55	70	70			
Nannippus	*minor*	UF 69933	PL	70					
Nannippus	*minor*	UF 201431	LL				11.25	19.34	0.58
Nannippus	*minor*	UF 224207	PNL				11.44	10.70	1.07
Nannippus	*minor*	UF 224215	PL	75	75	100			
Parahippus	sp.	MCZ uncat.	PNL				6.56	7.59	0.86
Parahippus	sp.	MCZ uncat.	ML			70			
Parahippus	*leonensis*	UF 163493	PNL				8.61	9.91	0.87
Parahippus	*leonensis*	UF 172621	PNL				12.45	11.32	1.10
Parahippus	*leonensis*	UF 199217	LL				11.33	22.36	0.51
Parahippus	*leonensis*	UF 255764	LL				11.17	20.60	0.54
Parahippus	*leonensis*	UF 299538	LL				10.40	21.25	0.49
Parahippus	*pawniensis*	AMNH F:AM 71705	PL	60					
Pliohippus	*pernix*	AMNH F:AM 60803	ML	70	80	80			
Pliohippus	*pernix*	AMNH F:AM 60803	ML	75	75	75			
Pliohippus	*pernix*	AMNH F:AM 60803	PL	80					
Pliohippus	*pernix*	AMNH F:AM 60803	PL	75	80	70			
Pliohippus	*pernix*	AMNH F:AM 60803	PNL	80	70	80	11.72	17.99	0.65
Pliohippus	*pernix*	AMNH F:AM 60803	PNL	85	80	80	17.10	28.79	0.59

APPENDIX 9. Craniocaudal variation in centrum dimensions of Equidae

CH, centrum height; CL, centrum length; CW, centrum width; AREA, centrum area.

Height and width are scaled by area. Centrum length is scaled by length of T8 where the

thoracic vertebrae are preserved, or L1 where only lumbars are preserved.

Hyracotherium grangeri UM 115547

Vertebra	CL	CW	CH	AREA	CH/AREA	CW/AREA	CL/T8
T1	12.3	10	6	7.75	0.77	1.29	1.10
T2							
T3	11.2	8.9	5.9	7.25	0.81	1.23	1.00
T4	11.4	8.6	5.4	6.81	0.79	1.26	1.02
T5	10.7	8.5					0.96
T6	11	8.7					0.98
T7	10.8	8.8					0.96
T8	11.2	9.5	6.5	7.86	0.83	1.21	1.00
T9	11.3	9.5	6.5	7.86	0.83	1.21	1.01
T10	11.7	9.5	6.5	7.86	0.83	1.21	1.04
T11	12	9.4	6.5	7.82	0.83	1.20	1.07
T12	12.3	9.5	6.6	7.92	0.83	1.20	1.10
T13	12.7	10.5	6.6	8.32	0.79	1.26	1.13
T14	14.7	10.6	6.7	8.43	0.80	1.26	1.31
T15	14	10.5	7.4	8.81	0.84	1.19	1.25
T16	15.8	11.8	7.6	9.47	0.80	1.25	1.41
T17	17.7	12.4	7.8	9.83	0.79	1.26	1.58
L1	17.2	12.4	7.8	9.83	0.79	1.26	1.54
L2	17.2	14.5	8.8	11.30	0.78	1.28	1.54
L3	17.5	13	7.3	9.74	0.75	1.33	1.56
L4	18.9	12.6	8.1	10.10	0.80	1.25	1.69
L5	18.9	13.3	8.3	10.51	0.79	1.27	1.69
L6	18.3	15.5	6	9.64	0.62	1.61	1.63
L7	16	20.6	6.7	11.75	0.57	1.75	1.36

Mesohippus bairdii composite

Vertebra	Specimen number	CL	CW	CH	AREA	CH/AREA	CW/AREA	CL/L1
T17	YPM 13791	18.78	17.81	11.16	14.10	0.79	1.26	0.94
L1	YPM 13791	20.03	16.86	11.22	13.75	0.82	1.23	1.00
L2	YPM 13791	21.35	17.78	12.81	15.09	0.85	1.18	1.07
L3	YPM 13791	20.94	17.94	11.94	14.64	0.82	1.23	1.05
L4	YPM 13791	22.38	18.43	11.01	14.24	0.77	1.29	1.12
L5	YPM 13791	20.54		10.22				1.03
L6	YPM 13791	18.04	18.39	9.10	12.93	0.70	1.42	0.90
L3	YPM 11376	21.37	17.18	11.37	13.97	0.81	1.23	1.07
L4	YPM 11376	21.15	17.12	10.21	13.22	0.77	1.30	1.06
L5	YPM 11376	21.53	17.99	11.27	14.24	0.79	1.26	1.07
L6	YPM 11376	23.57	17.53	9.45	12.87	0.73	1.36	1.18
L7	YPM 11376	19.78	17.06	7.62	11.40	0.67	1.50	0.99
L3	Mean of both	21.15	17.56	11.65	14.30	0.81	1.23	1.06
L4	Mean of both	21.77	17.78	10.61	13.73	0.77	1.29	1.09
L5	Mean of both	21.03	17.99	10.74	13.90	0.77	1.29	1.05
L6	Mean of both	20.81	17.96	9.27	12.90	0.72	1.39	1.04

Parahippus leonensis composite

Vertebra	Specimen no	CH	CW	CL	AREA	CH/AREA	CW/AREA	CL/L1
L1	UF 273270	13.99	20.86	23.92	17.08	0.82	1.22	1.00
L2	UF 205530	14.18	21.58	23.04	17.49	0.81	1.23	0.96
L3	UF 256115	14.15	25.40	25.85	18.96	0.75	1.34	1.08
L4	UF 260245	14.31	24.08	25.16	18.56	0.77	1.30	1.05
L5	UF 255585	14.24	23.00	25.93	18.10	0.79	1.27	1.08
L6	UF163493	10.77	22.01	25.59	15.39	0.70	1.43	1.07
L7	UF 199217	9.47	20.02	22.55	13.77	0.69	1.45	0.94

Pliohippus pernix AMNH 60803

Vertebra	CL	CW	CH	AREA	CH/AREA	CW/AREA	CL/L1
T17	34.86	33.49	22.23	27.29	0.81	1.23	0.95
L1	36.55	30.93	22.34	26.29	0.85	1.18	1.00
L2	36.05	32.24	23.22	27.36	0.85	1.18	0.99
L3	36.58	33.87	24.53	28.82	0.85	1.18	1.00
L4	36.51	33.13	23.07	27.65	0.83	1.20	1.00
L5	36.34	34.99	19.41	26.06	0.74	1.34	0.99
L6	33.64	34.59	17.92	24.89	0.72	1.39	0.92
L7/S1	31.69	28.14	14.15	19.95	0.71	1.41	0.87

Equus caballus, mean of all specimens (See Appendix 2)

Vertebra	CL	CW	CH	AREA	CH/AREA	CW/AREA	CL/T8
T1	49.50	61.03	35.78	46.73	0.77	1.31	1.39
T2	42.56	41.37	37.08	39.17	0.95	1.06	1.19
T3	40.54	38.26	38.88	38.57	1.01	0.99	1.14
T4	39.27	40.43	34.43	37.31	0.92	1.08	1.10
T5	38.28	42.35	36.20	39.16	0.92	1.08	1.07
T6	37.28	40.22	34.57	37.29	0.93	1.08	1.04
T7	36.97	38.96	32.77	35.73	0.92	1.09	1.04
T8	35.72	41.70	34.48	37.92	0.91	1.10	1.00
T9	37.57	38.82	33.98	36.32	0.94	1.07	1.05
T10	37.34	39.42	33.17	36.16	0.92	1.09	1.05
T11	38.67	39.61	36.04	37.78	0.95	1.05	1.08
T12	38.56	40.70	35.44	37.98	0.93	1.07	1.08
T13	37.82	40.69	33.73	37.04	0.91	1.10	1.06
T14	38.35	42.21	34.31	38.06	0.90	1.11	1.07
T15	38.97	44.00	35.35	39.44	0.90	1.12	1.09
T16	39.62	42.08	34.73	38.23	0.91	1.10	1.11
T17	40.53	45.43	36.70	40.83	0.90	1.11	1.13
T18	40.31	49.12	37.06	42.66	0.87	1.15	1.13
L1	42.77	49.05	40.19	44.40	0.91	1.10	1.20
L2	43.64	49.62	38.92	43.94	0.89	1.13	1.22
L3	43.71	53.66	37.75	45.01	0.84	1.19	1.22
L4	44.55	51.25	29.24	38.71	0.76	1.32	1.25
L5	42.12	49.19	25.99	35.76	0.73	1.38	1.18
L6	38.45	47.14	22.75	32.75	0.69	1.44	1.08

BIBLIOGRAPHY

Adams, D. C., and E. Otarola-Castillo. 2013. Geomorph: An R package for the collection and analysis of geometric morphometric shape data. Methods in Ecology and Evolution 4:393-399.

Adams, D. C., F. J. Rohlf, and D. E. Slice. 2004. Geometric morphometrics: ten years of progress following the 'revolution'. Italian Journal of Zoology 71:5-16.

Alberdi, M. T., J. L. Prado, and E. Ortizjaureguizar. 1995. Patterns of body-size changes in fossil and living Equini (Perissodactyla). Biological Journal of the Linnean Society 54:349-370.

Alexander, R. M. 1977. Allometry of limbs of antelopes (Bovidae). Journal of Zoology 183:125-146.

Alexander, R. M., N. J. Dimery, and R. F. Ker. 1985. Elastic structures in the back and their role in galloping in some mammals. Journal of Zoology 207:467-482.

Alexander, R. M., A. S. Jayes, G. M. O. Maloiy, and E. M. Wathuta. 1979. Allometry of the limb bones of mammals from shrews (*Sorex*) to elephant (*Loxodonta*). Journal of Zoology 189:305-314.

Alexander, R. M., A. S. Jayes, G. M. O. Maloiy, and E. M. Wathuta. 1981. Allometry of the leg muscles of mammals. Journal of Zoology 194:539-552.

Alvarez, A., M. D. Ercoli, and F. J. Prevosti. 2013. Locomotion in some small to medium-sized mammals: a geometric morphometric analysis of the penultimate lumbar vertebra, pelvis and hindlimbs. Zoology 116:356-371.

Anyonge, W. 1993. Body mass in large extant and extinct carnivores. Journal of Zoology 231:339-350.

Argot, C. 2003. Functional-adaptive anatomy of the axial skeleton of some extant marsupials and the paleobiology of the Paleocene marsupials *Mayulestes ferox* and *Pucadelphys andinus*. Journal of Morphology 255:279-300.

Argot, C. 2012. Postcranial analysis of a carnivoran-like archaic ungulate: The case of *Arctocyon primaevus* (Arctocyonidae, Mammalia) from the Late Paleocene of France. Journal of Mammalian Evolution 20:83-114.

Bebej, R. M., M. Ul-Haq, I. S. Zalmout, and P. D. Gingerich. 2012. Morphology and function of the vertebral column in *Remingtonocetus domandaensis* (Mammalia, Cetacea) from the middle Eocene Domanda Formation of Pakistan. Journal of Mammalian Evolution 19:77-104.

Bertram, J. E. A., and A. A. Biewener. 1990. Differential scaling of the long bones in the terrestrial Carnivora and other mammals. Journal of Morphology 204:157-169.

Bertram, J. E. A., and A. Gutmann. 2009. Motions of the running horse and cheetah revisited: fundamental mechanics of the transverse and rotary gallop. Journal of the Royal Society Interface 6:549-559.

Biancardi, C. M., and A. E. Minetti. 2013. Biomechanical determinants of transverse and rotary gallop in cursorial mammals. Journal of Experimental Biology 215:4144-4156.

Bibi, F. 2013. A multi-calibrated mitochondrial phylogeny of extant Bovidae (Artiodactyla, Ruminantia) and the importance of the fossil record to systematics. BMC Evolutionary Biology 13:1-15.

Biewener, A. A. 1983. Allometry of quadrupedal locomotion: the scaling of duty factor, bone curvature and limb orientation to body size. Journal of Experimental Biology 105:147-171.

Biewener, A. A. 1989. Scaling body support in mammals: limb posture and muscle mechanics. Science 245:45-48.

Biewener, A. A. 1990. Biomechanics of mammalian terrestrial locomotion. Science 250:1097-1103.

Biewener, A. A. 2000. Scaling of terrestrial support: differing solutions to mechanical constraints of size; pp. 51-66 *i*n J. H. Brown, and G. B. West (eds.), Scaling in Biology. Oxford University Press, Oxford.

Biewener, A. A. 2005. Biomechanical consequences of scaling. Journal of Experimental Biology 208:1665-1676.

Bogduk, N. 1980. The dorsal lumbar muscles of the cat. Anatomischer Anzeiger 148:55-67.

Bookstein, F. L. 1997. Two shape metrics for biomedical outline data: Bending energy, Procrustes distance, and the biometrical modeling of shape phenomena. 110-120 pp.

Boszczyk, B. M., A. A. Boszczyk, and R. Putz. 2001. Comparative and functional anatomy of the mammalian lumbar spine. Anatomical Record 264:157-168.

Bramble, D. M. 1989. Axial-appendicular dynamics and the integration of breathing and gait in mammals. American Zoologist 29:171-186.

Bramble, D. M., and D. Carrier. 1979. Locomotor-respiratory coupling in lagomorphs. American Zoologist 19:909-909.

Bramble, D. M., and D. R. Carrier. 1983. Running and breathing in mammals. Science 219:251-256.

Bramble, D. M., and F. A. Jenkins. 1993. Mammalian locomotor-respiratory integration: Implications for diaphragmatic and pulmonary design. Science 262:235-240.

Broek, C. M. A., A. J. Bakker, I. Varela-Lasheras, M. Bugiani, S. Van Dongen, and F. Galis. 2012. Evo-devo of the human vertebral column: on homeotic transformations, pathologies and prenatal selection. Evolutionary Biology 39:456-471.

Brown, J. H., G. B. West, and B. J. Enquist. 2000. Scaling in biology: Patterns and processes, causes and consequences; pp. 1-24 *i*n J. H. Brown, and G. B. West (eds.), Scaling in Biology. Oxford University Press, Oxford.

Buchholtz, E. 2014. Crossing the frontier: A hypothesis for the origins of meristic constraint in mammalian axial patterning. Zoology 117:64-69.

Buchholtz, E., J. Yang, H. Bailin, S. Laves, and L. Drozd. 2011. Localization of the diaphragm and axial patterning in mammals. Journal of Vertebrate Paleontology 31:79-79.

Buchholtz, E. A. 2001. Vertebral osteology and swimming style in living and fossil whales (Order: Cetacea). Journal of Zoology 253:175-190.

Buchholtz, E. A. 2007. Modular evolution of the cetacean vertebral column. Evolution & Development 9:278-289.

Buchholtz, E. A., and C. C. Stepien. 2009. Anatomical transformation in mammals: developmental origin of aberrant cervical anatomy in tree sloths. Evolution & Development 11:69-79.

Campione, N. E., and D. C. Evans. 2012. A universal scaling relationship between body mass and proximal limb bone dimensions in quadrupedal terrestrial tetrapods. BMC Biology 10.

Carrier, D. R. 1987. The evolution of locomotor stamina in tetrapods: Circumventing a mechanical constraint. Paleobiology 13:326-341.

Chen, X. M., N. Milne, and P. O'Higgins. 2005. Morphological variation of the thoracolumbar vertebrae in Macropodidae and its functional relevance. Journal of Morphology 266:167-181.

Christian, A., and H. Preuschoft. 1996. Deducing the body posture of extinct large vertebrates from the shape of the vertebral column. Palaeontology 39:801-812.

Christiansen, P. 1999a. Scaling of mammalian long bones: small and large mammals compared. Journal of Zoology 247:333-348.

Christiansen, P. 1999b. Scaling of the limb long bones to body mass in terrestrial mammals. Journal of Morphology 239:167-190.

Christiansen, P. 2007. Long-bone geometry in columnar-limbed animals: allometry of the proboscidean appendicular skeleton. Zoological Journal of the Linnean Society 149:423-436.

Cotter, M. M., S. W. Simpson, B. M. Latimer, and C. J. Hemandez. 2009a. Trabecular microarchitecture in thoracic vertebrae of extant hominoids. American Journal of Physical Anthropology:110-110.

Cotter, M. M., S. W. Simpson, B. M. Latimer, and C. J. Hernandez. 2009b. Trabecular microarchitecture of hominoid thoracic vertebrae. Anatomical Record 292:1098-1106.

Crisco, J. J., M. M. Panjabi, I. Yamamoto, and T. R. Oxland. 1992. Euler stability of the human ligamentous lumbar spine. Part II: Experiment. Clinical Biomechanics 7:27-32.

Daley, M. A., D. M. Bramble, and D. R. Carrier. 2013. Impact loading and locomotor-respiratory coordination significantly influence breathing dynamics in running humans. PLoS ONE 8.

Damuth, J. 1990. Problems in estimating body masses of archaic ungulates using dental measurements; pp. 229-253 *i*n J. Damuth, and B. J. MacFadden (eds.), Body Size in Mammalian Paleobiology: Estimation and Biological Implications. Cambridge University Press, Cambridge.

Day, L. M., and B. C. Jayne. 2007. Interspecific scaling of the morphology and posture of the limbs during the locomotion of cats (Felidae). Journal of Experimental Biology 210:642-654.

De Groote, I., C. A. Lockwood, and L. C. Aiello. 2010. Technical note: A new method for measuring long bone curvature using 3D landmarks and semi-landmarks. American Journal of Physical Anthropology 141:658-664.

Denis, F. 1983. The three column spine and its significance in the classification of acute thoracolumbar spinal injuries. Spine 8:817-831.

Denoix, J. M. D. 1999. Spinal biomechanics and functional anatomy. Veterinary Clinics of North America-Equine Practice 15:27-60.

Doube, M., A. W. Conroy, P. Christiansen, J. R. Hutchinson, and S. Shefelbine. 2009. Three-dimensional geometric analysis of felid limb bone allometry. PLoS ONE 4.

Economos, A. C. 1983. Elastic and or geometric similarity in mammalian design. Journal of Theoretical Biology 103:167-172.

English, A. W. 1980. The functions of the lumbar spine during stepping in the cat. Journal of Morphology 165:55-66.

Evans, H. E. 1993. Miller's Anatomy of the Dog, 3rd Edition. W. B. Saunders Company, Philadelphia.

Faber, M., C. Johnson, H. C. Schamhardt, P. R. Van Weeren, L. Roepstorff, and A. Barneveld. 2001a. Three-dimensional kinematics of the equine spine during canter. Equine Veterinary Journal 33:145-149.

Faber, M., C. Johnston, H. Schamhardt, R. van Weeren, L. Roepstorff, and A. Barneveld. 2001b. Basic three-dimensional kinematics of the vertebral column of horses trotting on a treadmill. American Journal of Veterinary Research 62:757-764.

Fabre, A. C., R. Cornette, G. Slater, C. Argot, S. Peigne, A. Goswami, and E. Pouydebat. 2013. Getting a grip on the evolution of grasping in musteloid carnivorans: a three-dimensional analysis of forelimb shape. Journal of Evolutionary Biology 26:1521-1535.

Fajardo, R. J., J. M. De Silva, L. M. MacLatchy, and M. L. Bouxsein. 2005. Relationships between body weight and vertebral bone architecture in primates that exhibit a 48-fold range in body weight. Bone 36:380.

Fajardo, R. J., J. M. Desilva, R. K. Manoharan, J. E. Schmitz, L. M. Maclatchy, and M. L. Bouxsein. 2013. Lumbar vertebral body bone microstructural scaling in small to medium-sized strepsirhines. Anatomical Record 296:210-226.

Felsenstein, J. 1985. Phylogenies and the comparative method. American Naturalist 125:1-15.

Fernandez, M. H., and E. S. Vrba. 2005. A complete estimate of the phylogenetic relationships in Ruminantia: a dated species-level supertree of the extant ruminants. Biological Reviews 80:269-302.

Filler, A. G. 1986. Axial character seriation in mammals: an historical and morphological exploration of the origin, development, use, and current collapse of the homology paradigm. Ph.D Dissertation, Harvard University, Department of Anthropology:349pp.

Filler, A. G. 2007. Homeotic evolution in the Mammalia: diversification of therian axial seriation and the morphogenetic basis of human origins. PLoS ONE 2:e1019.

Flower, W. H. 1885. An Introduction to the Osteology of the Mammalia. MacMillan, London.

Froehlich, D. J. 2002. Quo vadis *Eohippus*? The systematics and taxonomy of the early Eocene equids (Perissodactyla). Zoological Journal of the Linnean Society 134:141-256.

Gál, J. M. 1993. Mammalian spinal biomechanics 2: intervertebral lesion experiments and mechanisms of bending resistance. Journal of Experimental Biology 174:281-297.

Galis, F. 1999. Why do almost all mammals have seven cervical vertebrae? Developmental constraints, *Hox* genes, and cancer. Journal of Experimental Zoology 285:19-26.

Galis, F., D. R. Carrier, J. van Alphen, S. D. van der Mije, T. J. M. Van Dooren, J. A. J. Metz, and C. M. A. ten Broek. 2014. Fast running restricts evolutionary change of

the vertebral column in mammals. Proceedings of the National Academy of Sciences of the United States of America 111:11401-11406.

Gambaryan, P. P. 1974. How Mammals Run. 367 pp. Halsted Press, New York.

Garland, T. 1983. The relation between maximal running speed and body mass in terrestrial mammals. Journal of Zoology 199:157-170.

Garland, T., A. W. Dickerman, C. M. Janis, and J. A. Jones. 1993. Phylogenetic Analysis of Covariance by Computer-Simulation. Systematic Biology 42:265-292.

Garland, T., P. H. Harvey, and A. R. Ives. 1992. Procedures for the analysis of comparative data using phylogenetically independent contrasts. Systematic Biology 41:18-32.

Garland, T., and A. R. Ives. 2000. Using the past to predict the present: Confidence intervals for regression equations in phylogenetic comparative methods. American Naturalist 155:346-364.

Gaudin, T. J., and A. A. Biewener. 1992. The functional morphology of xenarthrous vertebrae in the armadillo *Dasypus novemcinctus* (Mammalia, Xenarthra). Journal of Morphology 214:63-81.

Geomagic Studio. 2010. Geomagic Inc. Version 12.1.2.

Gingerich, P. D., S. M. Raza, M. Arif, M. Anwar, and X. Y. Zhou. 1994. New whale from the Eocene of Pakistan and the origin of cetacean swimming. Nature 368:844-847.

Gingerich, P. D., B. H. Smith, and K. Rosenberg. 1982. Allometric scaling in the dentition of primates and prediction of body-weight from tooth size in fossils. American Journal of Physical Anthropology 58:81-100.

Gould, F. D. H. 2014. To 3D or not to 3D, that is the question: do 3D surface analyses improve the ecomorphological power of the distal femur in placental mammals? PLoS ONE 9.

Grafen, A. 1989. The Phylogenetic Regression. Philosophical Transactions of the Royal Society of London Series B-Biological Sciences 326:119-157.

Grand, T. I. 1997. How muscle mass is part of the fabric of behavioral ecology in East African bovids (*Madoqua, Gazella, Damaliscus, Hippotragus*). Anatomy and Embryology 195:375-386.

Halpert, A. P., F. A. Jenkins, Jr., and H. Franks. 1987. Structure and scaling of the lumbar vertebrae in African bovids (Mammalia, Artiodactyla). Journal of Zoology 211:239-258.

Harty, T. H. 2010. The role of the vertebral column during jumping in quadrupedal mammals: In *Zoology*, Vol. Ph.D. Oregon State University.

Hassanin, A., F. Delsuc, A. Ropiquet, C. Hammer, B. J. van Vuuren, C. Matthee, M. Ruiz-Garcia, F. Catzeflis, V. Areskoug, T. T. Nguyen, and A. Couloux. 2012. Pattern and timing of diversification of Cetartiodactyla (Mammalia, Laurasiatheria), as revealed by a comprehensive analysis of mitochondrial genomes. Comptes Rendus Biologies 335:32-50.

Hassanin, A., and E. J. P. Douzery. 1999. The tribal radiation of the family Bovidae (Artiodactyla) and the evolution of the mitochondrial cytochrome b gene. Molecular Phylogenetics and Evolution 13:227-243.

Hatt, R. T. 1932. The vertebral columns of ricochetal rodents. Bulletin of the American Museum of Natural History 63:599-738.

Haussler, K. K., J. E. A. Bertram, K. Gellman, and J. W. Hermanson. 2001. Segmental *in vivo* vertebral kinematics at the walk, trot and canter: a preliminary study. Equine Veterinary Journal 33:160-164.

Hermanson, J. W., and B. J. MacFadden. 1992. Evolutionary and functional morphology of the shoulder region and stay-apparatus in fossil and extant horses (Equidae). Journal of Vertebrate Paleontology 12:377-386.

Hermanson, J. W., and B. J. MacFadden. 1996. Evolutionary and functional morphology of the knee in fossil and extant horses (Equidae). Journal of Vertebrate Paleontology 16:349-357.

Hernandez, C. J., D. A. Loomis, M. M. Cotter, A. L. Schifle, L. C. Anderson, L. Elsmore, C. Kunos, and B. Latimer. 2009. Biomechanical allometry in hominoid thoracic vertebrae. Journal of Human Evolution 56:462-470.

Heylings, D. J. A. 1980. Supraspinous and interspinous ligaments in dog, cat and baboon. Journal of Anatomy 130:223-228.

Hildebrand, M. 1959. Motions of the running cheetah and horse. Journal of Mammalogy 40:481-495.

Hildebrand, M. 1962. Walking, running, and jumping. American Zoologist 2:151-155.

Hildebrand, M. 1995. The Analysis of Vertebrate Structure. 657 pp. John Wiley & Sons, New York.

Hooker, J. J. 1994. The beginning of the equoid radiation. Zoological Journal of the Linnean Society 112:29-63.

Howell, A. B. 1944. Speed in Animals. 270 pp. University of Chicago Press, Chicago.

Hudson, P. E., S. A. Corr, and A. M. Wilson. 2012. High speed galloping in the cheetah (*Acinonyx jubatus*) and the racing greyhound (*Canis familiaris*): spatio-temporal and kinetic characteristics. Journal of Experimental Biology 215:2425-2434.

Hukins, D. W. L., and J. R. Meakin. 2000. Relationship between structure and mechanical function of the tissues of the intervertebral joint. American Zoologist 40:42-52.

Hulbert, R. C., and B. J. MacFadden. 1991. Morphological transformation and cladogenesis at the base of the adaptive radiation of Miocene hypsodont horses. American Museum Novitates 3000:1-61.

Hurov, J. R. 1987. Terrestrial locomotion and back anatomy in vervets (*Cercopithecus Aethiops*) and patas monkeys (*Erythrocebus Patas*). American Journal of Primatology 13:297-311.

Hussain, S. T. 1975. Evolutionary and functional anatomy of pelvic limb in fossil and recent Equidae (Perissodactyla, Mammalia). Anatomia Histologia Embryologia 4:193-222.

Huxley, J. S. 1932. Problems of Relative Growth. Methuen and Co. Ltd., London.

Janis, C. M. 1990. Correlation of cranial and dental variables with body size in ungulates and macropodids; pp. 255-300 *i*n J. Damuth, and B. J. MacFadden (eds.), Body Size Estimation in Mammalian Paleobiology: Estimation and Biological Implications. Cambridge University Press, Cambridge.

Jayne, H. 1898. The Skeleton of the Cat. J. B. Lippincott Company, Philadelphia.

Jeffcott, L. B., and G. Dalin. 1980. Natural rigidity of the horses backbone. Equine Veterinary Journal 12:101-108.

Jenkins, F. A., Jr. 1970. Anatomy and function of expanded ribs in certain edentates and primates. Journal of Mammalogy 51:288-301.

Johnson, S. E., and L. J. Shapiro. 1998. Positional behavior and vertebral morphology in atelines and cebines. American Journal of Physical Anthropology 105:333-354.

Johnson, W. E., E. Eizirik, J. Pecon-Slattery, W. J. Murphy, A. Antunes, E. Teeling, and S. J. O'Brien. 2006. The Late Miocene radiation of modern Felidae: A genetic assessment. Science 311:73-77.

Jones, K. E., and R. Z. German. 2014. Ontogenetic allometry in the thoracolumbar spine of mammal species with differing gait use. Evolution & Development 16:110-120.

Kessel, M., and P. Gruss. 1991. Homeotic transformations of murine vertebrae and concomitant alteration of *Hox* codes induced by retinoic acid. Cell 67:89-104.

Klingenberg, C. P. 2011a. MorphoJ: an integrated software package for geometric morphometrics. Molecular Ecology Resources 11:353-357.

Klingenberg, C. P. 2011b. MorphoJ, pp. an integrated software package for geometric morphometrics. Molecular Ecology Resources, advance online.

Koob, T. J., and J. H. Long. 2000. The vertebrate body axis: Evolution and mechanical function. American Zoologist 40:1-18.

Long, J. H., D. A. Pabst, W. R. Shepherd, and W. A. McLellan. 1997. Locomotor design of dolphin vertebral columns: bending mechanics and morphology of *Delphinus delphis*. Journal of Experimental Biology 200:65-81.

MacFadden, B. J. 1986. Fossil horses from *Eohippus* (*Hyracotherium*) to *Equus*: Scaling, Cope's Law, and the evolution of body size. Paleobiology 12:355-369.

MacFadden, B. J. 1992. Fossil Horses: Systematics, Paleobiology and Evolution of the Family Equidae. Cambridge University Press, Cambridge.

Macpherson, J. M., and J. Fung. 1998. Activity of thoracic and lumbar epaxial extensors during postural responses in the cat. Experimental Brain Research 119:315-323.

Macpherson, J. M., and Y. Ye. 1998. The cat vertebral column: stance configuration and range of motion. Experimental Brain Research 119:324-332.

Maddison, W. P., and D. R. Maddison. 2010. Mesquite: a modular system for evolutionary analysis. Version 2.73. http://mesquiteproject.org.

Majoral, M., C. Berge, A. Casinons, and F. K. Jouffroy. 1997. The length of the vertebral column in primates. Folia Primatologica 68:57-76.

McMahon, T. 1973. Size and shape in biology. Science 179:1201-1204.

McMahon, T. A. 1975a. Allometry and biomechanics: limb bones in adult ungulates. American Naturalist 109:547-563.

McMahon, T. A. 1975b. Using body size to understand the structural design of animals: quarupedal locomotion. Journal of Applied Physiology 39:619-627.

Molnar, J. L., S. E. Pierce, and J. R. Hutchinson. 2014. An experimental and morphometric test of the relationship between vertebral morphology and joint stiffness in Nile crocodiles (*Crocodylus niloticus*). Journal of Experimental Biology 217:758-768.

Moritz, S., M. S. Fischer, and N. Schilling. 2007a. The consequences of having a long trunk: functional morphology in the ferret. Journal of Morphology 268:1109-1109.

Moritz, S., M. S. Fischer, and N. Schilling. 2007b. Three-dimensional fibre-type distribution in the paravertebral muscles of the domestic ferret (*Mustela putorius f. furo*) with relation to functional demands during locomotion. Zoology 110:197-211.

Nagel, D. A., P. C. Kramers, B. A. Rahn, J. Cordey, and S. M. Perren. 1991. A paradigm of delayed union and non-union in the lumbosacral joint: a study of motion and bone-grafting of the lumbosacral spine in sheep. Spine 16:553-559.

Nakatsukasa, M., and Y. Hirose. 2003. Scaling of lumbar vertebrae in anthropoids and implications for evolution of the hominoid axial skeleton. Primates 44:127-135.

Narita, Y., and S. Kuratani. 2005. Evolution of the vertebral formulae in mammals: A perspective on developmental constraints. Journal of Experimental Zoology Part B: Molecular and Developmental Evolution 304B:91-106.

Nyakatura, K., and O. R. P. Bininda-Emonds. 2012. Updating the evolutionary history of Carnivora (Mammalia): a new species-level supertree complete with divergence time estimates. BMC Biology 10:12.

O'Higgins, P., and D. R. Johnson. 1993. The inheritance of vertebral shape in the mouse II: A study using fourier analysis to examine the inheritance of patterns of vertebral variation in the cervical and upper thoracic vertebral column. Journal of Anatomy 182:65-73.

Osborn, H. F. 1900. *Oxyaena* and *Patriofelis* re-studied as terrestrial creodonts. Bulletin of the American Museum of Natural History 13:269-279.

Osborn, H. F. 1923. Remounted skeleton of *Phenacodus primaevus*. Bulletin of the American Museum of Natural History 10:159-164.

Otts, C. 1991. Postural and locomotor capabilities of the phenacodontid condylarths (Mammalia), Vol. Ph.D dissertation, pp. 566. University of Arizona.

Pal, G. P., and R. V. Routal. 1999. Mechanism of change in the orientation of the articular process of the zygapophyseal joint at the thoracolumbar junction. Journal of Anatomy 195:199-209.

Patwardhan, A. G., R. M. Havey, K. P. Meade, B. Lee, and B. Dunlap. 1999. A follower load increases the load-carrying capacity of the lumbar spine in compression. Spine 24:1003-1009.

Pierce, S. E. 2013. Morpho-functional characteristics of the axial skeleton in stem tetrapods. International Congress of Vertebrate Morphology. Symposium: Axial systems and their actuation: new twists on the ancient body of vertebrates.

Pierce, S. E., J. A. Clack, and J. R. Hutchinson. 2011. Comparative axial morphology in pinnipeds and its correlation with aquatic locomotory behaviour. Journal of Anatomy 219:502-514.

Pilliner, S., S. Elmhurst, and Z. Davies. 2002. The Horse in Motion: The Anatomy and Physiology of Equine Locomotion. Blackwell Science Ltd.

Polly, P. D., J. J. Head, and M. J. Cohn. 2001. Testing modularity and dissociation: The evolution of regional proportions in snakes; pp. 305-335 *in* M. Zelditch (ed.), Beyond Heterochrony: The Evolution of Development. Wiley-Liss.

Pridmore, P. A. 1992. Trunk movements during locomotion in the marsupial *Monodelphis domestica* (Didelphidae). Journal of Morphology 211:137-146.

Prothero, D. R., and P. C. Sereno. 1982. Allometry and paleoecology of Middle Miocene dwarf rhinoceroses from Texas Gulf Coastal-Plain. Paleobiology 8:16-30.

R. 2009. R Development Core Team. A Language and Environment for Statistical Computing.

Radinsky, L. 1966. The adaptive radiation of the phenacodontid condylarths and the origin of the Perissodactyla. Evolution 20:408-417.

Rasband, W. S. 2004. ImageJ. National Institutes of Health, Bethesda, Maryland, USA.

Rawls, A., and R. E. Fisher. 2010. Development and functional anatomy of the spine; pp. 21-46 *in* K. Kusumi, and S. L. Dunwoodie (eds.), The Genetics and Development of Scoliosis. Springer, New York.

Reddy, D., J. Kim, and R. Raaum. 2006. Resample.exe.

Reilly, S. M., and T. D. White. 2009. Breathing with your belly: Abdominal exhalation, loco-ventilatory integration and size constraints on locomotion in small mammals. Zoology 112:161-168.

Ritruechai, P. 2009. Novel insights into the anatomy and function of the equine back: In *Department of Veterinary Basic Sciences*, Vol. Ph.D., pp. 181. University of London, London.

Rohlf, F. J. 2005. tpsDig, version 2.05, pp. See http://life.bio.sunysb.edu/morph. Department of Ecology and Evolution, State University of New York at Stony Brook.

Rohlf, F. J. 2010. TPS:Relative warps. Ecology and Evolution, SUNY at Stony Brook.

Rose, K. D. 2006. The Beginning of the Age of Mammals. Johns Hopkins University Press, Baltimore.

Rose, M. D. 1975. Functional proportions of primate lumbar vertebral bodies. Journal of Human Evolution 4:21-38.

Ruff, C. B. 1986. Prediction of body weight from lower-limb bone lengths and cross-sectional dimensions in primates. American Journal of Physical Anthropology 69:259-259.

Russo, G. A. 2010. Prezygapophyseal articular facet shape in the catarrhine thoracolumbar vertebral column. American Journal of Physical Anthropology 142:600-612.

Sanders, W. J. 1998. Comparative morphometric study of the australopithecine vertebral series Stw-H8/H41. Journal of Human Evolution 34:249-302.

Sargis, E. J. 2001. A preliminary qualitative analysis of the axial skeleton of tupaiids (Mammalia, Scandentia): functional morphology and phylogenetic implications. Journal of Zoology 253:473-483.

Scan Studio HD. 2006. Version 1.3.0. Shape Tools LLC and NextEngine, Inc. Scan, Aligh, Fuse, Polish and Export,.

Schendel, M. J., K. B. Wood, G. R. Buttermann, J. L. Lewis, and J. W. Ogilvie. 1993. Experimental measurement of ligament force, facet force, and segment motion in the human lumbar spine. Journal of Biomechanics 26:427-438.

Schilling, N. 2009. Metabolic profile of the perivertebral muscles in small therian mammals: Implications for the evolution of the mammalian trunk musculature. Zoology 112:279-304.

Schilling, N. 2011. Evolution of the axial system in craniates: Morphology and function of the perivertebral musculature. Frontiers in Zoology 8:4-23.

Schilling, N., and D. R. Carrier. 2010. Function of the epaxial muscles in walking, trotting and galloping dogs: implications for the evolution of epaxial muscle function in tetrapods. Journal of Experimental Biology 213:1490-1502.

Schilling, N., and R. Hackert. 2006. Sagittal spine movements of small therian mammals during asymmetrical gaits. Journal of Experimental Biology 209:3925-3939.

Schmidt-Nielsen, K. 1984. Scaling: Why is Animal Size so Important? Cambridge University Press, Cambridge.

Scott, K. M. 1983. Prediction of body weight of fossil Artiodactyla. Zoological Journal of the Linnean Society 77:199-215.

Scott, K. M. 1985. Allometric trends and locomotor adaptations in the Bovidae. Bulletin of the American Museum of Natural History 179:193-288.

Scott, K. M. 1990. Postcranial dimensions of ungulates as predictors of body mass; pp. 301-336 *i*n J. Damuth, and B. J. MacFadden (eds.), Body Size in Mammalian Paleobiology: Estimation and Biological Implications. Cambridge University Press, Cambridge.

Scott, K. M., and C. M. Janis. 1993. Relationships of the Ruminantia (Artiodactyla) and an analysis of the characters used in ruminant taxonomy; pp. 282-302 *i*n F. S. Szalay, M. J. Novacek, and M. C. McKenna (eds.), Mammal Phylogeny: Placentals. Springer-Verlag, New York.

Shapiro, L. J. 1993. Functional morphology of the vertebral column in primates; pp. 121–49 *i*n D. L. Gebo (ed.), Postcranial Adaptation in Nonhuman Primates. Northern Illinois University Press, DeKalb.

Shapiro, L. J. 1995. Functional morphology of indrid lumbar vertebrae. American Journal of Physical Anthropology 98:323-342.

Shapiro, L. J., C. V. M. Seiffert, L. R. Godfrey, W. L. Jungers, E. L. Simons, and G. F. N. Randria. 2005. Morphometric analysis of lumbar vertebrae in extinct Malagasy strepsirrhines. American Journal of Physical Anthropology 126:1-17.

Shapiro, L. J., and C. V. M. Simons. 2002. Functional aspects of strepsirrhine lumbar vertebral bodies and spinous processes. Journal of Human Evolution 42:753-783.

Shirazi-Adl, A. 1994. Nonlinear stress analysis of the whole lumbar spine in torsion: mechanics of the facet articulation. Journal of Biomechanics 27:289-299.

Shirazi-Adl, A., and G. Drouin. 1987. Load-bearing role of facets in a lumbar segment under sagittal plane loadings. Journal of Biomechanics 20:601-613.

Simpson, G. G. 1932. Mounted skeletons of *Eohippus*, *Merychippus*, and *Hesperosiren*. American Museum Novitates 587:1-8.

Simpson, G. G. 1951. Horses. 323 pp. Doubleday and Co., Garden City, N.Y.

Sinclair, W. J. 1925. The mounted skeleton of a new *Mesohippus* from the Protoceras beds. Proceedings of the American Philosophical Society 64:55-63.

Sisson, S. 1975a. Equine syndesmology; pp. 349-375 *i*n R. Getty (ed.), Sisson and Grossman's The Anatomy of the Domestic Animals. W. B. Saunders Company, Philadelphia.

Sisson, S. 1975b. Ruminant syndesmology; pp. 787-790 *i*n R. Getty (ed.), Sisson and Grossman's The Anatomy of the Domestic Animals. W. B. Saunders Company, Philadelphia.

Sisson, S. 1975c. Sisson and Grossman's The Anatomy of the Domestic Animals. W. B. Saunders Company, Philadelphia.

Slijper, E. J. 1946. Comparative biologic-anatomical investigations on the vertebral column and spinal musculature of mammals. Verhandelingen der Koninklijke Nederlandse Akademie van Wetenschappen, Afdeling Natuurkunde 42:1-128.

Smeathers, J. E. 1981. A mechanical analysis of the mammalian lumbar spine: In *Department of Zoology*, Vol. Ph.D Thesis. University of Reading.

Smit, T. H. 2002. The use of a quadruped as an in vivo model for the study of the spine: biomechanical considerations. European Spine Journal 11:137-144.

Smith, J. M., and R. J. G. Savage. 1956. Some locomotory adaptations in mammals. Journal of the Linnean Society 42:603-622.

Sondaar, P. Y. 1968. The osteology of the manus of fossil and recent Equidae. Verhandelingen der Koninklijke Nederlandse Akademie van Wetenschappen Afdeling Natuurkunde 25:15-75.

SPSS for Windows. 2001. SPSS Inc., Version 11.0.1, Chicago.

Steudel, K., and J. Beattie. 1993. Scaling of cursoriality in mammals. Journal of Morphology 217:55-63.

Stromberg, C. A. E. 2006. Evolution of hypsodonty in equids: testing a hypothesis of adaptation. Paleobiology 32:236-258.

Sylvester, A. D. 2013. A geometric morphometric analysis of the medial tibial condyle of African hominids. Anatomical Record 296:1518-1525.

SYSTAT 13 for Windows. 2009. SYSTAT Software Inc.

Thomason, J. J. 1985. Estimation of locomotory forces and stresses in the limb bones of recent and extinct equids. Paleobiology 11:209-220.

Thomason, J. J. 1986. The functional morphology of the manus in tridactyl equids *Merychippus* and *Mesohippus:* Paleontological inferences from neontological models. Journal of Vertebrate Paleontology 6:143-161.

Thompson, D. A. W. 1917. On Growth and Form. Cambridge University Press, Cambridge.

Thompson, R. E., T. M. Barker, and M. J. Pearcy. 2003. Defining the Neutral Zone of sheep intervertebral joints during dynamic motions: an in vitro study. Clinical Biomechanics 18:89-98.

Townsend, H. G. G., and D. H. Leach. 1984. Relationship between intervertebral joint morphology and mobility in the equine thoracolumbar spine. Equine Veterinary Journal 16:461-465.

Townsend, H. G. G., D. H. Leach, and P. B. Fretz. 1983. Kinematics of the equine thoracolumbar spine. Equine Veterinary Journal 15:117-122.

Van Valkenburgh, B. 1985. Locomotor diversity within past and present guilds of large predatory mammals. Paleobiology 11:406-428.

Van Valkenburgh, B. 1990. Skeletal and dental predictors of body mass in carnivores; pp. 181-206 *in* J. Damuth, and B. J. MacFadden (eds.), Body Size in Mammalian Paleobiology. Cambridge University Press, Cambridge.

Vaughan, T. A., J. M. Ryan, and N. J. Czaplewski. 2011. Mammalogy. Jones and Bartlett Publishers, PLC, Burlington, MA.

Vinagre, T., N. Moncaut, M. Carapuco, A. Novoa, J. Bom, and M. Mallo. 2010. Evidence for a myotomal *Hox/Myf* cascade governing non-autonomous control of rib specification within global vertebral domains. Developmental Cell 18:655-661.

Wang, M. K., Y. M. Chu, S. L. Qiu, and Y. P. Jiang. 2012. Bounds for the perimeter of an ellipse. Journal of Approximation Theory 164:928-937.

Ward, C. V., and B. Latimer. 1993. The thoracic and lumbar vertebrae; pp. *i*n A. Walker (ed.), The Nariokotome *Homo erectus* Skeleton. Cambridge University Press, Cambridge.

Wellik, D. M. 2007. *Hox* patterning of the vertebrate axial skeleton. Developmental Dynamics 236:2454-2463.

Wellik, D. M., and M. R. Capecchi. 2003. *Hox10* and *Hox11* genes are required to globally pattern the mammalian skeleton. Science 301:363-367.

Wilke, H. J., A. Kettler, and L. E. Claes. 1997a. Are sheep spines a valid biomechanical model for human spines? Spine 22:2365-2374.

Wilke, H. J., A. Kettler, K. H. Wenger, and L. E. Claes. 1997b. Anatomy of the sheep spine and its comparison to the human spine. Anatomical Record 247:542-555.

Williams, S. A. 2012a. Placement of the diaphragmatic vertebra in catarrhines: Implications for the evolution of dorsostability in hominoids and bipedalism in hominins. American Journal of Physical Anthropology 148:111-122.

Williams, S. A. 2012b. Variation in hominoid vertebral formulae: implications for the evolution of the hominin vertebral column. American Journal of Physical Anthropology 147:304-304.

Wilson, A. M., K. Roskilly, J. Lowe, P. Hudson, K. Golabek, and J. Mcnutt. 2013. Dynamics of high speed locomotion and hunting in free ranging cheetah. Integrative and Comparative Biology 53:229.

Wilson, D. E., and D. M. Reeder. 2005. Mammal Species of the World: A Taxonomic and Geographic Reference. 3rd Ed. 2142 pp. Johns Hopkins University Press, Baltimore.

Wood, A. R., R. M. Bebej, C. L. Manz, D. L. Begun, and P. D. Gingerich. 2011. Postcranial functional morphology of *Hyracotherium* (Equidae, Perissodactyla) and locomotion in the earliest horses. Journal of Mammalian Evolution 18:1-32.

Wortman, J. L. 1894. Osteology of *Patriofelis,* a Middle Eocene creodont. Bulletin of the American Museum of Natural History 6:129-165.

Zaneb, H., C. Peham, and C. Stanek. 2013. Functional anatomy and biomechanics of the equine thoracolumbar spine: a review. Turkish Journal of Veterinary & Animal Sciences 37:380-389.

Zar, J. H. 1999. Biostatistical Analysis: Fourth Edition. Pearson Education, Singapore.

Zelditch, M., D. Swiderski, H. D. Sheets, and W. Fink. 2004. Geometric Morphometrics for Biologists: A Primer. 416 pp. Elsevier Academic Press, Boston, MA.

Zhou, X., W. J. Sanders, and P. D. Gingerich. 1992. Functional and behavioral implications of vertebral structure in *Pachyaena ossifraga* (Mammalia, Mesonychia). Contributions from the Museum of Paleontology, The University of Michigan 28:289-319.

CURRICULUM VITA

KATRINA E. JONES

Functional Anatomy and Evolution, Suite 305,
1830 E. Monument St., Baltimore, MD21205
Web: http://www.hopkinsmedicine.org/fae/KJ.htm
Email: kjone108@jhmi.edu
DOB: 7.22.1986, Liverpool UK

EDUCATION

2014   **Ph.D.** Functional Anatomy and Evolution, Johns Hopkins University.
Thesis: *Allometry of the thoracolumbar region in running mammals*.
Advisor: Kenneth D. Rose.

2008   **MSci.** Earth Sciences, Cambridge University.
Thesis*: Morphometric Analysis of Cranial Morphology in Pinnipeds (Mammalia, Carnivora)*.
Advisor*:* Anjali Goswami.

2007   **B.A. (Hons).** Natural Sciences, Trinity Hall, Cambridge University.
Thesis: *Sedimentary Geology of Lundbreck Falls, Alberta.*

PUBLICATIONS

1. **Jones, K. E.,** Goswami, A. and Smaers, J. *in review.* Impact of the terrestrial-aquatic transition on disparity and rates of evolution in the carnivoran skull. BMC Evolutionary Biology.
2. **Jones, K. E.** and German, R. Z. 2014. Ontogenetic allometry of the thoracolumbar spine during post-natal growth. Evolution and Development. 16 (2): 110-120.
3. **Jones, K. E**., Rose, K. D. and Perry, J. M. G. 2014. Body size and premolar evolution in the Early-Middle Eocene euprimates of Wyoming. American Journal of Physical Anthropology. 153 (1): 15-28.
4. **Jones, K. E**., Ruff, C. B. and Goswami. A. 2013. Biomechanics of the pinniped jaw: Mandibular evolution without mastication. Anatomical Record. 296(7):1049-1062.
5. **Jones, K. E**. and Goswami, A. 2010. Quantitative analysis of the influences of phylogeny and ecology on phocid and otariid pinniped (Mammalia; Carnivora) cranial morphology. Journal of Zoology. 280(3):297-308.
6. **Jones, K. E**. and Goswami, A. 2010. Morphometric analysis of cranial morphology in pinnipeds (Mammalia, Carnivora): convergence, ecology, ontogeny, and dimorphism. In: Goswami A. and Friscia A., editors. Carnivoran Evolution: New Views on Phylogeny, Form and Function. Cambridge University Press. p342-373.

CONFERENCE PRESENTATIONS

Talks

1. **Jones, K. E.,** Goswami, A. and Ruff, C. 2013. Seals, skulls, and sexual dimorphism. American Society of Mammalogists. Philadelphia.
2. **Jones, K. E.** and Rose, K. D. 2011. Premolar evolution in the earliest euprimates of Wyoming. Supplement to the online Journal of Vertebrate Paleontology, P133. SVP. Los Vegas.
3. **Jones, K. E.** and Goswami, A. 2010. Discordant morphological disparity and taxonomic diversity in pinniped versus fissiped carnivorans. Supplement to the online Journal of Vertebrate Paleontology, P113A. SVP. Pittsburgh.
4. **Jones, K. E.** and Weishampel, D. 2010. Understanding conflicting topologies: The role of character complexes in tree incongruency. The Annual Symposium of Palaeonotology and Comparative Anatomy. Cambridge, UK.
5. **Jones, K. E.** and Goswami, A. 2008. Morphometric analysis of cranial morphology in pinnipeds (Mammalia, Carnivora): Disparity, dimorphism, ecology and ontogeny. The Annual Symposium of Palaeonotology and Comparative Anatomy. Dublin, Ireland.

Posters

1. **Jones, K. E.** and Wood, A. 2013. Lumbar morphology of *Arenahippus* and *Mesohippus*, and implications for the evolution of equid locomotion. Supplement to the online Journal of Vertebrate Paleontology, P145. SVP. Los Angeles.
2. **Jones, K. E** and German, R. Z. 2013. The influence of locomotion and modularity on craniocaudal patterns of vertebral growth. FASEB J. 27:755.10. American Association of Anatomists. Boston.
3. **Jones, K. E** and German, R. Z. 2013. Differential vertebral growth produces variations in adult thoracolumbar proportions in half-bounding mammals. Society of Integrative and Comparative Biology. San Francisco.
4. **Jones, K. E**. and Ruff, C. B. 2011. Male-male combat drives bite force dimorphism in the absence of mastication. FASEB J. 25:867.1. American Association of Anatomists. Washington DC.
5. **Jones, K. E**. and Ruff. C. B., Goswami, A. 2010. Novel adaptations of the pinniped (Mammalia: Carnivora) jaw anatomy to aquatic prey-capture. FASEB J. 24: lb8. American Association of Anatomists. Anaheim, CA.
6. **Jones, K. E**. and Goswami, A. 2008. Morphometric analysis of cranial morphology in pinnipeds (Mammalia, Carnivora): Disparity, dimorphism, ecology and ontogeny. Journal of Vertebrate Paleontology. 28 (supplement to 3):97A. SVP. Cleveland.

AWARDS & GRANTS

Research grants

2013	American Society of Mammalogists, Grant-in-aid of Research	$1500
-	American Museum of Natural History, Theodore Roosevelt Grant	$1500
-	Sigma-Xi, Grant-in-aid of Research	$1000

Travel awards

2013	American Society of Mammalogists Travel Award. *Abstract selected in top 20 of 110 students.*	$300
-	American Association of Anatomists (AAA) Travel Award.	$350
-	Society of Integrative and Comparative Biology, Charlotte Magnum Award. *Accommodation costs covered.*	
2011	JHU Graduate Student Association (GSA) Travel Award.	$200
-	AAA Travel Award.	$350
2010	JHU GSA Travel Award.	$300
-	AAA Travel Award.	$250
2008	SVP Jackson School of Geosciences Student Travel Grant	$400
2006	Cambridge University, Trinity Hall Travel Award.	£300
-	Cambridge University, Earth Sciences Student Travel Award.	£400

TEACHING EXPERIENCE

JHU Medical Gross Anatomy. Two months. *Cadaver based.*

2013	Guest instructor, exam grading, tutoring
2012	Guest instructor, exam grading, tutoring
2011	Full-time lab instructor
2010	Prosections

JHU Physical and Medical Rehabilitation Resident Anatomy. *Cadaver based.*

2012-2014	Prosections

Towson University Physician Assistant Anatomy. One month. *Cadaver Based.*

2012-2014	Lecturing to small groups and lab demonstration (8 sessions)

JHU Summer Anatomy. One month. *Cadaver based.*

2011 & 2010	Dissections, lecturing to small groups, tutoring, grading

Comparative Anatomy through Dissection. Two-week intensive dissection class.

2012	Co-designed comparative anatomy class for graduate students.

JHU Undergraduate Mammalian Evolution. One Semester.

2010	Lecturing, led review sessions, exam grading

Graduate classes with student-led seminar component: Embryology, Histology, Variation, Mammal Evolution, Biomechanics, Cladistics.

SERVICE

Educational Outreach

2013   **SICB Student Journalist.** Published article for popular science audience.
                 http://www.sicb.org/students/jonesk.php

2012-2013   **MINDS.** Mentoring to Inspire Diversity in Science.
                 Led group science experiments with high school biology class once a month.

2011,2013   **JHU Science Day.**
                 Gave science presentations to groups of elementary school students from Baltimore.

2007-2008   **Time Truck.**
                 Presented earth and environmental science concepts to elementary school children near Cambridge, using interactive exhibits on board a haulage truck. Designed and refurbished exhibits.

Committee Experience

2014 -   **SVP Media Liaison Committee member**

2010-2011   **Vice-President, Graduate Student Association**. JHU.
                 Planned and implemented graduate student networking events, represented students at admin meetings.

2007-2008   **President, Time Truck**. Department of Earth Sciences, Cambridge.
                 Coordinated student-run science outreach program.

2006-2007   **Secretary, Trinity Hall JCR**. Cambridge.
                 Produced weekly news letter and represented student interests at committee meetings.

FIELDWORK & MUSEUM EXPERIENCE

2010-2014   Research Student Appointment, National Museum of Natural History at the Smithsonian Institute (Washington DC)

2009, 2011, 2013   Bighorn Basin, Wyoming. JHU Paleontological Expedition.

2006   Crowsnest Pass, Alberta. Geological mapping of sedimentary deposits.

Research experience with recent and fossil mammals at: Cambridge Zoology Museum, Natural History Museum (London), National Museum of Natural History at the Smithsonian Institute (Washington DC) and American Museum of Natural History (New York).

PROFESSIONAL MEMBERSHIPS

Society of Vertebrate Paleontology	Since 2008
American Association of Anatomists	Since 2009
American Society of Mammologists	Since 2012
Society of Integrative and Comparative Biology	Since 2012
Sigma-Xi	Since 2012